Frequency Diversity Array: Theory and Design

By

Jingjing Huang

A thesis submitted for the degree of Doctor of Philosophy of

University College London

Faculty of Engineering Sciences

Department of Electronic and Electrical Engineering

University College London

United Kingdom

Sep 2010

I, Jingjing Huang, confirm that the work in this thesis is my own. Where information has been derived from other sources, I confirm that this has been indicated in the thesis.

_____

Abstract

This thesis presents a novel concept of beam scanning and forming by employing frequency diversity in an array antenna. It is shown that by applying a linear frequency shift to the CW signals across the elements, a periodically scanning beam pattern is generated and the main beam direction is a function of time and range. Moreover, when transmitting a pulse signal, the frequency diversity array (FDA) can be used for beam forming in radar applications. These properties offer a more flexible beam scanning and forming option over traditional phase shifter implementations. The thesis begins with the discussion on FDA's array factor. It is mathematically proven that the array factor is a periodic function of time and range and the scanning period itself is a function of the linear frequency shift. Then further discussion is made when a pulsed signal is transmitted by an FDA. The requirement on the pulse width for a certain linear frequency shift is specified and corresponding signal processing technique is provided for the frequency diverse signal receiver. The thesis subsequently goes on to an electromagnetic simulation of FDA. The CST Microwave Studio is utilized to model the FDA and simulate its transient field, which allows one to verify the relationship between the scanning period and the linear frequency shift. Finally, the implementation of FDA is considered with the focus laid on the generation of the required frequency diverse signals complying with the two basic assumptions. The PLL frequency synthesis technique is introduced as an effective approach of generating the frequency diverse signals. One low cost and profile design of integer-N frequency synthesizer is presented to illustrate the basic design considerations and guidelines. For comparison, a $\Sigma - \Delta$ fractional-N frequency synthesizer produced by Analog Device is introduced for designs where more budget is available.

Acknowledgements

I would like to thank my supervisors, Dr. Kenneth Tong and Prof. Chris Baker, for their supervision and many helpful comments. The UK Ministry of Defense generously sponsored this work. I would also like to thank the department staffs for their help during this research project. Finally, I would like to thank my parents for their consistent support.

Novel Research Contributions and Publications

The novel research contributions of this work are:

1. Derivation of FDA's array factor, bringing the factor of time into discussion [See Section 4.2]
2. Mathematical proof of periodicity of FDA's array factor [See Section 4.3]
3. Electromagnetic simulation of FDA and verification of the relationship between scanning period and frequency shift. [See Section 5.3]
4. Method of beam forming using a pulsed FDA and signal processing technique at the receiver [See Section 6.5]
5. Design of frequency diverse signal generator based on PLL frequency synthesis technique. [See Section 7.2]

The following papers were published as a result of this Ph.D. research programme:

1) Kin-Fai Tong, Jingjing Huang, Lacotte, G, "Wideband Single-fed Proximity Coupled Circularly Polarized Annular Slot Antenna", IET Microwaves, Antennas & Propagation (accepted in Nov 2009)

2) Kin-Fai Tong, Jingjing Huang, "New Proximity Coupled Feeding Method for Reconfigurable Circularly Polarized Microstrip Ring Antennas", IEEE Transactions on Antennas and Propagation, Volume: 56 , Issue: 7, Year: 2008 , Page(s): 1860 - 1866

3) Jingjing Huang, Kin-Fai Tong, Chris Baker, "Frequency Diverse Array: Simulation and Design", Antennas & Propagation Conference, 2009. LAPC 2009. Loughborough, UK, Nov 2009, Page(s): 253-256

4) Jingjing Huang, Kin-Fai Tong, Karl Woodbridge, Chris Baker, "Frequency Diverse

Array: Simulation and Design", 2009 IEEE Radar Conference, Pasadena, USA, May 2009, Page(s): 1-4

5) Jingjing Huang, Kin-Fai Tong, Chris Baker, "Frequency Diverse Array with Beam Scanning Feature", The 2008 IEEE International Symposium on Antennas and Propagation, San Diego, USA, July 2008,Page(s):1-4

6) Kin-Fai Tong, Lacotte, G, Jingjing Huang, "Novel Single-feed Proximity Coupled Wideband Circularly Polarized Slot Antenna ", 2008 Asia Pacific Microwave Conference, Hong Kong, China, Dec 2008, Page(s):1-4

7) Jingjing Huang, Kin-Fai Tong, Chris Baker, "A New Polarization Reconfigurable Microstrip Antenna for Diversity Array", 2008 IEEE Radar Conference, Rome, Italy, May 2008, Page(s):1-4

8) Kin-Fai Tong, Jie Du, Jingjing Huang, "Novel Sequential Rotation Technique for Broadband Circularly Polarized Microstrip Ring Antennas", LAPC 2008, Loughborough, U.K., March 2008, Page(s):325-328.

List of Figures

List of Symbols

$\vec{A}$ Magnetic vector potential

β Phase constant, $\beta = \frac{2\pi}{\lambda}$

c Speed of light

d Spacing between array elements

Δf Frequency shift

ε_0 Permittivity of free space, $\varepsilon_0 = 8.854 \times 10^{-12} F / m$

$\vec{E}$ Electric field

$\vec{H}$ Magnetic field

f_i Frequency of the i^{th} element

j Imaginary unit

λ Wavelength

ρ $\rho \square \frac{d}{\lambda}$

μ_0 Permeability of free space, $\mu_0 = 4 \times 10^{-7} N / A^2$

N Number of elements

R_i Range from the i^{th} element to a point target

θ Angle with respect to z axis

$\vec{J}$ Electrical current density

$\vec{M}$ Magnetic current density

$\vec{I_e}$ Electric currents

η Intrinsic impedance ($377\,\Omega$ in free space)

λ_g Waveguide wavelength in the feed line

ω Angular speed

k Wave number $k = \frac{2\pi}{\lambda}$

$AF_{\Delta f,\rho}(\theta,t,r)$ Array factor of a CW FDA with $\Delta f, \lambda, d$

t_s Start time of a pulse

t_e End time of a pulse

$AF(\theta,t,r)^{P}_{\Delta f,\rho}$ Array factor of a pulsed FDA with $\Delta f, \lambda, d$

τ_0 Time delay

ν_0 Doppler frequency shift

$h_{\tau,\nu}(t)$ Matched filter

$o_T(\tau,\nu)$ Ambiguity function

f_p Working frequency of a pulsed FDA

l_p Length of a pulse transmitted by an FDA

f_{ref} Frequency of reference signal

f_{vco} VCO's output frequency

N_T Total divide value

F Fractional index of a fractional-N frequency synthesizer

List of Abbreviations

CDMA Code Division Multiple Access

CW Continuous Wave

dB Decibel

dBc Decibel relative to Carrier

DDS Direct Digital Synthesis

DSSS Direct Sequence Spread Spectrum

EM Electromagnetic

FDA Frequency diverse array

FHSS Frequency Hopping Spread Spectrum

GHz Gigahertz

IEEE Institute of Electrical and Electronics Engineers, Inc

kHz kilohertz

LFM Linear frequency modulation

MHz Megahertz

OFDM Orthogonal Frequency Division Multiplex

PN Phase Noise

RCS Radar Cross Section

RF Radio Frequency

STAP Space Time Adaptive Processing

TEM Transverse Electromagnetic Mode

TCXO Temperature Compensated Crystal Oscillator

WLAN Wireless Local Area Network

Table of Contents

Chapter 1

Introduction

1.1 Background

This research evolved out of a study exploring the opportunities of using waveform diversity to achieve electronically beam scanning and forming. Traditionally a phased array antenna is used for beam scanning and forming purpose. Although the cost of electronically beam scanning arrays has decreased significantly in the last ten years, affordability is still a challenge [1]-[3].

On the other hand, MIMO has become a focus of intensive research since its concept was proposed in 1993. With multiple independent paths created between multiple transmit and receive antennas, MIMO was first used in wireless communication systems to reduce fading and increase channel capacity [4], [5]. MIMO has recently been applied to radar systems [6]-[29]. The first MIMO radar employed multiple antennas placed far from each other, so that a target would be illuminated from different angles. In this way, the fluctuation of target's RCS is reduced and better detection performance is achieved [7], [8], [10]-[12], [16], [18]. Informally, the RCS of an object is the cross-sectional area of a perfectly reflecting sphere that would produce the same strength reflection as would the object in question. Such MIMO schemes were typically considered for distributed sensor systems. More recent developments have considered coherent MIMO approaches for closely spaced antennas. In MIMO radar using closely spaced transmit and receive antennas, one can create a very long virtual array with a small number of antennas with properly designed positions [6], [14], [26]. Thus the spatial resolution can be greatly

improved at a relatively low cost. With multiple closely spaced transmit antennas, transmit beam synthesis can be achieved by transmitting properly designed waveforms from multiple transmit antennas [9], [12]-[14], [19], [20], [22], [29].

Here we propose to explore new design freedoms of electronically beam scanning arrays by applying frequency diversity in an array antenna. Frequency diversity when applied temporally has been the subject of much research. However, the benefits of frequency diversity applied spatially are unknown. In this thesis, the characteristics of FDA where waveforms of different frequencies are spatially transmitted are examined. In FDA's simplest configuration, a continuous wave (CW) sinuous signal is radiated from each element. In contrast to conventional phased array, a linear frequency increment, rather than a phase increment, is applied across the elements. It is shown that this small frequency shift results in a beam pattern whose main beam direction is a periodic function of time and range. This is significantly different from the conventional phased array, whose beam direction is independent of range and time. The FDA is also different from co-located antennas in MIMO radar for transmit beam synthesis because there are more constraints on the parameters of waveforms transmitted by a given FDA. In other words, waveforms transmitted in MIMO radar with co-located antennas can have different frequencies, phases, durations, polarizations, etc; while the waveforms transmitted by an FDA are only different in their frequencies.

This work is motivated by the intention to examine the properties of array antennas that use frequency diversity. There has been much interest in the development and application of electronically scanned antennas in many radar applications. Much research has been done in order to develop adaptive beam forming techniques [30]-[36] in small scaled phased array. However, there has been almost no research on the advantages and disadvantages of addressing different antenna elements or

sub-arrays with different waveforms. It is demonstrated that FDA offers a new design freedom in achieving beam forming and scanning, which is hitherto unexplored.

1.2 Research Aims

The main aim of this research is to examine the relationships between frequency diversity and an electronically scanned antenna array. The research efforts are summarized below:

1) Build the mathematical model of FDA and identify physical parameters that determine its radiation behavior
2) Derive the array factor of FDA under CW case and perform a parametric study on FDA's array factor
3) Extend the discussion from CW FDA to pulsed FDA and explore the mechanism of achieving beam forming using pulsed FDA
4) Create the electromagnetic simulation that can demonstrate the performance of frequency diverse signals in an 8-element array
5) Design the frequency diverse signal generator that can produce the required frequency diverse signals

1.3 Thesis Layout

This thesis has 8 Chapters in total. Chapter 1 introduces the background and objective of this research project. Chapter 2 discusses relevant research on waveform diversity and antenna arrays, including phased arrays and MIMO systems. Chapter 3 gives a review of array fundamentals based on which the theory of FDA is developed. Chapter 4 describes the theory of an FDA in detail, focusing on the array factor of FDA. Chapter 5 is an extension of Chapter 4, discussing the mechanism of beam forming using pulsed FDA, as well as signal processing technique for systems using FDA. Chapter 6 presents the results of electromagnetic simulations of the frequency diverse array, providing a proof of FDA's beam scanning feature. Chapter 7 describes the hardware implementation of FDA. A PLL based design of frequency diverse signal generator is presented. Conclusions of the research and potential future work are finally presented in Chapter 8.

Chapter 2

Context of the Work

2.1 Literature Review

This Section provides a review of the prior work in the joint design of waveform and antenna array. It is not possible to cite all prior work in related areas, thus only those important accomplishments relevant to the development of the FDA are cited. Prior work in the development of phased array antenna, waveform diversity, and MIMO systems is primarily concerned. The review begins with an introduction to the phased array antenna. Then the review turns to developments in waveform diversity. Early work in the joint design of waveform and antenna array is mentioned, as well as recent work in MIMO systems.

2.1.1 Phased Array Antenna

A phased array antenna is a directive antenna composed of a number of individual elements. It can steer the beam electronically by varying the phase of signal at each element [1]-[2]. Unlike conventional mechanically scanned antennas, phased array antennas offer the advantage of rapid and flexible scan without mechanical rotation, and the ability to form multiple beams at the same time. Since they first gained interest and development throughout the 1950s and 1960s [37]-[44], phased arrays have come a long way in the last five decades. Over time, the enabling technologies of phased array antenna have improved. However, the underlying theory of the phased array antenna has changed little.

Historically, electronically steerable phased arrays are designed in two ways, the passive Electronically Steerable Array (ESA) which utilizes a single transmitter and receiver and the active ESA that utilizes multiple Transmit/Receive (T/R) modules, typically one per element, to provide amplitude and phase control.

The first generation of phased array is passive ESA, such as AN/MPQ-53 Radar for Patriot missile (see Figure 2.1). The second generation of phased array is active ESA using discrete solid state components. An example is PAVE PAWS radar for missile warning and space surveillance (see Figure 2.2). The third generation is also active ESA, but uses microwave analog integrated circuits. AN/APG-77 Radar used by F-22 fighter is such an example which supports the F-22's stealthy design by exhibiting a very low Radar Cross Section (RCS).

Figure 2.1: Patriot Radar AN/MPQ-53 [45].

Figure 2.2: PAVE PAWS radar of Missile Early Warning System [46].

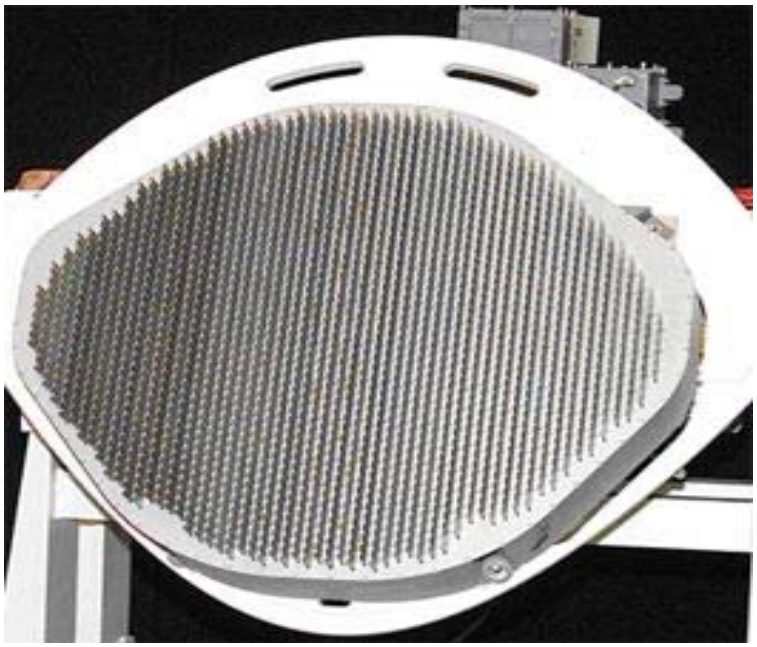

Figure 2.3: AN/APG-77 Radar used by F-22 fighter [47].

The advantages of the passive ESA include simple design and wide availability of components. One major disadvantage of the passive array is degraded SNR related to

the location of LNA. In a passive array, phase shifters and feeding network between radiation elements and LNA causes signal loss and phase noise increase. Another major disadvantage of the passive array is related to reliability. If the transmitter fails, the whole system will fail.

While in the active ESA design, the LNA can be placed immediately after the radiating element. The system experiences "graceful degradation" which means that some T/R (transmit/receive) Modules can fail without causing total system failure. The overall size of the system is significantly reduced due to the high levels of component integration on the T/R Module substrate. As for the disadvantages of the active phased array, cost was considered to be a large obstacle. Active arrays provide added system capability and reliability, but they did not receive extensive attention until the last 15 years because they were too complex and expensive. However, the advent of relatively low-cost GaAs MMICs [48]-[50] and low-cost high-speed DSP make the active ESA the preferred approach for many radar systems and communication systems requiring rapid scanning.

Phased arrays consist of multiple stationary radiating elements each of which are fed by tunable phase or time-delay control units to steer the beam. A phase shifting network is necessary to generate the phase shift necessary to steer the wave front in the required direction. Cost considerations limit the number of discrete bits of a phase shifter, resulting in periodic phase or amplitude errors across the array because of the quantization of each element. It is shown in [3] that for the actual pattern to greatly approach that of the ideal phase shifter, the number of bits should be at least 8. To reduce system size, it makes sense to integrate as many components as possible on a single chip. The integration of phase shifters on the T/R Module increases the size of the circuit. Increasing the number of bits creates a larger phase shifter, which in turn causes an increase in size and cost. Therefore cost has become a trade off,

particularly when the phase shifter is integrated on the T/R Module. Recently MEMS [51]-[55] has been used in phase shifters as a way to reduce the cost and insertion loss associated with these components.

Beam steering in a phased array is typically achieved by applying a linear phase shift across the aperture. As the frequency of the radiated signal varies, the electrical spacing between elements also varies, causing the phase progression across the aperture to change. This causes the antenna beam to scan as frequency varies, which limits the effective bandwidth of the array [56]. The aperture scanning effect can be eliminated through the use of True Time Delay (TTD) [56]-[59]. In TTD, the time of propagation for the paths of all radiating elements is made to be equal, causing all signals to add in phase for every frequency component in the waveform. However, this is costly to implement at the element level, so that TTD is usually implemented in each sub-array, rather than each element, in a big array [56], [58], [59]. However, more recent advances in direct digital synthesis (DDS) [60]-[62] of the local oscillator at each element make TTD at the element level more practical.

2.1.2 Waveform Diversity

Waveform diversity is a recent development in both radar and communications. Waveform diversity refers to the use of various waveforms in both transmitter and receiver to improve the overall performance of radar and communication systems. Examples of possible diversity dimensions are: spatial diversity – different waveforms transmitted from different spatial locations, time diversity – different waveforms transmitted at different times, frequency diversity – waveforms differ in frequency, polarization diversity – waveforms differ in polarization, etc. When waveforms are transmitted and received simultaneously by multiple antennas, it is

referred to as MIMO system, which has been developed as a separate topic from waveform diversity. Relevant research in MIMO communication and radar will be reviewed in Section 2.1.3. In this Section, only one antenna is employed at transmitter and receiver.

Before 1990s, waveform diversity did not exist as a separate research area. The 1960s saw an explosion of interest in waveform design for clutter rejection, electromagnetic compatibility, and spread spectrum techniques for communication and radar [63]-[71]. Interest in wireless communications increased rapidly in the 1990s, and waveform diversity began to emerge as a distinct technology. Besides communications, renewed research interest was shown in optimal waveforms for radar applications [72]-[81] where the joint design of transmit and receive waveforms in the presence of targets and interference was investigated.

Relevant research on waveform diversity in communications and radar will be reviewed separately in Section 2.1.2.2 and 2.1.2.3. Before that, the wireless communication and radar systems are compared so that one can understand the emphasis of

2.1.2.2 Comparison of Wireless Communications and Radar

1) Radar and wireless communication systems use electromagnetic waves of different frequencies. Radar's operating frequency is higher than that of wireless communications, in order to avoid interference.

2) The purpose of wireless communications is to achieve point-to-point information transfer with the use of electromagnetic waves. Information is carried by

systematically changing some property of the radiated waves, such as amplitude, frequency, phase, pulse width, etc. Advanced signal processing and channel coding techniques are applied to increase the system capacity and the transmission data rate. Radar, which is an acronym for RAdio Detection And Ranging, is an object-detection system that uses specially designed electromagnetic waveforms to identify the range, altitude, direction, or speed of both moving and fixed objects such as aircraft, ships, weather formations, terrain, etc. A radar system has a transmitter that transmits radar signals in predetermined directions. When these signals come into contact with an object they are usually reflected and/or scattered in many directions. At the receiver more sophisticated methods of signal processing are used in order to recover useful radar signals.

3) The main considerations in wireless communications include the capacity of the transmission channel, confidentiality of the transmitted signals and how to achieve endure less signal distortion during transmission; while the main considerations in radar are how to detect a target more quickly and at a further distance, and how to get more accurate target information from the reflected signal under limited/certain transmit power constraints.

4) From the perspective of signal processing, the main task of radar signal processing is to improve the SNR so that the detection possibility can be increased, no matter whether signal waveforms endure distortion or not; while in wireless communications signal waveform distortion must be considered, and received SNR is generally higher than that in a radar system.

2.1.2.2 Waveform Diversity in Communications

It is well known with the huge increase in the number of cellular users, capacity of the existing cellular system has become an issue. Waveform diversity techniques have been exploited to provide multiple independent channels in order to increase capacity and reduce BER. Examples of waveform diversity in communication include Direct Sequence Spread Spectrum (DSSS), Frequency Hopping Spread Spectrum (FHSS), Orthogonal Frequency Division Multiplexing (OFDM), MIMO system (see Section 2.1.3), etc

In 1997 IEEE defined the 802.11 Wireless LAN (WLAN) standards which allow wireless clients (laptops, mobile phones, etc) to communicate with Access Points, which are base stations in a wireless network. One of the radio technologies on which WLANs are based is known as spread spectrum [82]-[86]. Spread spectrum generally makes use of a sequential noise-like signal structure to spread the normally narrowband information signal over a relatively wideband (radio) band of frequencies. The receiver correlates the received signals to retrieve the original information signal. This technique decreases the potential interference to other receivers while achieving privacy. These techniques are used for a variety of reasons, including the establishment of secure communications, increasing resistance to natural interference and jamming, to prevent detection, and to limit power flux density (e.g. in satellite downlinks).There are basically two types of Spread Spectrum modulation techniques: FHSS and DSSS.

In a DSSS system, a user data sequence is multiplied by a high-speed pseudo-random number (PRN) sequence to generate a spread signal (see Figure 4.3). Since the frequency of the spreading code is much higher than the symbol rate, a higher-rate higher-bandwidth sequence is constructed, which is called “Spread Spectrum”. At the receiver, the incoming spread-spectrum signal is multiplied with

the same PRN code to de-spread the signal, allowing the original data sequence to be extracted. At the same time, any narrow-band interferers at the receiver are spread and appear to the demodulator as wideband noise. The allocation of different PRN codes to each user in the system allows isolation between users in the same frequency band. This is known as Code Division Multiple Access (CDMA).

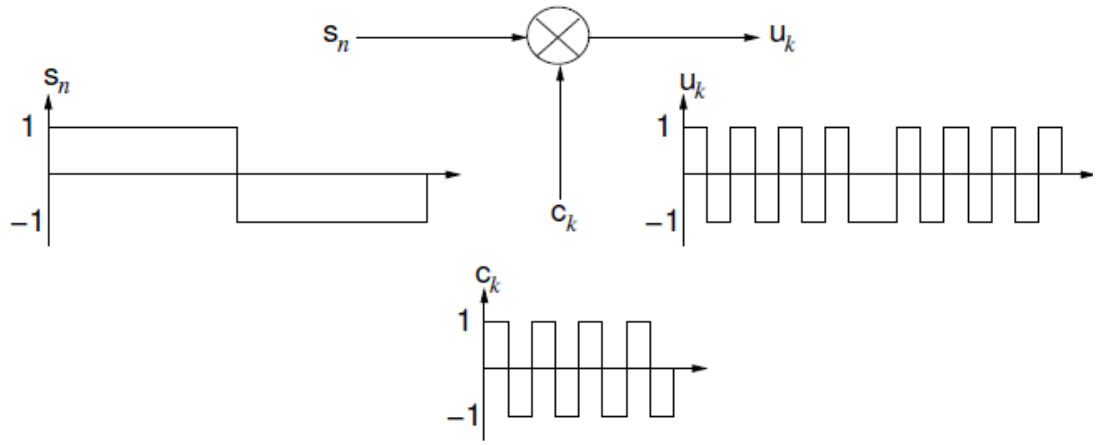

Figure 2.4: Conceptual diagram of DSSS [87]

Using CDMA techniques, it is possible to have multiple users which simultaneously transmit information over a single channel. Ideally the spreading codes in a multi-user DSSS system are orthogonal and there is zero interference between users provided that the data streams are synchronized. However, in practice, the spreading codes are only approximately orthogonal and the data streams of multiple users are not likely to be synchronized. As a result, the number of users for a specified probability of error is limited [88].

Another Spread Spectrum modulation technique is FHSS where user data sequences are modulated with pseudorandom carrier frequencies. The carrier frequency is periodically changed following a specified sequence that is known as the “spreading code” known both by the receiver and transmitter. The amount of time spent on each hop is known as “dwell time” during which a narrow band signal is generated. But if the frequency hopping process is performed over a longer period, the energy of the

narrow band signal is spread over a wider frequency band. At the receiver, the pre-determined sequence of carrier frequencies is then used to demodulate the data symbols. Again, any narrow-band interferers at the receiver are spread and appear to the demodulator as wideband noise.

DSSS has the advantage of providing higher capacities than FHSS (typically 11 Mbps vs. 3Mbps), but it is a very sensitive to environmental factors (mainly reflections). Typical DSSS applications include indoor wireless LAN, point to base station links in cellular systems, etc. On the other hand, FHSS is a very robust technology, with little influence from noises, reflections, other radio stations or other environmental factors. In addition, the number of simultaneously active systems in the same area ("collocated systems") is significantly higher than the number for DSSS systems. FHSS technology is typically selected for designs covering big areas where a large number of collocated systems exist and the use of directional antennas to minimize environmental factors is impossible.

Both DSSS and FHSS can be considered to be frequency diversity applied in a single-channel multi-user system. Data streams from different users are modulated separately using a unique "spreading code" form an orthogonal code set which allows parallel transmission of data from multiple users without interference. OFDM also uses multiple carrier frequencies, but the difference between OFDM and FHSS is that multiple carrier frequencies in OFDM are used simultaneously, rather than sequentially. OFDM applies the principle of frequency diversity by dividing the symbol stream into symbol sub-streams, each with a lower rate and requiring a smaller bandwidth, and modulating each sub-stream with a separate carrier [87], [89]-[91]. A large number of closely-spaced orthogonal carriers, as seen in Figure 2.4, are used to carry separate sub-streams. In practice, this is achieved by applying an inverse fast Fourier transform (IFFT) to the symbol stream and using the result to modulate a single carrier. The reverse process occurs at the receiver.

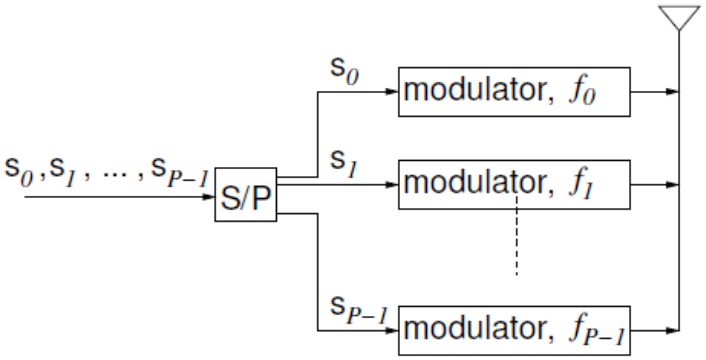

Figure 2.5: Conceptual diagram of OFDM transmitter [87]

2.1.2.2 Waveform Diversity and Design (WDD) in Radar

In traditional phased array radar, the system can only transmit scaled versions of a single waveform. Because only a single waveform is used, the phased array radar is also called SIMO (single-input multiple-output) radar. The transmitting antenna transmits a pulse in a chosen direction and the receiving antenna array under consideration has multiple equally spaced spatial channels. In the 1960s and 1970s, Space-Time Adaptive Processing (STAP) began to be developed [91], [92]. STAP techniques were originally developed for airborne moving target indication (AMTI), demonstrating superior interference rejection over non-adaptive techniques. There have been many algorithms proposed [93]-[98] for improving the performance of STAP (mainly its complexity and convergence speed) in SIMO radar. STAP can remove unwanted signal interference and enable exploitation of spatial and temporal super-resolution.

Traditional STAP algorithms assume an ideal linear array of equally spaced, isotropic point elements, ignoring real physical effects such as mutual coupling. Thus traditional STAP algorithms suffer from significant performance loss in real scenarios that include non-homogeneous data and antenna array effects. To overcome the drawback of traditional STAP algorithms, knowledge-based STAP

(KB-STAP) [99]-[104] has been developed. Knowledge-based processing takes advantage of known information about the target and interference environment, and alters algorithms, data, and parameters based on this information.

STAP and KB-STAP provide adaptivity at the receiver side of the radar system. Recent work has extended adaptivity to the transmitted waveform as well [105]-[115]. Polarization diversity has been applied to imaging radar system [105]-[107] to improve target detection and identification in the presence of clutter (e.g. ship detection in the presence of sea clutter). Several waveform design methods [108]-[114] have been proposed for the optimization of the ambiguity function in the traditional SIMO radar. The joint design of transmit and receive waveforms in the presence of targets and interference [115], [116] has also been investigated. Building on transmit waveform design and KB-STAP, a fully adaptive radar system is now possible, where the radiated waveforms and the processing of those waveforms can be dynamically chosen and mathematically optimized in response to the environment.

Due to the development in adaptive transmit technology, IEEE has adopted a new definition of waveform diversity: “Adaptivity of the radar waveform to dynamically optimize the radar performance for the particular scenario and tasks. Waveform diversity may also exploit adaptivity in other domains, including the antenna radiation pattern (both on transmit and receive), time domain, frequency domain, coding domain and polarization domain”. Notice that the IEEE definition of waveform diversity explicitly includes multiple dimensions, including spatial domain. In other words, waveform diversity includes scenarios where independent waveforms are transmitted/received simultaneously from multiple spatially separated transmit/receive antennas. This has been developed into a separate research area referred as MIMO.

2.1.3 MIMO System

MIMO techniques utilize multiple transmit and receive antennas, where each transmit antenna simultaneously transmits a different signal. The idea of increasing the capacity of a wireless communication system by applying multiple input and output antennas goes back to 1970, when Kaye and George first proposed a multiple-input multiple-output scheme that tried to improve bandwidth efficiency of a wireless communication system [117]. Spatial multiplexing using MIMO was first patented in 1993 by Paulraj and Kailath[4], [5]. Bell labs demonstrated spatial multiplexing in 1998. Today MIMO based solutions for IEEE 802.16e WIMAX have been developed by Beceem Communications, Samsung, Runcom Technologies, etc. Other companies like Broadcom and Intel have successfully applied MIMO-OFDM in IEEE802.11n. In 2004 Fishler [6], [7] and Robey [8] first proposed the concept of MIMO radar, which has become the focus of intensive research [6]-[22], [26]-[29].

2.1.3.1 MIMO in Communications

In MIMO systems (see Figure 2.6), a transmitter sends multiple data streams by multiple transmit antennas. The transmit data streams go through a channel which consists of multiple paths between multiple transmit antennas at the transmitter and multiple receive antennas at the receiver. Then, the receiver gets the received signals from the multiple receive antennas and decodes the received signals. Here is a MIMO system model:

$$Y = HX + N \tag{2-1}$$

where *Y* and *X* are the receive and transmit vectors, respectively. In addition, *H* and *N* are the channel matrix and the noise vector, respectively.

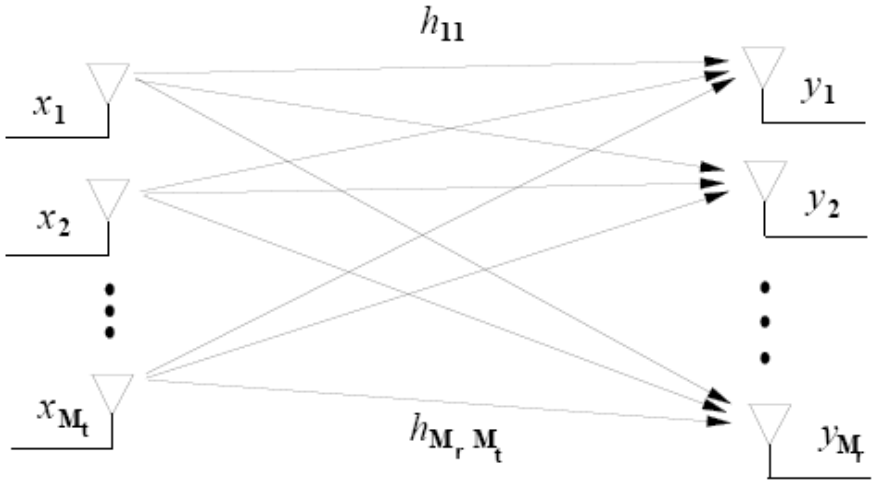

Figure 2.6: MIMO Systems [25]

If the gain of each individual transmit–receive path fades (or fluctuates) independently, multiple parallel channels can be created. A high rate signal is split into multiple lower rate streams and each stream is transmitted from a different transmit antenna in the same frequency channel. If these signals arrive at the receiver antenna array with sufficiently different spatial signatures, the receiver can separate these streams into parallel channels. Thus a MIMO system can provide spatial multiplexing, which is a powerful technique for increasing channel capacity.

The essence of MIMO communications is: (i) using multiple transmitters to transmit multiple signals over the same carrier simultaneously; and (ii) using some signal processing technique to separate individual transmitted signals from the received signals at a receiving antenna array.

2.1.3.2 MIMO Radar

The MIMO radar concept is to employ multiple antennas for transmitting several orthogonal (In general, the waveforms do not need to be orthogonal) waveforms and multiple antennas for receiving the echoes reflected by the target. The concept for MIMO radar to transmit multiple orthogonal waveforms from different antennas is usually referred to as waveform diversity. Consequently, the waveform design and optimization has been the main focus of the research in MIMO radar [6]-[29].

Based on the array configurations, MIMO radars can be classified into two main types. The first type uses widely separated transmit/receive antennas so that the spatial diversity of target's RCS can be obtained [10]. Since the transmitting antenna elements are widely separated, the target's RCS are independent random variables for different transmitting paths. Therefore, each of the echoes extracted at the receiver contains independent information about the target and a better detection performance can be obtained. The second MIMO radar type employs arrays of closely spaced transmit/receive antennas to form a beam towards a certain direction in space [9], [14], [19], [23]. In this case, the transmitting antennas are co-located such that the RCS observed by each transmitting element is identical. The echoes extracted at each receiving antenna contain the information of a transmitting path from one of the transmitting antenna elements to one of the receiving antenna elements. By using the information about all of the transmitting paths, a better spatial resolution can be obtained. The phase differences caused by different transmitting antennas along with the phase differences caused by different receiving antennas can form a new virtual array steering vector. With properly designed antenna positions, one can create a very long array steering vector with a small number of antennas. Thus the spatial resolution for clutter can be greatly improved at a relatively low cost [26], [27]. It has been shown that this kind of radar system has many advantages

such as excellent clutter interference rejection capability [15], [28], improved parameter identifiability [29], and enhanced flexibility for transmit beam pattern design [9], [20]. Through the choice of a transmit signal cross-correlation matrix, one can create spatial beam patterns ranging from the high directionality of phased-array systems to the omni-directionality of MIMO systems with orthogonal signals.

2.1.4 FDA

FDA combines frequency diversity and spatial diversity; therefore differ from any waveform diversity schemes with single antenna configuration. FDA is also different from phased scanning array, frequency scanning array and co-located transmit antennas in MIMO radar. Phased arrays transmit a single waveform from all elements and achieve beam forming by applying a linear phase shift across the aperture. In frequency scanning arrays beam steering is achieved by changing the frequency from time to time, but only one frequency is used at any given time. Co-located transmit antennas in MIMO radars have more freedoms in the design of waveforms than FDAs, since waveforms in co-located MIMO radars can differ in frequency, phase, duration, etc; while the waveforms in an FDA must have the same duration, linearly increasing/decreasing frequencies and special requirements on initial phase.

The concept of FDA was proposed by Paul Antonik et al. at 2006 IEEE Radar Conference [118]. In a linear FDA, the frequency of the waveform radiated from each element was incremented by a small amount (Δf) from element-to-element. This is illustrated in Figure 2.7.

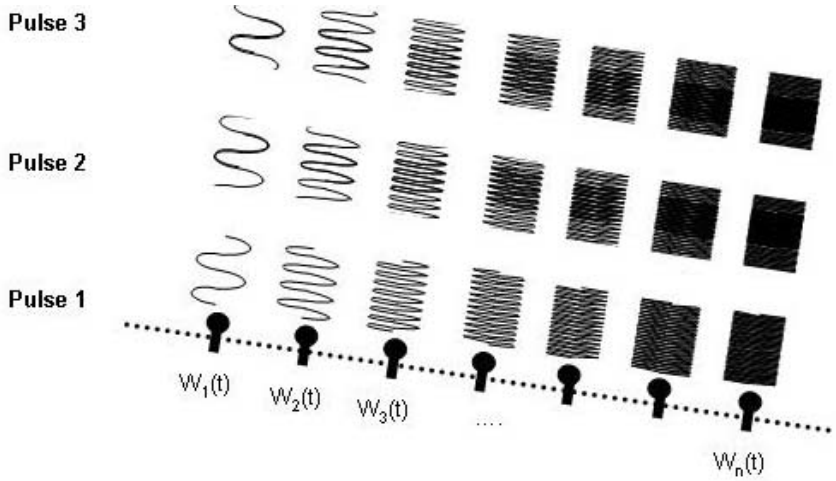

Figure 2.7: An element-to-element frequency offset is applied [118].

In [118], the FDA was described as a "range-dependent beamformer" whose apparent scan angle was written as:

$$\theta' = \arcsin\left\{\frac{2R_1\Delta f}{c}\right\} \tag{2-2}$$

Let the element spacing be λ/2, a "range-dependent beam pattern" was generated by FDA with Δf to be 350 Hz.

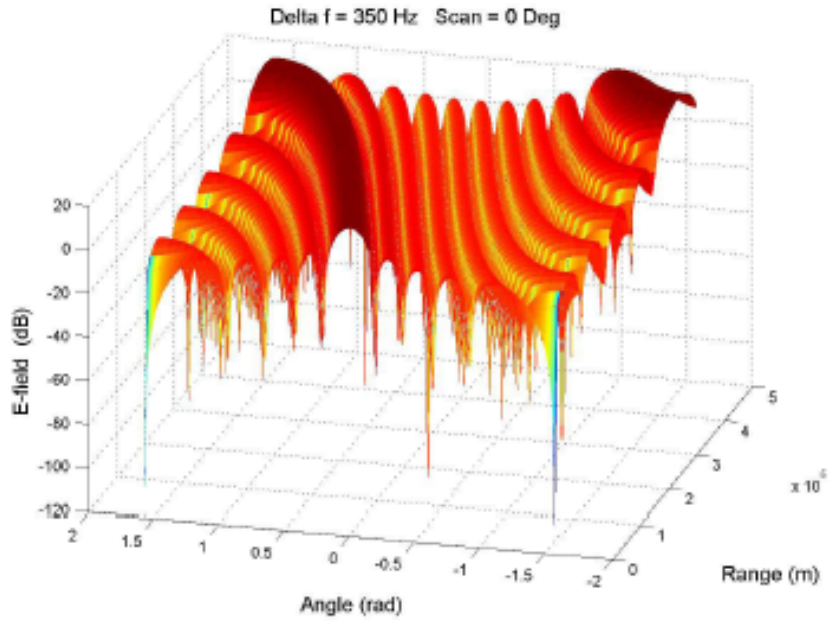

Figure 2.8: Range-dependent beam pattern with 350 Hz frequency offset [118].

In [118], the beam pattern of FDA was considered to be a function of range, thus FDA was called "range-dependent beamformer". Obviously, time was not included into consideration. In this thesis an electromagnetic simulation of 8-element linear FDA with $\Delta f = 0.01$ GHz was performed, showing that the beam pattern of FDA was also a function of time. As a result, a paper describing FDA's "beam scanning feature" [119] was published in 2008. Moreover, in [119] the scanning period was proved to be 100 ns, which is the inverse of the frequency increment $\Delta f = 0.01$ GHz between two neighboring elements. That is,

$$T_{period} = \frac{1}{\Delta f}. \tag{2-3}$$

In this thesis a compact design of FDA transmitter based on PLL frequency synthesis technique was proposed and published in 2009 [120]. 4 PLL frequency synthesizers sharing the same reference signal (see Figure 2.9) are used for generating the desired signals. The output frequencies can be easily configured and flexibly changed by 16 bit parallel programming.

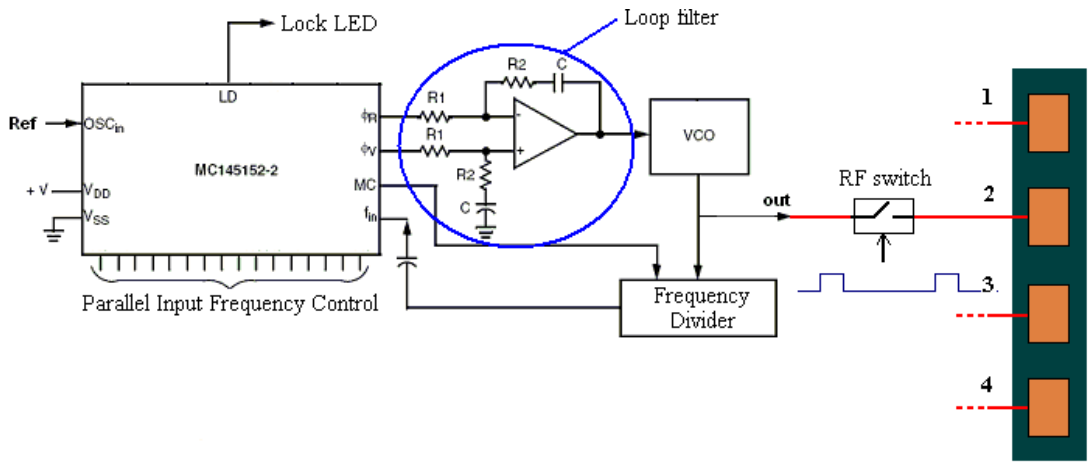

Figure 2.9: A PLL frequency synthesizer designed for FDA [120].

As an application of FDA in pulsed radar system, the mechanism of beam forming with FDA transmitting a pulse signal was explained in [121]. When the same pulse is repeated every $1/\Delta f$, the same beam pattern will be generated by each pulse. Further, when the pulse width is much shorter compared to the scanning period, the main beam will just scan such a very small angle (e.g. less than 1°) that the main beam can be considered to remain "static".

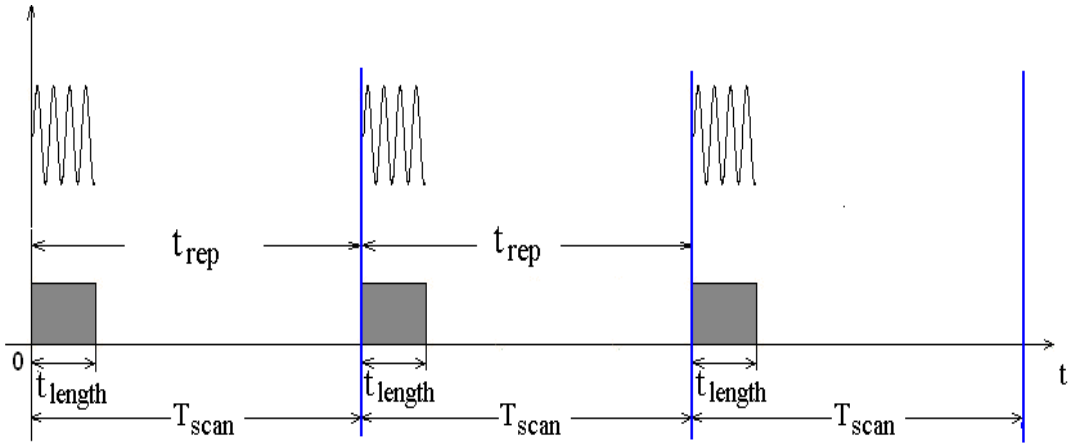

Figure 2.10: Pulse train for fixed beam [121].

Paul Antonik later included the factor of time in his PhD thesis on FDA [122] and concluded that the time signal radiated by an FDA was a function of time, range and angle. The block diagram of transmitter in Paul Antonik's experiment was shown in Figure 2.11. A 3 GHz transmit antenna was constructed of an array of 15 microstrip patch radiators. The 3 elements in each column were combined into a single sub-array, resulting in 5 spatial channels. Each 3-element column sub-array of the constructed frequency diverse array was driven by a separate signal generator. A CW tone was radiated from each column, with the frequency of each tone increased by Δf from channel-to-channel. All signal generators were triggered by a common clock. The signal in each channel was amplified and phase corrected, and then split by a 1-to-4 power divider.

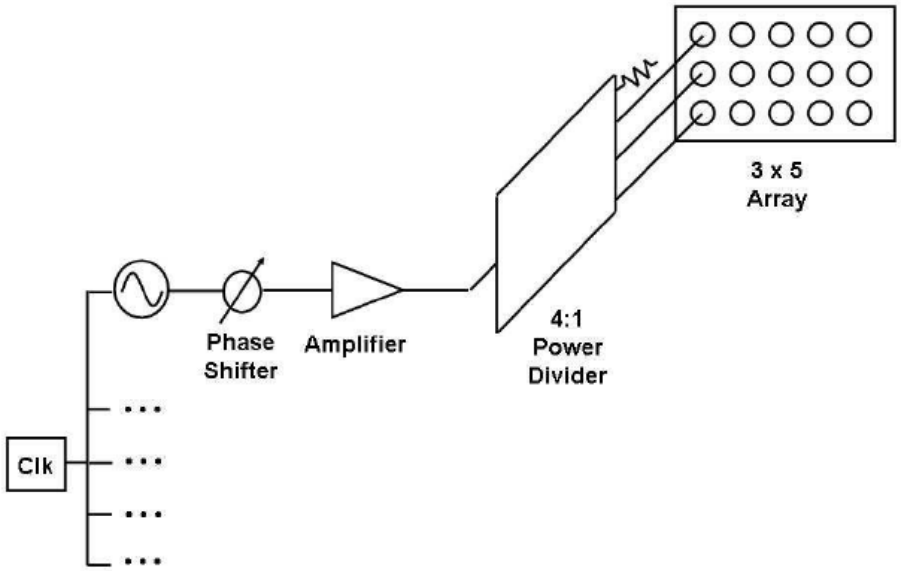

Figure 2.11: Block diagram of a transmitter channel [122].

Figure 2.12 shows the transmitter (without the signal generator set) used in Paul Antonik's experiment. One can see that the volume of the transmitter is quite big.

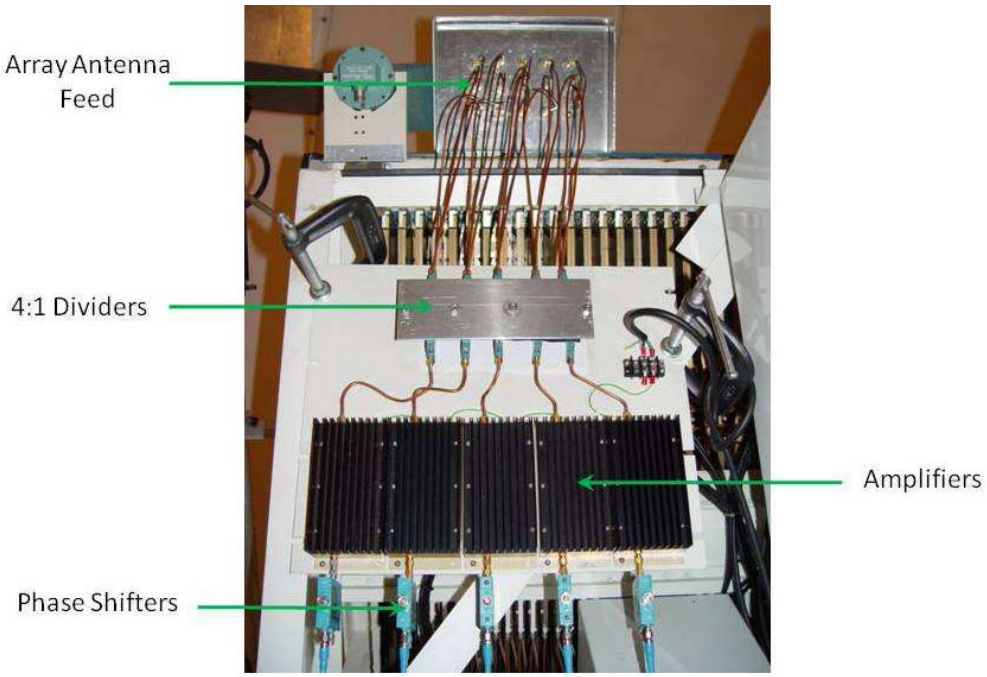

Figure 2.12: Assembled transmitter channels mounted in place [122].

In Paul Antonik's first experiment, the time signal of an FDA at boresight was examined. A probe was placed approximately 2 m from the transmit array. The

received signal was recorded by a digital oscilloscope. Since the time signal of FDA is a function of angle, range and time, in the first measurement the time signal is just a function of time with both range and angle fixed. A close-range probe measurement for a 5-channel system with $\Delta f = 100$ Hz showed a period of $1/\Delta f = 10$ ms, which verified the relationship between signal's period and frequency increment Δf.

The second experiment was performed to demonstrate the auto-scanning property of the FDA. The transmitted signals were recorded simultaneously by two receivers placed at known angular separations. Since the time signal of FDA is a function of time, range and angle, in this experiment the time signal should be a function of angle and time. Because data at two receive antennas was recorded simultaneously, the delay (difference) between two received signals should be a function of angle only. The delays between the simultaneously recorded signals were then measured in relation to the frequency shift Δf. Delay can be observed to increase progressively with angle. The agreements between the expected and measured delays were generally quite good.

The last experiment was performed to examine how an FDA's time signal varies with range. Two receivers were placed at a location approximately 2 km from, and within line-of-sight of, the transmit array. The receivers were separated by distances of 0, 30, 49, and 60 m, and two transmit channels were utilized with a frequency offset between channels of 2.5 MHz. Since the time signal of FDA is a function of time, range and angle, in this experiment the time signal should be a function of range and time. Because data at two receive antennas was recorded simultaneously, the delay (difference) between two received signals should be a function of range only. Delay can be observed to increase progressively with range. Again the agreements between the expected and measured delays were generally quite good.

2.2 Summary of Prior Work

Paul Antonik has done some work in the research area of FDA, proposing its concept and providing large amount of experimental data. However, the experimental FDA system composed of multiple signal generators, with its large volume and cost, may not be suitable for applications where either low volume or cost is desired.

The research presented in this thesis began in 2007 with electromagnetic modeling and simulation of FDA. Supported by electromagnetic simulation results, the beam scanning feature of FDA was published in 2008, showing that the beam pattern of FDA is also a function of time. Further in 2009, two more paper were published proposing a PLL based compact design for FDA, as well as the method of beam forming/scanning with an FDA transmitting a pulse signal.

The study on FDA's beam pattern is independently carried out in this thesis, including derivation of FDA's array factor and thorough discussions. Electromagnetic simulation based on Finite Integration Technique (FIT), was performed to verify the theory on FDA in this thesis. CW FDA's beaming scanning feature is theoretically analyzed and the method of achieving beam forming with FDA is proposed. The hardware implementation of the FDA is also considered and a phase lock loop (PLL) based hardware design is presented.

A review of the relevant literature shows that the research on FDA in this thesis is separate and distinct from previously published works. The FDA provides new design freedom in range, angle, and time and novel ways to control antenna radiation patterns. The described research provides antenna patterns that are periodic in time, and that scan in angle without the need for phase shifters or mechanical steering. In addition, extended versions of the FDA concept may allow for new radar designs.

Chapter 3

Phased Array Theory

In this Chapter, the basic theory of antenna array is introduced. This provides the comparison on what novelties the frequency diversity concepts are developed in Chapter 4.

3.1 Basic Concepts of Antenna Array

3.1.1 Radiated Fields of Electrical/Magnetic Current Source

In the analysis of radiation problems, it is a very common to introduce auxiliary functions, known as vector potentials. While it is possible to determine the $\vec{E}$ and $\vec{H}$ fields directly from the electrical current density $\vec{J}$ and magnetic current density $\vec{M}$, it is usually much simpler to find the auxiliary potential functions first and then determine the $\vec{E}$ and $\vec{H}$. The most common vector potential functions are the $\vec{A}$ (magnetic vector potential) and $\vec{F}$ (electric vector potential). Here the vector potential $\vec{A}$ for an electrical current density $\vec{J}$ is discussed while the solution of magnetic current density $\vec{M}$ can be obtained by the duality theorem.

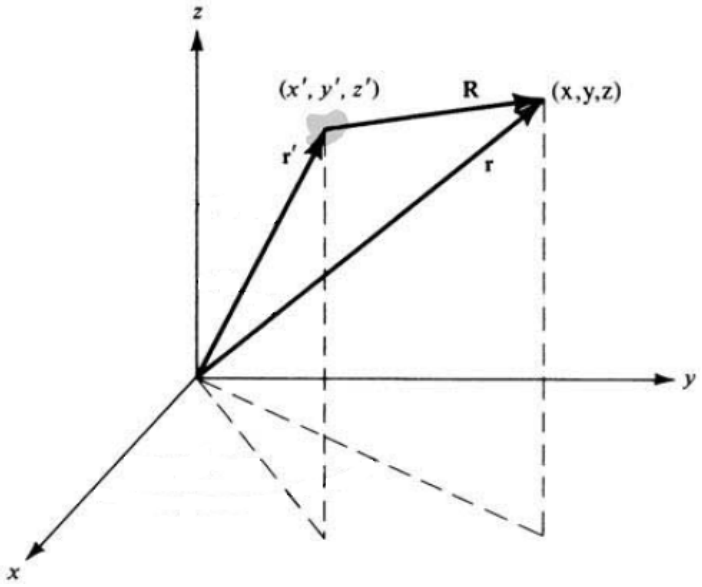

Figure 3.1: Source placed at (x',y',z').

If the source is placed at a position represented by the primed coordinates (x',y',z'), as shown in Figure 3.1, the magnetic vector potential $\vec{A}$ can be written as [123]

$$\vec{A}(x,y,z)=\frac{\mu}{4\pi}\iiint_v \vec{J}\left(x',y',z'\right)\frac{e^{-jkR}}{R}dv', \tag{3-1}$$

where the primed coordinates represent the source, the unprimed the observation point, and *R* the distance from any point on the source to the observation point.

For electric currents $\vec{I_e}$, (3-1) reduces to line integrals of the form

$$\vec{A}(x,y,z)=\frac{\mu}{4\pi}\int_C \vec{I_e}(x',y',z')\frac{e^{-jkR}}{R}dl'. \tag{3-2}$$

Once A is known, the radiated E-field $\vec{E_A}$ can be derived as [123]

$$\overrightarrow{E_A} = -j\omega\vec{A} - j\frac{1}{\omega\mu\varepsilon}\nabla(\nabla\cdot\vec{A}). \tag{3-3}$$

3.1.2 An Example: Far Fields of Infinitesimal Electrical Dipole

An infinitesimal electric dipole with a finite length l ($l \ll \lambda$) is positioned symmetrically at the origin of the coordinate system and oriented **along the z axis**, as shown in Figure 3.2. And the spatial distribution of the current is assumed to be constant and given by

$$I\left(z'\right) = \hat{a}_z I_0, \tag{3-4}$$

where I_0 is a constant.

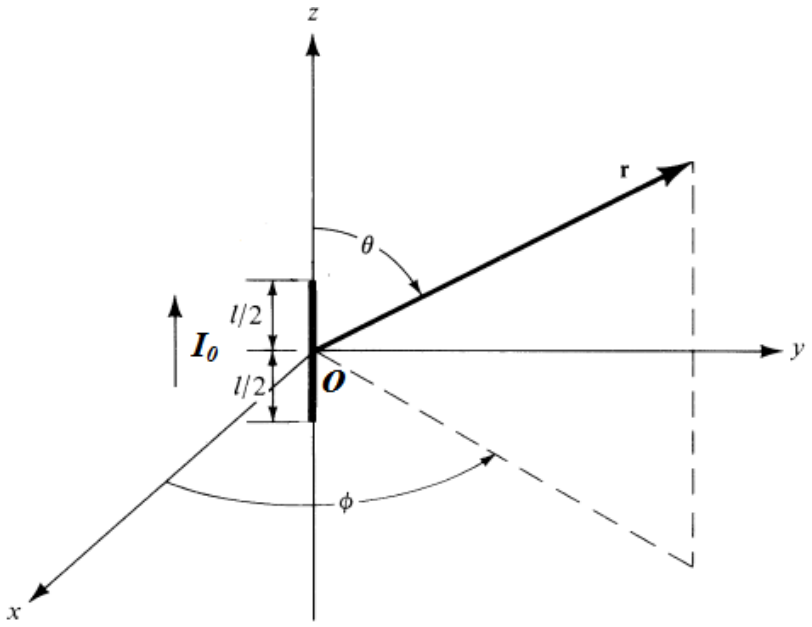

Figure 3.2: An infinitesimal electric dipole with finite length positioned at the origin along the **z** axis.

According to (3-2), the vector potential function $\vec{A}$ can be written as

$$\vec{A}(x,y,z) = \hat{a}_z \frac{\mu I_0}{4\pi r} e^{-jkr} \int_{-l/2}^{+l/2} dz' = \hat{a}_z \frac{\mu I_0 l}{4\pi r} e^{-jkr} . \tag{3-5}$$

Using (3-3), the radiated fields in the far-field region where $kr \gg 1$ ($r \gg \lambda$) can be written as [123]

$$E_\theta \approx j\eta \frac{kI_0 l e^{-jkr}}{4\pi r} \sin\theta , \tag{3-6}$$

$$E_r \approx E_\phi = 0 ,$$

where η is the intrinsic impedance ($377 \approx 120\pi\ \Omega$ for free-space).

The $\vec{E}$ and $\vec{H}$-field components are perpendicular to each other, transverse to the radial direction of propagation, and the fields form a Transverse ElectroMagnetic (TEM) wave whose wave impedance is equal to the intrinsic impedance of the medium. Since the r variations are separable from those of θ and ϕ, the shape of the pattern is not a function of the radial distance r. Actually this relationship is applicable in the far-field region of all antennas of finite dimensions.

3.1.3 Far Field of Antenna Array: Array factor and Pattern Multiplication

In Section 3.1.2, the radiation characteristics of single-element antenna were discussed and analyzed. Based on that, the far field of an array antenna composed of *N* elements can be derived. The simplest and most practical array is formed by placing the elements along a straight line as shown in Figure 3.3.

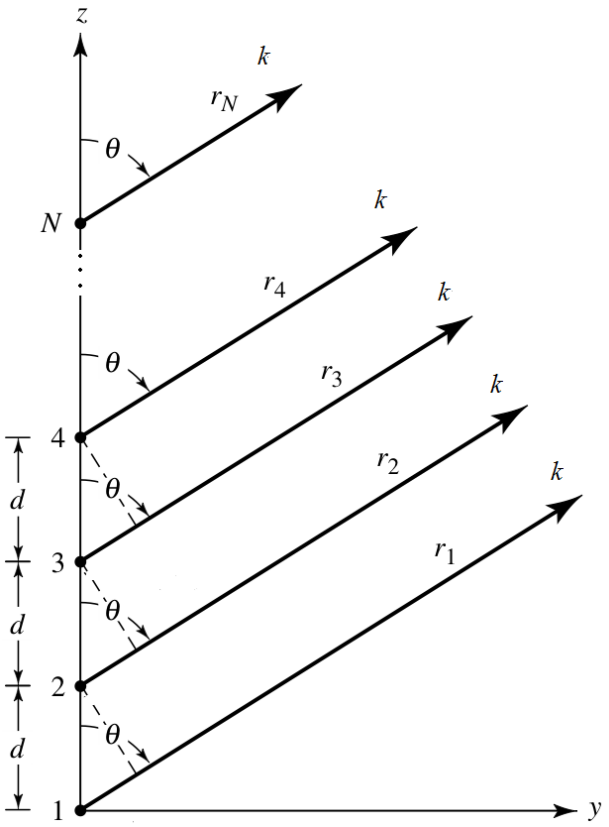

Figure 3.3: An *N*-element linear array.

The total field radiated by *N* elements, assuming no coupling between the elements, is equal to the sum of the individual field and in the y-z plane. It is given by

$$\overrightarrow{E_t} = \hat{a}_\theta \, j\eta \frac{kI_0 l}{4\pi r} \sin\theta \sum_{n=1}^{N} e^{j(n-1)\left(kd\cos\theta+\beta\right)}, \tag{3-7}$$

where β is the difference in phase excitation between the elements. The excitation magnitude of the radiators is identical.

It is apparent from (3-7) that the total field of the array is equal to the field of a single element positioned at the origin ($\hat{a}_\theta \, j\eta \frac{kI_0 l}{4\pi r} \sin\theta$) multiplied by a factor which is widely referred to as the array factor. This is referred to as pattern multiplication

[124] for arrays of identical elements. For the N-element array of constant amplitude, the array factor is given by

$$AF = \sum_{n=1}^{N} e^{j(n-1)\psi} , \tag{3-8}$$

where $\psi = kd\cos\theta + \beta$.

The array factor of a constant amplitude array is a function of the geometry of the array and the excitation phase. By varying the separation d and β the phase between the elements, the characteristics of the array factor and of the total field of the array can be controlled.

The array factor, in general, is a function of the number of elements, their geometrical arrangement, their relative magnitude, their relative phase, and their spacing. The array factor will be of simpler form if the elements have identical amplitude, phase, and spacing. Since the array factor does not depend on the directional characteristics of the radiating elements themselves, it can be formulated by replacing the actual elements with isotropic (point) sources. Once the array factor has been derived using the point-source array, the total field of the actual array is obtained by the use of pattern multiplication.

In Chapter 4, we will derive the array factor for an FDA and one will see that the array factor of an FDA is also a function of time and range.

3.1.4 More on Array Factor: Null, Maximum, Grating lobe, Element space

The array factor of (3-8) can also be expressed in a closed form as:

$$\left|AF\right| = \left|\frac{\sin\left(\frac{N}{2}\psi\right)}{\sin\left(\frac{1}{2}\psi\right)}\right|, \tag{3-9}$$

where $\psi = kd\cos\theta + \beta$.

To find the nulls of the array factor (3-9) is set equal to zero.

$$\theta_n = \cos^{-1}\left[\frac{\lambda}{2\pi d}\left(-\beta \pm \frac{2n}{N}\pi\right)\right] \quad \begin{matrix} n = 1,2,3,... \\ n \neq N, 2N, 3N, ... \end{matrix} \tag{3-10}$$

Moreover, for a zero to exist, the argument of the arccosine cannot exceed unity, i.e.

$$\left|\frac{\lambda}{2\pi d}\left(-\beta \pm \frac{2n}{N}\pi\right)\right| \leq 1. \tag{3-11}$$

Thus for an *N*-element array, the number of nulls that can exist will be a function of the element separation *d* and the phase excitation difference β. The values of *n* determine the order of the nulls (1st, 2nd, etc.).

Similarly, the maximum value of array factor occur when

$$\theta_m = \cos^{-1}\left[\frac{\lambda}{2\pi d}\left(-\beta \pm 2m\pi\right)\right] \quad m = 0,1,2,... \tag{3-12}$$

For a maximum to exist, the argument of the arccosine cannot exceed unity, i.e.,

$$\left|\frac{\lambda}{2\pi d}\left(-\beta \pm 2m\pi\right)\right| \le 1. \tag{3-13}$$

In many applications it is desirable to have the maximum radiation of an array directed normal to the axis of the array ($\theta_0 = 90^\circ$). If first maximum θ_0 (m = 0 in 3-12) of the array factor occurs at $\theta_0 = 90^\circ$ then

$$\psi = kd\cos\theta_0 + \beta\Big|_{\theta_0=90^\circ} = 0 \Rightarrow \beta = 0. \tag{3-14}$$

To have the maximum of the array factor of a uniform linear array directed broadside to the axis of the array, it is necessary that all the elements have the same phase excitation ($\beta = 0$). The array factor of (3-9) is shown in Figure 3.4 for an 8-element linear array with d=0.45λ, $\beta = 0$.

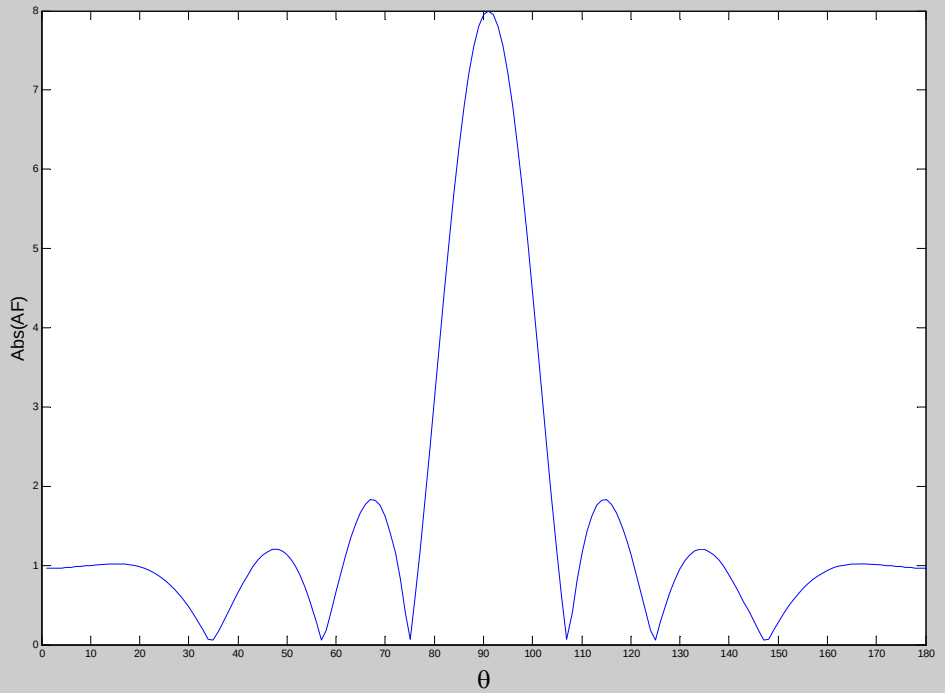

Figure 3.4: Array factor of an 8-element linear array with d=0.45λ, $\beta = 0$.

The separation between the elements can be of any value. When d = $\lambda, \beta = 0$, the array factor of (3-9) is shown in Figure 3.5 for comparison.

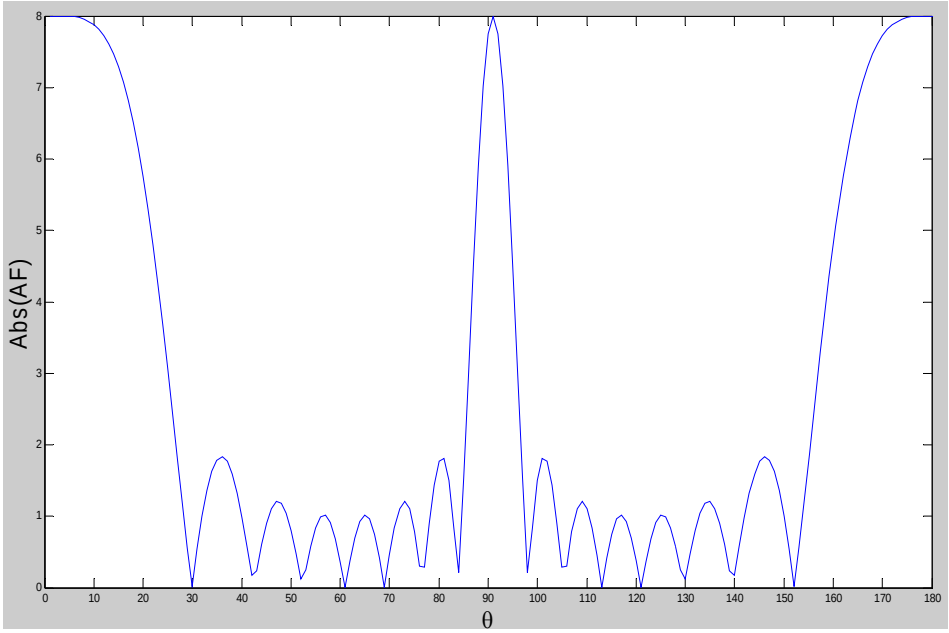

Figure 3.5: Array factor of an 8-element linear array with d = $\lambda, \beta = 0$.

To ensure that there are no principal maxima in other directions, which are referred to as grating lobes, the largest spacing between the elements in a broadside array should be less than one wavelength ($d_{\max} < \lambda$) when $\beta = 0$ to avoid any grating lobe [125].

Instead of having the maximum radiation broadside to the axis of the array, it may be desirable to direct it along the axis of the array (end-fire). To direct the first maximum towards $\theta_0 = 0^\circ$,

$$\psi = kd\cos\theta_0 + \beta\Big|_{\theta_0=0^\circ} = 0 \Rightarrow \beta = -kd\,. \tag{3-15}$$

Or if the first maximum is desired toward $\theta_0 = 180^\circ$, then

$$\psi = kd\cos\theta_0 + \beta\Big|_{\theta_0=180^\circ} = 0 \Rightarrow \beta = kd\,. \tag{3-16}$$

Thus, end-fire radiation is accomplished when $\beta = -kd$ (for $\theta_0 = 0^\circ$) or $\beta = kd$ (for $\theta_0 = 180^\circ$). As an example, the array factor of (3-9) is shown in Figure 3.6 for an 8-element linear array with $\rho = 0.5, \beta = \pi\ (or - \pi)$.

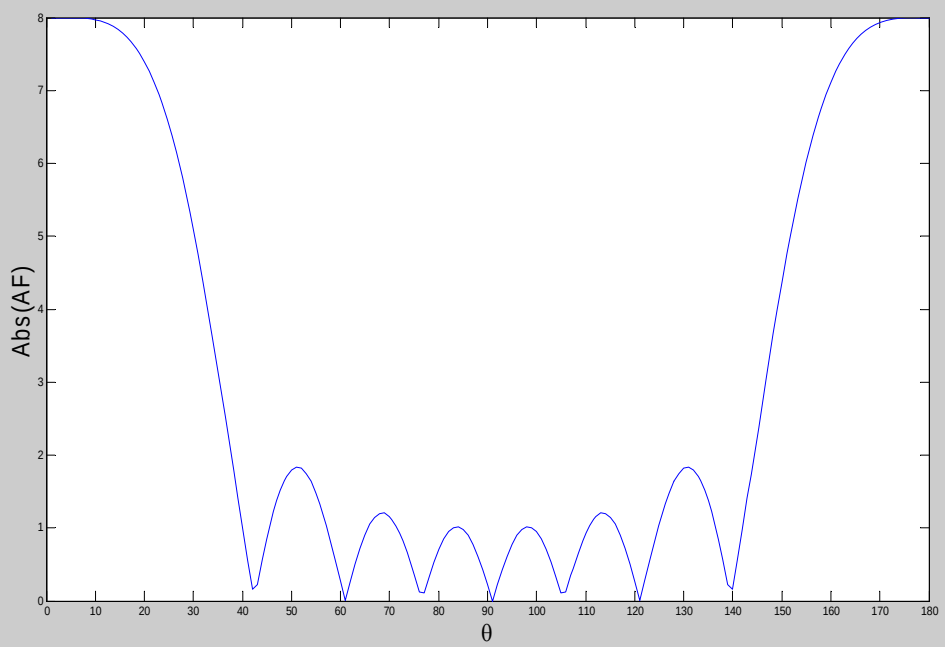

Figure 3.6: Array factor of an 8-element linear array with $\rho = 0.5, \beta = \pi\ (or - \pi)$

To have only one end-fire maximum (either $\theta_0 = 0^\circ$ or $\theta_0 = 180^\circ$) and to avoid any grating lobes, the maximum spacing between the elements should be less than $\rho < 0.5\ \left(d_{\max} < \lambda/2\right)$ [125]. The array factor of (3-9) is shown in Figure 3.7 for an 8-element linear array with $\rho = 0.45, \beta = -kd = -0.9\pi$.

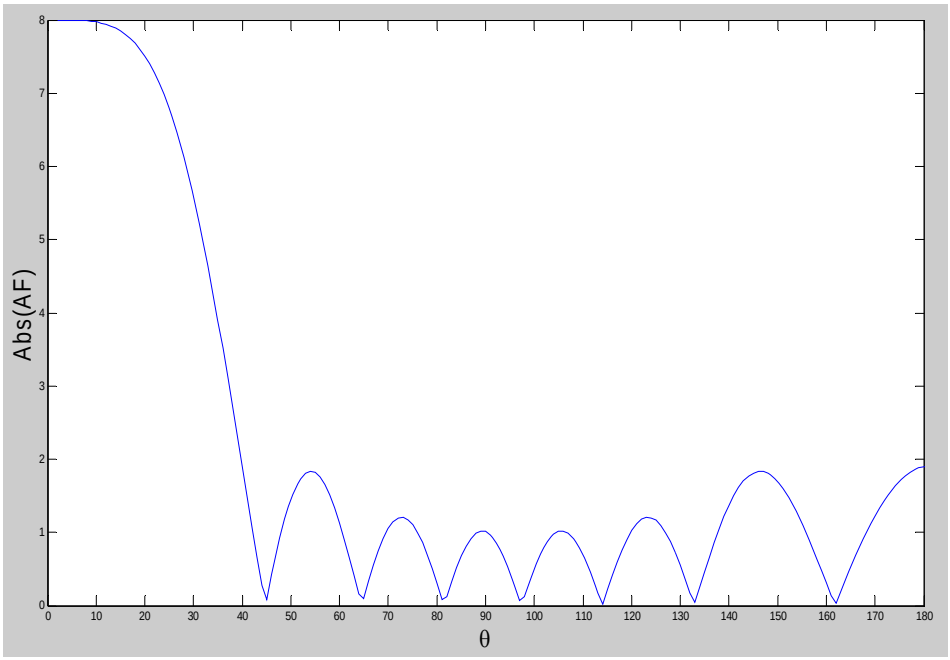

Figure 3.7: Array factor of an 8-element linear array with $\rho = 0.45$, $\beta = -kd = -0.9\pi$

And for an 8-element linear array with $d = 0.45\lambda,\ \beta = kd = 0.9\pi$ the array factor of (3-9) is shown in Figure 3.8.

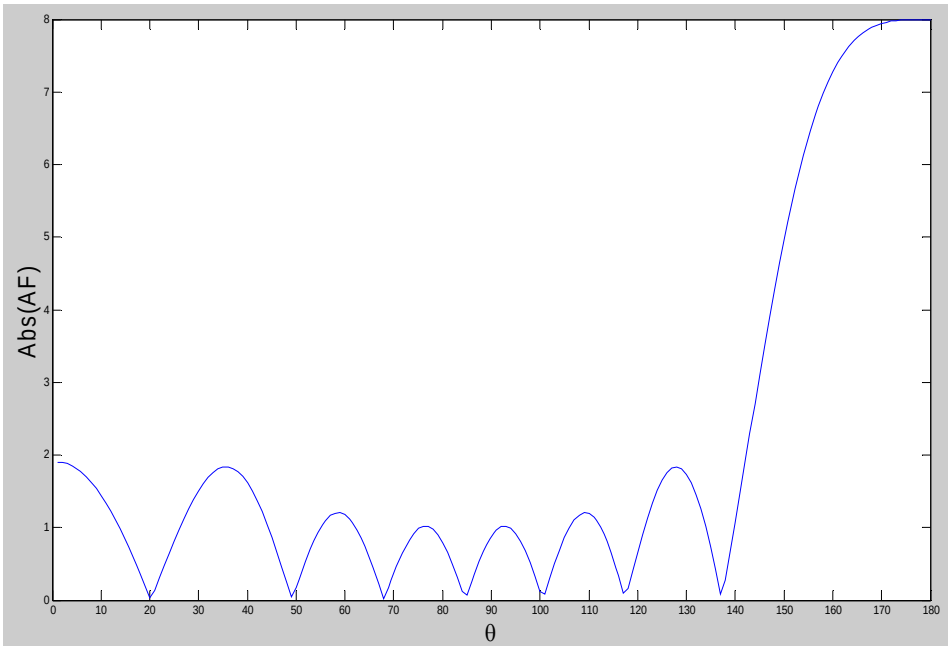

Figure 3.8: Array factor of an 8-element linear array with $\rho = 0.45, \beta = kd = 0.9\pi$.

3.2 Beam steering and phase shifting

3.2.1 Beam Steering

In the previous Section it was shown how to steer the beam by controlling the phase difference between the elements, in broadside and end fire direction of the array. It is then natural to assume that the maximum radiation can be oriented in any direction to form a scanning array. Let us assume that the maximum radiation of the array is required to be oriented at an angle θ_0. To accomplish this, the phase excitation difference $\beta \in [-kd, kd]$ between the elements must be adjusted so that

$$\psi = kd\cos\theta + \beta\Big|_{\theta=\theta_0} = 0 \Rightarrow \beta = -kd\cos\theta_0 . \tag{3-17}$$

As an example, for an 8-element array with $d = 0.45\lambda$ to form a main beam at $\theta_0 = 0^\circ, 60^\circ, 90^\circ, 120^\circ, 180^\circ$ separately, the corresponding phase shift β should be $-0.9\pi, -0.45\pi, 0, 0.45\pi, 0.9\pi$.

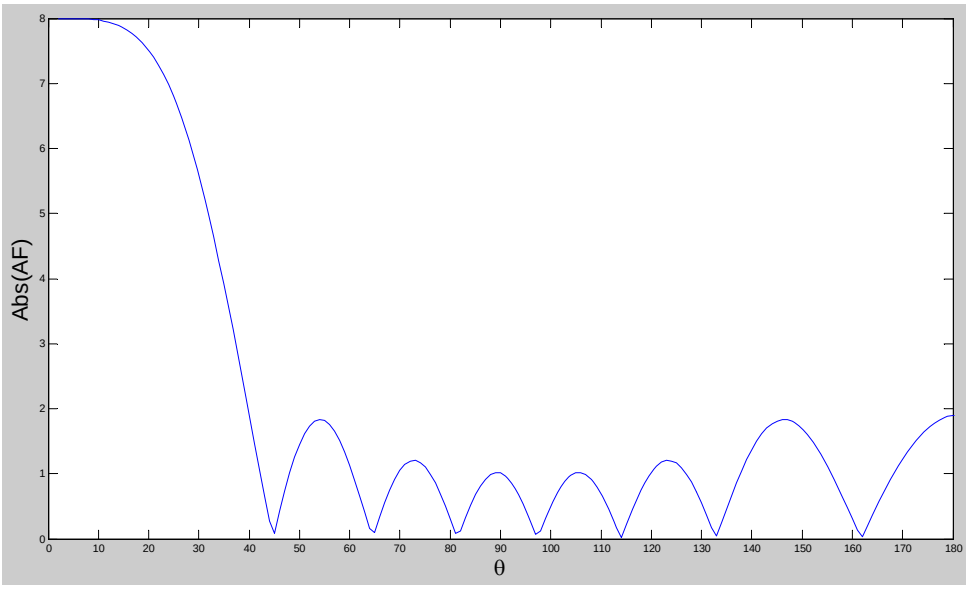

(a) $\theta_0 = 0^\circ$ with $\beta = -0.9\pi$

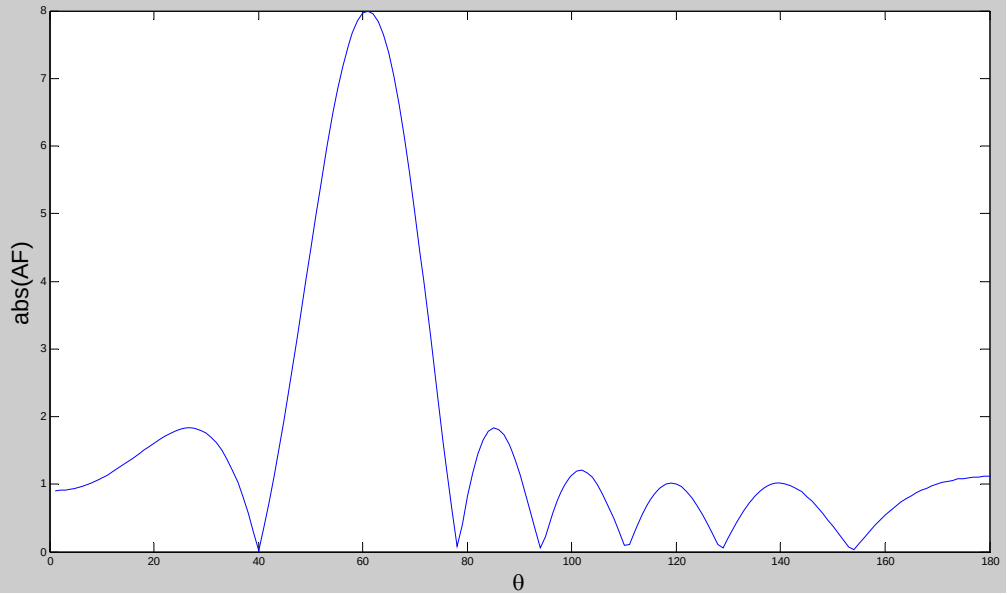

(b) $\theta_0 = 60^\circ$ with $\beta = -0.45\pi$

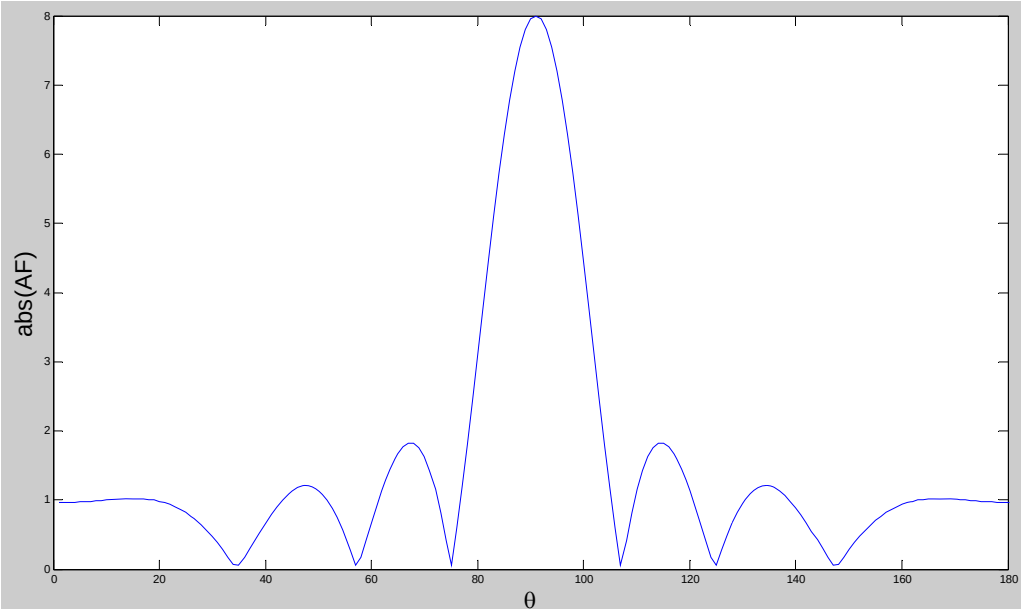

(c) $\theta_0 = 90^\circ$ with $\beta = 0$

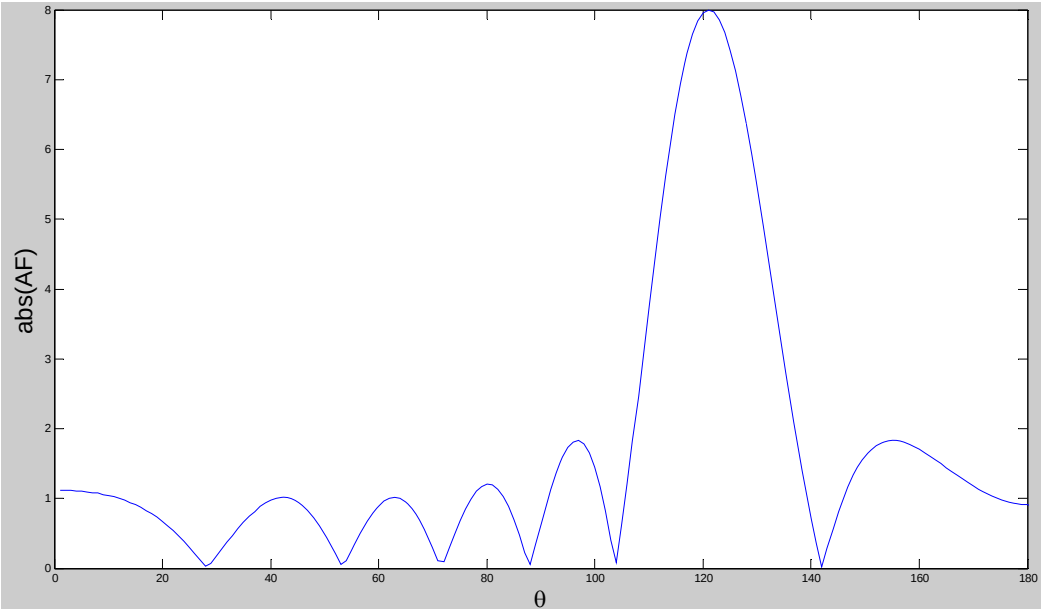

(d) $\theta_0 = 120^\circ$ with $\beta = 0.45\pi$

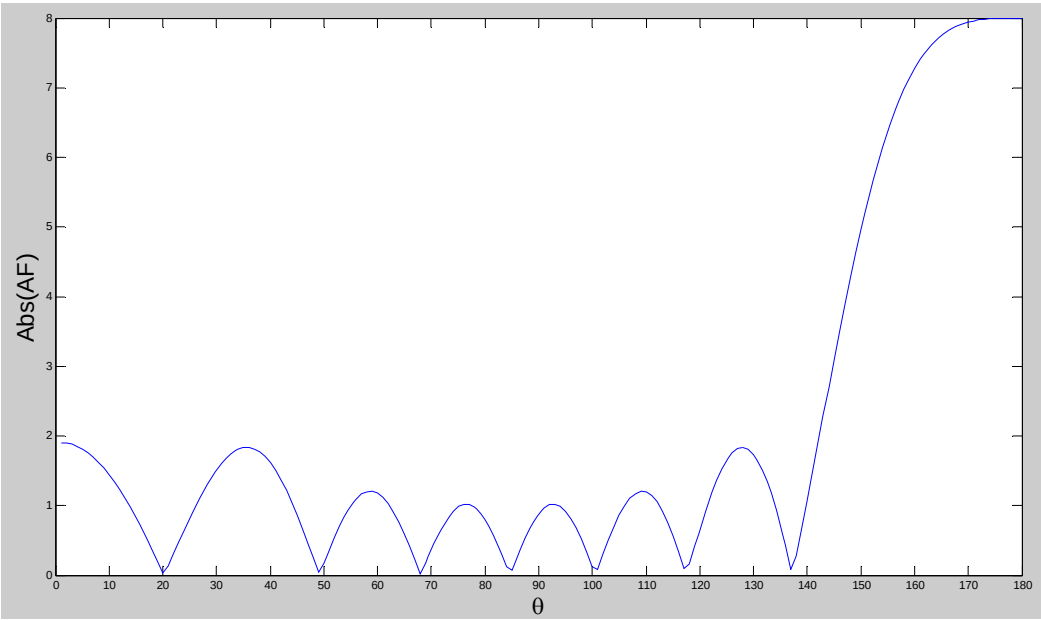

(e) $\theta_0 = 180^\circ$ with $\beta = 0.9\pi$

Figure 3.9: Beam steering with different phase shifts.

Thus by controlling the progressive phase difference between the elements, the maximum radiation can be steered in any desired direction to form a scanning array. This is the basic principle of scanning array operation. To ensure that there are no principal maxima in other directions, the maximum spacing between the elements should be less than $d_{\max} < \lambda / 2$ in a scanning array [125].

So far, we have discussed the phased array antenna beam positioning by applying a phase shift to the linear array antenna elements without specifying how this phase shifting may be accomplished. In this Section, we will briefly outline some (certainly not all) methods available for accomplishing a desired phase shift.

3.2.2 Phase Shifting by Changing Physical Length

One way of accomplishing a desired phase shift is by changing physical lengths. A schematic view of a cascaded, four-bit, digitally switched phase shifter is shown in Figure 3.10.

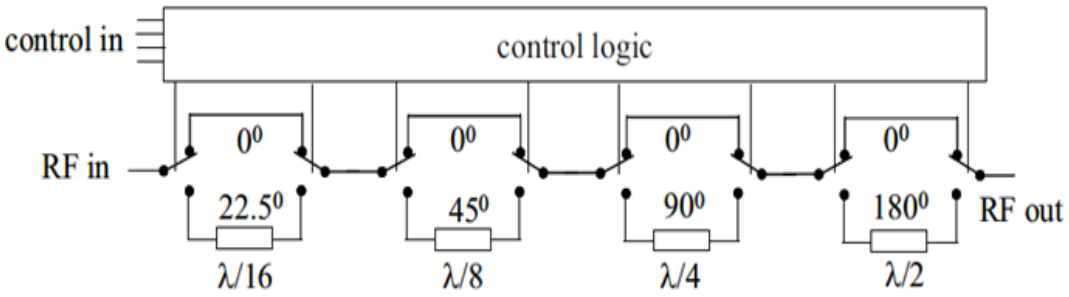

Figure 3.10: A cascaded 4-bit digitally switched phase shifter [126].

The switches in every Section are used to either switch a standard length of transmission line into the network or a piece of transmission line that adds to this

standard length a piece of predetermined length. These lengths are chosen such that when the cascade of standard length is taken as reference having a phase $\psi = 0^{\circ}$, while 16 phases, ranging from $\psi = 0^{\circ}$ to $\psi = 337.5^{\circ}$ in steps of 22.5°, may be selected.

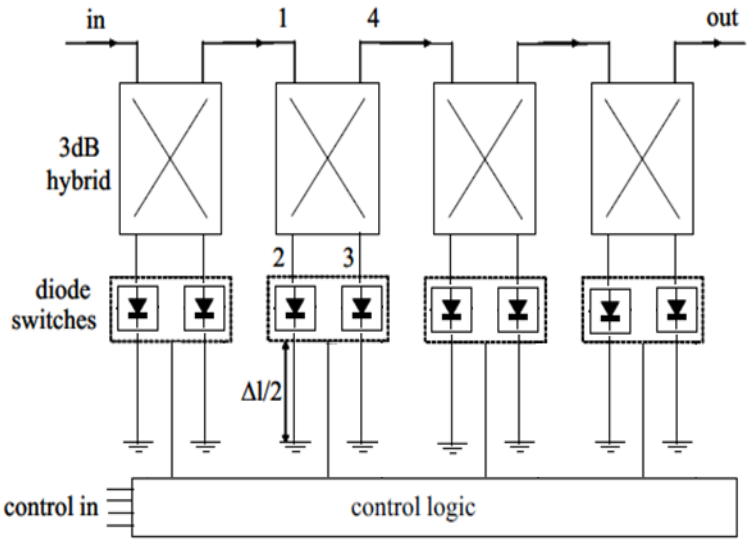

Figure 3.11: A cascaded 4-bit digitally switched phase shifter [126].

Another way of switching physical line lengths is found in the cascaded hybrid-coupled phase shifter. A 3dB hybrid divides the power at input port 1, equally over ports 2 and 3 and passes no power to port 4, see Figure 3.11. The reflected signals from ports 2 and 3 return into the hybrid and combine at output port 4, with no power returned to port 1. The diode switches in every segment (bit) of the cascaded hybrid-coupled phase shifter either reflect the signals at ports 2 and 3 directly, or after having travelled the extra line length Δl twice.

3.2.3 Phase Shifting by Changing Frequency

Phase shifting by changing frequency is accomplished by series feeding the array antenna elements, having the elements equidistantly positioned along the line and changing the frequency of input signal, see Figure 3.12.

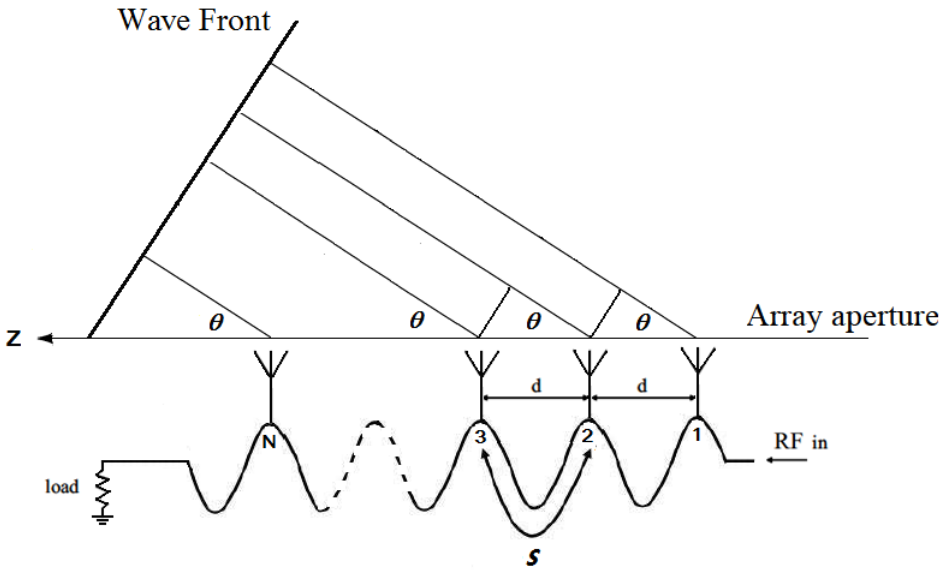

Figure 3.12: A frequency scanning array.

We have seen that changing the physical length makes the phase change. Another way of achieve this phase change is taking the electrical length into account. Similarly as in Section 3.1.3, we can get the array factor of the frequency scanning array in Figure 3.12, as

$$AF = \sum_{n=1}^{N} e^{j(n-1)\psi}, \tag{3-18}$$

where $\psi = \frac{2\pi}{\lambda} d\cos\theta - \frac{2\pi}{\lambda_g} s$,

λ is the wavelength in free space,

d is the distance between radiating elements,

λ_g is the waveguide wavelength in the feed line,

s is the length of feed line between elements.

The maximum value of (3-18) occurs when

$$\sin\left(\frac{1}{2}\psi\right)=0\Rightarrow\frac{1}{2}\psi\Big|_{\theta=\theta_m}=\pm m\pi \qquad m=0,1,2... \tag{3-19}$$

Since $s>d$, $\lambda_g<\lambda$, $\left|\cos\theta_m\right|\le 1$, ψ is always negative. Thus,

$$\frac{2\pi}{\lambda}d\cos\theta_m-\frac{2\pi}{\lambda_g}s=-2m\pi \qquad m=1,2,3,... \tag{3-20}$$

Or
$$\theta_m=\cos^{-1}\left(\frac{\lambda}{d}\left(\frac{s}{\lambda_g}-m\right)\right)\ m=1,2,3,... \tag{3-21}$$

For a maximum to exist, the argument of the arccosine cannot exceed unity. That is,

$$\left|\frac{\lambda}{d}\left(\frac{s}{\lambda_g}-m\right)\right|\le 1\Rightarrow\frac{s}{\lambda_g}-\frac{d}{\lambda}\le m\le\frac{s}{\lambda_g}+\frac{d}{\lambda}. \tag{3-22}$$

To avoid any grating lobes the maximum spacing between the elements should be less than $d_{\max}<\lambda/2$, because when $d<\lambda/2$ there is no more than 1 integer in $\left[\frac{s}{\lambda_g}-\frac{d}{\lambda},\frac{s}{\lambda_g}+\frac{d}{\lambda}\right]$.

In frequency scanned arrays the path lengths of feed lines to the radiators are not equal. The increasing line lengths along the array introduce a linearly progressive phase shift, and the frequency-sensitive properties of the transmission line result in a scan with frequency.

For example, the array factor of an 8-element frequency scanning array with d = 40 *mm*, s = 80 *mm* and $\sqrt{\varepsilon_{re}} = 2.5$ is computed using (3-18) when f is 2.5 GHz, 2.7GHz, 3 GHz, 3.3 GHz, 3.5 GHz, 3.7 GHz and 3.75 GHz and shown in Figures 3.13-3.19 respectively. One can see that the main beam scans from 180° to 0° with the frequency increases from 2.5 GHz to 3.75 GHz.

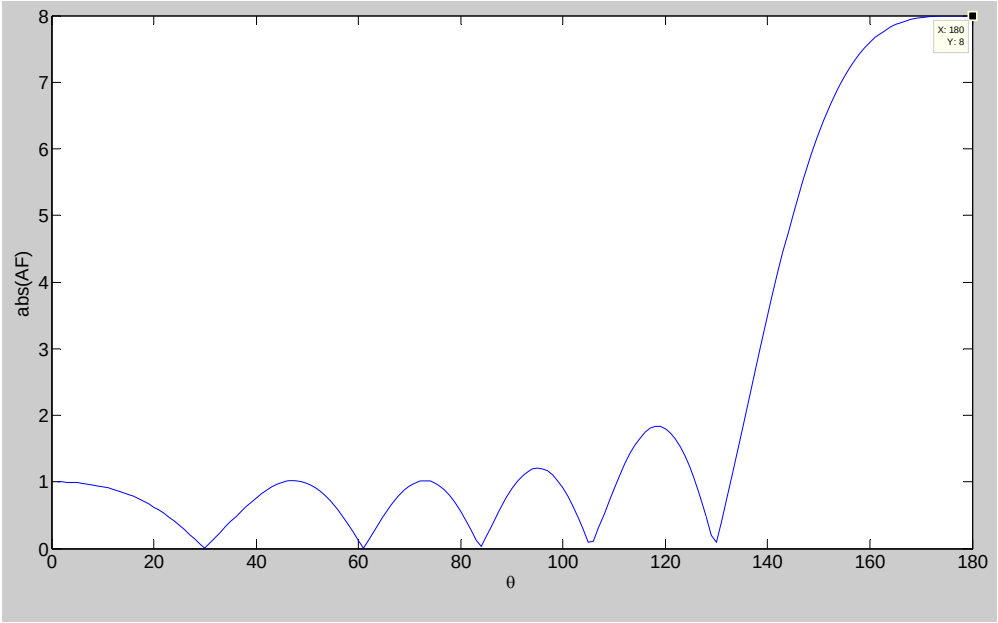

Figure 3.13: The array factor of an 8-element frequency scanning array at 2.5 GHz.

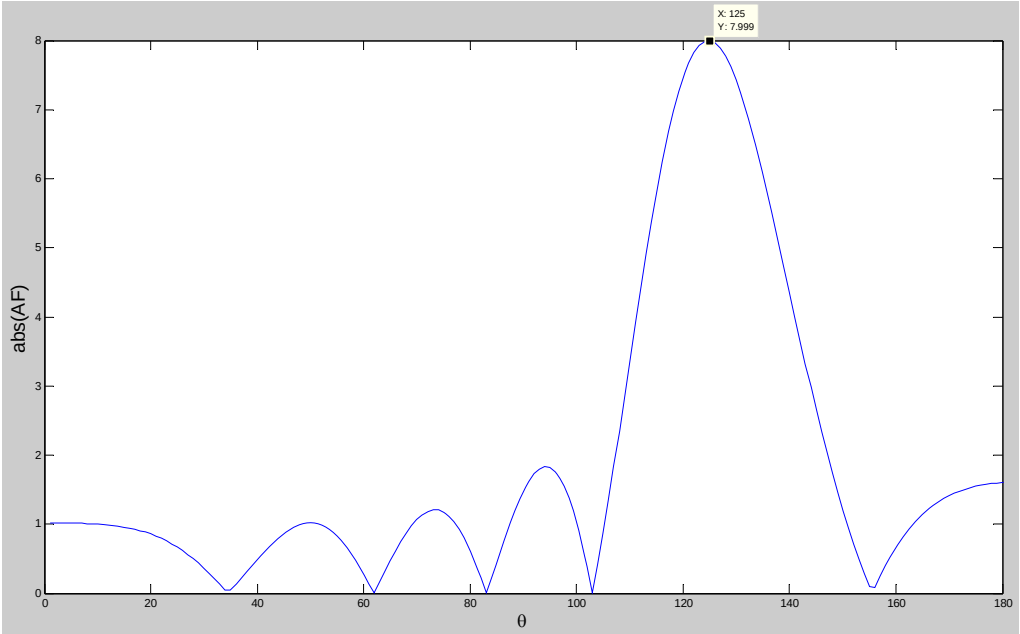

Figure 3.14: The array factor of an 8-element frequency scanning array at 2.7 GHz.

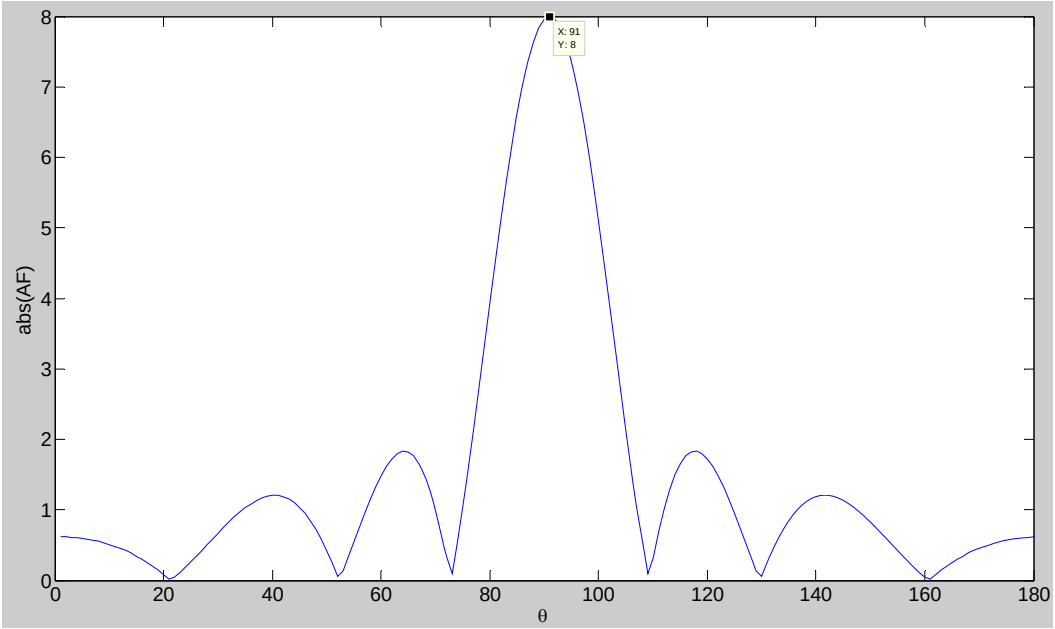

Figure 3.15: The array factor of an 8-element frequency scanning array at 3 GHz.

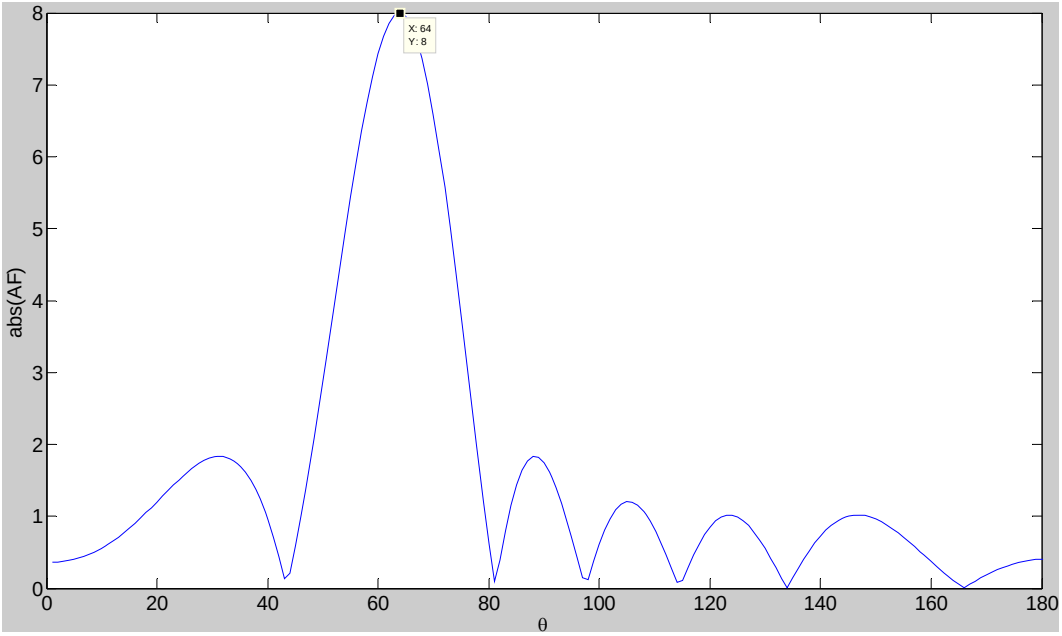

Figure 3.16: The array factor of an 8-element frequency scanning array at 3.3 GHz.

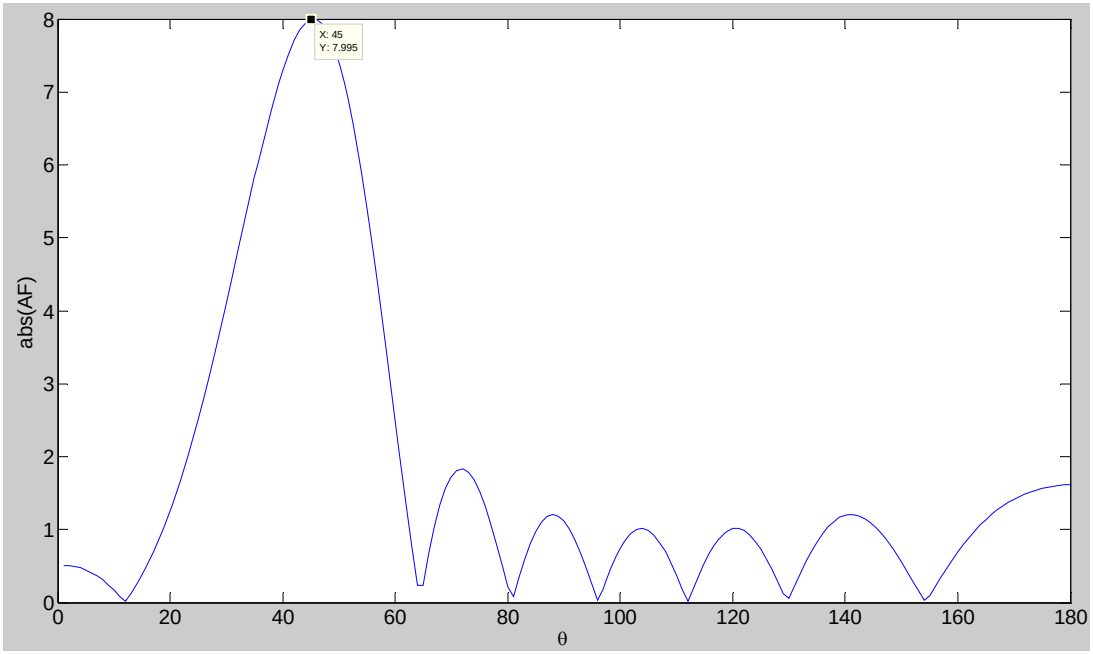

Figure 3.17: The array factor of an 8-element frequency scanning array at 3.5 GHz.

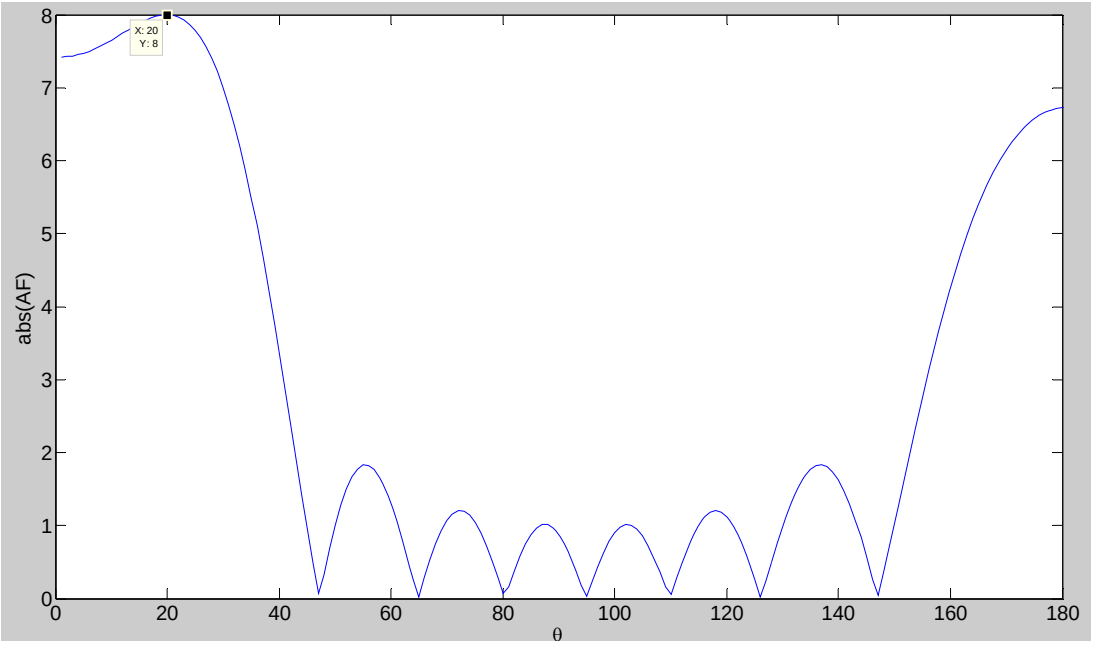

Figure 3.18: The array factor of an 8-element frequency scanning array at 3.7 GHz.

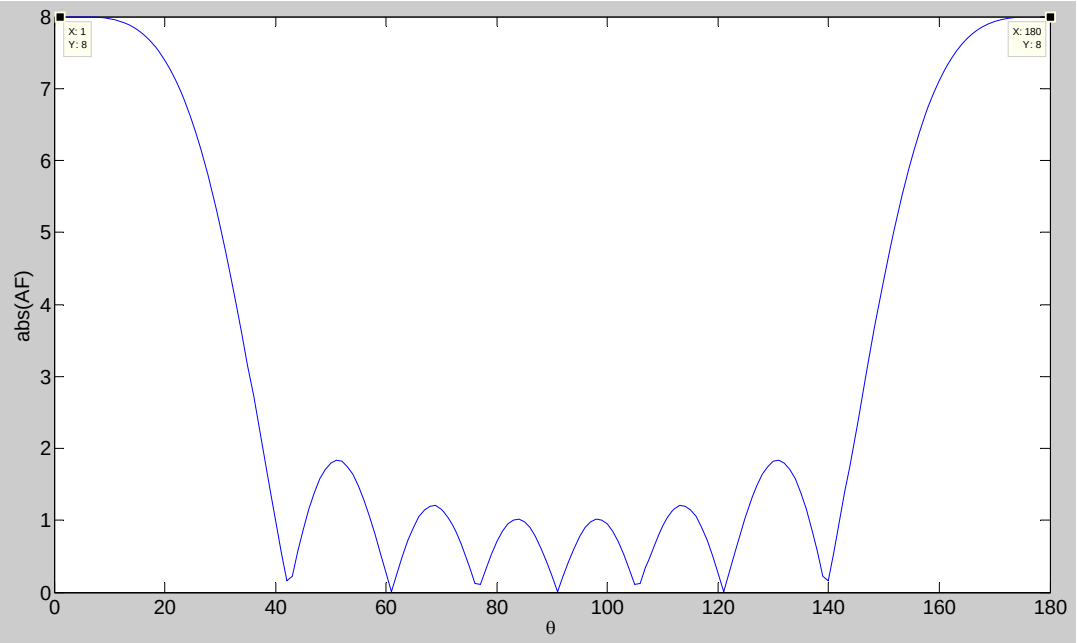

Figure 3.19: The array factor of an 8-element frequency scanning array at 3.75 GHz.

This chapter discussed conventional array theory, including beam steering and frequency scanned arrays. A key characteristic of the frequency scanned array is that the same signal is applied to all radiating elements, and frequency is varied over time to effect beam steering. The next Chapter will discuss the new development of an FDA. The FDA is fundamentally different from the frequency scanned array in that it applies different signals of various frequencies simultaneously to each spatial channel. It will be shown that this provides additional degrees of freedom for the control of antenna patterns.

Chapter 4

Theory of FDA

4.1 Concept

This Chapter discusses the theory of FDAs. An FDA provides additional degrees of freedom for the design of array antennas which leads to novel beam formation techniques and control methods.

In a conventional phased scanning array, the frequency of signal input to each radiator in an array is identical as shown in Figure 4.1, with a phase shift applied for beam steering and possible amplitude weighting for side lobe control. While in an FDA, a unique CW signal is radiated from each array element and a frequency increment Δf is applied between neighboring elements, see Figure 4.2. This frequency shift results in a beam pattern for which the beam direction changes as a function of range, angle, and time. This is significantly different from the conventional phased array, where the beam pointing direction is independent of range and time in the far-field.

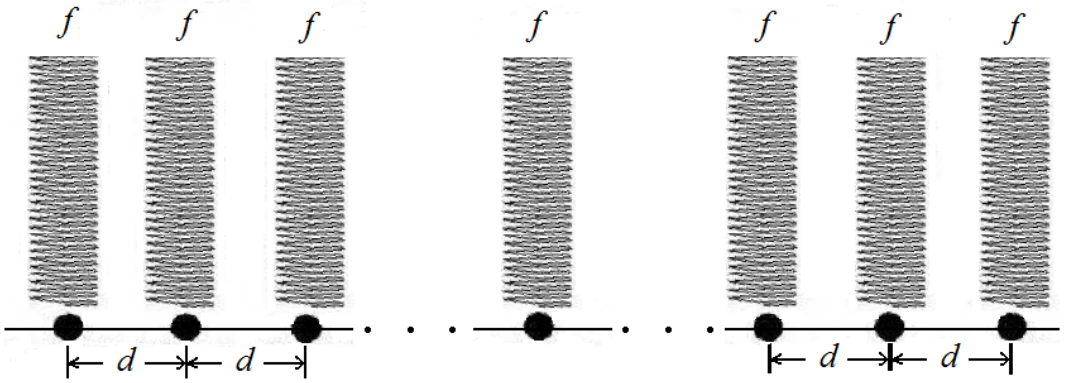

Figure 4.1: Signals of same frequency transmitted by phased scanning array.

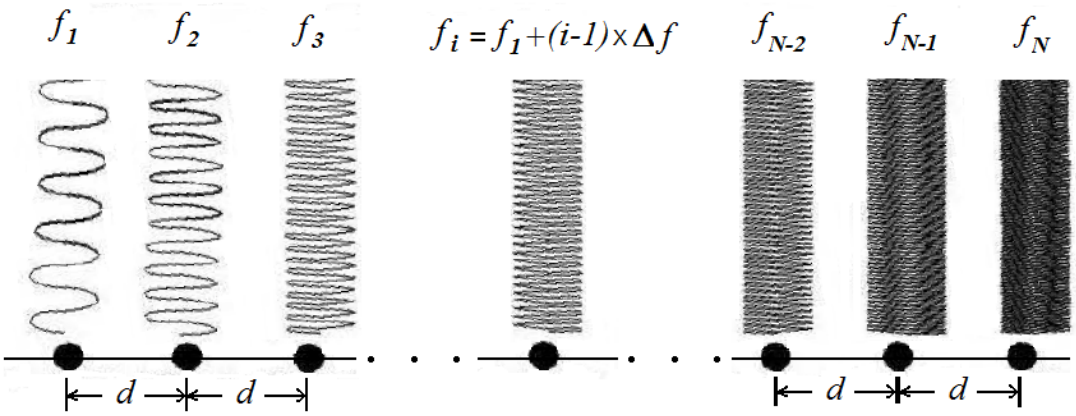

Figure 4.2: A linear frequency shift Δf is applied across the elements in FDA.

4.2 Array Factor of FDA

To derive the array factor of FDA, we start by identifying the phase of a signal. In all our calculations so far we have assumed the signals to be time harmonic, which means that a physical realizable signal $s(\omega)$ varies according to the real part of the complex signal $e^{j\omega t}$,

$$s(\omega) \square e^{j\omega t}, \tag{4-1}$$

where $\omega = 2\pi f$, f being the frequency of the signal. The argument of the cosine is known as the phase

$$\psi = 2\pi ft. \tag{4-2}$$

Consider a linear FDA composed of N elements (infinitesimal electric dipole in Section 3.1.2) along **Z** axis, as shown in Figure 4.3.

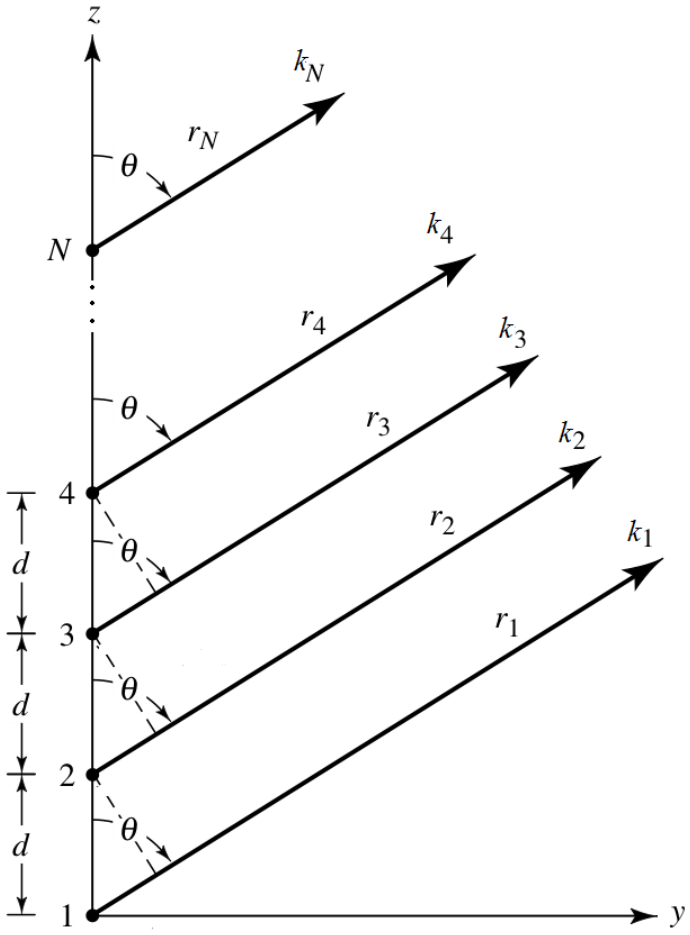

Figure 4.3: An *N*-element linear FDA

As seen in Section 3.1.3, the radiated E-fields of an infinitesimal dipole $I\left(z'\right)=\hat{a}_z I_0 e^{j2\pi ft}$ in the far-field region where $r \gg \lambda$ can be written as

$$E_\theta \approx j\eta I_0 l \sin\theta \frac{k e^{j2\pi ft} e^{-jkr}}{4\pi r},$$

$$E_r \approx E_\phi = 0, \tag{4-3}$$

where $k=\frac{2\pi f}{c}$ and c is the velocity of signal (light) in free space.

As in a conventional phase scanning array all signals radiated from each element have the same frequency, and at any time *t* the $e^{j2\pi ft}$ term has the same value for all elements thus it is neglected. However, this is not the case for FDA as *f* is different for each element.

The total field radiated by *N* elements, assuming no coupling between the elements, is equal to the sum of the individual field and in the y-z plane it is given by

$$\begin{aligned}\overrightarrow{E_t} &= \overrightarrow{E_1} + \overrightarrow{E_2} + \cdots + \overrightarrow{E_N} \\ &= \hat{a}_\theta \; j\eta \frac{I_0 l}{4\pi} \sin\theta \left\{ \frac{k_1 e^{j2\pi f_1 t} e^{-jk_1 r_1}}{r_1} + \frac{k_2 e^{j2\pi f_2 t} e^{-jk_2 r_2}}{r_2} + \cdots + \frac{k_N e^{j2\pi f_N t} e^{-jk_N r_N}}{r_N} \right\}. \end{aligned} \quad (4\text{-}4)$$

From $k = \frac{2\pi f}{c}$ and $f_i = f_1 + (i-1)\Delta f$, we have

$$k_i = k_1 + (i-1)\Delta k , \quad (4\text{-}5)$$

where $\Delta k = \frac{2\pi \Delta f}{c}$.

To simplify (4-4), we introduce an assumption of FDA:

$$\Delta f \; \square \; f_i . \quad (4\text{-}6)$$

(4-6) indicates that the frequency increment Δf is much smaller when compared to f_1 . In this thesis, Δf is less than $\frac{1}{1000} \times f_1$ to comply with (4-6).

Given $\Delta f \ll f_1$ ($\Delta k \ll k_1$), assuming far-field observations and referring to Figure 4.3, we have

$$\left.\begin{aligned} r_1 &\approx r_2 \approx r_3 \approx \cdots \approx r_N \\ k_1 &\approx k_2 \approx k_3 \approx \cdots \approx k_N \end{aligned}\right\} \text{ for amplitude variations} \qquad (4\text{-}6)$$

$$\left.\begin{aligned} r_1 &= r \\ r_2 &\approx r - d\cos\theta \\ r_3 &\approx r - 2d\cos\theta \\ &\vdots \\ r_N &\approx r - (N-1)d\cos\theta \end{aligned}\right\} \text{ for phase variations} \qquad (4\text{-}7)$$

Then, (4-4) reduces to

$$\begin{aligned} \overrightarrow{E_t} &= \hat{a}_\theta \, j\eta \frac{kI_0 l}{4\pi r}\sin\theta \left\{ e^{j2\pi f_1 t} e^{-jk_1 r_1} + e^{j2\pi f_2 t} e^{-jk_2 r_2} + \cdots + e^{j2\pi f_N t} e^{-jk_N r_N} \right\} \qquad (4\text{-}8) \\ &= \hat{a}_\theta \, j\eta \frac{kI_0 l}{4\pi r}\sin\theta e^{j2\pi f_1 t} e^{-jk_1 r_1} \left\{ 1 + e^{j2\pi\Delta f t} e^{j(k_1 r_1 - k_2 r_2)} + \cdots + e^{(N-1)*j2\pi\Delta f t} e^{j(k_1 r_1 - k_N r_N)} \right\}. \end{aligned}$$

If we take a look at $(k_1 r_1 - k_i r_i)$, we can find

$$\begin{aligned} k_1 r_1 - k_i r_i &= k_1 r_1 - \left[k_1 + (i-1)\Delta k \right]\left[r_1 - (i-1)d\cos\theta \right] \\ &= (i-1)k_1 d\cos\theta - (i-1)\Delta k r_1 + (i-1)^2 \Delta k d\cos\theta \end{aligned}. \qquad (4\text{-}9)$$

Under the assumption of $\left.\begin{aligned} \Delta k &\ll k_1 \\ d &\ll r_1 \end{aligned}\right\} \Rightarrow \left\{\begin{aligned} \Delta k d\cos\theta &\ll k_1 d\cos\theta \\ \Delta k d\cos\theta &\ll \Delta k r_1 \end{aligned}\right.$,

$(i-1)^2 \Delta k d\cos\theta$ is discarded and thus we have

$$k_1 r_1 - k_i r_i \approx (i-1)k_1 d\cos\theta - (i-1)\Delta k r_1. \qquad (4\text{-}10)$$

Plugging this back into (4-8) reduces to

$$\overrightarrow{E_t} = \hat{a}_\theta \, e^{j\left(2\pi f_1 t - k_1 r_1\right)} j\eta \frac{kI_0 l}{4\pi r} \sin\theta \sum_{n=1}^{N} e^{j\left(n-1\right)\left(2\pi\Delta f t + k_1 d\cos\theta - \Delta k r_1\right)} . \quad (4\text{-}11)$$

It is apparent from (4-11) that the total field of FDA is equal to the field of a single element positioned at the origin ($\hat{a}_\theta \, j\eta \frac{kI_0 l}{4\pi r}\sin\theta$) multiplied by its array factor $\sum_{n=1}^{N} e^{j\left(n-1\right)\left(2\pi\Delta f t + k_1 d\cos\theta - \Delta k r_1\right)}$. For the *N*-element FDA of constant amplitude, the array factor is given by

$$AF = \sum_{n=1}^{N} e^{j(n-1)\psi} ,$$

where $$\psi = 2\pi\cos\theta\times\rho + 2\pi\times\left(\frac{t}{1/\Delta f}\right) - 2\pi\times\left(\frac{r}{c/\Delta f}\right), \quad \rho = \frac{d}{\lambda}. \quad (4\text{-}12)$$

One may recall, the array factor of a conventional phase scanning array is

$$AF = \sum_{n=1}^{N} e^{j(n-1)\psi} ,$$

where $$\psi = 2\pi\cos\theta\times\rho + \beta , \quad \rho = \frac{d}{\lambda}.$$

Given ρ, the array factor of a convention phase scanning array is just a function of θ and phase excitation β. And the array factor of a conventional phased array does not change with *t* or *r* as *t* and *r* are not included in the array factor at all. However, for an FDA with given Δf and ρ, its array factor is a function of θ, *r* and *t*. Thus FDA provides additional design freedoms for the beam forming and control, while without using phase shifters.

4.3 Discussions on FDA's Array Factor

So far it has been shown that for a specific CW FDA with physical parameters of Δf and ρ and, its array factor *AF* is a function of θ, r and *t*. That is,

$$AF_{\Delta f,\rho} = AF_{\Delta f,\rho}(\theta, t, r). \tag{4-13}$$

To better explain the behavior of $AF(\theta, t, r)$, which is dependent on three parameters, we will examine $AF(\theta, r)|t = t_0$ and $AF(\theta, t)|r = r_0$ by holding one parameter "*t*" (or "*r*") as constant while examining how the radiation pattern varies with the other variable "*r*" (or "*t*"). Before carrying on further discussions, the value range of "*r*" and "*t*" should be specified.

4.3.1 Values Range of "*t*" and "*r*"

Generally, *t* should be between 0 and infinity for CW signals, that is $t \in [0, +\infty)$. At the time $t = 0$, all elements start to transmit signals simultaneously and there was no signal before that. In addition, although the signal transmitted by each element has a different frequency, all the signals have a phase of 0° at $t = 0$.

The constraint between *r* and *t* is

$$r \le t \times c, \tag{4-14}$$

or

$$t \ge \frac{r}{c}. \tag{4-15}$$

Basically, within the time of t the maximum distance the signal could reach is $t \times c$, beyond that range there is no signal. Equivalently, it is not until the time of $\frac{r}{c}$ that a signal can reach the distance of r.

Thus we re-define the array factor of FDA as follows.

$$AF_{\Delta f,\rho} = AF\left(\theta,t,r\right)_{\Delta f,\rho} \begin{cases} 0 & when \quad r > t \times c \quad (t < r/c) \\ \sum_{n=1}^{N} e^{j(n-1)\psi} & when \quad r \le t \times c \quad \left(t \ge r/c\right) \end{cases} \tag{4-16}$$

where $\psi = 2\pi \cos\theta \times \rho + 2\pi \times \left(\frac{t}{1/\Delta f}\right) - 2\pi \times \left(\frac{r}{c/\Delta f}\right)$.

Correspondently, $AF\left(\theta,t\right)\big|r = r_0$ has a non-zero value after the time of r_0/c; while $AF\left(\theta,r\right)\big|t = t_0$ has a non-zero value within the range of $t_0 \times c$.

4.3.2 Periodicity of $AF_{\Delta f,\rho}\left(\theta,t,r\right)$

From (4-16) one can directly see that for a specific CW FDA with physical parameters of Δf and ρ, its array factor $AF_{\Delta f,\rho}\left(\theta,t,r\right)$ is periodic with t and r. And we will examine the periodicity of $AF\left(\theta,t\right)_{\Delta f,\rho}\big|r = r_0$ and $AF\left(\theta,r\right)_{\Delta f,\rho}\big|t = t_0$ respectively.

4.3.2.1 Periodicity of $AF(\theta,t)_{\Delta f,\rho}|r=r_0$

When $r=r_0$, the array factor (4-16) becomes

$$AF(\theta,t)_{\Delta f,\rho}|r=r_0 \triangleq \begin{cases} 0 & when\ t<r_0/c, \\ \sum_{n=1}^{N} e^{j(n-1)\psi} & when\ t\geq r_0/c, \end{cases} \tag{4-17}$$

where $\psi = 2\pi\cos\theta\times\rho + 2\pi\times\left(\frac{t}{1/\Delta f}\right) - 2\pi\times\left(\frac{r_0}{c/\Delta f}\right)$.

We conclude that $AF(\theta,t)_{\Delta f,\rho}|r=r_0 \ \left(t\geq r_0/c\right)$ is periodic in t with a time period of $1/\Delta f$ because

$$\begin{aligned} AF_{\Delta f,\rho}\left(\theta,t+\frac{1}{\Delta f}\right)|r=r_0 &\triangleq \sum_{n=1}^{N} e^{j(n-1)\left(2\pi\times\frac{t+1/\Delta f}{1/\Delta f}+\frac{2\pi f}{c}d\cos\theta-2\pi\times\frac{r_0}{c/\Delta f}\right)} \\ &= \sum_{n=1}^{N} e^{j(n-1)\left(2\pi+2\pi\times\frac{t}{1/\Delta f}+\frac{2\pi f}{c}d\cos\theta-2\pi\times\frac{r_0}{c/\Delta f}\right)} \\ &= \sum_{n=1}^{N} e^{j(n-1)\times 2\pi} e^{j(n-1)\left(2\pi\times\frac{t}{1/\Delta f}+\frac{2\pi f}{c}d\cos\theta-2\pi\times\frac{r_0}{c/\Delta f}\right)} \\ &= \sum_{n=1}^{N} e^{j(n-1)\left(2\pi\times\frac{t}{1/\Delta f}+\frac{2\pi f}{c}d\cos\theta-2\pi\times\frac{r_0}{c/\Delta f}\right)} \\ &= AF_{\Delta f,\rho}(\theta,t)|r=r_0 \ \left(t\geq r_0/c\right). \end{aligned}$$

As an example, the array factor $AF(\theta,t)_{\Delta f,\rho}|r=r_0$ of an 8-element FDA with $N=8,\ \Delta f=1kHz,\ \rho=0.45$ is depicted in Figure 4.4 . The range is fixed at $r_0 = 1\times c/\Delta f = 3\times10^5\,\mathrm{m}$.

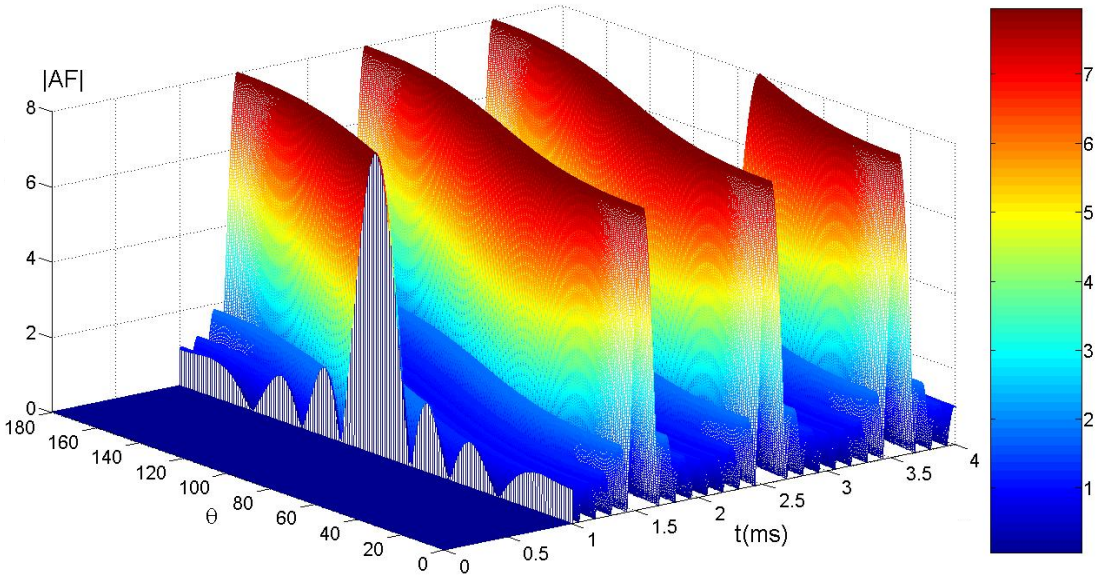

(a) 3d view

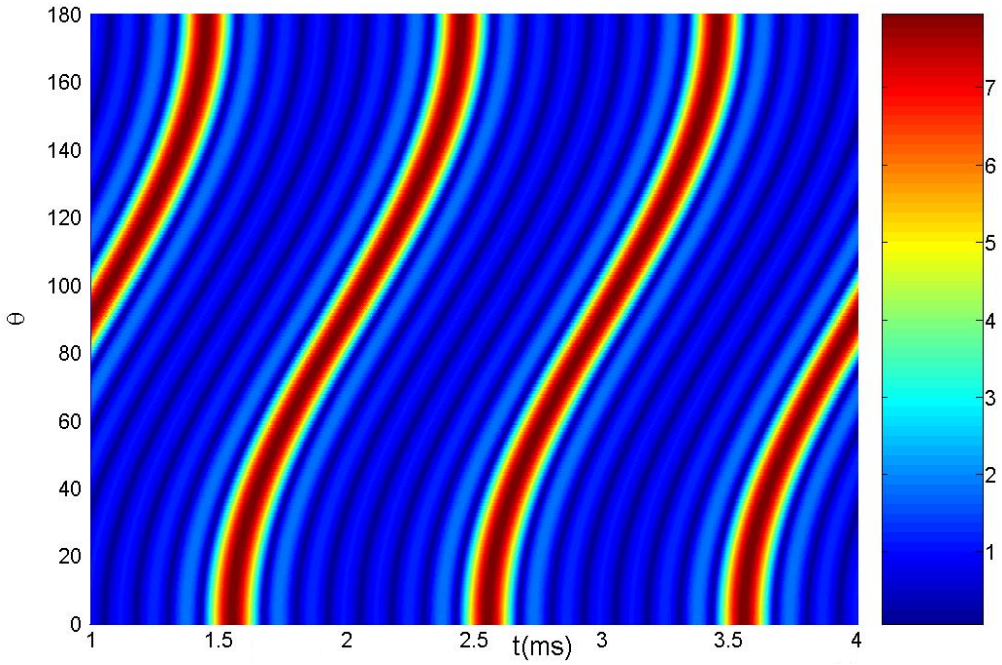

(b) top view

Figure 4.4: Array factor of an FDA at $r_0 = 3\times10^5\,\mathrm{m}$.

We can see the beam at $r_0 = 3\times10^5\,\mathrm{m}$ starts scanning from the time of $\frac{r_0}{c} = 1\,\mathrm{ms}$ and the angle of $\theta = 90^\circ$ and it is directly shown in Figure 4.5 that beam periodically scans from 0° to 180° in every time length of $\frac{1}{\Delta f} = 1\,\mathrm{ms}$.

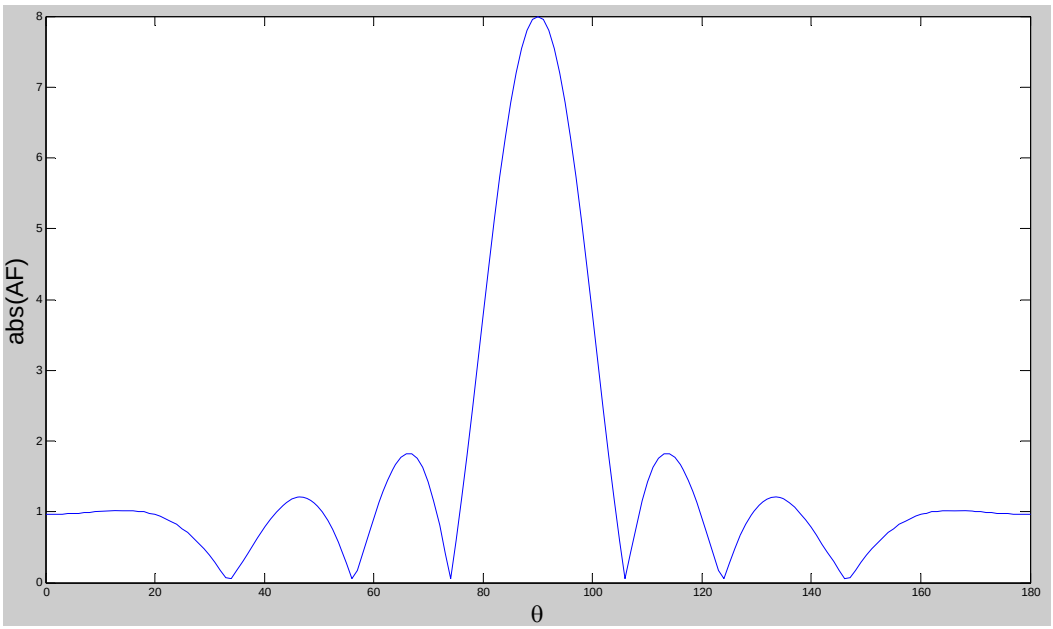

(a) Array factor at $r_0 = 3\times10^5$ m, $t = 1$ ms

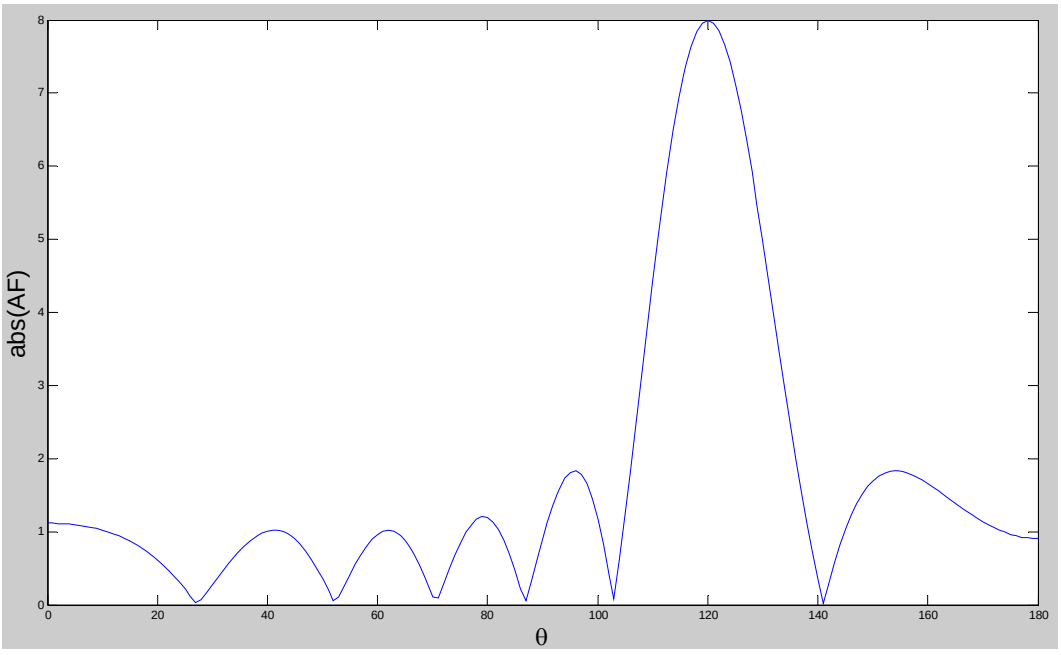

(b) Array factor at $r_0 = 3\times10^5$ m, $t = 1.225$ ms

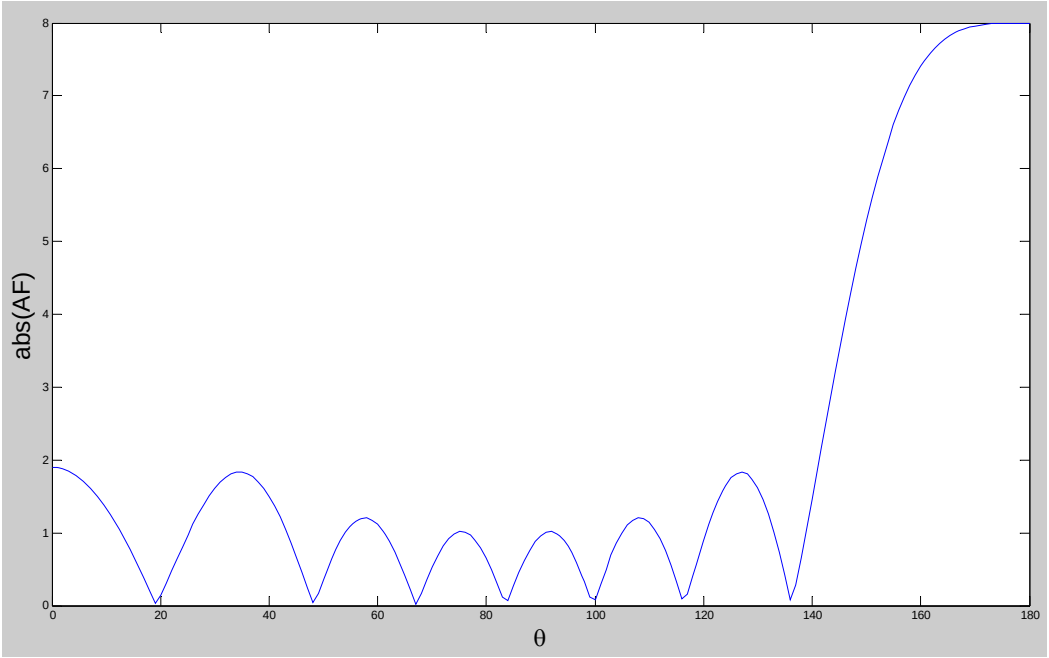

(c) Array factor at $r_0 = 3\times10^5$ m, $t = 1.45$ ms

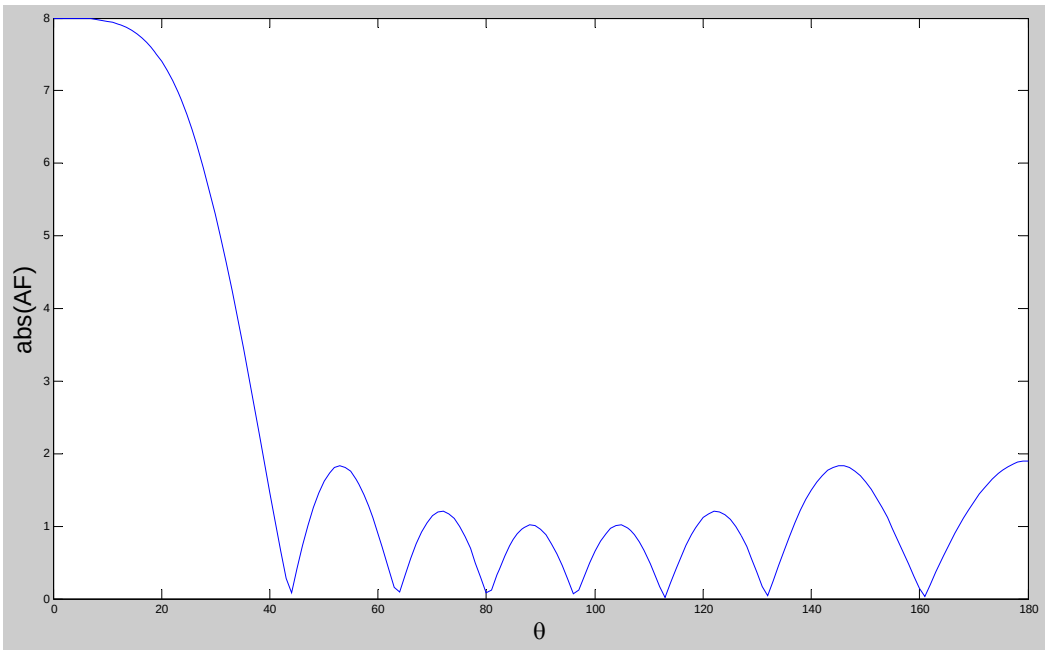

(d) Array factor at $r_0 = 3\times10^5$ m, $t = 1.55$ ms

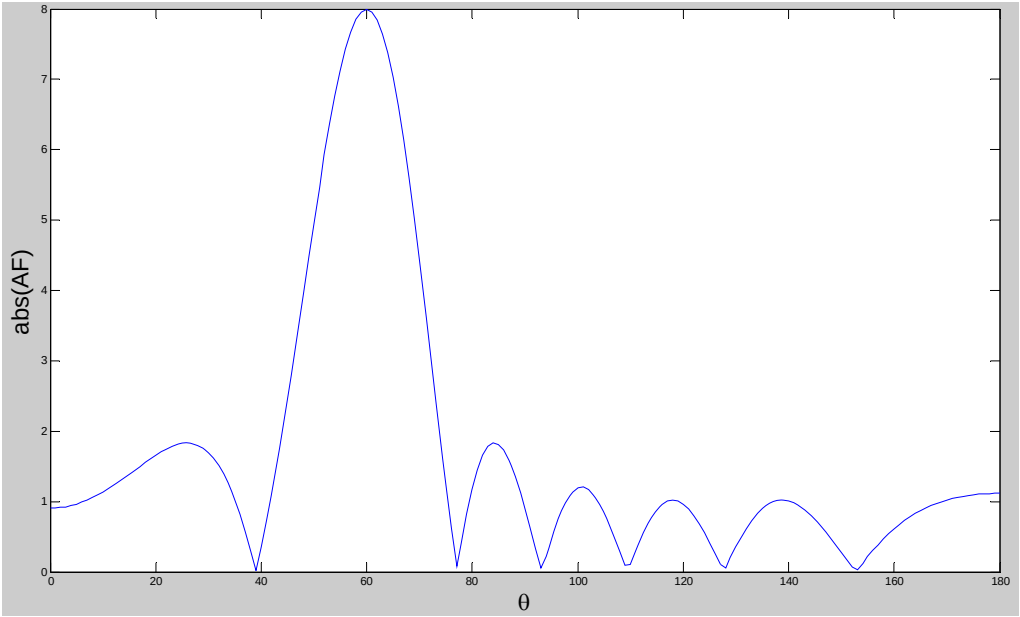

(e) Array factor at $r_0 = 3\times10^5$ m, $t = 1.775$ ms

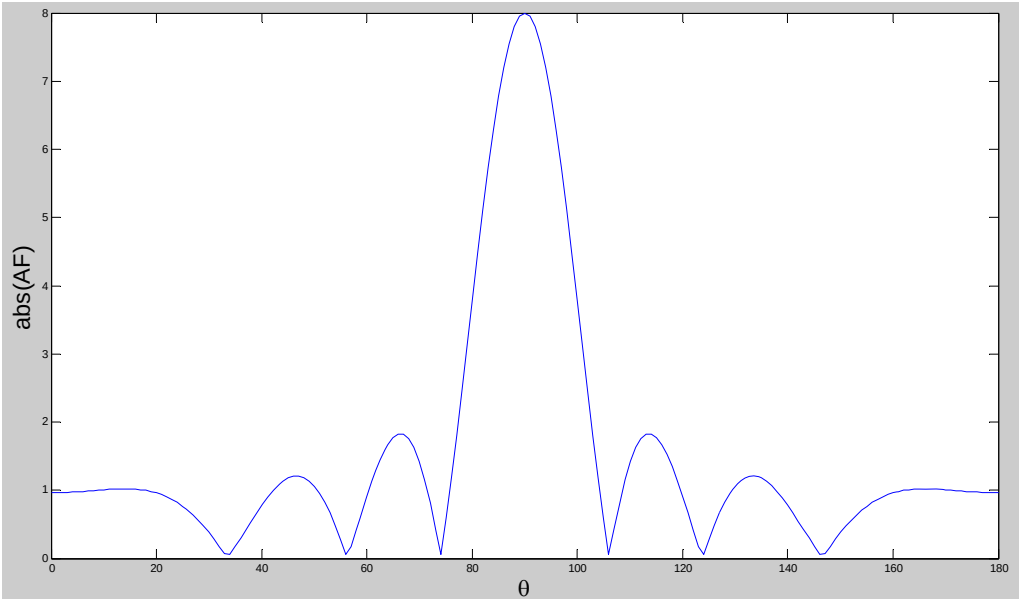

(f) Array factor at $r_0 = 3\times10^5$ m, $t = 2$ ms

Figure 4.5: Beam scanning with $\frac{1}{\Delta f}$ time period.

We can see that when t and r are both fixed, the array factor of the FDA $AF_{\Delta f,\rho}(\theta)\big|t=t_0, r=r_0$ has the same shape as that of the conventional phase scanning array.

4.3.2.2 Periodicity of $AF_{\Delta f,\rho}(\theta,r)\big|t=t_0$

When $t=t_0$, the array factor (4-16) becomes

$$AF_{\Delta f,\rho}(\theta,r)\big|t=t_0 \triangleq \begin{cases} 0 & when\ \ r > t_0 \times c, \\ \sum_{n=1}^{N} e^{j(n-1)\psi} & when\ \ r \le t_0 \times c, \end{cases} \tag{4-17}$$

where $\psi = 2\pi\cos\theta\times\rho + 2\pi\times\left(\frac{t_0}{1/\Delta f}\right) - 2\pi\times\left(\frac{r}{c/\Delta f}\right)$.

Similarly, we can prove that $AF_{\Delta f,\rho}(\theta,r)\big|t=t_0$ $\left(r \le t_0 \times c\right)$ is periodic in r with a period of $c/\Delta f$.

$$\begin{aligned} AF_{\Delta f,\rho}\left(\theta, r+\frac{c}{\Delta f}\right)\Big|t=t_0 &\triangleq \sum_{n=1}^{N} e^{j(n-1)\left(2\pi\times\frac{t_0}{1/\Delta f}+\frac{2\pi f}{c}d\cos\theta-2\pi\times\frac{r+c/\Delta f}{c/\Delta f}\right)} \\ &= \sum_{n=1}^{N} e^{j(n-1)\left(2\pi\times\frac{t_0}{1/\Delta f}+\frac{2\pi f}{c}d\cos\theta-2\pi\times\frac{r}{c/\Delta f}-2\pi\right)} \\ &= \sum_{n=1}^{N} e^{-j(n-1)\times 2\pi} e^{j(n-1)\left(2\pi\times\frac{t_0}{1/\Delta f}+\frac{2\pi f}{c}d\cos\theta-2\pi\times\frac{r}{c/\Delta f}\right)} \\ &= \sum_{n=1}^{N} e^{j(n-1)\left(2\pi\times\frac{t}{1/\Delta f}+\frac{2\pi f}{c}d\cos\theta-2\pi\times\frac{r_0}{c/\Delta f}\right)} \\ &= AF_{\Delta f,\rho}(\theta,r)\big|t=t_0 \quad \left(r \le t_0 \times c\right). \end{aligned}$$

As an example, the array factor $AF_{\Delta f,\rho}(\theta, r)\big|t = t_0$ of the same 8-element FDA with $\Delta f = 1$ kHz, $\rho = 0.45$ is examined. The time is chosen at $t_0 = 3 \times 1/\Delta f$ and therefore $AF_{\Delta f,\rho}(\theta, r)\big|t = t_0$ has a non-zero value within the range of $r = t_0 \times c = 9 \times 10^5$ m.

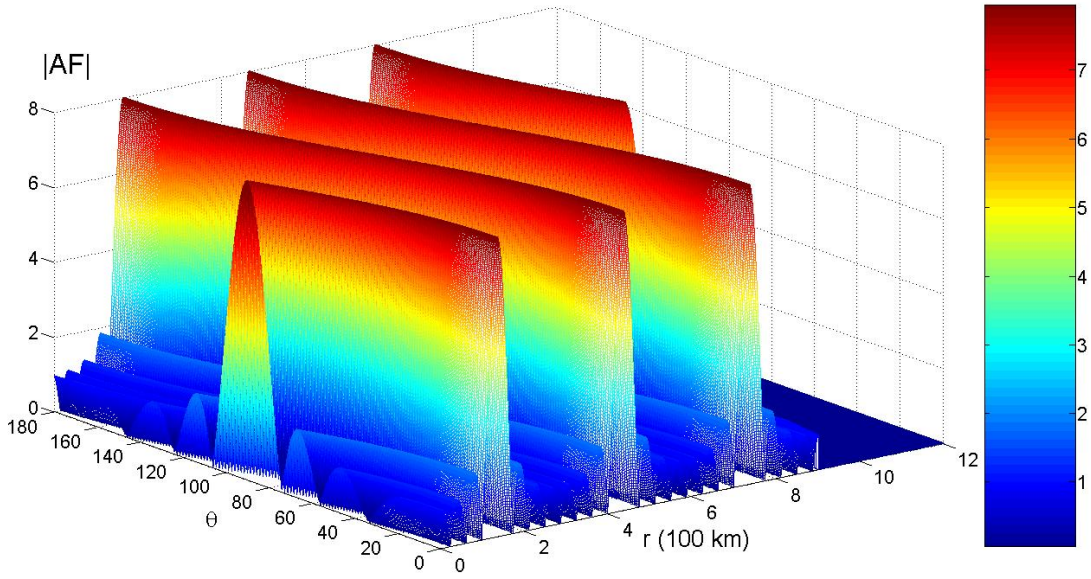

(a) 3D view

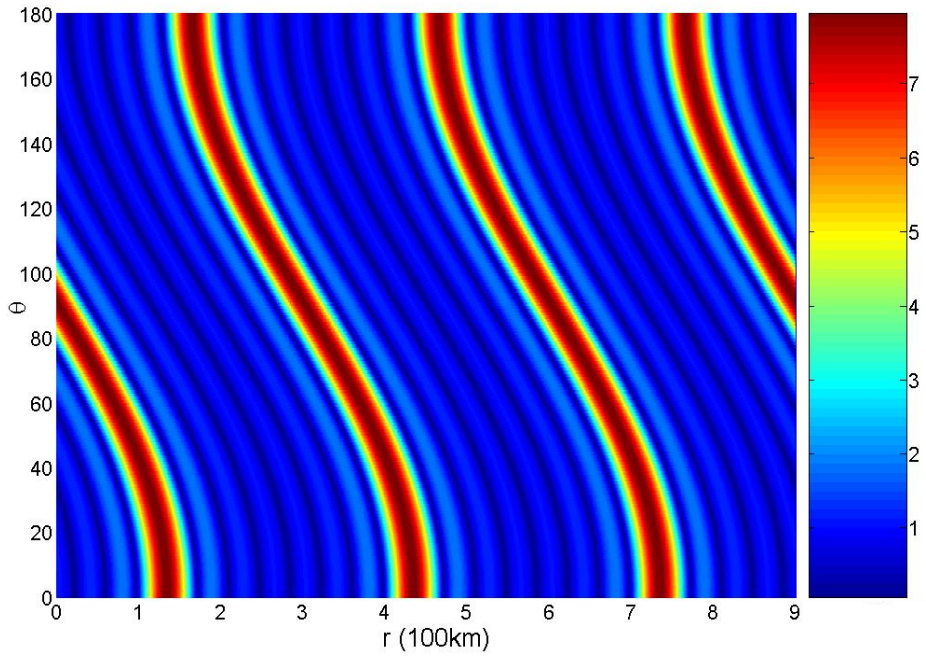

(b) Top view

Figure 4.6: Array factor of an FDA at $t_0 = 3$ ms.

We can see at $t_0 = 3$ ms, the array factor $AF_{\Delta f,\rho}(\theta, r)\big|t = t_0$ is periodic in r and it is directly shown in Figure 4.7 (from 1 to 6) that beam periodically repeats itself every $\frac{c}{\Delta f} = 3\times10^5$ m.

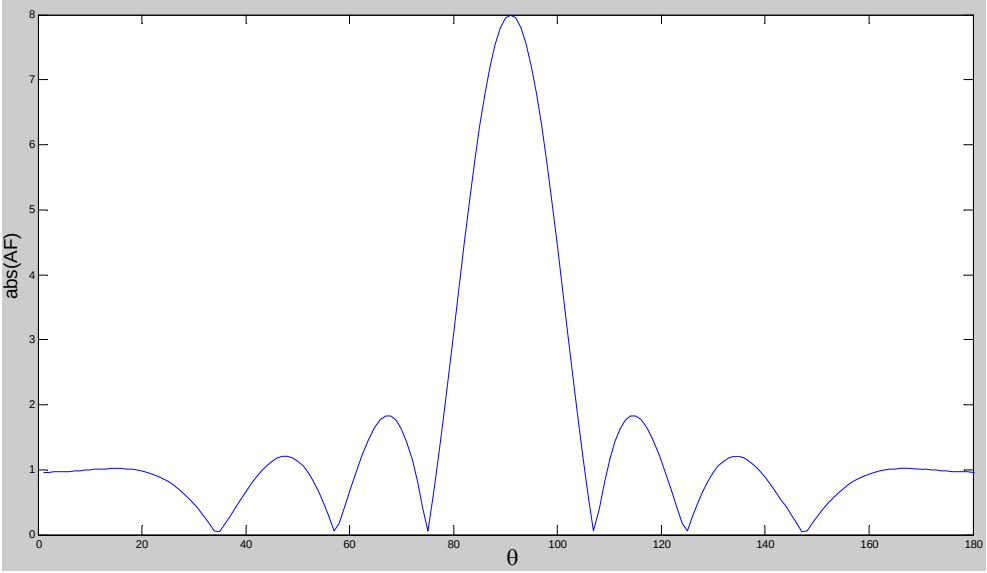

(1) Array factor at $t_0 = 3$ ms, $r = 6\times10^5$ m

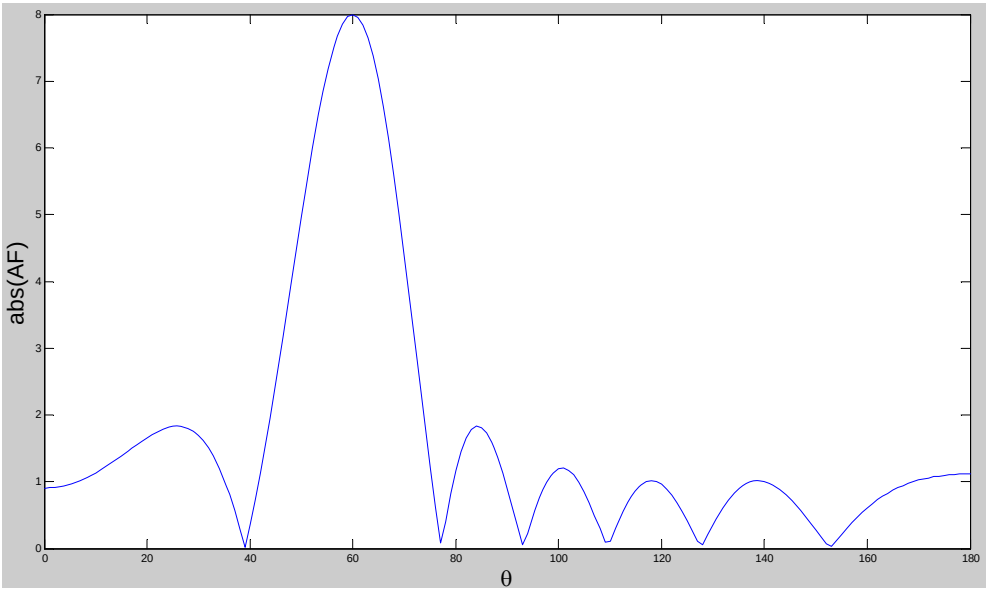

(2) Array factor at $t_0 = 3$ ms, $r = 6.675\times10^5$ m

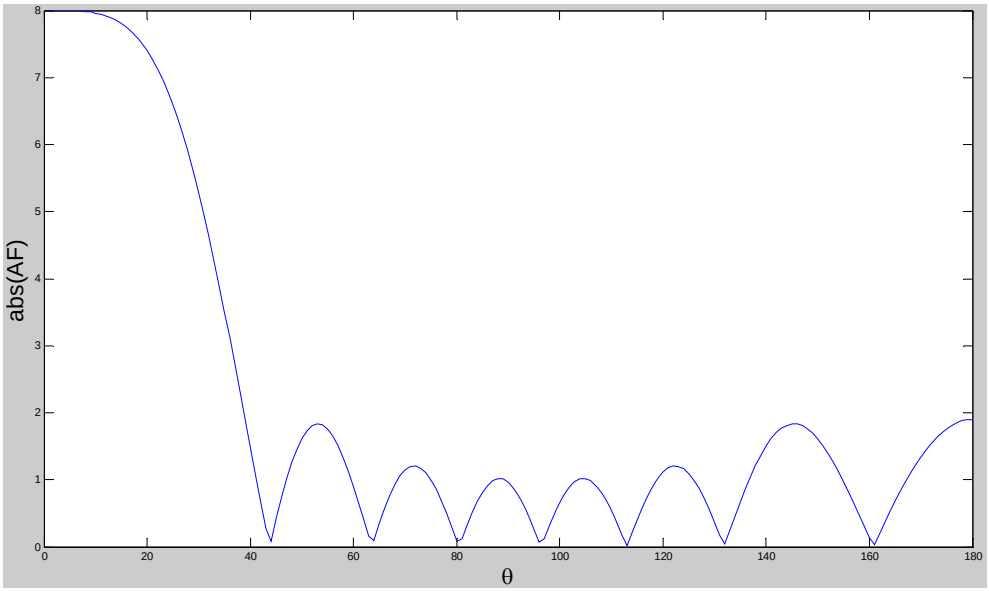

(3) Array factor at $t_0 = 3$ ms, $r = 7.35 \times 10^5$ m

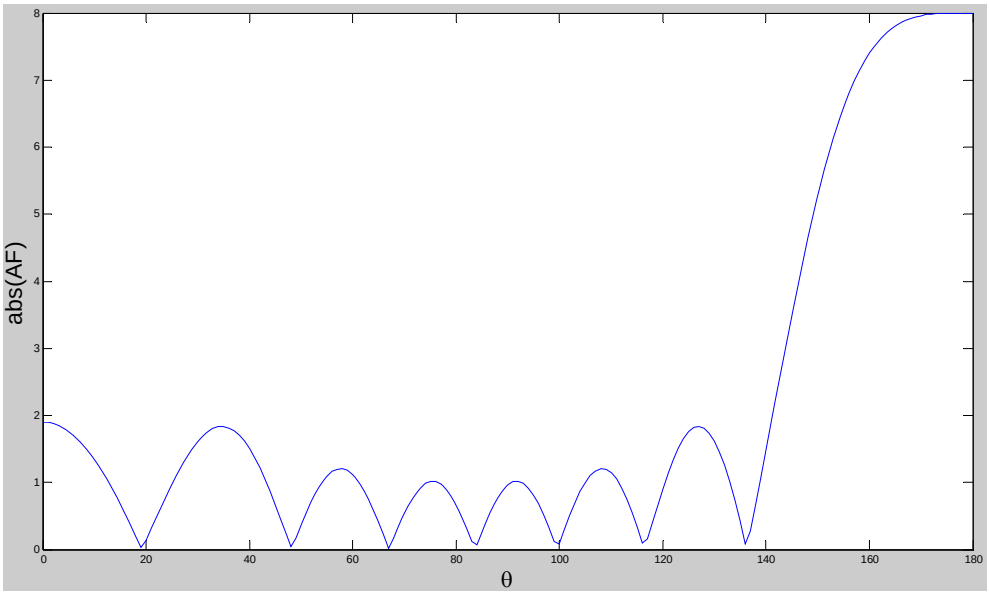

(4) Array factor at $t_0 = 3$ ms, $r = 7.65 \times 10^5$ m

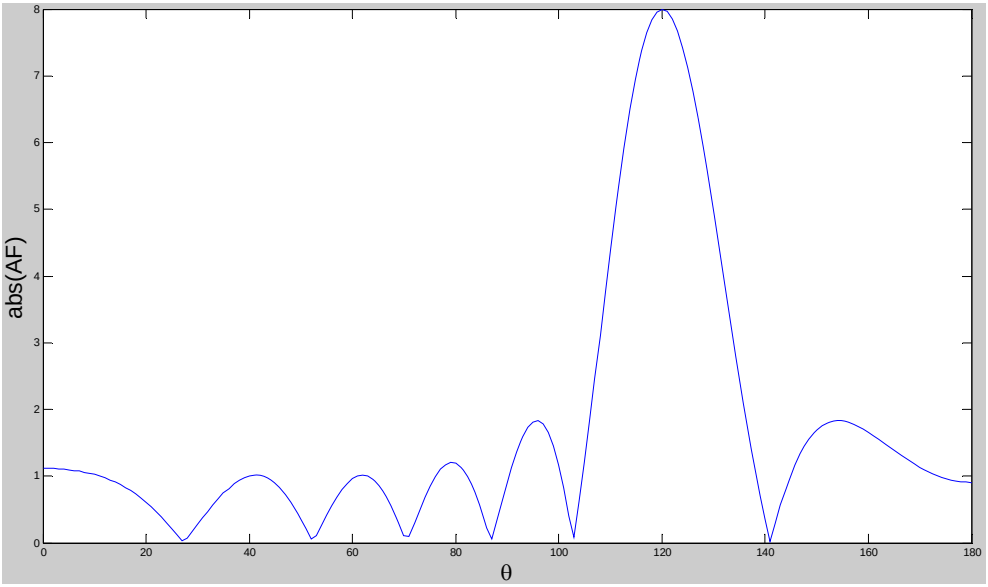

(5) Array factor at $r = 8.325 \times 10^5$ m

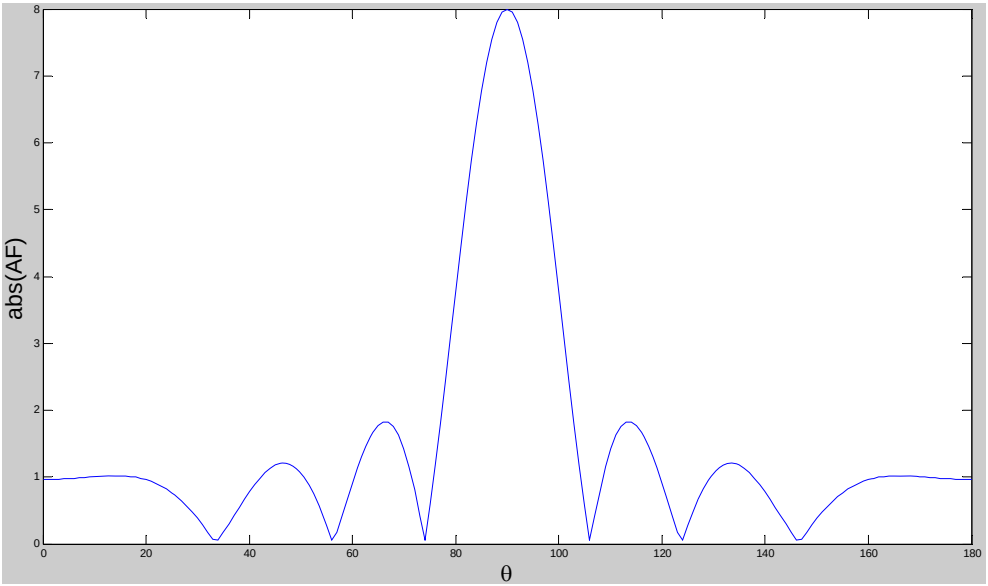

(6) Array factor at $t_0 = 3$ ms, $r = 9 \times 10^5$ m

Figure 4.7: Beam scanning in range with period of $\frac{c}{\Delta f}$.

4.3.3 More about $AF_{\Delta f,\rho}(\theta,t,r)$: Null, Maximum, Grating lobe

The array factor of (4-16) can also be expressed in a closed form. This is accomplished by

$$\left|AF\right| = \left|\sum_{n=1}^{N} e^{j(n-1)\psi}\right| = \left|\frac{\sin\left(\frac{N}{2}\psi\right)}{\sin\left(\frac{1}{2}\psi\right)}\right|, \tag{4-18}$$

where $\psi = 2\pi\cos\theta\times\rho + 2\pi\times\left(\frac{t}{1/\Delta f}\right) - 2\pi\times\left(\frac{r}{c/\Delta f}\right)$ $\left(t \geq r/c\right)$.

4.3.3.1 Nulls of $AF_{\Delta f,\rho}(\theta,t,r)$

To find the nulls of the array factor (4-18) is set equal to zero. That is,

$$\begin{cases} \sin\left(\frac{N}{2}\psi\right) = 0 \\ \sin\left(\frac{1}{2}\psi\right) \neq 0 \end{cases} \Rightarrow \begin{cases} \frac{N}{2}\psi\Big|_{\theta=\theta_n} = \pm n\pi \\ \frac{1}{2}\psi\Big|_{\theta=\theta_n} \neq \pm m\pi \end{cases} \Rightarrow$$

$$\theta_n = \cos^{-1}\left\{\rho\left[\Delta f\left(\frac{r}{c} - t\right) \pm \frac{n}{N}\right]\right\} \qquad \begin{matrix} n = 1,2,3,... \\ n \neq N, 2N, 3N, ... \end{matrix} \tag{4-19}$$

Moreover, for a zero to exist the argument of the arccosine cannot exceed unity. That is,

$$\left|\rho\left[\Delta f\left(\frac{r}{c} - t\right) \pm \frac{n}{N}\right]\right| \leq 1. \tag{4-20}$$

The number of nulls and the angle positions of the nulls can be derived as follows.

a) *if* $\left(\frac{t}{1/\Delta f}-\frac{r/c}{1/\Delta f}\right)\geq \rho$

$$\Rightarrow\begin{cases}\mathrm{N}\times\left(\frac{t}{1/\Delta f}-\frac{r/c}{1/\Delta f}-\rho\right)\leq n\leq \mathrm{N}\times\left(\frac{t}{1/\Delta f}-\frac{r/c}{1/\Delta f}+\rho\right)\\ n=1,2,3,...\\ n\neq N,2N,3N,...\\ \theta_n=\cos^{-1}\left\{\frac{1}{\rho}\left[\Delta f\left(\frac{r}{c}-t\right)+\frac{n}{N}\right]\right\}\end{cases}$$

b) *if* $0\leq\left(\frac{t}{1/\Delta f}-\frac{r/c}{1/\Delta f}\right)<\rho$

$$\Rightarrow\begin{cases}1\leq n\leq \mathrm{N}\times\left(\frac{r/c}{1/\Delta f}-\frac{t}{1/\Delta f}+\rho\right)\\ n=1,2,3,...\\ n\neq N,2N,3N,...\\ \theta_n=\cos^{-1}\left\{\frac{1}{\rho}\left[\Delta f\left(\frac{r}{c}-t\right)-\frac{n}{N}\right]\right\}\end{cases}\quad \text{or}\quad \begin{cases}1\leq n\leq \mathrm{N}\times\left(\frac{t}{1/\Delta f}-\frac{r/c}{1/\Delta f}+\rho\right)\\ n=1,2,3,...\\ n\neq N,2N,3N,...\\ \theta_n=\cos^{-1}\left\{\frac{1}{\rho}\left[\Delta f\left(\frac{r}{c}-t\right)+\frac{n}{N}\right]\right\}\end{cases}$$

Thus for an *N*-element FDA with given Δf and ρ, the number of nulls that can exist as well as their angle position will be a function of time *t* and distance *r*.

As an example, the nulls of array factor of an FDA with $N=8,\ \Delta f=1\ \text{kHz},\ \rho=0.45$ are computed following the above routine and pre-computed array factor are depicted in Figures 4.8 and 4.9 for comparison. One can see that the positions of the nulls computed using the above routine and Matlab are perfectly matched.

i) $r_0 = 3\times10^5\,\text{m},\ t = 1.775\text{ms}$

$$\because \frac{t}{1/\Delta f} - \frac{r/c}{1/\Delta f} - \rho = 0.315 > 0$$

$$\Rightarrow \begin{cases} \text{N}\times\left(\dfrac{t}{1/\Delta f} - \dfrac{r/c}{1/\Delta f} - \rho\right) \le n \le \text{N}\times\left(\dfrac{t}{1/\Delta f} - \dfrac{r/c}{1/\Delta f} + \rho\right) \\ n = 1, 2, 3, \ldots \\ n \ne N, 2N, 3N, \ldots \\ \theta_n = \cos^{-1}\left\{\dfrac{1}{\rho}\left[\Delta f\left(\dfrac{r}{c} - t\right) + \dfrac{n}{N}\right]\right\} \end{cases}$$

$$\Rightarrow \begin{cases} 2.52 \le n \le 9.8 \\ n = 1, 2, 3, \ldots \\ n \ne 8, 16, 24, \ldots \\ \theta_n = \cos^{-1}\left[\dfrac{1}{0.45}\left(\dfrac{n}{8} - 0.775\right)\right] \end{cases}$$

$$\Rightarrow \begin{cases} \theta_3 = 152.73^\circ \\ \theta_4 = 127.67^\circ \\ \theta_5 = 109.47^\circ \\ \theta_6 = 93.18^\circ \\ \theta_7 = 77.16^\circ \\ \theta_9 = 38.94^\circ \end{cases}$$

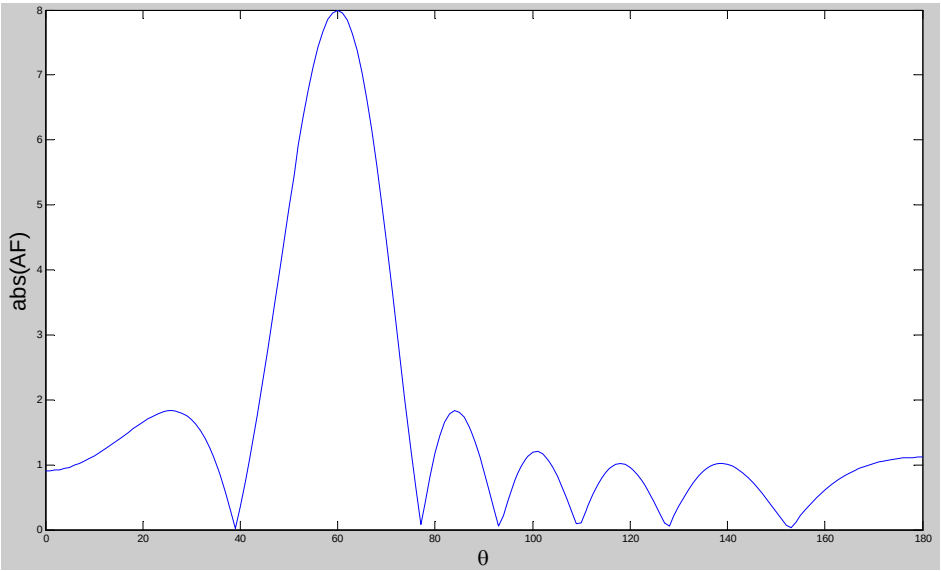

Figure 4.8: Matlab computed nulls when $r_0 = 3\times10^5\,\text{m},\ t = 1.775\text{ms}$.

ii) $t_0 = 3$ ms, $r = 8.325\times10^5$ m

$$\because \frac{t}{1/\Delta f} - \frac{r/c}{1/\Delta f} - \rho = -0.225 < 0 \Rightarrow$$

$$\Rightarrow \begin{cases} 1 \le n \le \mathrm{N}\times\left(\dfrac{r/c}{1/\Delta f} - \dfrac{t}{1/\Delta f} + \rho\right) \\ n = 1,2,3,\ldots \\ n \ne N, 2N, 3N, \ldots \\ \theta_n = \cos^{-1}\left\{\dfrac{1}{\rho}\left[\Delta f\left(\dfrac{r}{c} - t\right) - \dfrac{n}{N}\right]\right\} \end{cases} \quad \text{or} \quad \begin{cases} 1 \le n \le \mathrm{N}\times\left(\dfrac{t}{1/\Delta f} - \dfrac{r/c}{1/\Delta f} + \rho\right) \\ n = 1,2,3,\ldots \\ n \ne N, 2N, 3N, \ldots \\ \theta_n = \cos^{-1}\left\{\dfrac{1}{\rho}\left[\Delta f\left(\dfrac{r}{c} - t\right) + \dfrac{n}{N}\right]\right\} \end{cases}$$

$$\Rightarrow \begin{cases} 1 \le n \le 1.8 \\ n = 1,2,3,\ldots \\ n \ne 8,16,24,\ldots \\ \theta_n = \cos^{-1}\left[\dfrac{1}{0.45}\left(-0.225 - \dfrac{n}{8}\right)\right] \end{cases} \quad \text{or} \quad \begin{cases} 1 \le n \le 5.4 \\ n = 1,2,3,\ldots \\ n \ne 8,16,24,\ldots \\ \theta_n = \cos^{-1}\left[\dfrac{1}{0.45}\left(-0.225 + \dfrac{n}{8}\right)\right] \end{cases}$$

$$\Rightarrow \theta_1 = 141.06^\circ \quad \text{or} \quad \begin{cases} \theta_1 = 102.84^\circ \\ \theta_2 = 86.82^\circ \\ \theta_3 = 70.53^\circ \\ \theta_4 = 52.33^\circ \\ \theta_5 = 27.27^\circ \end{cases}$$

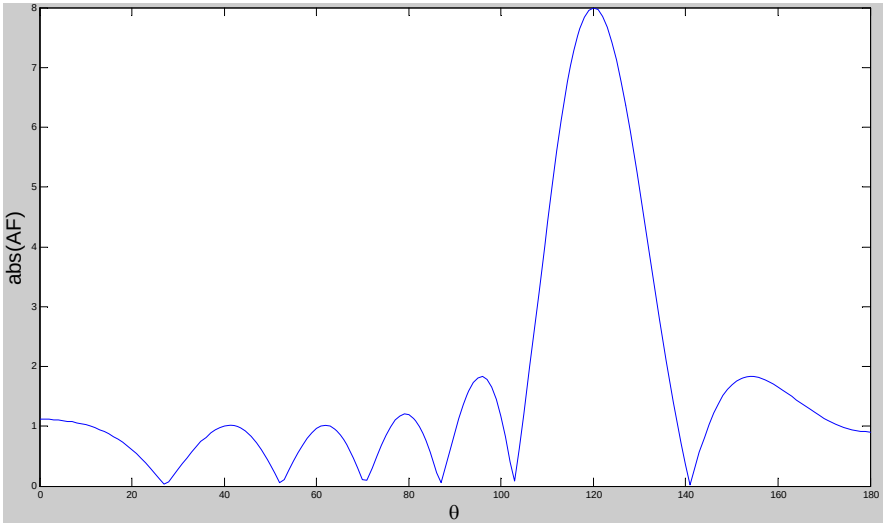

Figure 4.9: Matlab computed nulls when $t_0 = 3$ ms, $r = 8.325\times10^5$ m.

4.3.3.2 Maximum of $AF_{\Delta f,\rho}(\theta,t,r)$

Similarly, the maximum value of (4-18) is equal to N and occurs when

$$\sin\left(\frac{1}{2}\psi\right)=0 \tag{4-21}$$

$$\Rightarrow \theta_m=\cos^{-1}\left\{\frac{1}{\rho}\left[\Delta f\left(\frac{r}{c}-t\right)\pm m\right]\right\} \qquad m=0,1,2,... \tag{4-22}$$

For a maximum to exist, the argument of the arccosine cannot exceed unity. That is,

$$\left|\frac{1}{\rho}\left[\Delta f\left(\frac{r}{c}-t\right)\pm m\right]\right|\le 1. \tag{4-23}$$

The number and angle positions of the maxima can be derived as follows.

a) if $\left(\dfrac{t}{1/\Delta f}-\dfrac{r/c}{1/\Delta f}\right)\ge\rho$

$$\Rightarrow\begin{cases}\dfrac{t}{1/\Delta f}-\dfrac{r/c}{1/\Delta f}-\rho\le m\le\dfrac{t}{1/\Delta f}-\dfrac{r/c}{1/\Delta f}+\rho\\ m=0,1,2,...\\ \theta_m=\cos^{-1}\left\{\dfrac{1}{\rho}\left[\Delta f\left(\dfrac{r}{c}-t\right)+m\right]\right\}\end{cases}$$

b) if $0\le\left(\dfrac{t}{1/\Delta f}-\dfrac{r/c}{1/\Delta f}\right)<\rho$

$$\Rightarrow\begin{cases}0\le m\le\dfrac{t}{1/\Delta f}-\dfrac{r/c}{1/\Delta f}+\rho\\ m=0,1,2,...\\ \theta_m=\cos^{-1}\left\{\dfrac{1}{\rho}\left[\Delta f\left(\dfrac{r}{c}-t\right)+m\right]\right\}\end{cases}\quad\text{or}\quad\begin{cases}0\le m\le\dfrac{r/c}{1/\Delta f}-\dfrac{t}{1/\Delta f}+\rho\\ m=0,1,2,...\\ \theta_m=\cos^{-1}\left\{\dfrac{1}{\rho}\left[\Delta f\left(\dfrac{r}{c}-t\right)-m\right]\right\}.\end{cases}$$

We will compute the maximum(s) of the same FDA in previous Section with $N=8,\ \Delta f=1\,\text{kHz},\ \rho=0.45$ and compare them with the Matlab computed results in Figures 4.10 and 4.11.

i) $r_0=3\times10^5\,\text{m},\ t=1.775\text{ms}$

$$\because \frac{t}{1/\Delta f}-\frac{r/c}{1/\Delta f}-\rho=0.315>0$$

$$\Rightarrow\begin{cases}\dfrac{t}{1/\Delta f}-\dfrac{r/c}{1/\Delta f}-\rho\le m\le\dfrac{t}{1/\Delta f}-\dfrac{r/c}{1/\Delta f}+\rho\\ m=0,1,2,...\\ \theta_m=\cos^{-1}\left\{\dfrac{1}{\rho}\left[\Delta f\left(\dfrac{r}{c}-t\right)+m\right]\right\}\end{cases}$$

$$\Rightarrow\begin{cases}0.315\le m\le1.225\\ m=0,1,2,...\\ \theta_m=\cos^{-1}\left[\dfrac{1}{0.45}(m-0.775)\right]\end{cases}$$

$$\Rightarrow\theta_1=60^\circ$$

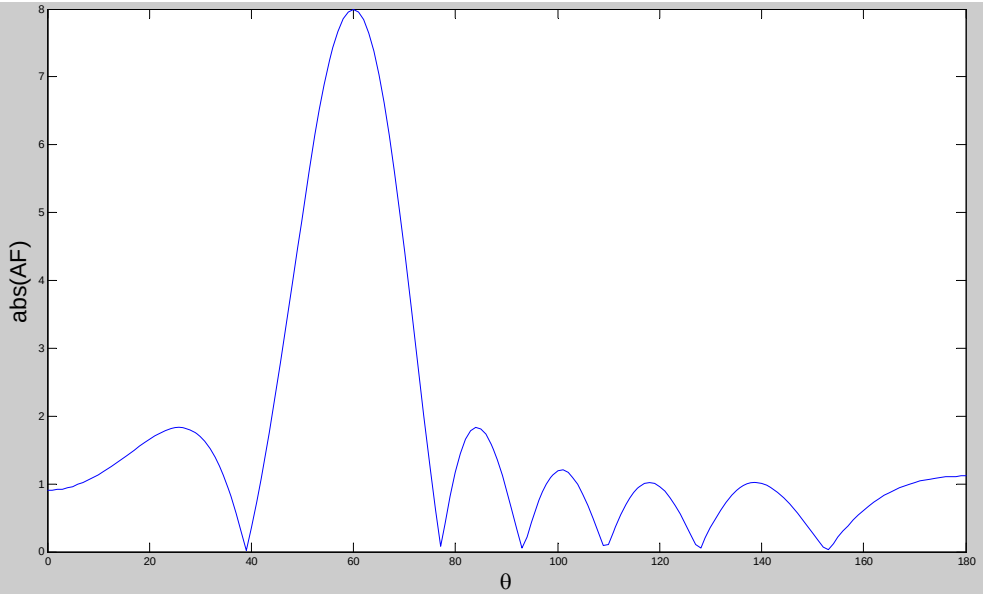

Figure 4.10: Matlab computed maximum when $r_0=3\times10^5\,\text{m},\ t=1.775\text{ms}$.

ii) $t_0 = 3$ ms, $r = 8.325\times10^5$ m

$$\because \frac{t}{1/\Delta f} - \frac{r/c}{1/\Delta f} - \rho = -0.225 < 0$$

$$\Rightarrow \begin{cases} 0 \le m \le \dfrac{t}{1/\Delta f} - \dfrac{r/c}{1/\Delta f} + \rho \\ m = 0,1,2,\ldots \\ \theta_m = \cos^{-1}\left\{\dfrac{1}{\rho}\left[\Delta f\left(\dfrac{r}{c} - t\right) + m\right]\right\} \end{cases} \quad \text{or} \quad \begin{cases} 0 \le m \le \dfrac{r/c}{1/\Delta f} - \dfrac{t}{1/\Delta f} + \rho \\ m = 0,1,2,\ldots \\ \theta_m = \cos^{-1}\left\{\dfrac{1}{\rho}\left[\Delta f\left(\dfrac{r}{c} - t\right) - m\right]\right\} \end{cases}$$

$$\Rightarrow \begin{cases} 0 \le m \le 0.675 \\ m = 0,1,2,\ldots \\ \theta_m = \cos^{-1}\left[\dfrac{1}{0.45}(-0.225 + m)\right] \end{cases} \quad \text{or} \quad \begin{cases} 0 \le m \le 0.225 \\ m = 0,1,2,\ldots \\ \theta_m = \cos^{-1}\left[\dfrac{1}{0.45}(-0.225 - m)\right] \end{cases}$$

$$\Rightarrow \theta_0 = 120^\circ$$

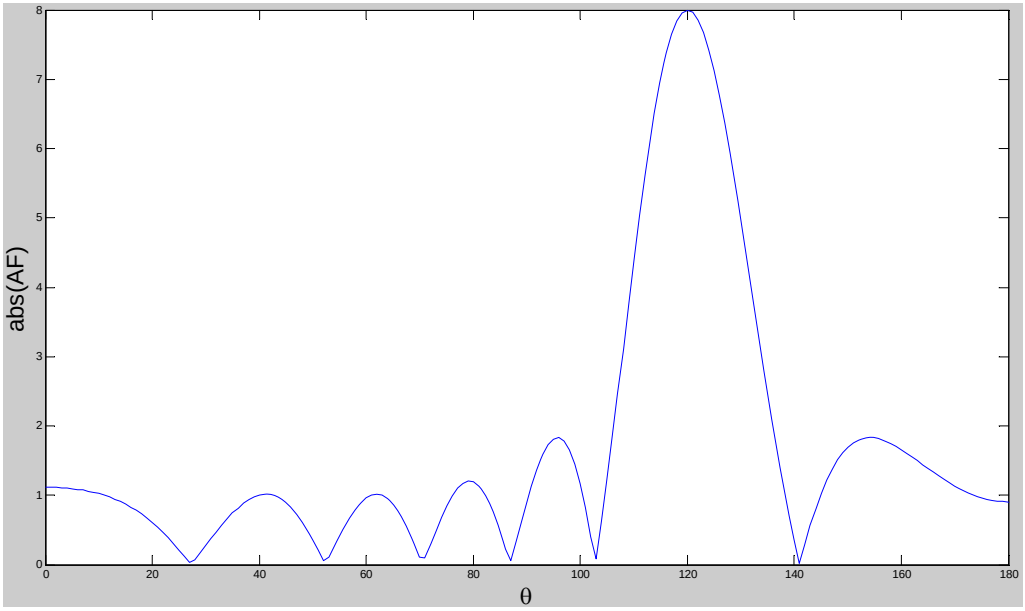

Figure 4.11: Matlab computed maximum when $t_0 = 3$ ms, $r = 8.325\times10^5$ m.

Thus for an *N*-element FDA with given Δf and ρ, the number of maximum that can exist as well as their angle position will be a function of time *t* and distance *r*.

We shall mention that when (*t*,*r*) is given, the above routine to compute the maximum of $AF_{\Delta f,\rho}(\theta,t,r)$ does not guarantee a maximum's existence, as one may not be able to find an integer "*m*" at all.

For example, the array factor of an FDA ($N=8,\ \Delta f=1\,\text{kHz},\ \rho=0.45$) is computed when distance is fixed at $r_0=3\times10^5\,\text{m}$. We can see that between 1.45ms and 1.55ms in Figure 4.12, there is no maximum at all.

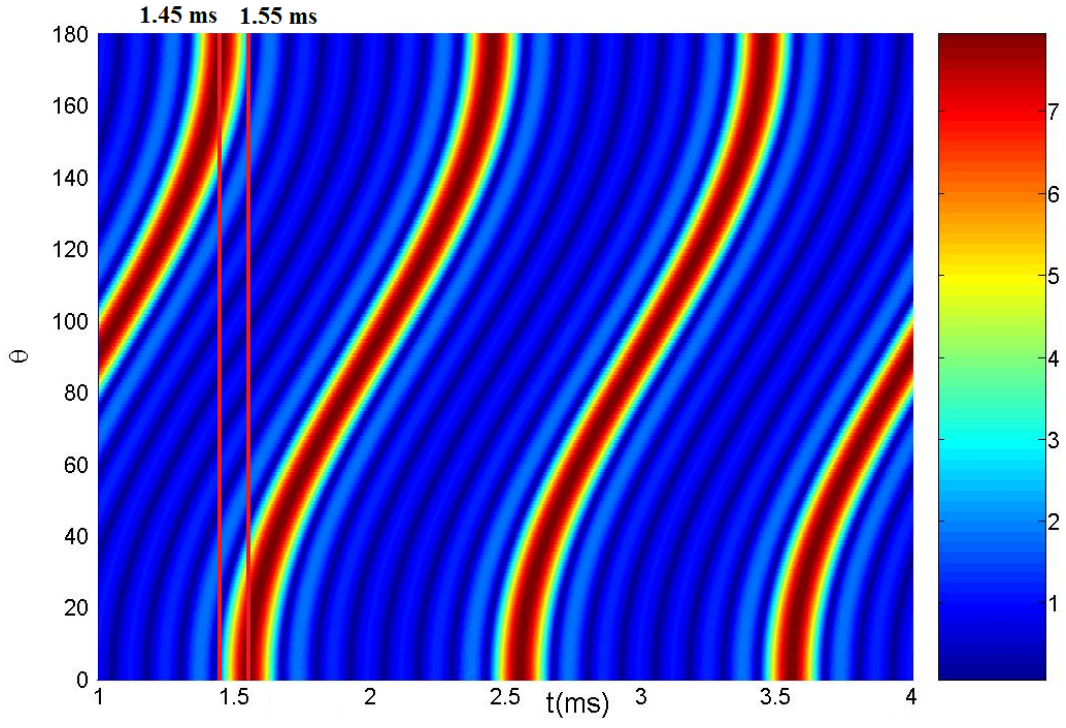

Figure 4.12: No maximum between "1.45 ms" and "1.55 ms".

If we let t = 1.5ms and follow the same routine to compute the maximum, we shall find

$$\because \frac{t}{1/\Delta f} - \frac{r/c}{1/\Delta f} - \rho = 0.05 > 0$$

$$\Rightarrow \begin{cases} \dfrac{t}{1/\Delta f} - \dfrac{r/c}{1/\Delta f} - \rho \le m \le \dfrac{t}{1/\Delta f} - \dfrac{r/c}{1/\Delta f} + \rho \\ m = 0,1,2,... \\ \theta_m = \cos^{-1}\left\{ \dfrac{1}{\rho}\left[\Delta f \left(\dfrac{r}{c} - t \right) + m \right] \right\} \end{cases}$$

$$\Rightarrow \begin{cases} 0.05 \le m \le 0.95 \\ m = 0,1,2,... \\ \theta_m = \cos^{-1}\left[\dfrac{1}{0.45}(m - 0.775) \right] \end{cases}$$

$\Rightarrow m$ does not exist.

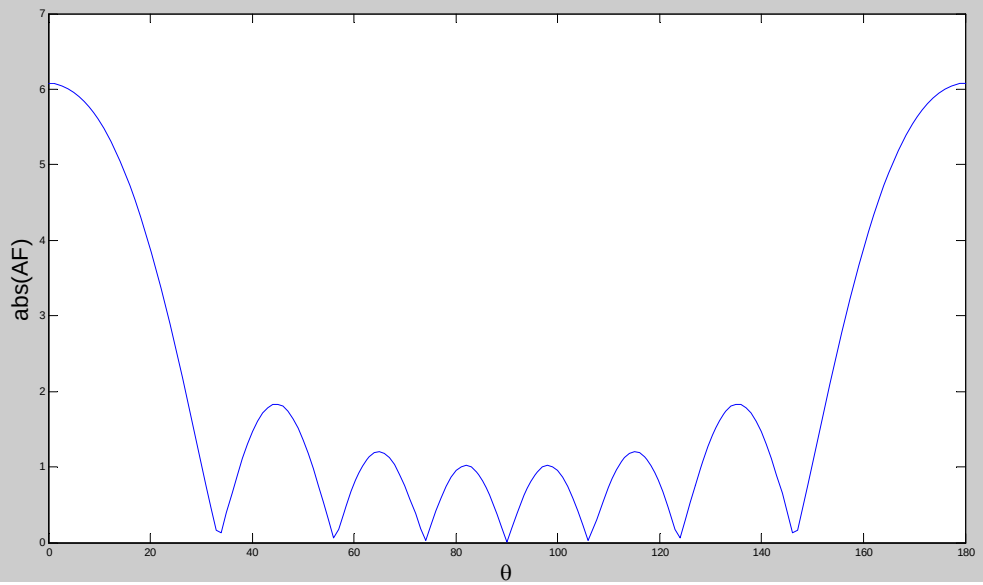

Figure 4.13: Matlab computed array when $r_0 = 3\times10^5$ m, $t = 1.5$ms.

Actually the array factor of an FDA ($N = 8$, $\Delta f = 1$ kHz, $\rho = 0.45$) at $r_0 = 3\times10^5$ m, $t = 1.5$ms is computed in Matlab and depicted in Figure 4.13. One can

see that the maximum value of $|AF|$ is less than 8 so there is no maxima at $r_0 = 3\times10^5\,\text{m},\ t = 1.5\text{ms}$.

4.3.3.3 Grating lobes of $AF_{\Delta f,\rho}(\theta,t,r)$

In previous Sections the array factor of the FDA with $N = 8,\ \Delta f = 1\,\text{kHz},\ \rho = 0.45$ is examined at $r_0 = 3\times10^5\,\text{m},\ t = 1.775\text{ms}$ and $t_0 = 3\text{ms},\ r = 8.325\times10^5\,\text{m}$. In both cases, there is only one principle maximum of the array factor at any time *t* or distance *r*. However, if the element space *d* is increased so that $\rho = 1.2$, there will be multiple principle maxims as shown in Figure 4.14.

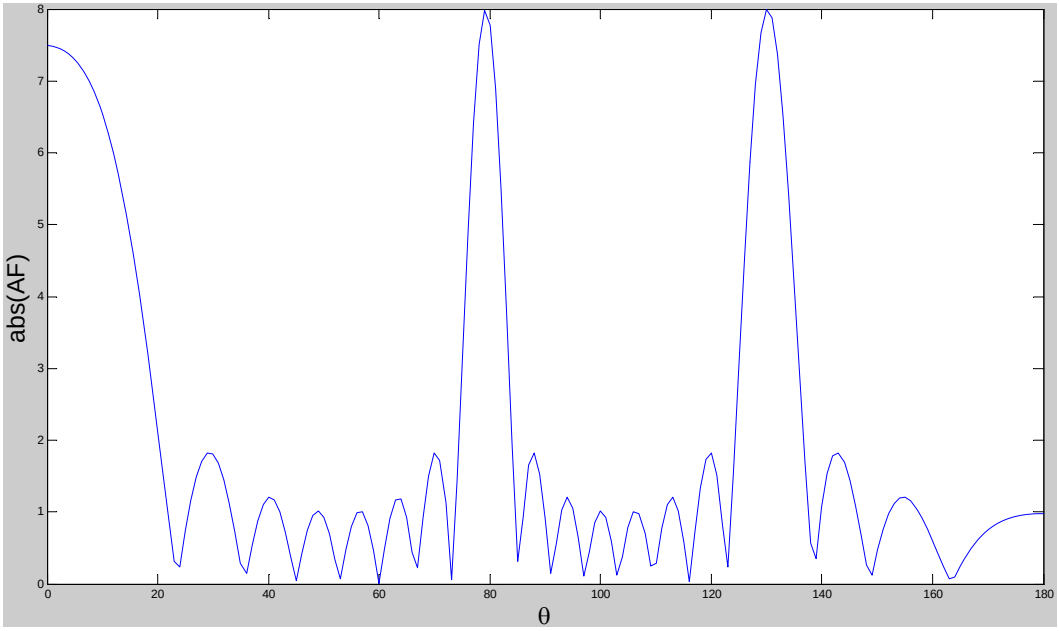

(a) Array factor at $r_0 = 3\times10^5\,\text{m},\ t = 1.775\text{ms}$

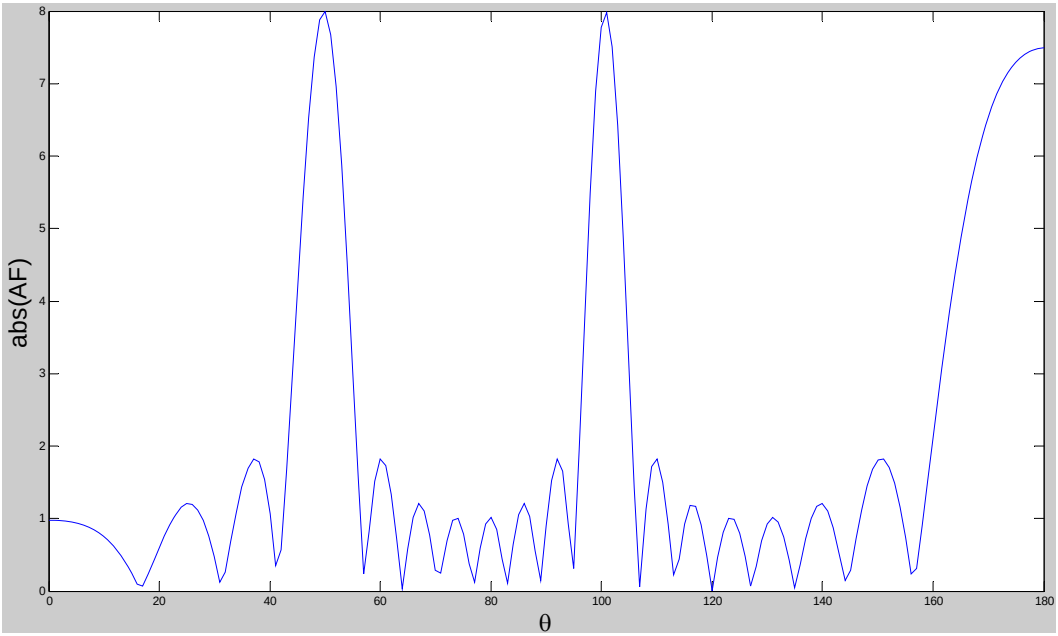

(b) Array factor at $t_0 = 3\text{ms},\ r = 8.325\times10^5\,\text{m}$

Figure 4.14: Matlab computed array factor when $\rho = 1.2$.

To ensure that there are no principal maxima in other directions, "*m*" should have at most one value under each circumstance. From (4-22) and (4-23) we can analyze the number of maxima as follows.

$$1 > if \quad \frac{t}{1/\Delta f} - \frac{r/c}{1/\Delta f} > \rho$$

$$\Rightarrow \begin{cases} \dfrac{t}{1/\Delta f} - \dfrac{r/c}{1/\Delta f} - \rho \le m \le \dfrac{t}{1/\Delta f} - \dfrac{r/c}{1/\Delta f} + \rho \\ m = 0,1,2,\ldots \end{cases} \Rightarrow 2\times\rho < 1 \Rightarrow \rho < 0.5$$

$$2 > if \quad \frac{t}{1/\Delta f} - \frac{r/c}{1/\Delta f} = \rho \Rightarrow \begin{cases} 0 \le m \le \rho \\ m = 0,1,2,\ldots \end{cases} \Rightarrow \begin{cases} \rho<1 \\ m = 0 \end{cases}$$

$$3 > if \quad 0 \le \frac{t}{1/\Delta f} - \frac{r/c}{1/\Delta f} < \rho$$

$$\Rightarrow \begin{cases} 0 \le m \le \dfrac{t}{1/\Delta f} - \dfrac{r/c}{1/\Delta f} + \rho \\ m = 0,1,2,\ldots \end{cases} \quad \text{or} \quad \begin{cases} 0 \le m \le \dfrac{r/c}{1/\Delta f} - \dfrac{t}{1/\Delta f} + \rho \\ m = 0,1,2,\ldots \end{cases}$$

$$\Rightarrow \begin{cases} 0 \le m < 2 \times \rho \\ m = 0,1,2,... \end{cases} \quad \text{or} \quad \begin{cases} 0 \le m \le \rho \\ m = 0,1,2,... \end{cases}$$

$$\Rightarrow \begin{cases} \rho \le 0.5 \\ m = 0 \end{cases} \quad \text{or} \quad \begin{cases} \rho < 1 \\ m = 0 \end{cases}$$

$$\Rightarrow \begin{cases} \rho < 1 \\ m = 0 \end{cases}$$

Thus the largest spacing between the elements in an FDA $(\Delta f, \rho)$ should be less than half wavelength $\left(\rho = \frac{d}{\lambda} < 0.5\right)$ to avoid any grating lobe when a principle occurs at any angle θ, time *t* and distance *r*.

4.4 Beam Steering Using $AF_{\Delta f,\rho}(\theta, t, r)$

In Chapter 4.2 we have derived the array factor of an FDA with given $\Delta f, \rho$. In Chapter 4.3 the nulls and maxima of $AF_{\Delta f,\rho}(\theta, t, r)$ are examined. Given any values of t and r, the number and position of nulls/maxima can be derived accordingly. Moreover, when element space is less than half wavelength $(\rho < 0.5)$, there is no grating lobe at any time *t* and distance *r*. When $\rho < 0.5$ the "-" sign before "*m*" in (4-22) cannot be taken and (4-22) reduces to

$$\theta_m = \cos^{-1}\left\{\frac{1}{\rho}\left[\Delta f\left(\frac{r}{c} - t\right) + m\right]\right\} \quad m = 0,1,2,... \qquad (4\text{-}23)$$

The angle position of the maximum can be derived following the routine in Section 4.3.3.2.

Another question is how to choose the values of t and r, if a maximum of $\hat{\theta}$ $(\rho < 0.5)$ is desired. If a maximum occurs at $\hat{\theta}$ $(\rho < 0.5)$, we have

$$t - \frac{r}{c} = \frac{m - \rho\cos\hat{\theta}}{\Delta f} \quad (m = 0,1,2,\ldots \text{ and } t \geq r/c). \tag{4-24}$$

It can be seen from (4-24) that for a given $\hat{\theta}$, there are multiple values of t and r for a beam to be formed towards $\hat{\theta}$. When computing the values of t and r, the value of m should be chosen according to the value of $\hat{\theta}$.

a) If $0^\circ \leq \hat{\theta} < 90^\circ$

$$\begin{cases} m = 1,2,3,\ldots \\ t - \dfrac{r}{c} = \dfrac{m - \rho\cos\hat{\theta}}{\Delta f} \end{cases} \tag{4-25}$$

b) If $\hat{\theta} = 90^\circ$, $m = 0,1,2,\ldots$

$$\begin{cases} m = 0,1,2,\ldots \\ t - \dfrac{r}{c} = \dfrac{m}{\Delta f} \end{cases} \tag{4-26}$$

c) If $90^\circ < \hat{\theta} \leq 180^\circ$, $m = 0,1,2,\ldots$

$$\begin{cases} m = 0,1,2,\ldots \\ t - \dfrac{r}{c} = \dfrac{m - \rho\cos\hat{\theta}}{\Delta f} \end{cases} \tag{4-27}$$

We will use the example in Section 4.3.2.1 to verify the above argument. In Section 4.3.2.1 the array factor of an 8-element FDA ($N = 8$, $\Delta f = 1$ kHz, $\rho = 0.45$) is computed at $r_0 = 3\times10^5$ m.

a) If $\hat{\theta} = 0^{\circ} \Rightarrow \begin{cases} t = (m + 0.55) \text{ ms} \\ m = 1, 2, 3, \ldots \end{cases}$

When m = 1, t =1.55 ms ("*C*" in Figure 4.15 shows beam formed at 0°).

b) If $\hat{\theta} = 90^{\circ} \Rightarrow \begin{cases} t = (m + 1) \text{ ms} \\ m = 0, 1, 2, \ldots \end{cases}$

When m = 0 or 1, t =1 ms ("*A*" in Figure 4.15 shows beam formed at 90°) or 2ms ("*D*" in Figure 4.15 shows beam formed at 90°).

c) If $\hat{\theta} = 180^{\circ} \Rightarrow \begin{cases} t = (m + 1.45) \text{ ms} \\ m = 0, 1, 2, \ldots \end{cases}$

When m = 0, t =1.45 ms ("*B*" in Figure 4.15 shows beam formed at 180°).

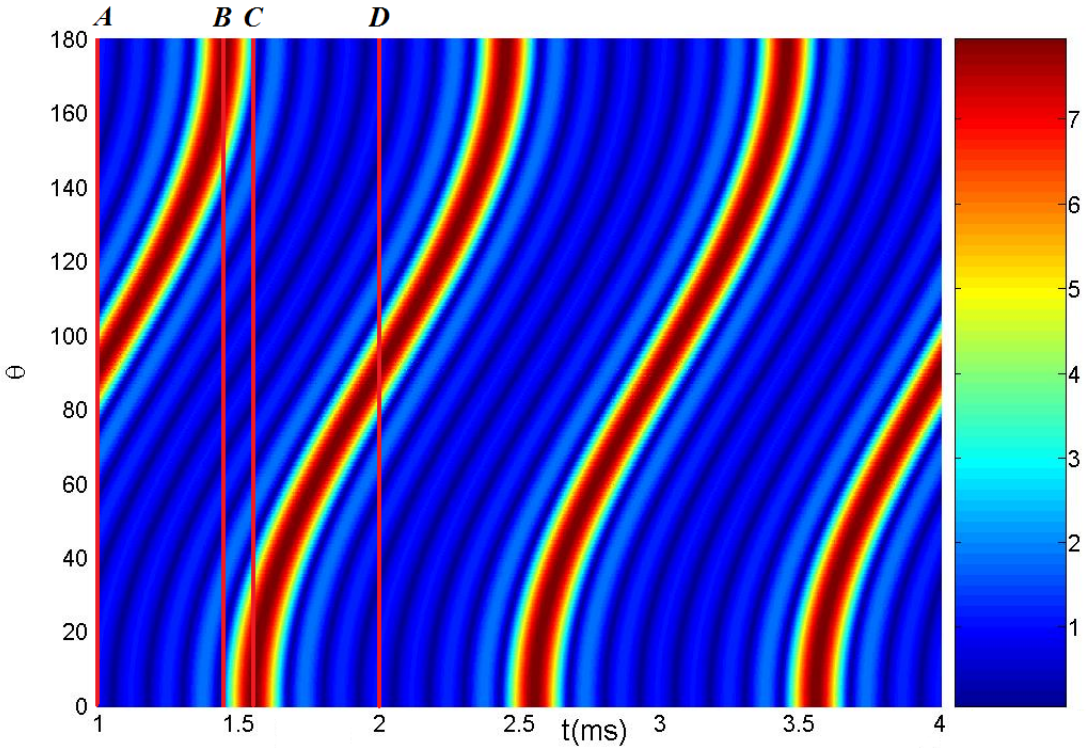

Figure 4.15: Matlab computed array factor at $r_0 = 3 \times 10^5$ m.

In many applications it is desirable to have the maximum radiation of an array directed normal to the axis of the array, which is referred as broadside radiation.

When $\hat{\theta} = 90^\circ$, we have

$$t = \frac{r}{c} + \frac{m}{\Delta f}, m = 0,1,2,... \tag{4-28}$$

Since all signals have 0° phase at $t = 0$, at $t = r/c$ all signals at the distance of r shall have 0° phase, which will result in a broadside radiation ($\hat{\theta} = 90^\circ$). Due to periodicity, at $t = \frac{r}{c} + m \times \frac{1}{\Delta f}, m = 0,1,2,...$, broadside radiation will also be expected.

Instead of having the maximum radiation broadside to the axis of the array, it may be desirable to direct it along the axis of the array (end-fire). To direct the maximum toward $\hat{\theta} = 0^\circ$

$$t = \frac{r}{c} + \frac{m}{\Delta f} - \frac{\rho}{\Delta f}, m = 1,2,3,... \tag{4-29}$$

Or if the maximum is desired toward $\hat{\theta} = 180^\circ$, then

$$t = \frac{r}{c} + \frac{m}{\Delta f} + \frac{\rho}{\Delta f}, m = 0,1,2,... \tag{4-30}$$

We can see the main beam scans from 0° to 180° in every time length of $\frac{2\rho}{\Delta f}$ while the scanning period is $\frac{1}{\Delta f}$. Since $\rho < 0.5$ is presumed, we have $\frac{2\rho}{\Delta f} < \frac{1}{\Delta f}$.

Therefore the gap between $\frac{2\rho}{\Delta f}$ and $\frac{1}{\Delta f}$ assures that there are no grating lobes, as shown in Figure 4.16.

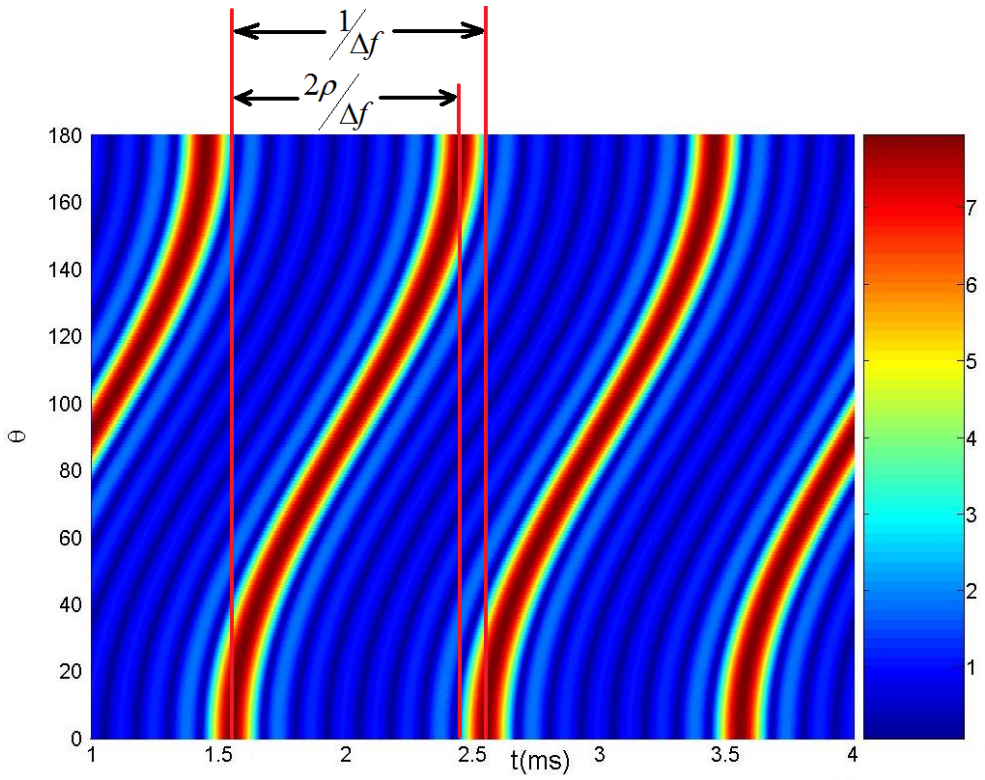

Figure 4.16: Gap between $\frac{2\rho}{\Delta f}$ and $\frac{1}{\Delta f}$.

4.5 Variation with ρ, $\Delta f = 1$ kHz

In Sections 4.3.3, it is shown that for an FDA to have no grating lobes the maximum element space should be less than half wavelength. That is, $\rho < 0.5$. This can be directly illustrated in Figure 4.16. The main beam scans from 0° to 180° in $\frac{2\rho}{\Delta f}$ which is less than the scanning period is $\frac{1}{\Delta f}$ given $\rho < 0.5$. The less ρ is than

0.5, the bigger the "gap" in Figure 4.16 becomes. On the other hand, the larger ρ is than 0.5, the more grating lobes an FDA has. In this section, different values of ρ are examined with given $\Delta f = 1$ KHz.

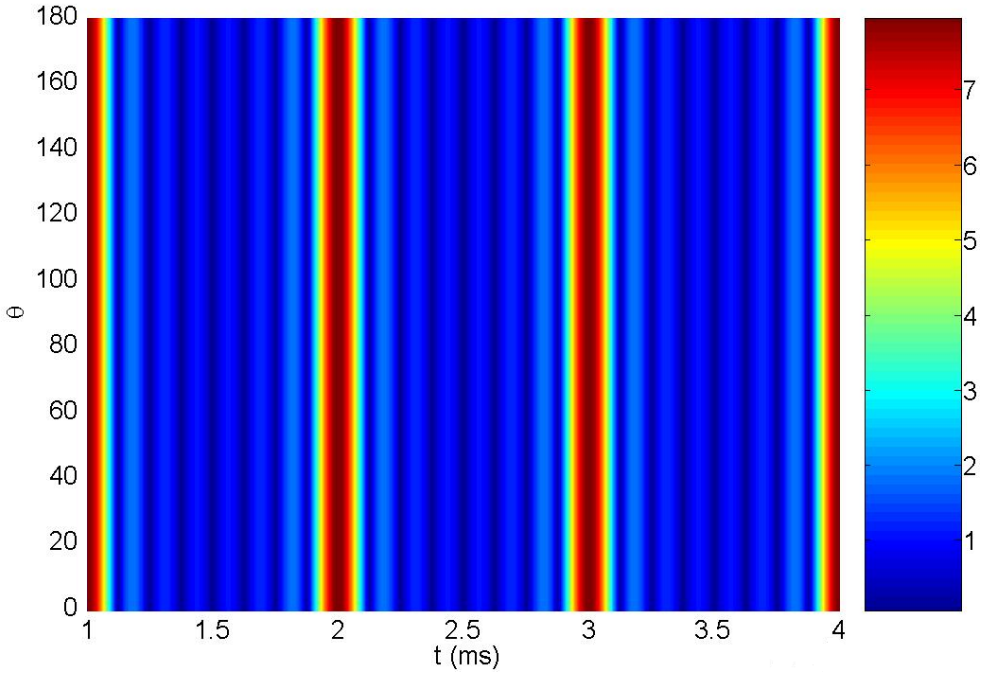

Figure 4.17: The array factor with $\rho = 0$ ($\Delta f = 1$ KHz).

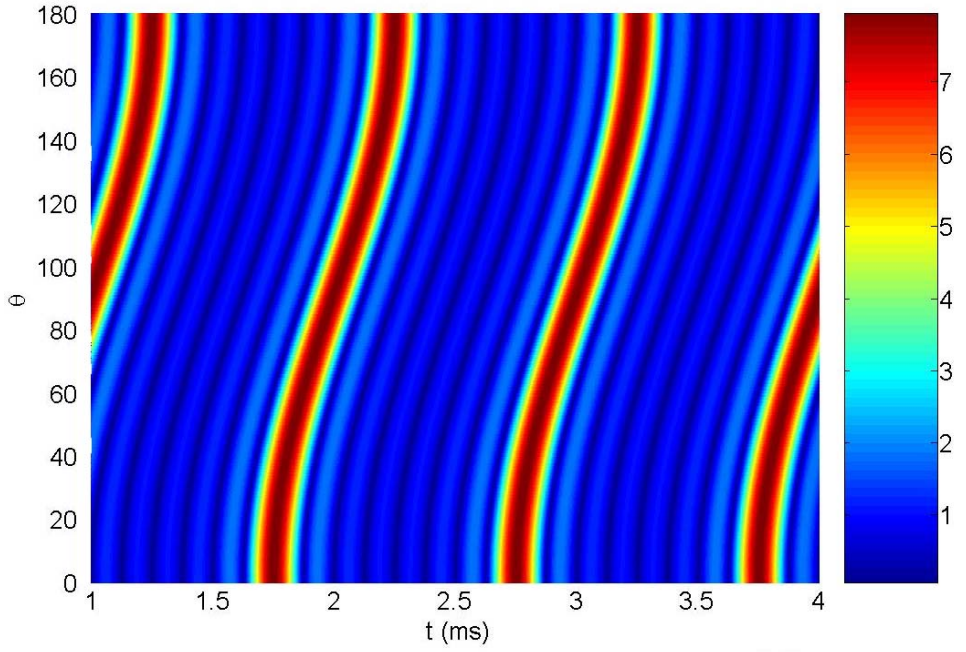

Figure 4.18: The array factor with $\rho = 0.25$ ($\Delta f = 1$ KHz).

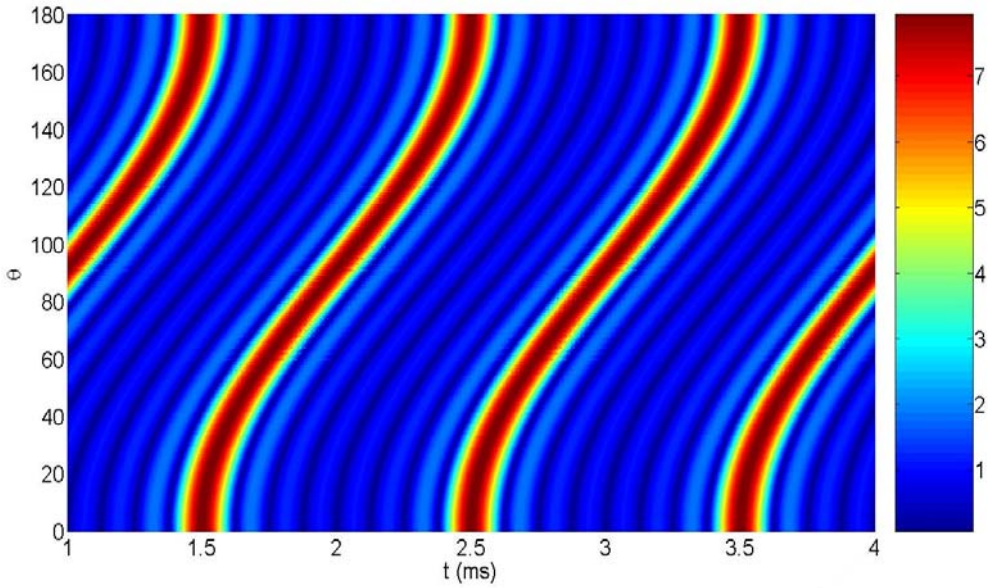

Figure 4.19: The array factor with $\rho = 0.5$ ($\Delta f = 1$ KHz).

From Figures 4.17 to 4.19, the value of ρ increases from 0 to 0.5 and the "gap" decreases from $\frac{1}{\Delta f}$ to 0. Since in three cases ρ is less than 0.5 ,no grating lobe is observed.

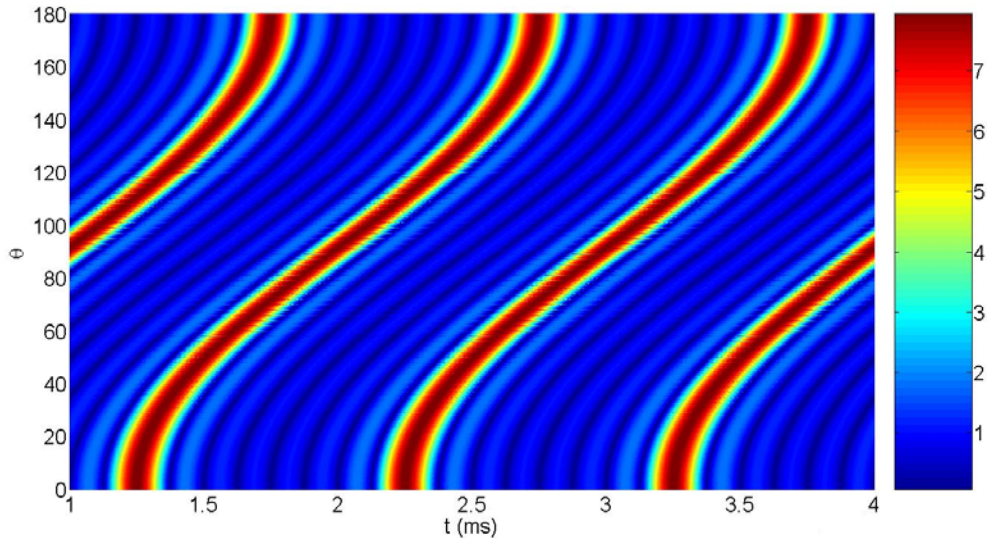

Figure 4.20: The array factor with $\rho = 0.75$ ($\Delta f = 1$ KHz).

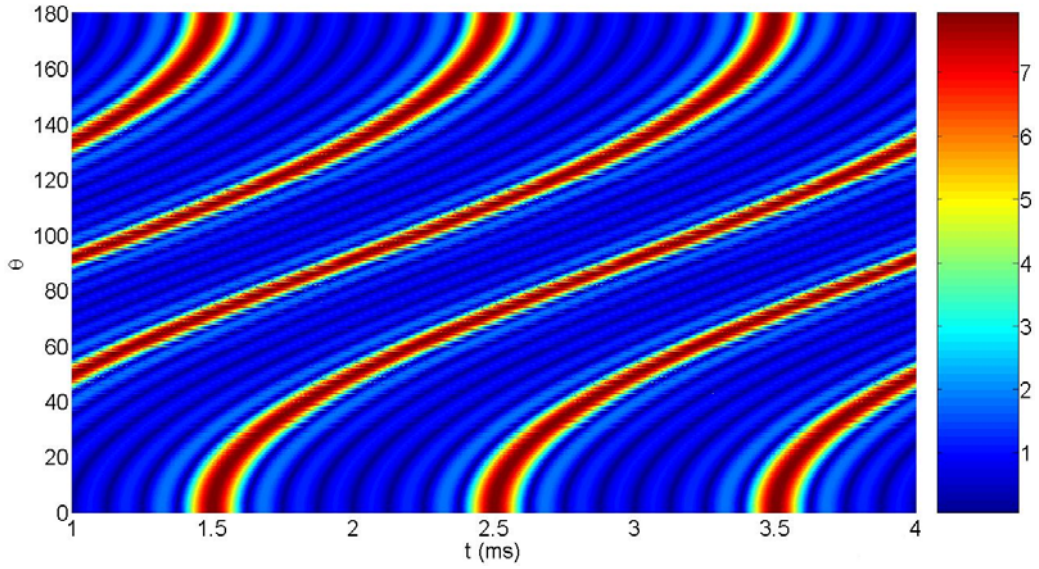

Figure 4.21: The array factor with $\rho = 1.5$ ($\Delta f = 1$ KHz).

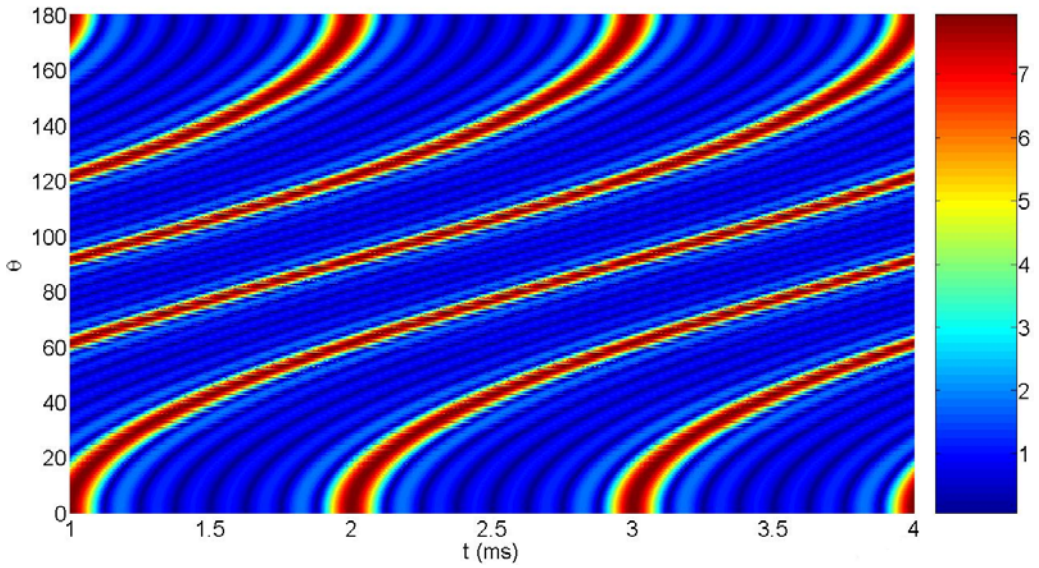

Figure 4.22: The array factor with $\rho = 2$ ($\Delta f = 1$ KHz).

From Figure 4.20 to 4.21, the value of ρ increases from 0.75 to 1.5 and number of grating lobes increases from 2 to 3. More grating lobes are expected when the value of ρ is further increased.

4.6 Variation with Δf , $\rho = 0.45$

Since the scanning period of an FDA with given Δf and ρ is $1/\Delta f$, the variation of Δf will cause an inverse variation of scanning period.. When Δf increases from 0.1 kHz to 10 kHz, the scanning period decreases from 10 ms to 0.1 ms as shown in Figures 4.23 to 4.25

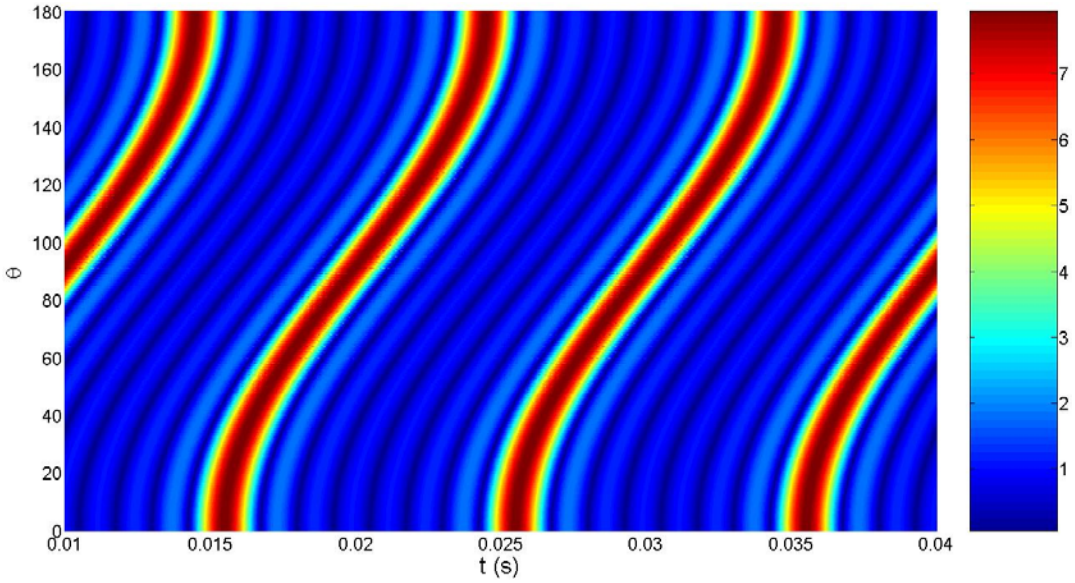

Figure 4.23: The array factor with $\Delta f = 100$ Hz ($\rho = 0.45$).

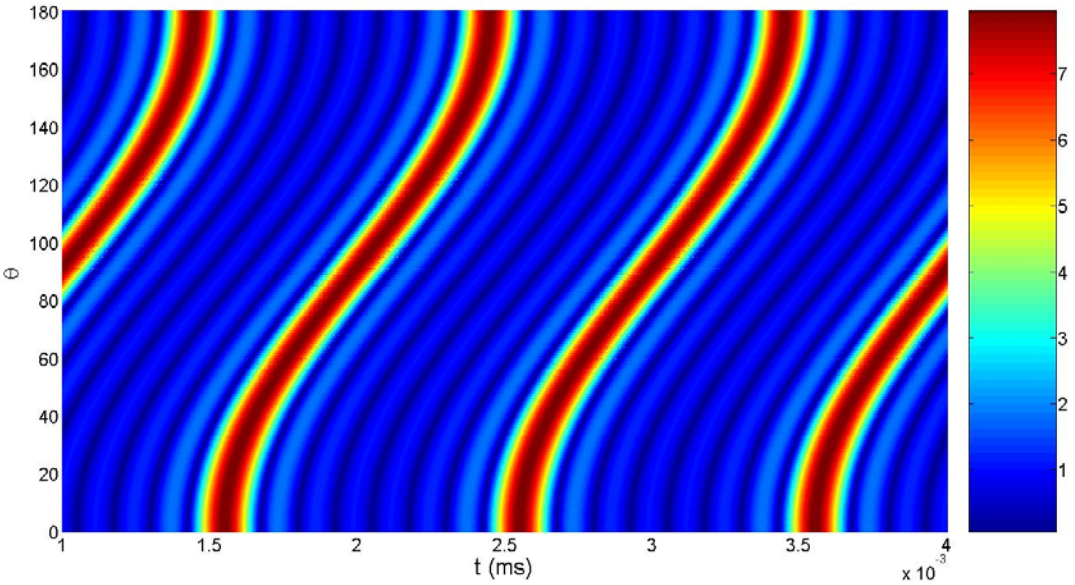

Figure 4.24: The array factor with $\Delta f = 1$ kHz ($\rho = 0.45$).

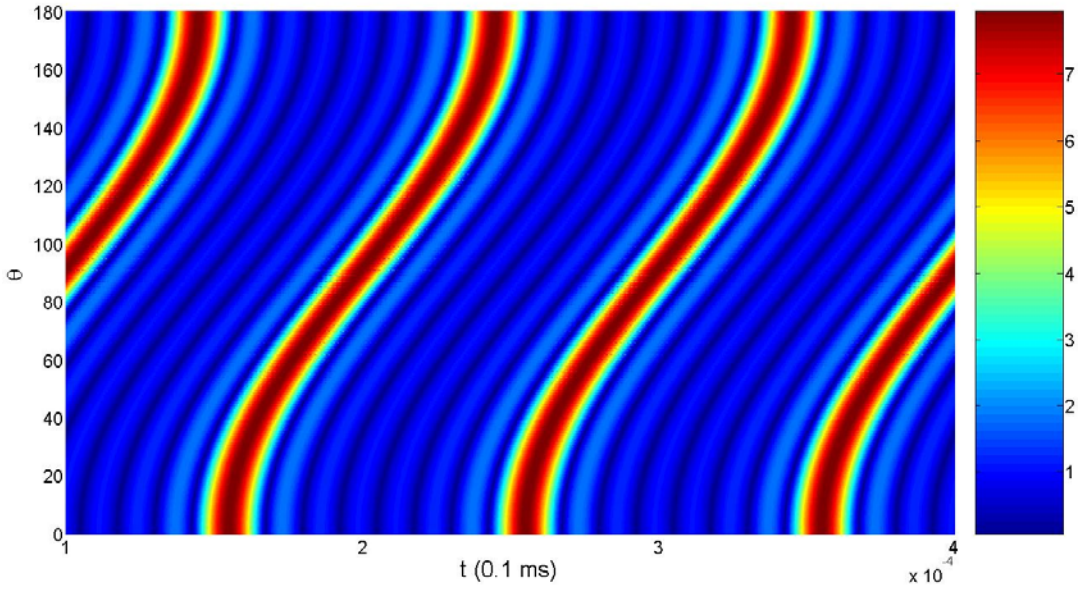

Figure 4.25: The array factor with $\Delta f = 10$ kHz ($\rho = 0.45$).

4.7 Summary

In this Chapter, the theory of FDA is developed through the derivation and discussion on its array factor. All the discussions are based on the assumption that the frequency shift Δf applied across the elements are much smaller than the working frequency of the array, also the initial phases of all signals are all 0°. For an FDA with specific Δf and ρ, its array factor $AF_{\Delta f,\rho}(\theta,t,r)$ is a function of angle, time and range. Different from a phased array whose array factor is a function of angle and phase shift, FDA offers new design freedoms (time and range) in beam forming and eliminates the use of phase shifters. The characteristics of FDA's array factor, including its periodicity, nulls, maxima and grating lobes, are thoroughly analyzed. The scanning time period is mathematically proven to be the inverse of

frequency shift Δf . It is also shown that to avoid grating lobes, the maximum element space of FDA should be less than half wavelength.

In Chapter 5, the beam scanning feature of CW FDA will be verified by electromagnetic simulation results. By analyzing how the transient E-field of a CW FDA varies with time, the periodicity of a CW FDA's beam pattern, together with the relationship between scanning period and frequency shift Δf , can be examined.

Chapter 5

Electromagnetic Simulation of CW FDA

5.1 Background

In Chapter 4, the radiation characteristics of CW FDA are explored through the examination of its array factor $AF_{\Delta f,\rho}(\theta,t,r)$. According to the pattern multiplication theorem in Chapter 3, the actual field of an FDA is equal to the field of a single element positioned at the origin multiplied by its array factor. It is known that the beam pattern of a single element, no matter what type of antenna is used, is a function of angle only and independent of time and range. Therefore the beam pattern of a CW FDA should also process the feature of $AF_{\Delta f,\rho}(\theta,t,r)$. For example, the actual beam pattern of a CW FDA should also be a periodic function of time and range. In this chapter, electromagnetic simulation of CW FDA is performed to verify the theory in Chapter 4.

Since the actual field of FDA is also expected to change with time and distance, the desired electromagnetic simulation should allow one to examine how the transient field at a fixed distance changes with time or how the transient field at a fixed time varies across distances. CST microwave studio is such a tool that allows one to examine the variation of the transient field distribution on a chosen plane. CST MICROWAVE STUDIO is part of the CST DESIGN STUDIO suite and offers a number of different solvers for different types of application. The most flexible tool is the transient solver, which can obtain the entire broadband frequency behavior of the simulated device from only one calculation run. It is based on the Finite Integration Technique (FIT).

5.2 EM Simulation of an 8-element FDA

CST Microwave Studio was used for the modeling and simulation of a linear FDA. Rectangular patch (see Figure 5.1) was chosen as the array element. The simulated substrate is Duriod 5880 with dielectric constant of 2.2 and thickness of 0.787 mm. The patch's dimension ($w = 13.92\ mm,\ l = 11.45\ mm$) and the feeding position ($d = 7.2\ mm$) are finely tuned to make sure it resonates around 8 GHz (-49 dB at 8.042 GHz as shown in Figure 5.2). Actually the array factor of FDA is independent on frequency, here 8 GHz is chosen in the consideration of wider operation bandwidth of the patch array.

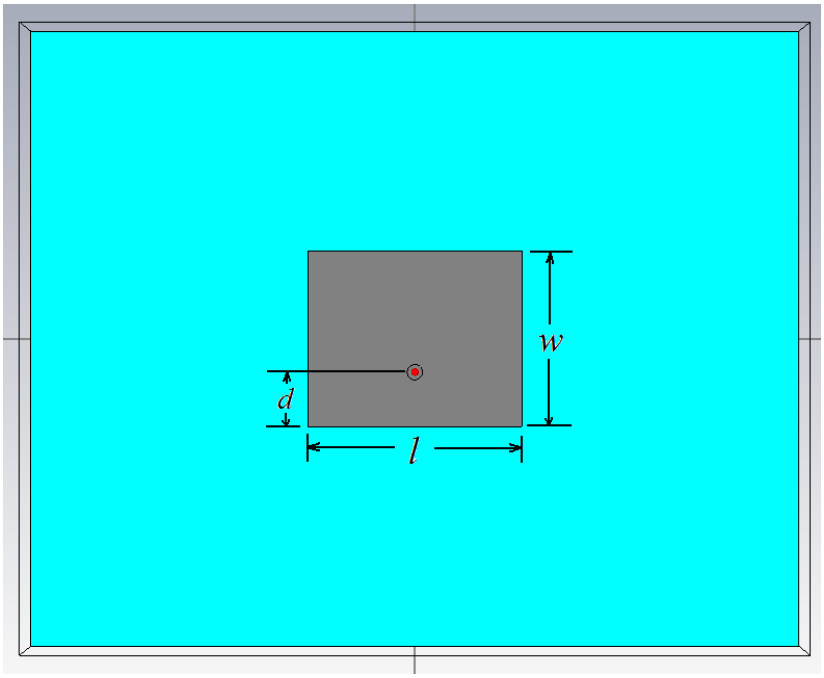

Figure 5.1: Dimension and feeding position of the patch antenna.

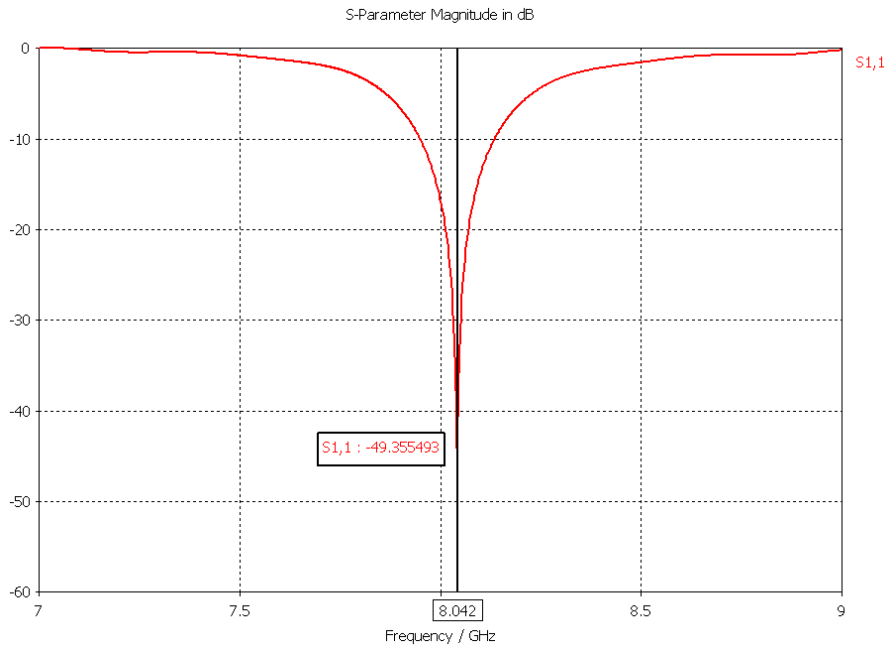

Figure 5.2: The simulated return loss of the patch antenna.

In Figures 5.3, the simulated radiation pattern on E-plane and H-plane is plotted. It is shown that the patch has a gain of 8.2 dBi at 8.042 GHz.

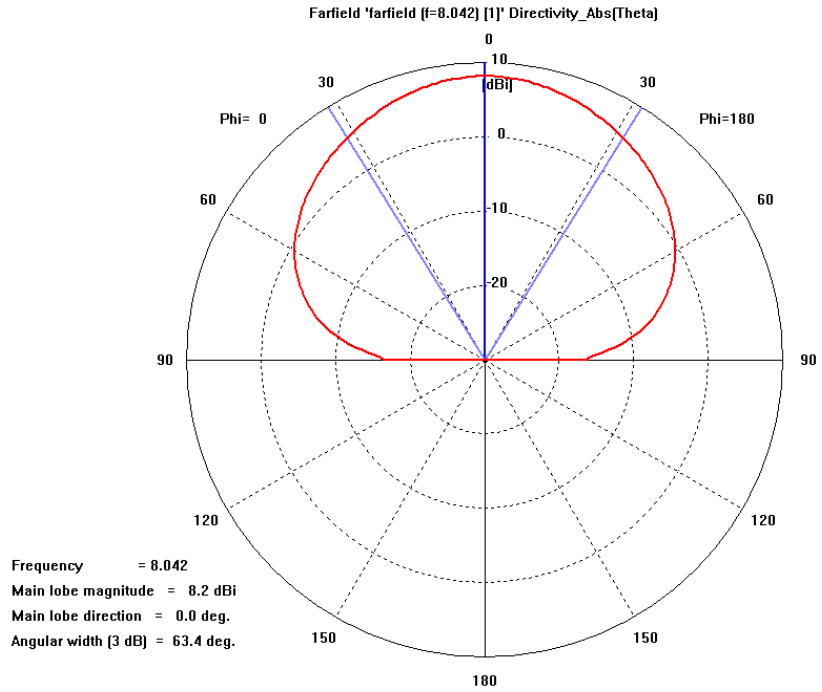

(a) E-plane

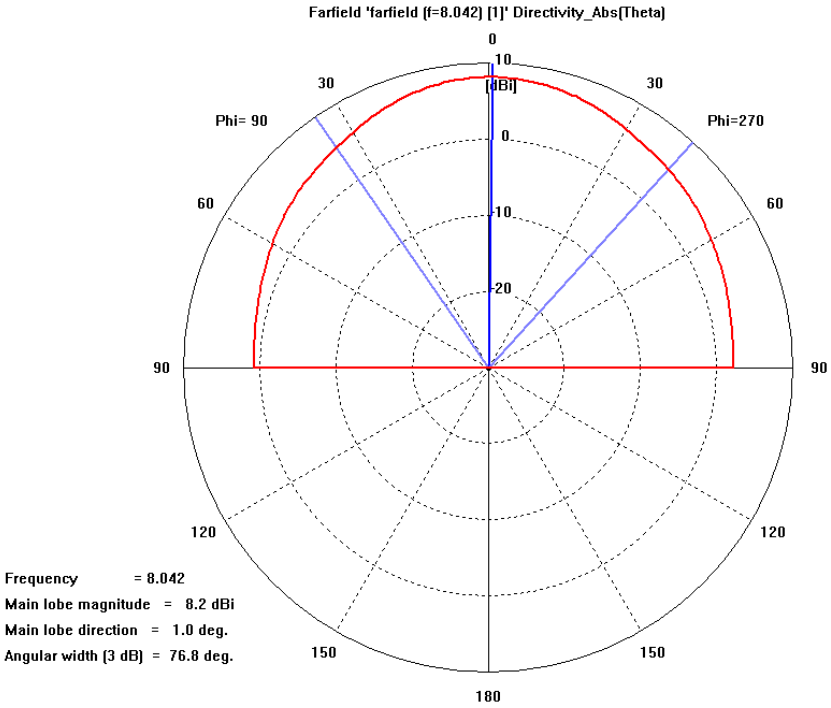

(b) H-plane

Figure 5.3: The simulated radiation pattern of the patch antenna at 8.042 GHz.

Using the designed patch, an 8-element linear FDA as shown in Figure 5.4 was built in CST. To avoid grating lobes, the element space was chosen to be half wavelength at 8 GHz (18.75 mm).

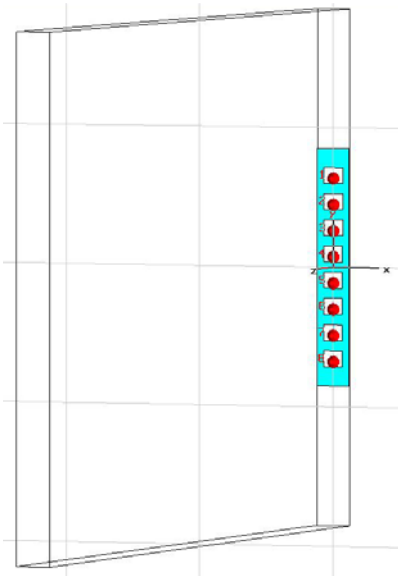

Figure 5.4: A model of an 8-element microstrip array for EM simulation.

The simulated S-parameters are given in Figure 5.5. One can see that the return loss at all ports S_{nn} (n=1-8) is below -35dB, which means all ports are well matched. Also it is shown that the coupling between 1 and the other ports is below -20dB, which means that mutual coupling has very small influence to single element and thus can be neglected as in previous discussions.

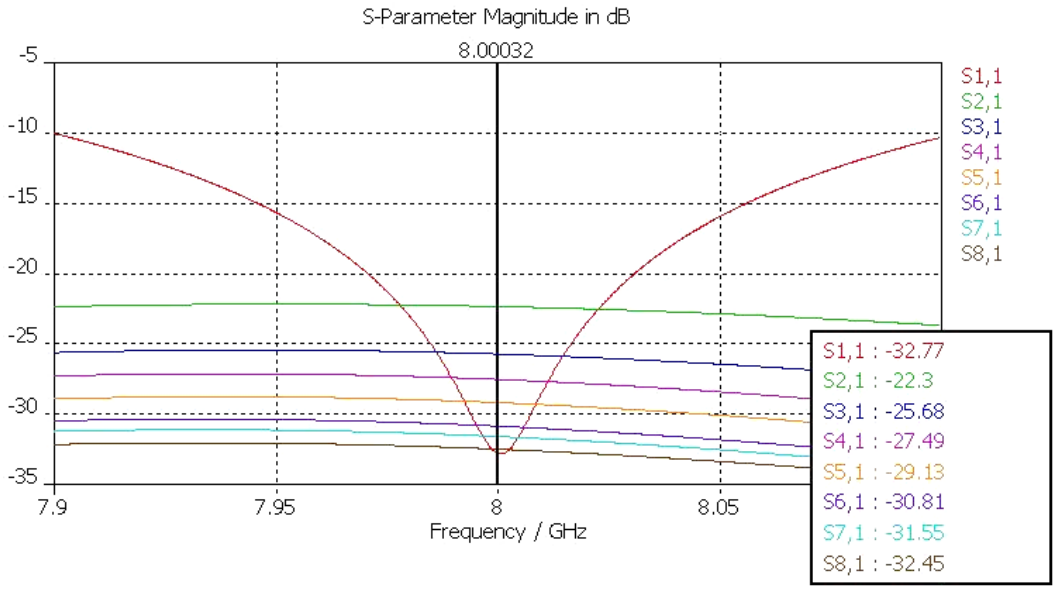

Freq	dB[S(1,1)]	dB[S(2,2)]	dB[S(3,3)]	dB[S(4,4)]	dB[S(5,5)]	dB[S(6,6)]	dB[S(7,7)]	dB[S(8,8)]
GHz	-32.8	-32.17	-33.71	-34.64	-34.89	-34.41	-33.41	-34.59

Figure 5.5: Simulated results of S-parameters of the array.

To perform the transient simulation, 8 sinuous signals “a” to “h” depicted in Figure 5.6, whose frequencies are separated by 0.025 GHz from 7.925 GHz to 8.1 GHz, are fed separately and simultaneously to port1 through port8. The duration of the excitation signals are all 80 ns, which covers 2 scanning periods. The spectrum of signal “a” and “h” are computed using the built-in FFT tool and depicted in Figures 5.7 -5.10.

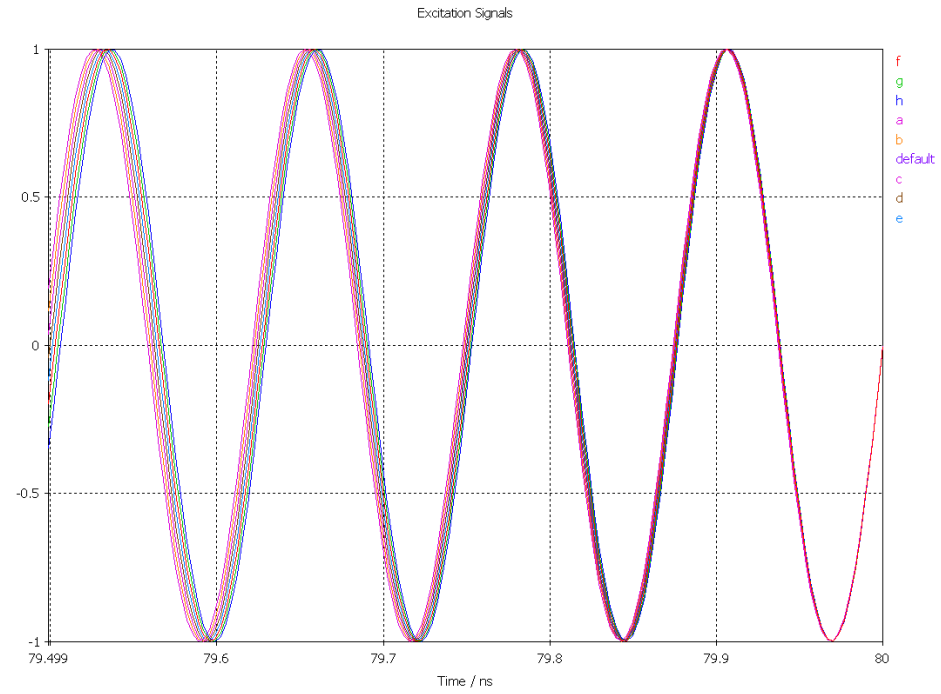

Figure 5.6: Time domain frequency diverse signals with $\Delta f = 0.025\text{GHz}$.

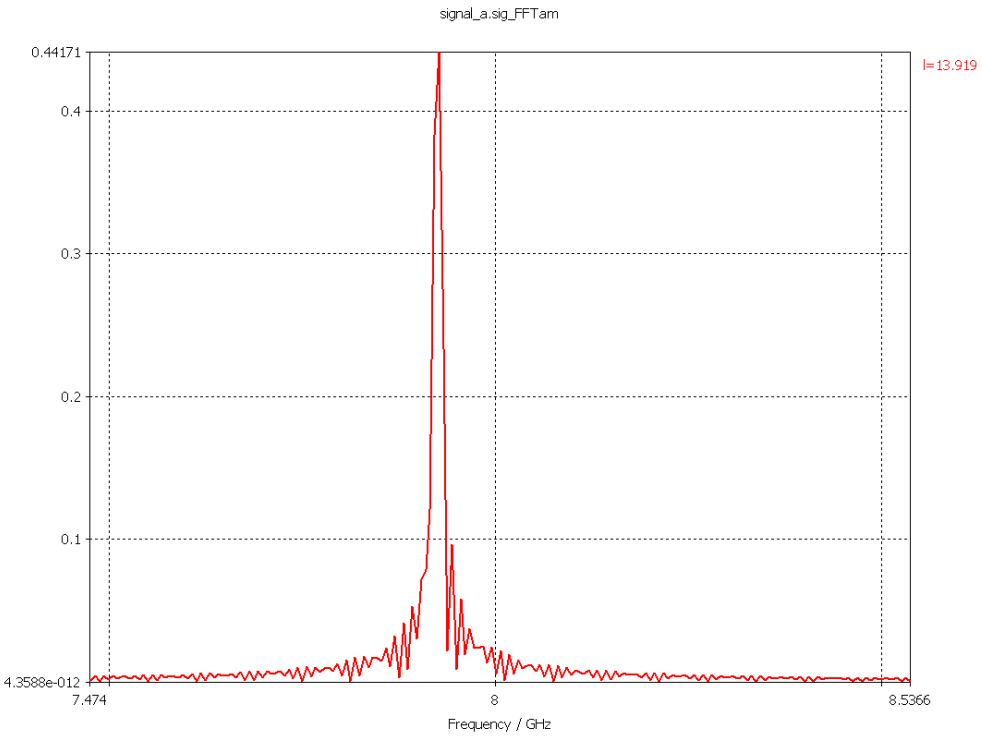

Figure 5.7: The spectrum of signal “a”.

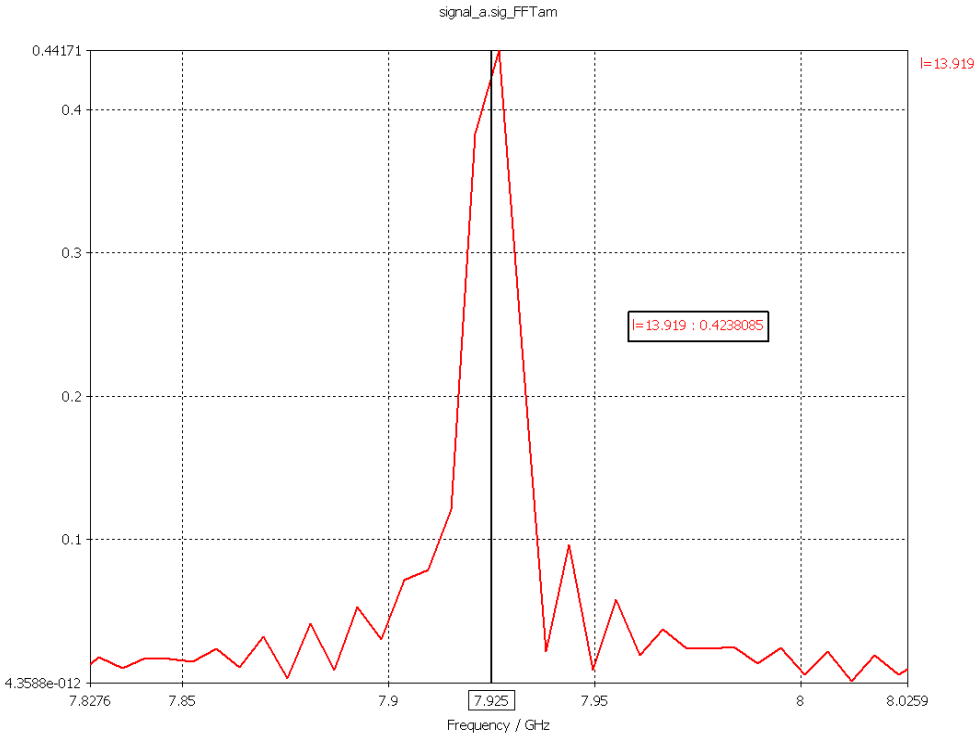

Figure 5.8: The frequency of signal “a” (7.925 GHz).

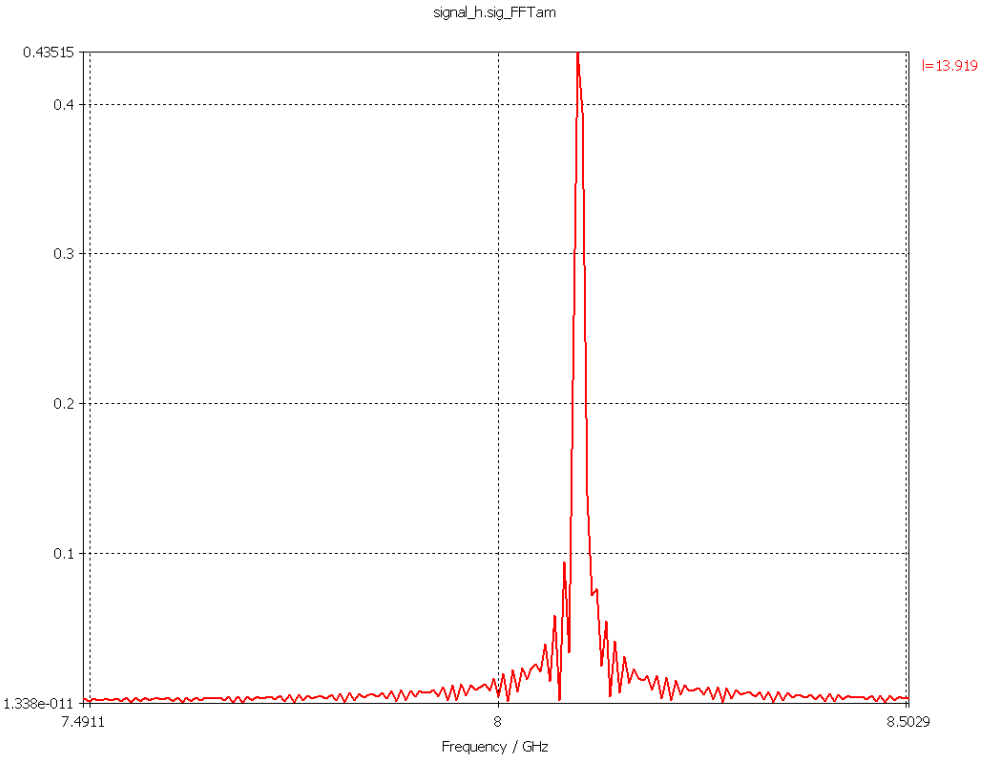

Figure 5.9: The spectrum of signal “h”.

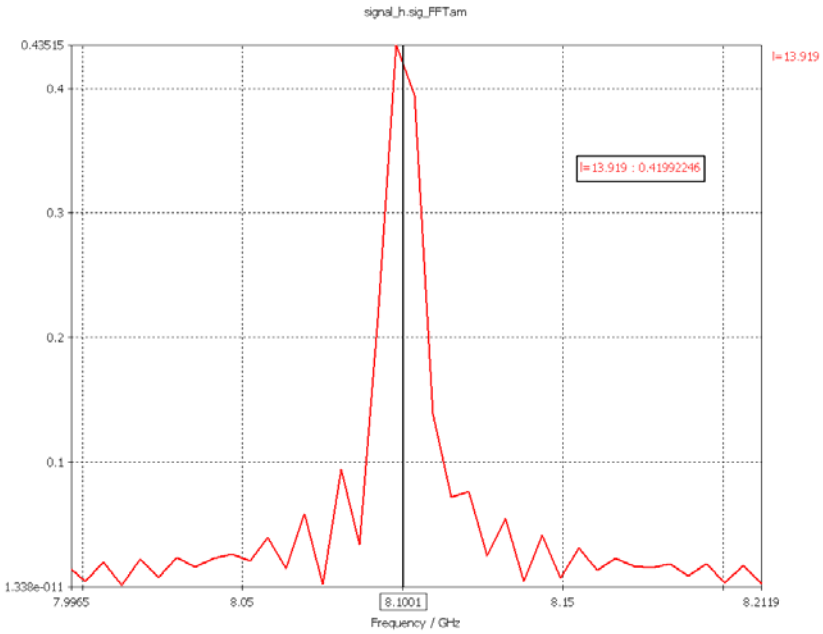

Figure 5.10: The frequency of signal "h" (8.1 GHz).

The frequency diverse signals are fed to the array simultaneously as shown in Figure 5.11. The transient E-field on the plane z = 600 mm is examined. This can be an approximation of the array factor $AF_{\Delta f,\rho}(\theta,t)\big|r=r_0$ since the plane z = 600 mm as in Figure 5.12 can be considered to be at a fixed distance to the array.

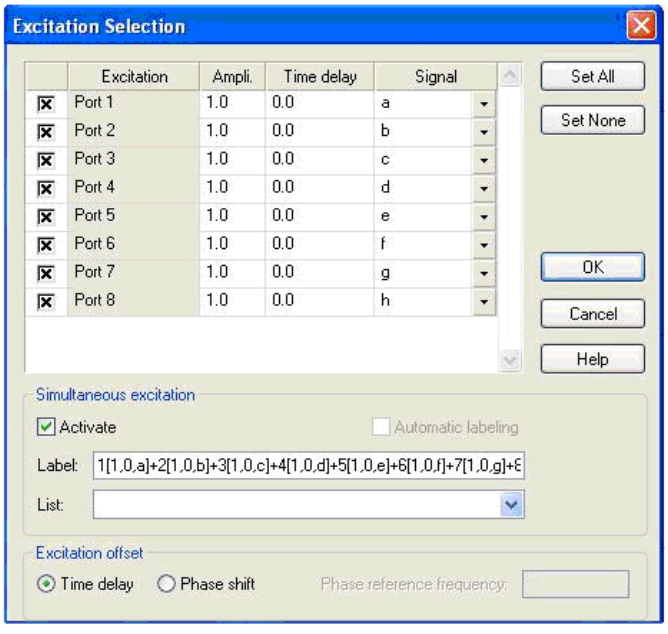

Figure 5.11: Transient simulation using simultaneous excitation.

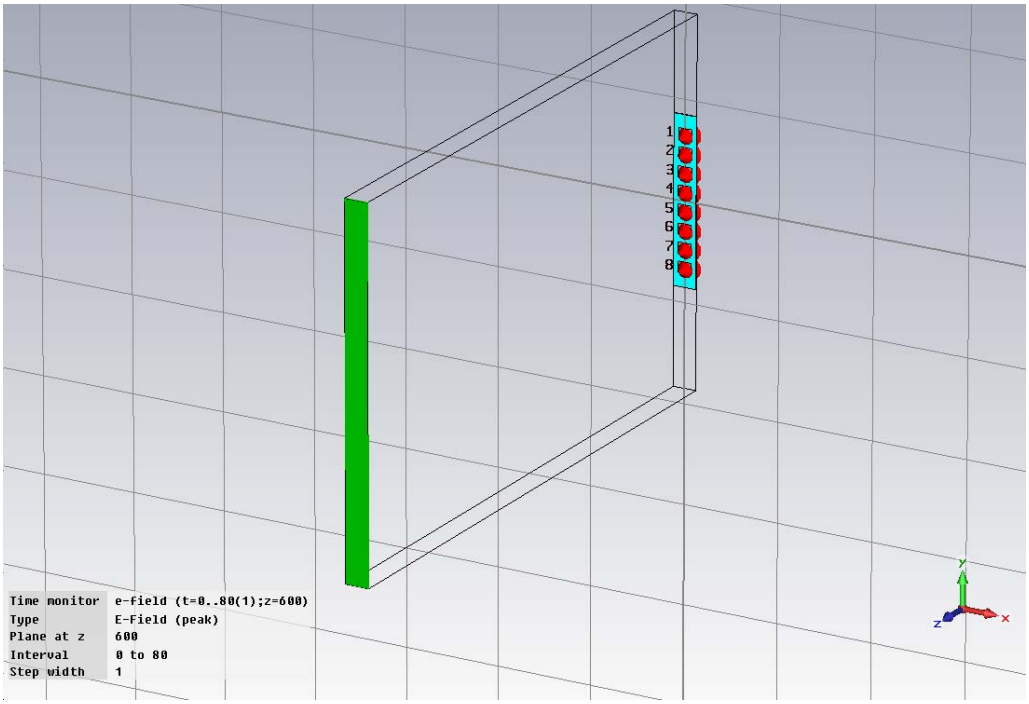

Figure 5.12: A field monitor placed at plane z = 600 mm.

11 consecutive snapshots of the transient E-field on the plane are captured and put together in Figure 5.13. From Figure 5.13 we can see that the main lobe is scanning from bottom to top, which agrees to the results in Chapter 4.

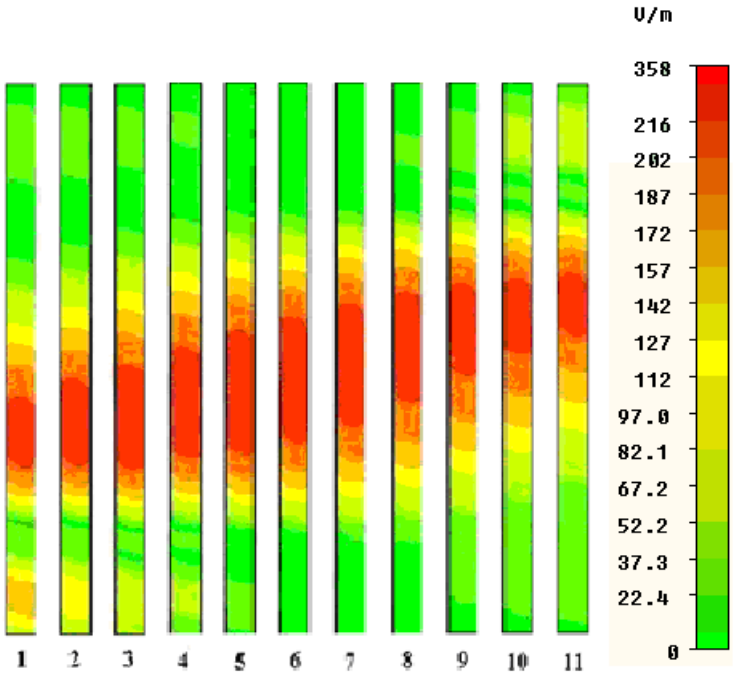

Figure 5.13: The variation of transient E-field at plane z = 600 mm in 10 ns.

To verify the relationship between scanning period and frequency shift, the transient E-field at 4 ns and 44 ns are captured for comparison. It is shown in Figure 5.14 that the E-field distribution is same at 2 moments separated by 40 ns, which is exactly the inverse of frequency shift, 0.025 GHz in this case.

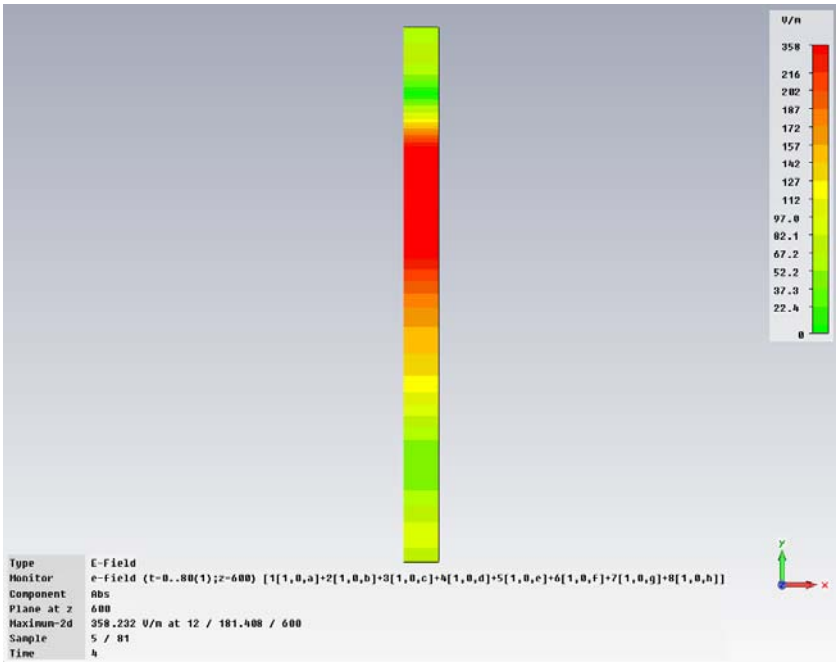

(a) Transient E-field at 4 ns

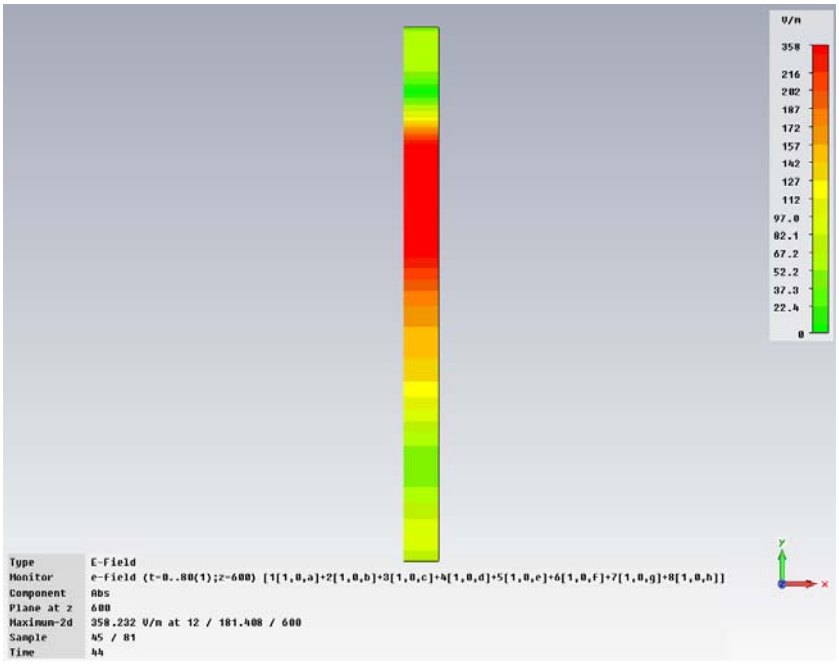

(b) Transient E-field at 44 ns

Figure 5.14: The transient E-field at 4 ns and 44 ns.

Another example is given to support the above argument. The transient E-field at 8 ns and 48 ns are shown in Figure 5.15. Again one can see that the E-field distribution is same at these 2 moments separated by 40 ns.

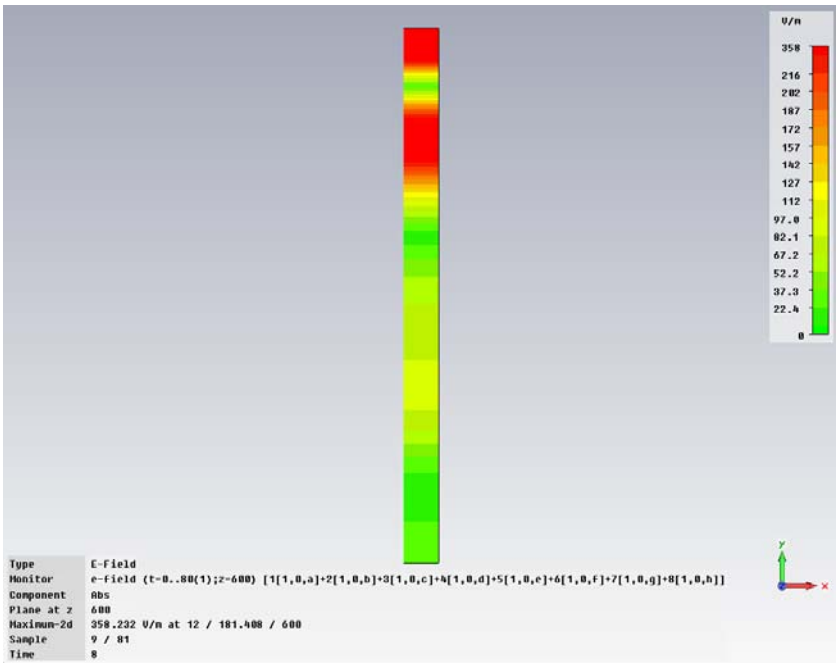

(a) Transient E-field at 8 ns

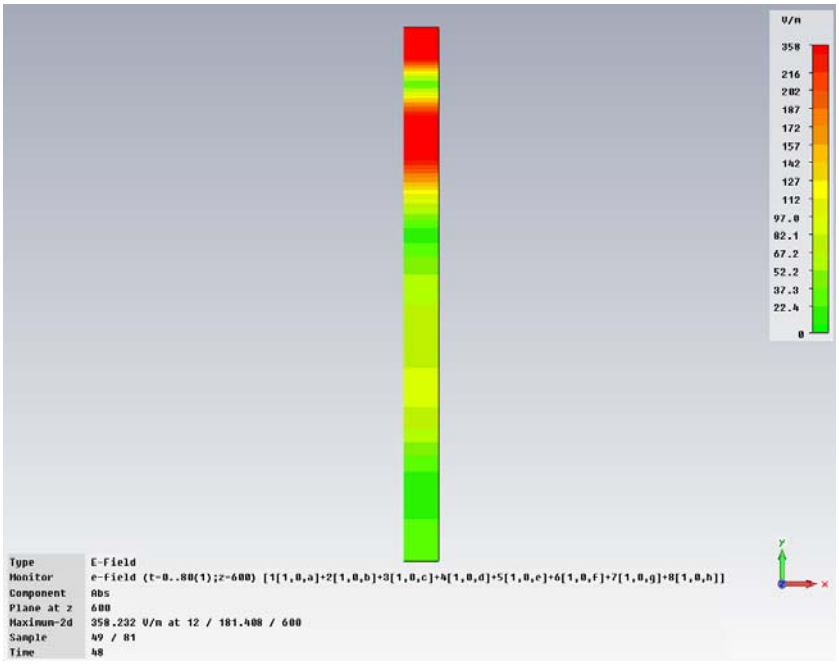

(b) Transient E-field at 48 ns

Figure 5.15: The transient E-field at 8 ns and 48 ns.

The periodically beam scanning phenomenon can be more intuitively observed when choosing the plane x = 2 mm as in Figure 5.16 and examine the transient E-field.

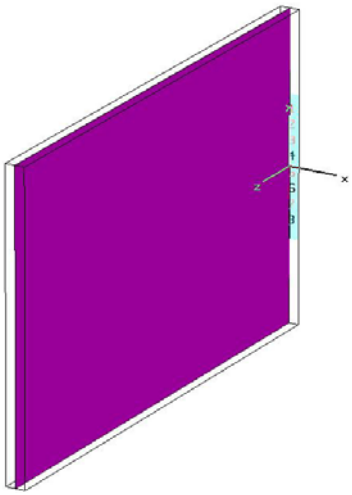

Figure 5.16: An E-field monitor placed at plane x = 2 mm.

During the whole simulated time of 80 ns, the transient E-field at 1 ns, 10 ns, 21 ns, 37 ns, 41 ns, 50 ns, 61 ns and 77 ns are captured.

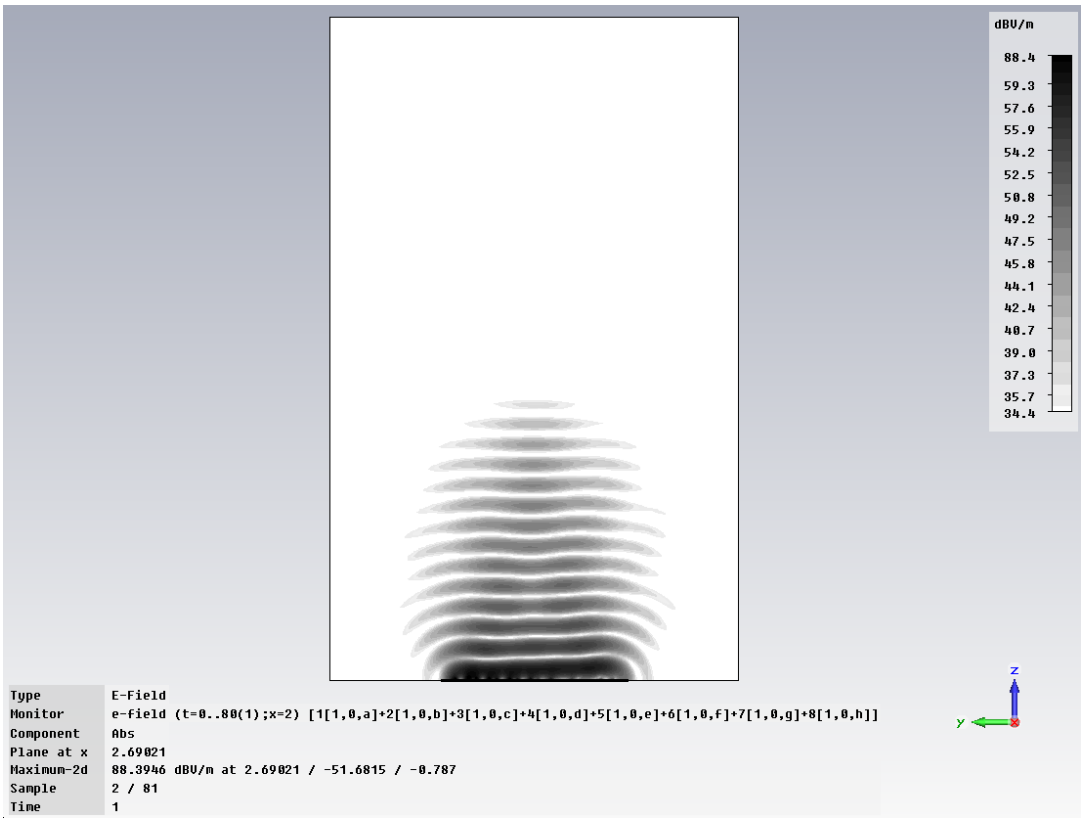

Figure 5.17: The transient E-field on plane x = 2 mm at 1 ns.

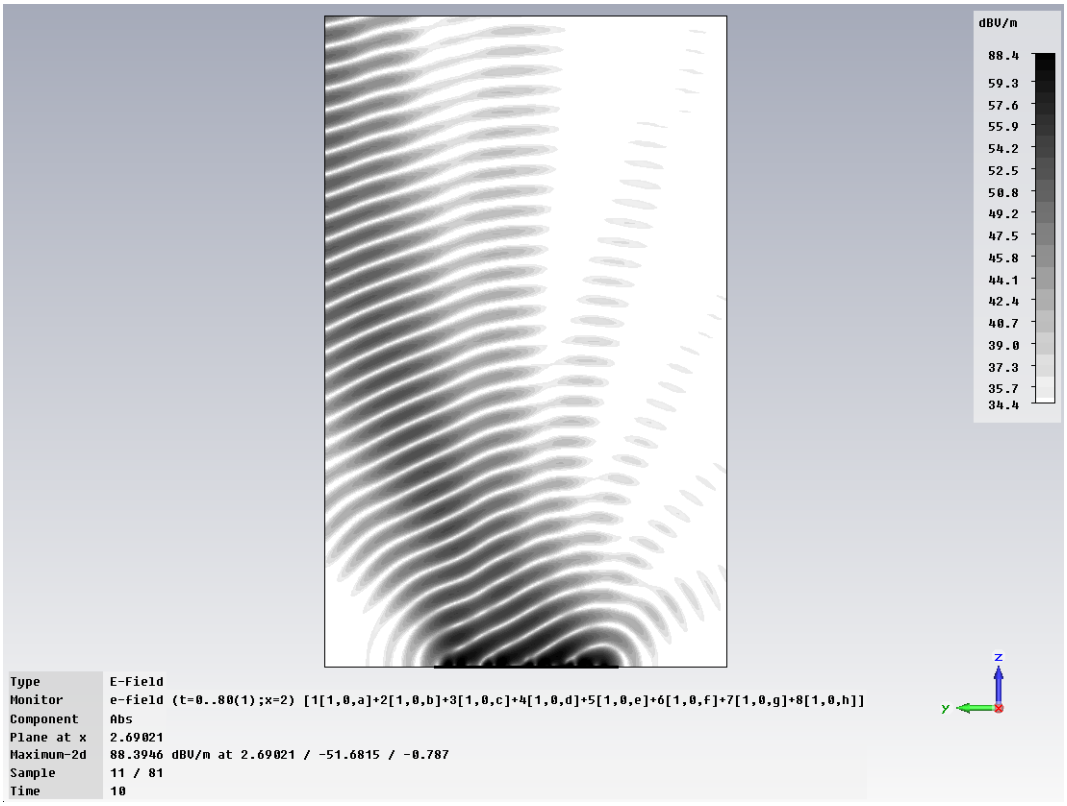

Figure 5.18: The transient E-field on plane x = 2 mm at 10 ns.

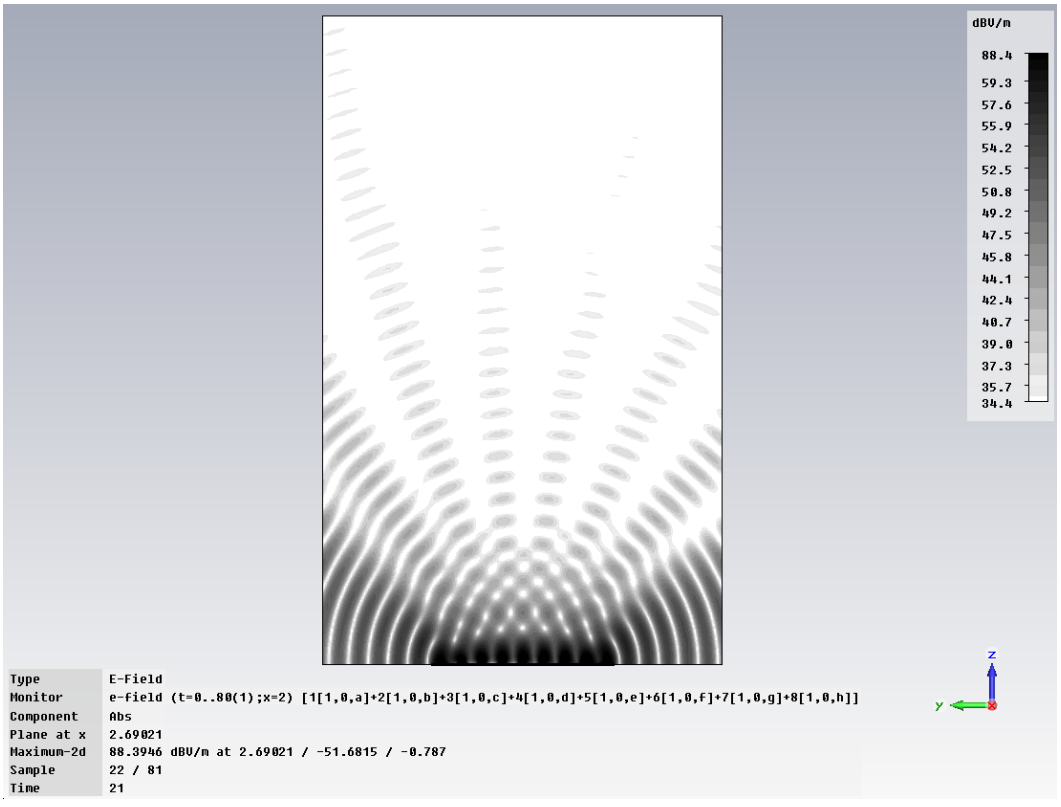

Figure 5.19: The transient E-field on plane x = 2 mm at 21 ns.

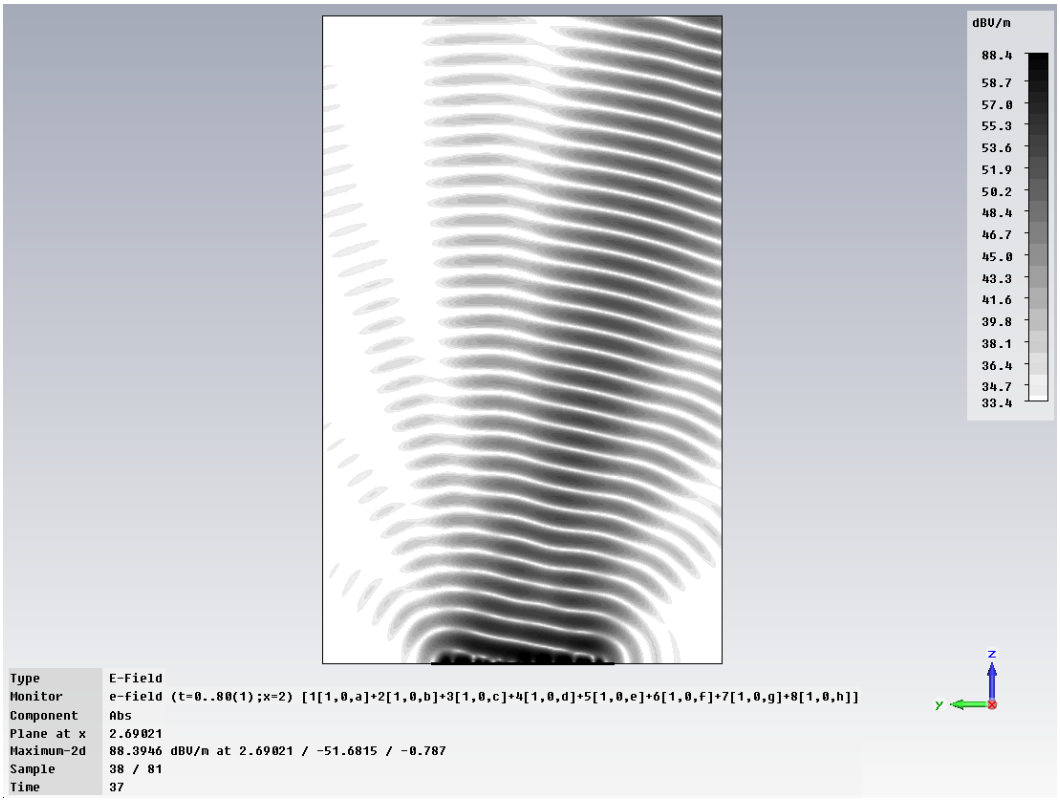

Figure 5.20: The transient E-field on plane x = 2 mm at 37 ns.

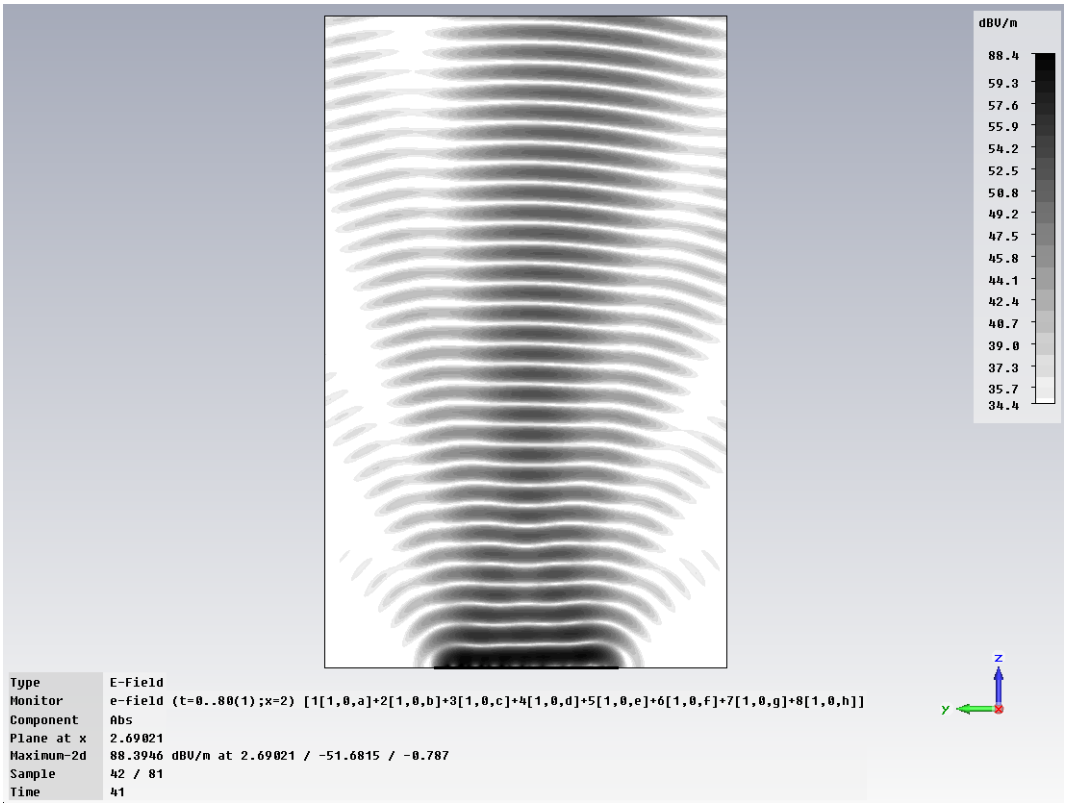

Figure 5.21: The transient E-field on plane x = 2 mm at 41 ns.

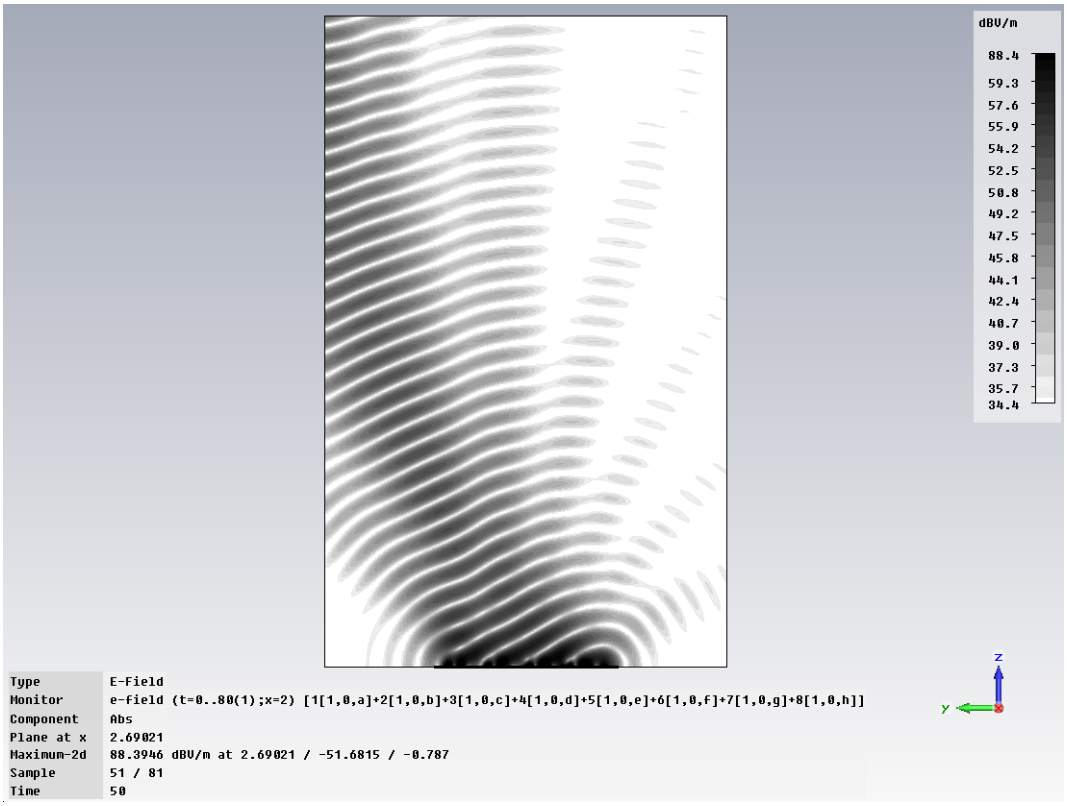

Figure 5.22: The transient E-field on plane x = 2 mm at 50 ns.

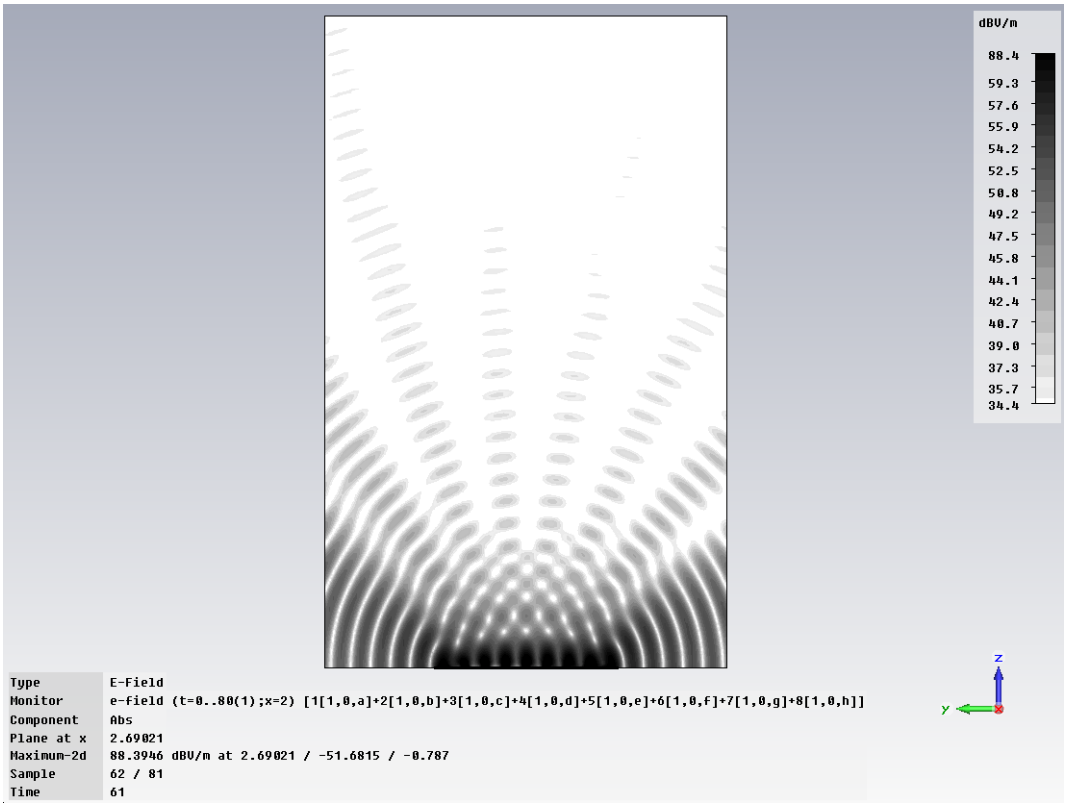

Figure 5.23: The transient E-field on plane x = 2 mm at 61 ns.

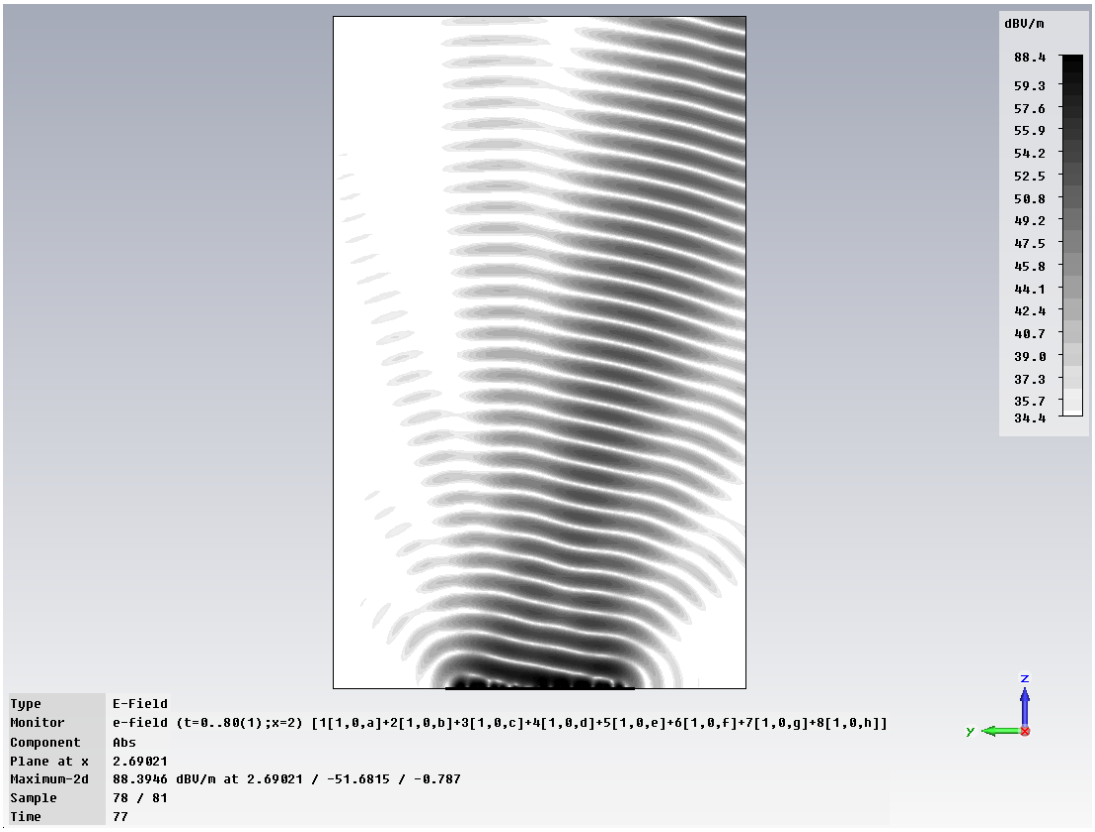

Figure 5.24: The transient E-field on plane x = 2 mm at 77 ns.

From Figures 5.17 to 5.24, it is shown that the main beam of an 8-element CW FDA ($N = 8,\ \Delta f = 0.025$ GHz, $\rho \approx 0.5$) finishes one entire anti-clockwise rotation in 40 ns, which is exactly the inverse of frequency shift $\Delta f = 0.025\text{GHz}$. As a result, the transient E-field distributions at 1 ns, 10 ns, 21 ns and 37 ns is identical to that at 41 ns, 50 ns, 61 ns and 77 ns respectively.

Moreover, the array factor $AF_{\Delta f,\rho}(\theta,t)\big|r = r_0$ is computed in Matlab with $N = 8,\ \Delta f = 0.025$ GHz, $\rho = 0.49,\ r_0 = 0.6$ m and depicted in Figure 5.25. One can see that at the main beam at $r_0 = 0.6$ m starts rotation from 2 ns and completes 2 cycles in 80 ns.

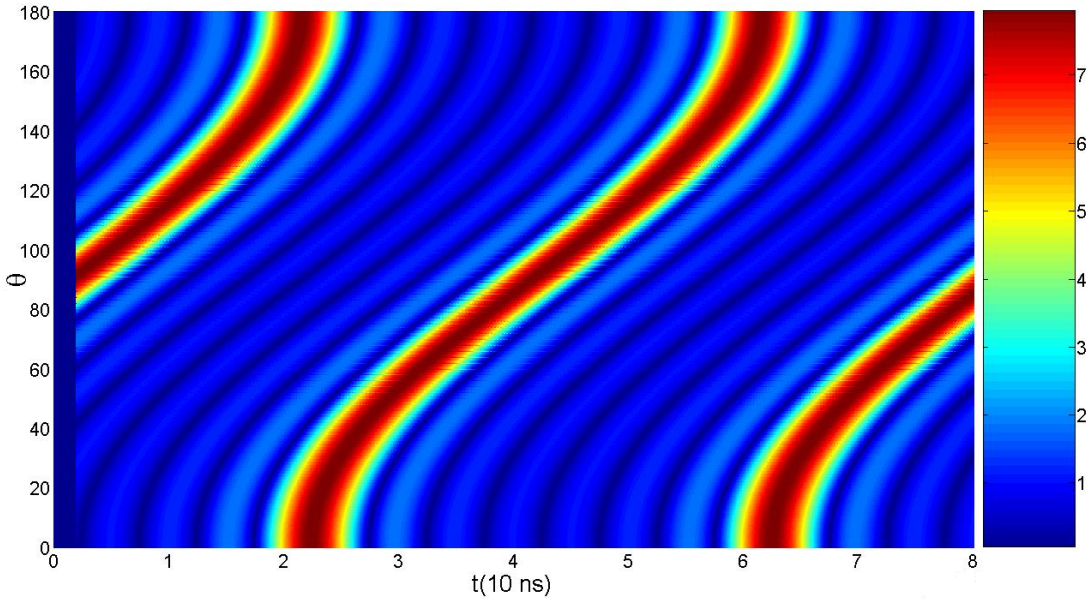

Figure 5.25: Matlab computed array factor $AF_{\Delta f,\rho}(\theta,t)\big|r=r_0$ with $N=8,\ \Delta f=0.025$ GHz, $\rho=0.49$ at $r_0=0.6$ m

The array factor at $r_0=0.6$ m, $t_0=21$ ns is shown in Figure 5.26 where the main beam is formed near 180° with 1 big side lobe pointing at 0°, same as the electromagnetic simulation result in Figure 5.19.

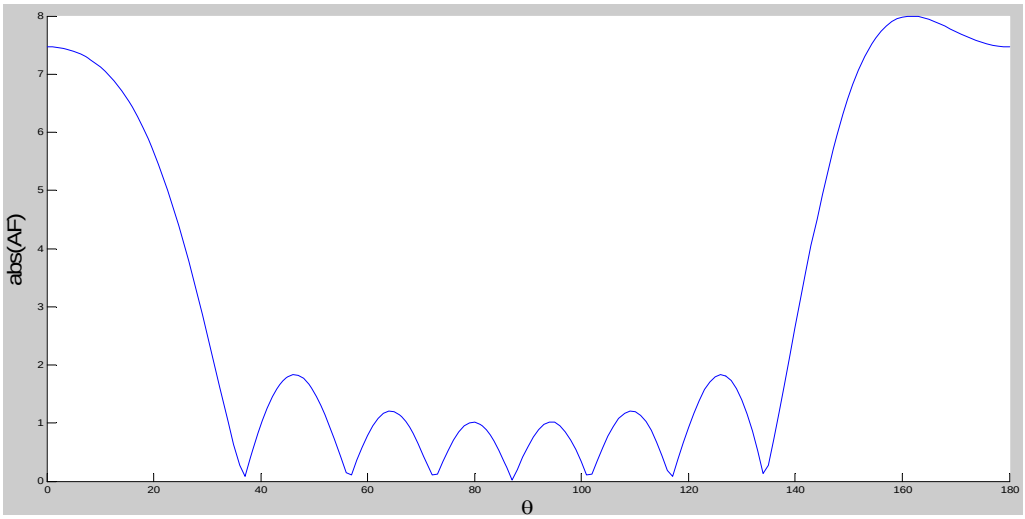

Figure 5.26: Matlab computed array factor with $N=8,\ \Delta f=0.025$GHz, $\rho=0.49$ at $r_0=0.6$ m, $t_0=21$ ns.

To give another example, the array factor at $r_0 = 0.6$ m, $t_0 = 41$ ns is shown in Figure 5.27. The main beam is formed near 90°, which again agrees with the electromagnetic simulation results in Figure 5.21.

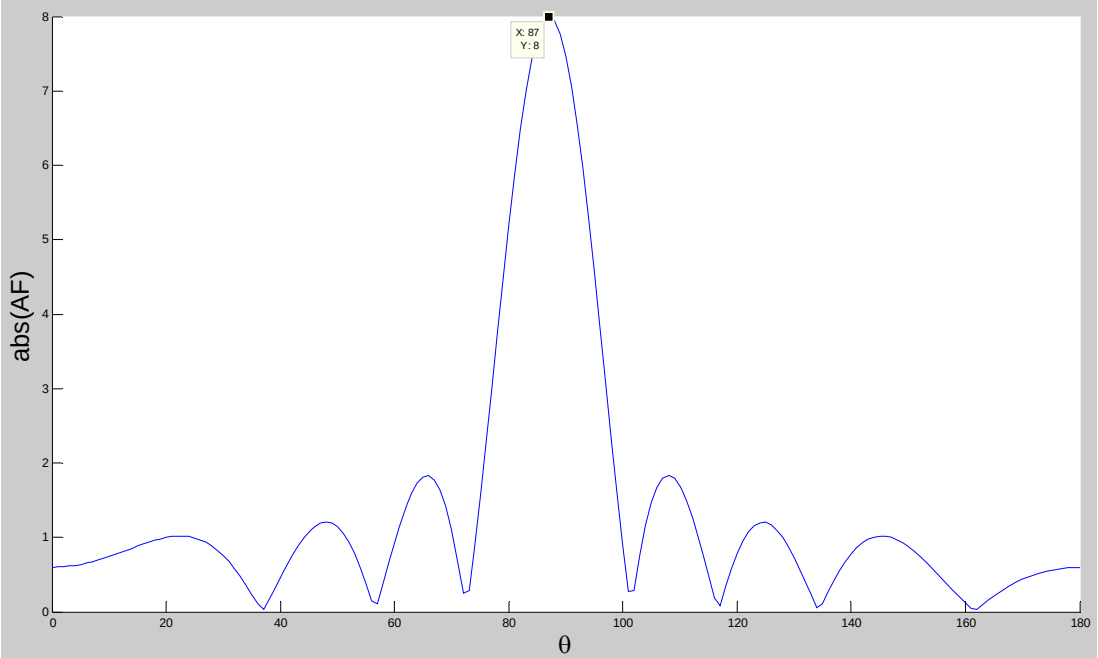

Figure 5.27: Matlab computed array factor with $N = 8$, $\Delta f = 0.025$ GHz, $\rho = 0.49$ at $r_0 = 0.6$ m, $t_0 = 41$ ns.

From the electromagnetic simulation results of an 8-element FDA, the periodically beam scanning phenomenon is again observed. Moreover, the relationship between scanning period and frequency shift is also verified at $\Delta f = 0.025$GHz. In order to make the argument more convincing, a 4-element FDA, which takes less time to simulate, is modeled and simulated with 2 different values of Δf. Corresponding scanning period is derived from simulation results, which is presented in Section 5.3.

5.3 Verification of Relationship between Scanning Period and Frequency Shift

In order to verify the relationship between scanning period and frequency increment of an FDA, a 4-element FDA as in Figure 5.28 is modeled in CST and the transient E-field on the plane x = 2 mm is examined. First the frequency increment Δf is set to be 0.02GHz. 4 sinuous signals, "sin1" to "sin4" in Figure 5.29, are fed to the 4-element array. Their frequencies are 7.98 GHz, 8 GHz, 8.02 GHz and 8.04 GHz respectively, as shown in Figure 5.30.

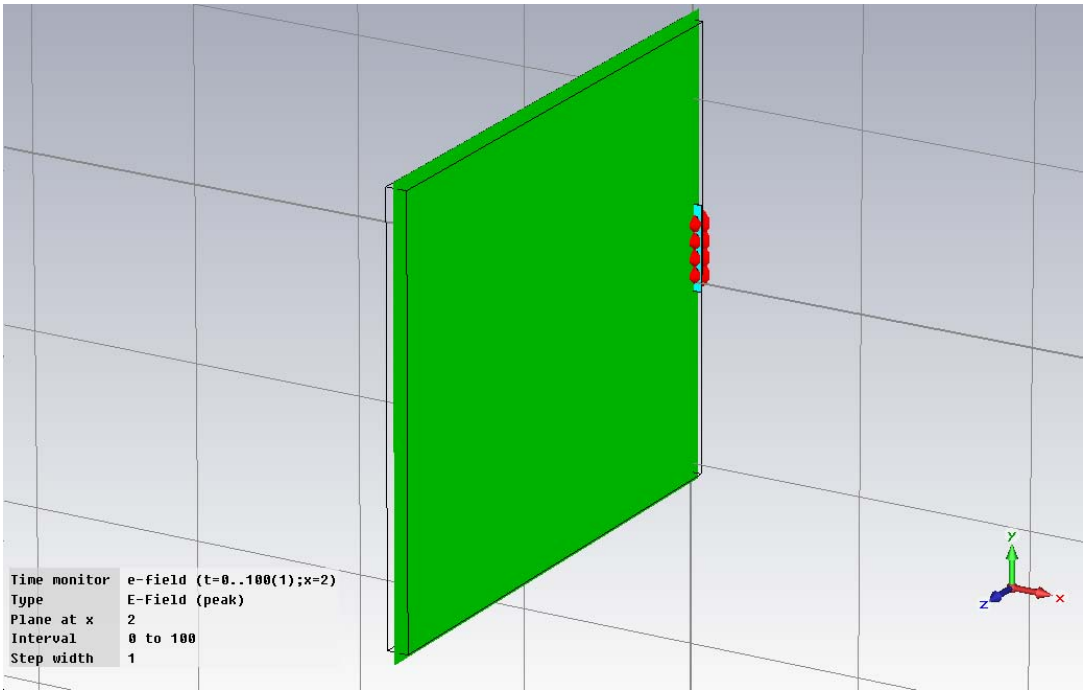

Figure 5.28: A 4-element FDA.

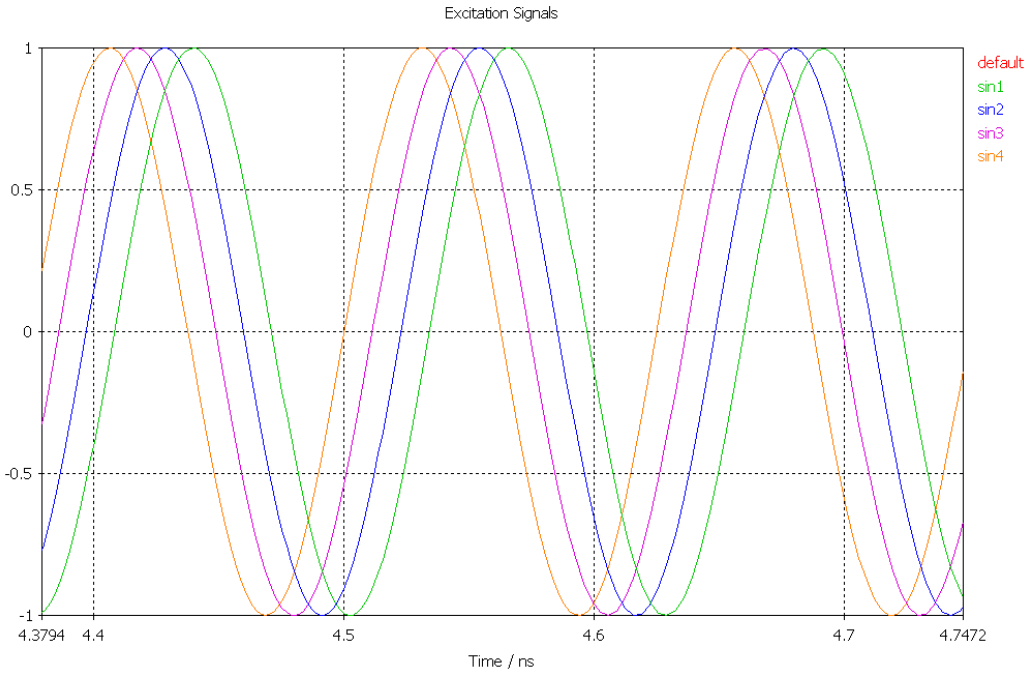

Figure 5.29: The 4 sinuous signals transmitted by the FDA.

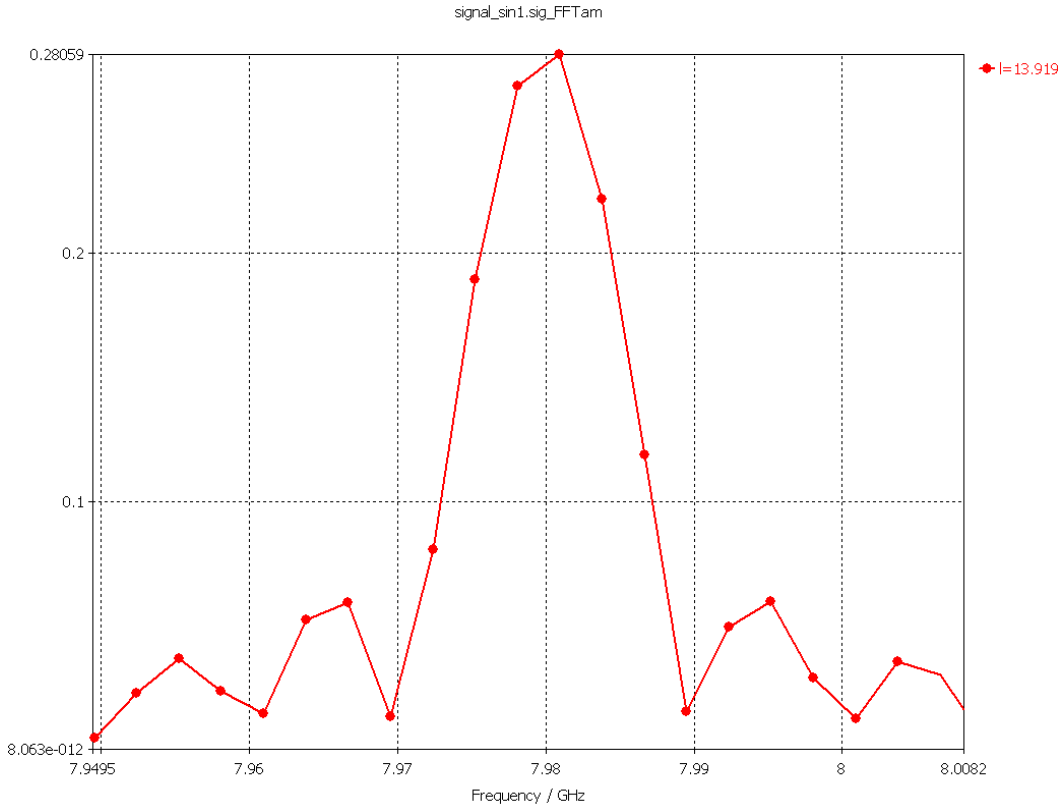

(a) The frequency of signal “sin1”: 7.98 GHz

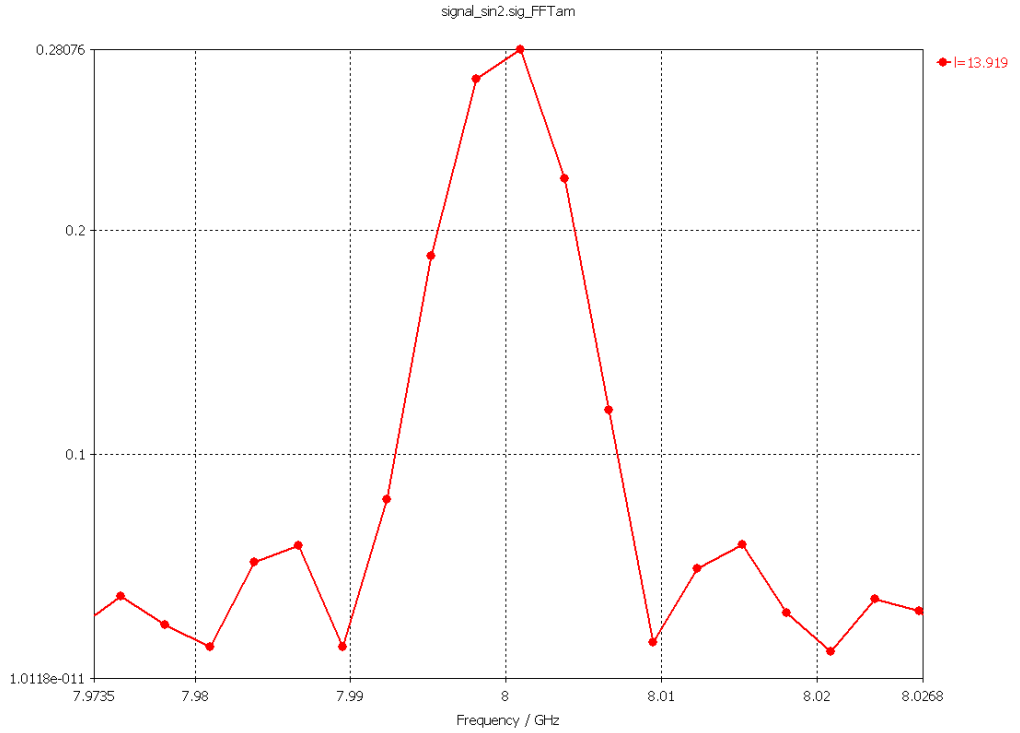

(b) The frequency of signal “sin2”: 8 GHz

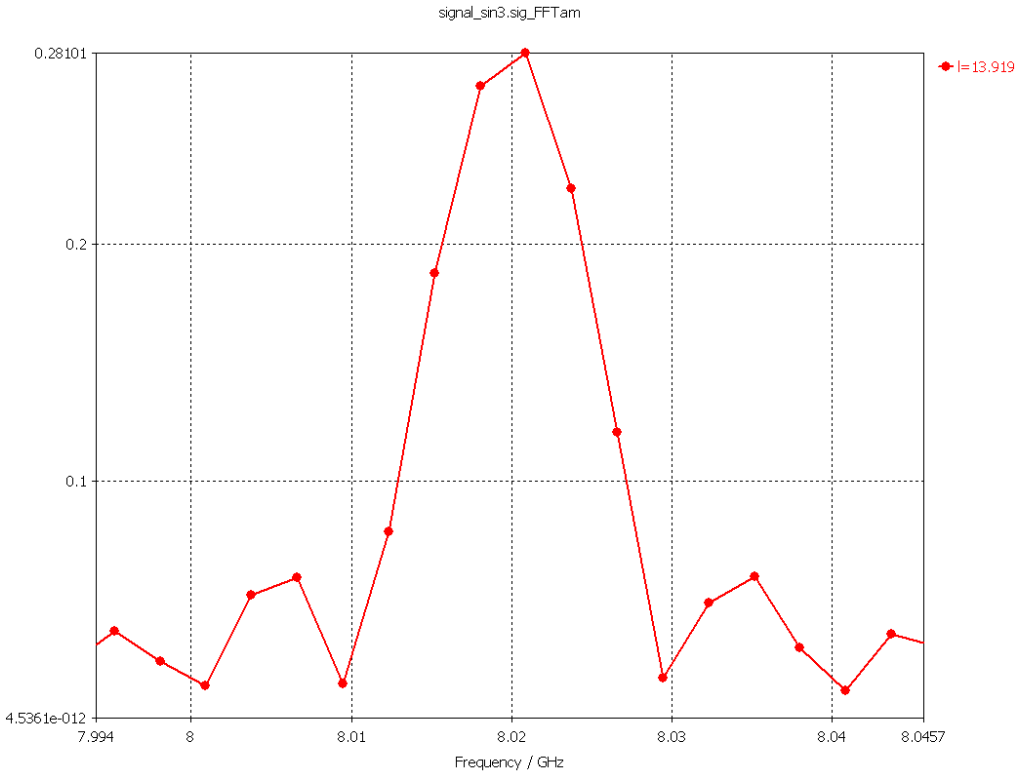

(c) The frequency of signal “sin3”: 8.02 GHz

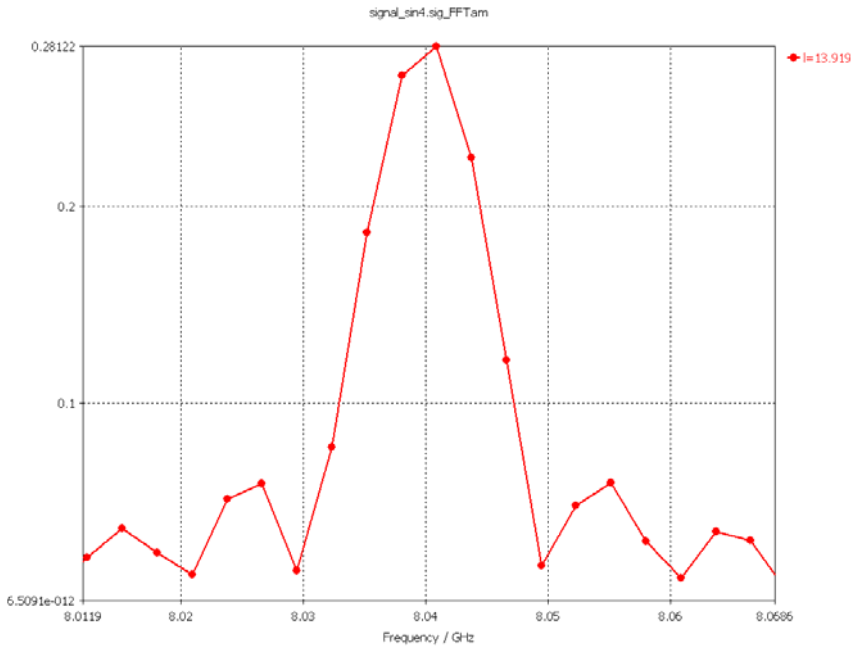

(d) The frequency of signal "sin4": 8.04 GHz

Figure 5.30: The spectrum of 4 sinuous signals with frequency shift of 0.02 GHz.

During the simulated time of 100 ns, the transient E-field at 1 ns, 11 ns, 27 ns, 41 ns, 51 ns, 61 ns, 77 ns and 91 ns are captured.

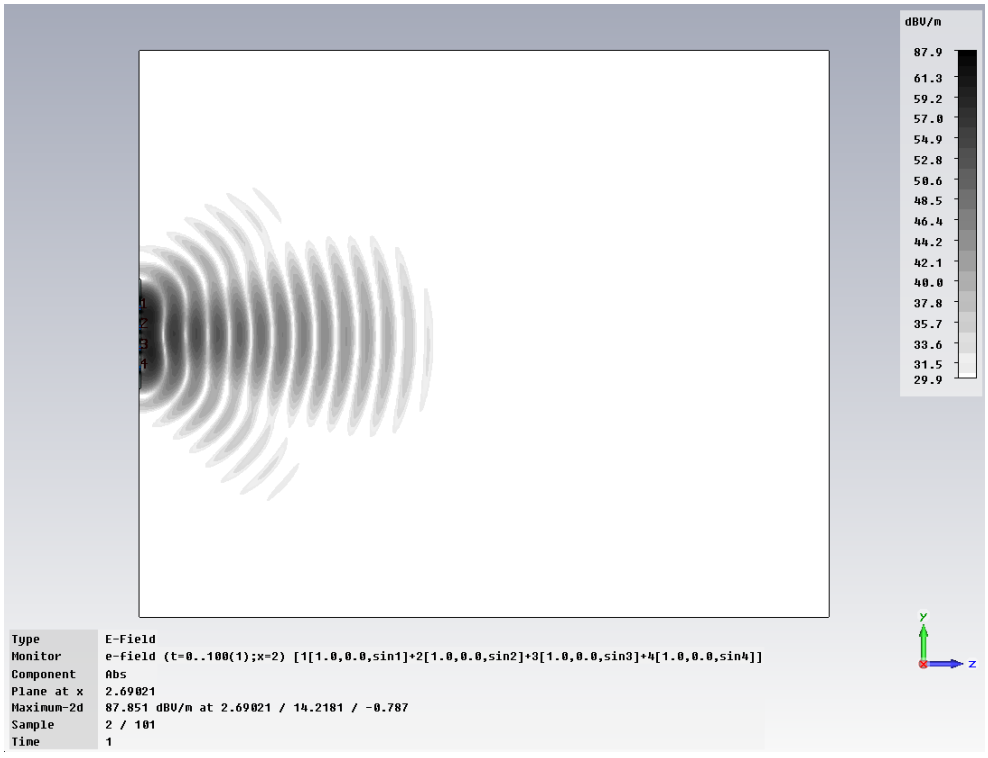

Figure 5.31: The transient E-field on plane x = 2 mm at 1 ns.

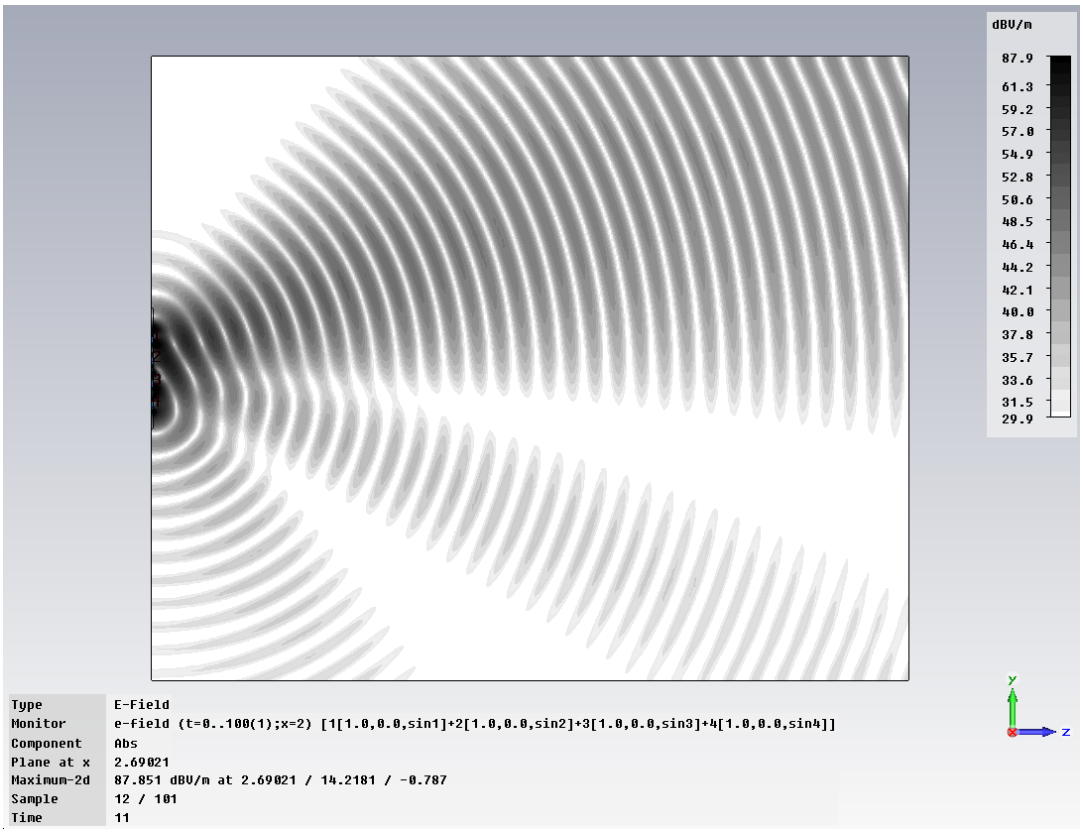

Figure 5.32: The transient E-field on plane x = 2 mm at 11 ns.

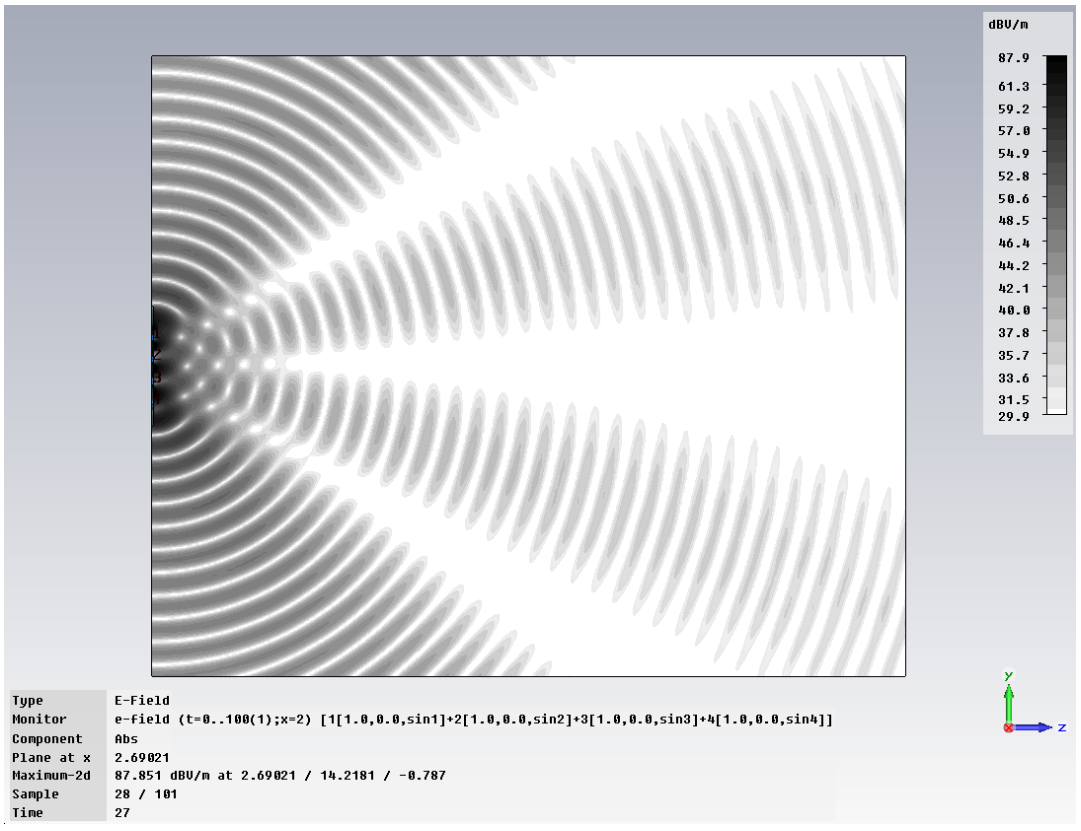

Figure 5.33: The transient E-field on plane x = 2 mm at 27 ns.

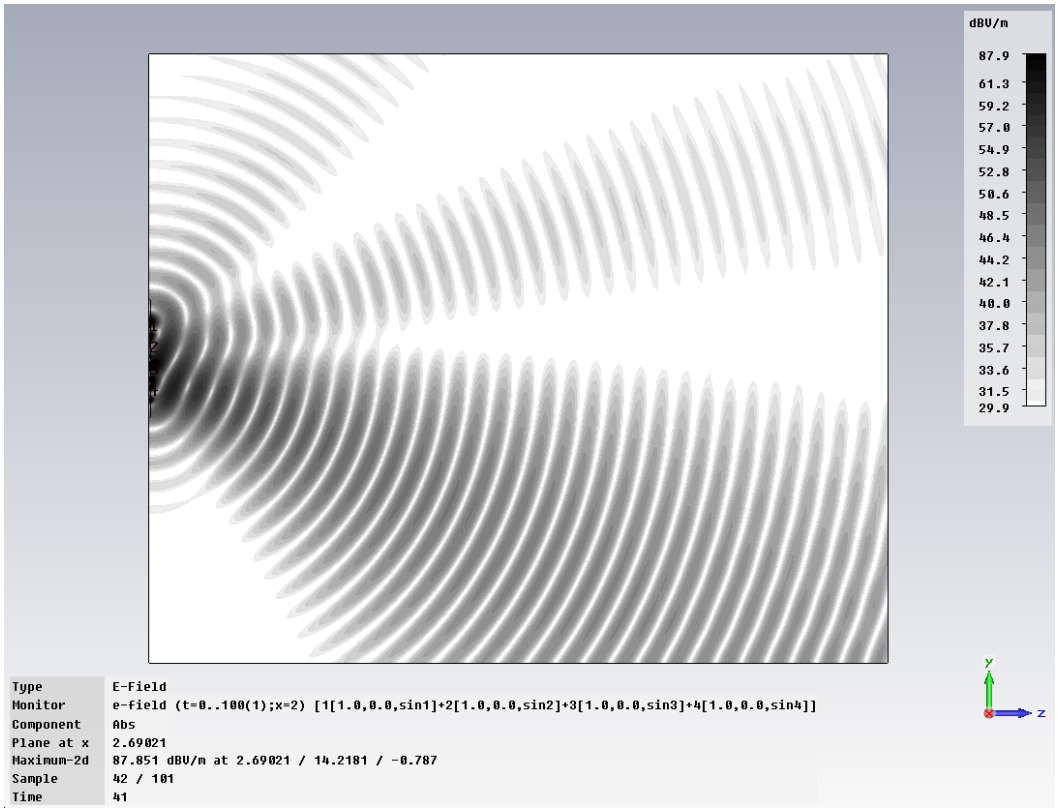

Figure 5.34: The transient E-field on plane x = 2 mm at 41 ns.

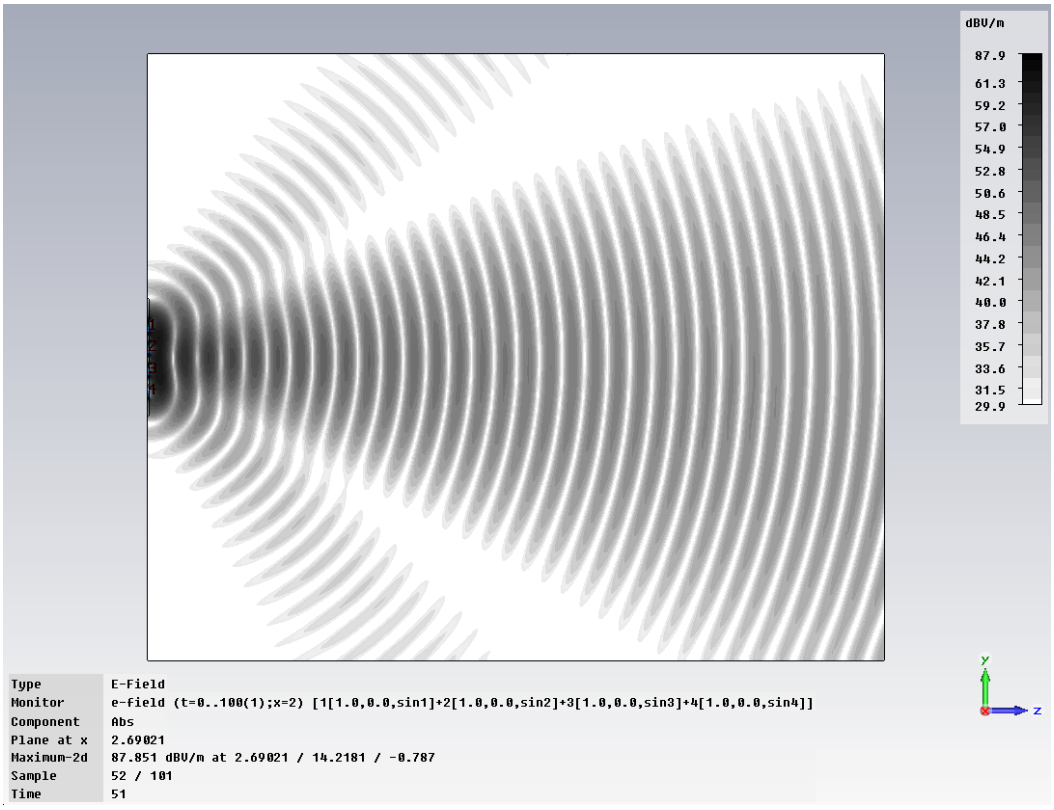

Figure 5.35: The transient E-field on plane x = 2 mm at 51 ns.

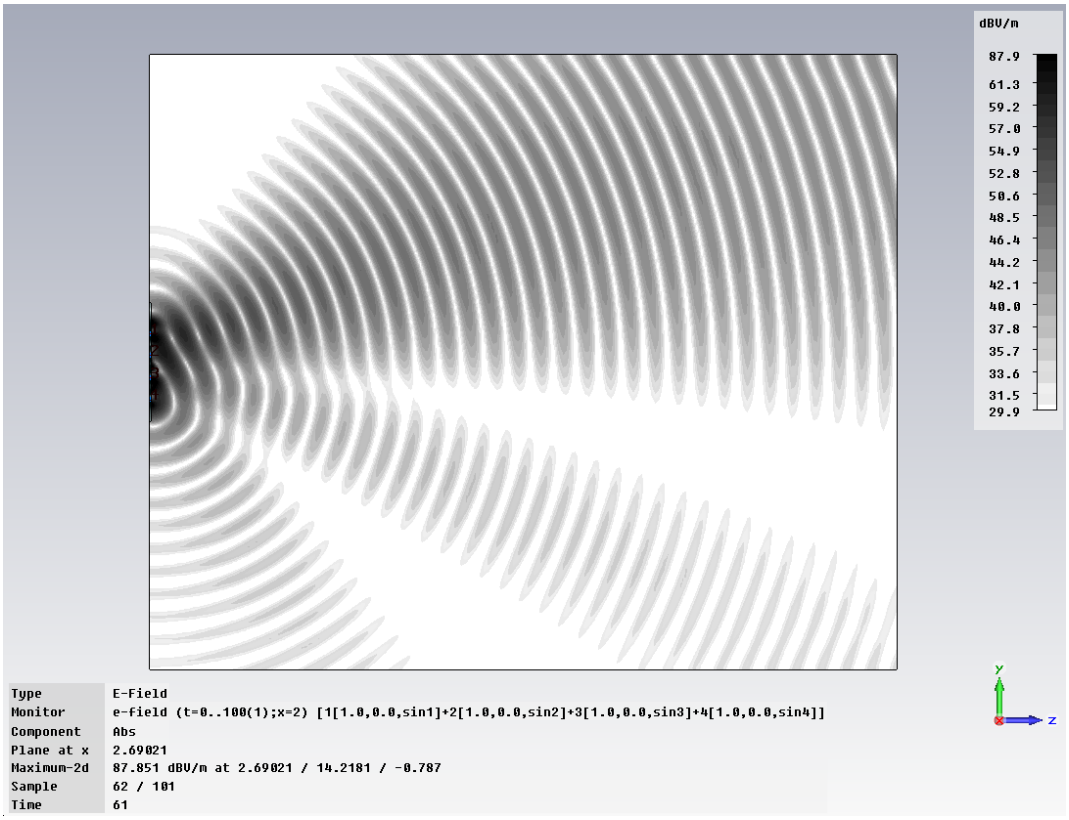

Figure 5.36: The transient E-field on plane x = 2 mm at 61 ns.

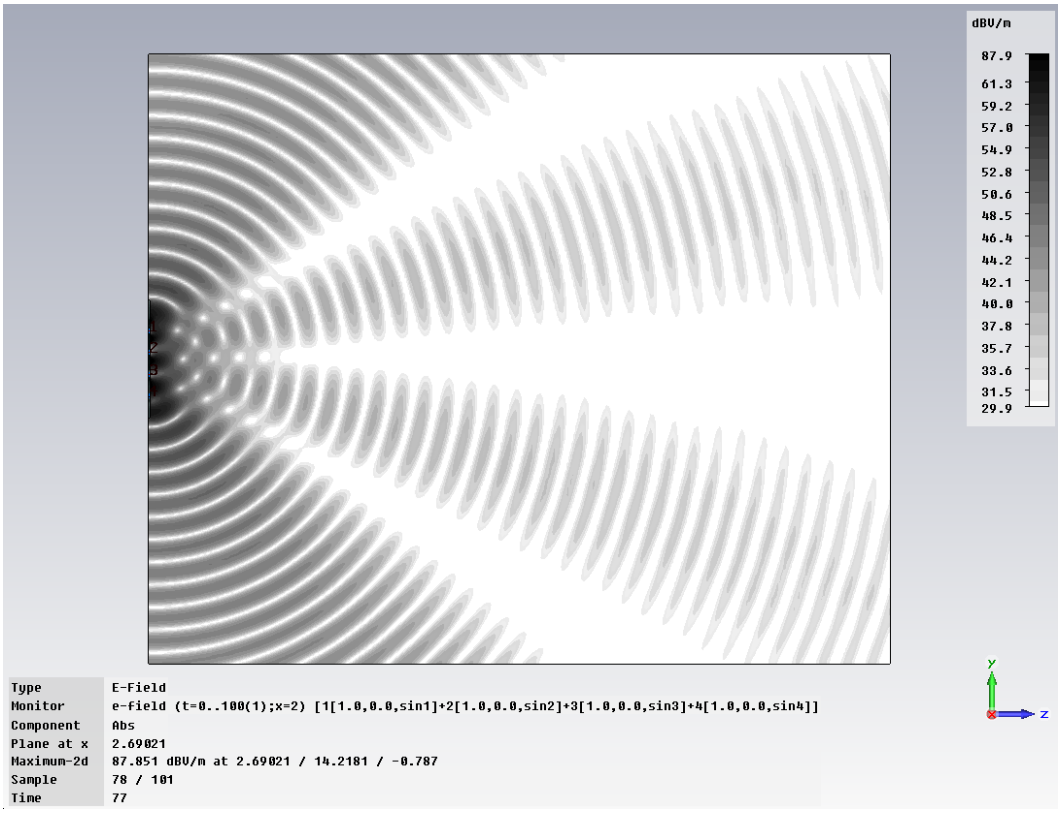

Figure 5.37: The transient E-field on plane x = 2 mm at 77 ns.

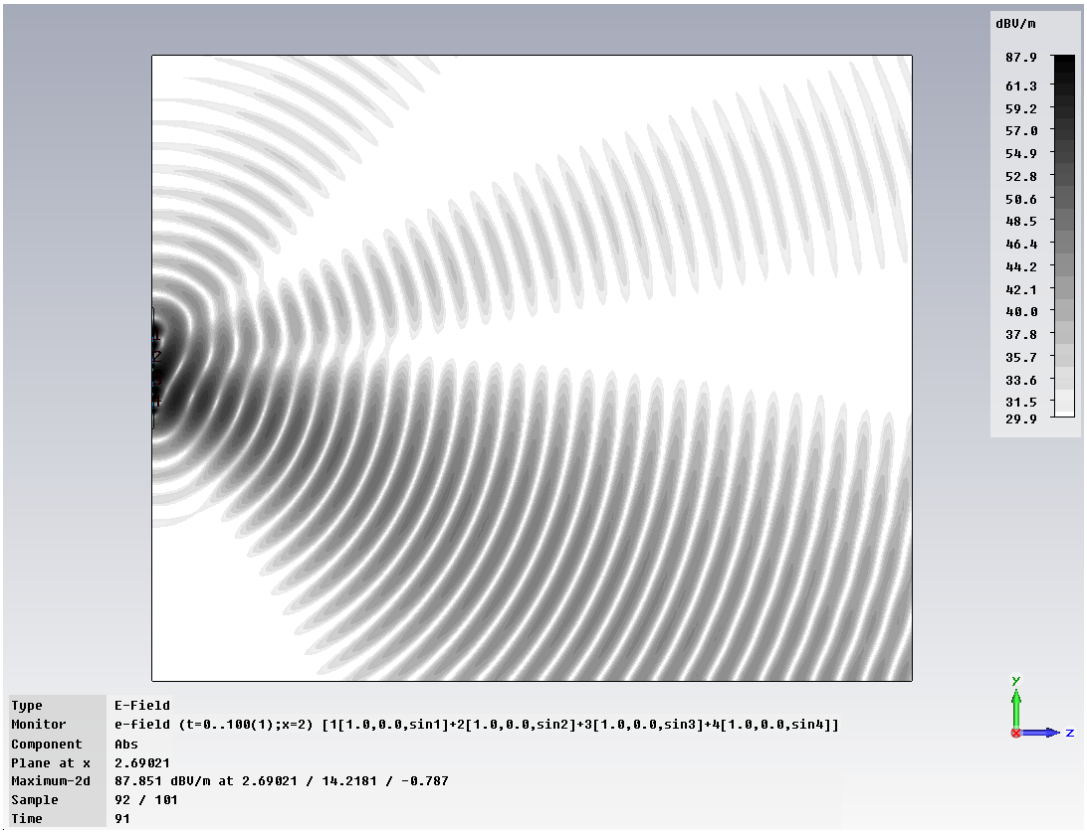

Figure 5.38: The transient E-field on plane x = 2 mm at 91 ns.

From Figures 5.31 to 5.38, it is shown that the beam scanning period of a 4-element FDA with ($\Delta f = 0.02$ GHz) is 50 ns, which is exactly the inverse of frequency shift Δf. As a result, the transient E-field distributions at 1 ns, 11 ns, 27 ns and 41 ns are identical to that at 51 ns, 61 ns, 77 ns and 97 ns respectively.

Then the frequency shift Δf is changed to 0.01 GHz and the frequencies of the 4 sinuous signals are 7.99 GHz, 8 GHz, 8.01 GHz and 8.02 GHz respectively as in Figure 5.39.

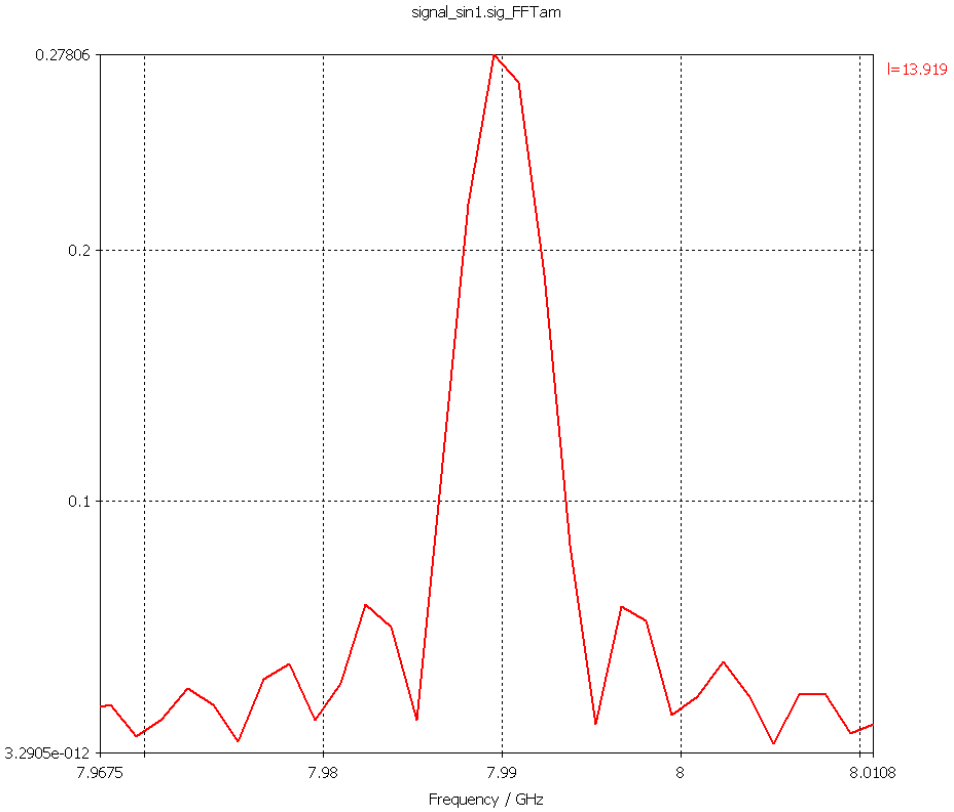

(a) The frequency of signal “sin1”: 7.99 GHz

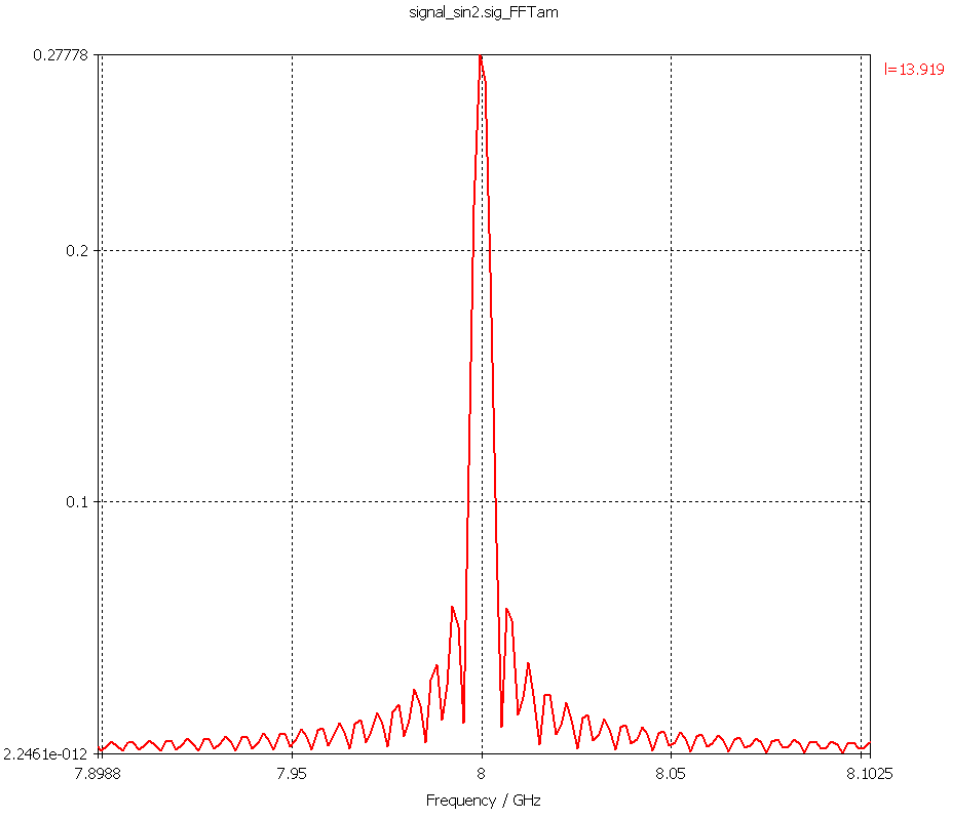

(b) The frequency of signal “sin2”: 8 GHz

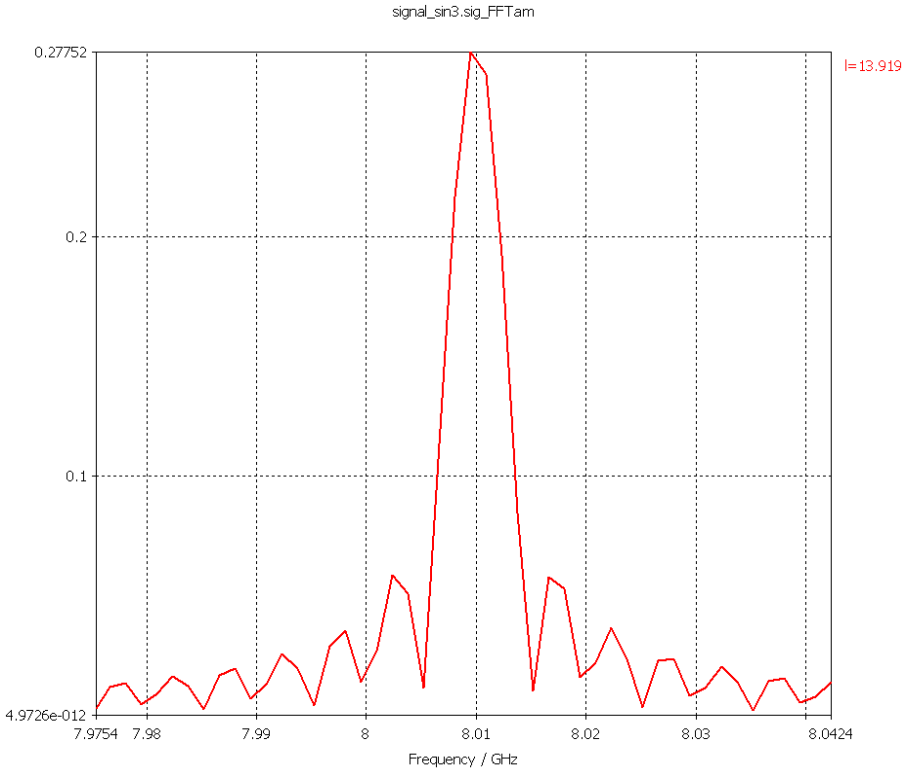

(c) The frequency of signal “sin3”: 8.01 GHz

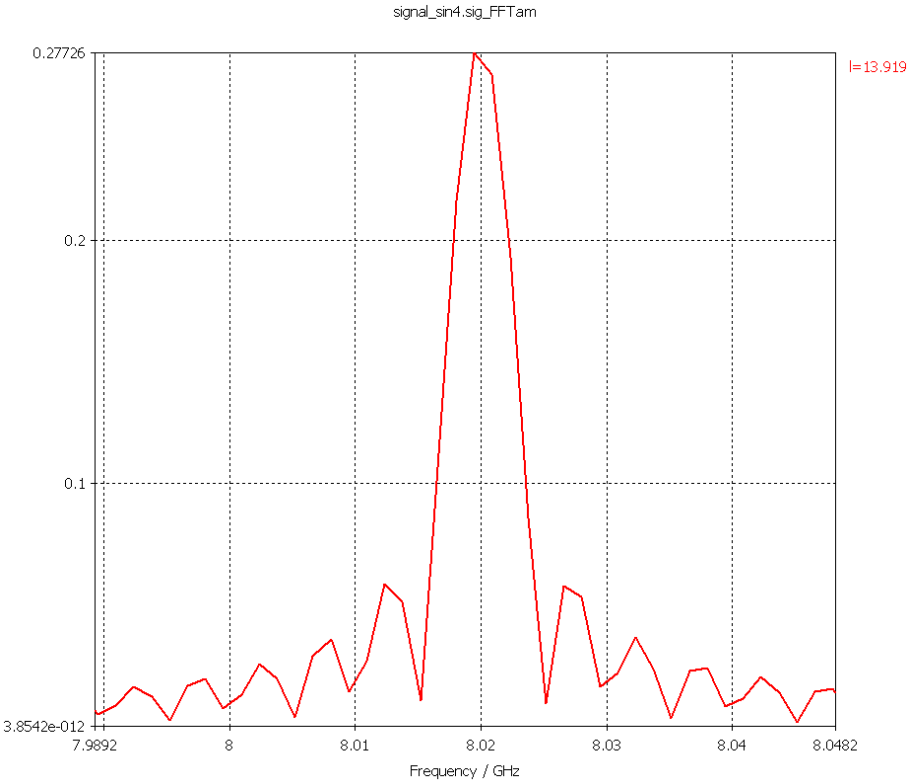

(d) The frequency of signal “sin4”: 8.02 GHz

Figure 5.39: The spectrum of 4 sinuous signals with frequency shift of 0.01 GHz.

During the simulated time of 200 ns, the transient E-field at 1 ns, 21 ns, 52 ns, 84 ns, 101 ns, 121 ns, 152 ns and 184 ns are captured.

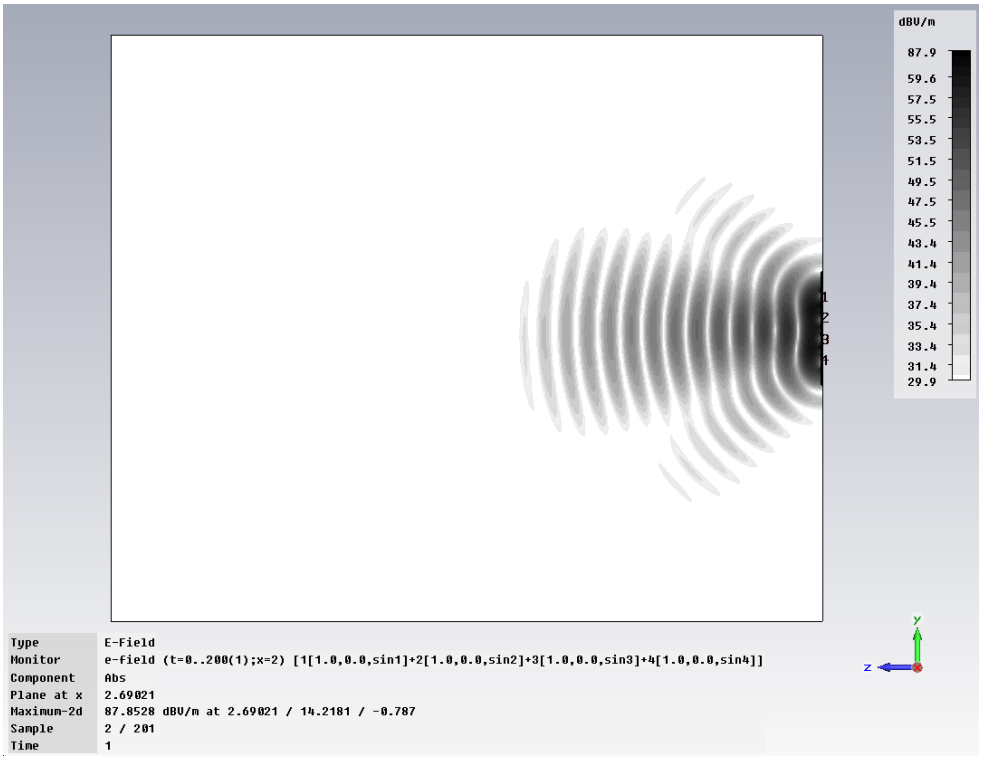

Figure 5.40: The transient E-field on plane x = 2 mm at 1 ns.

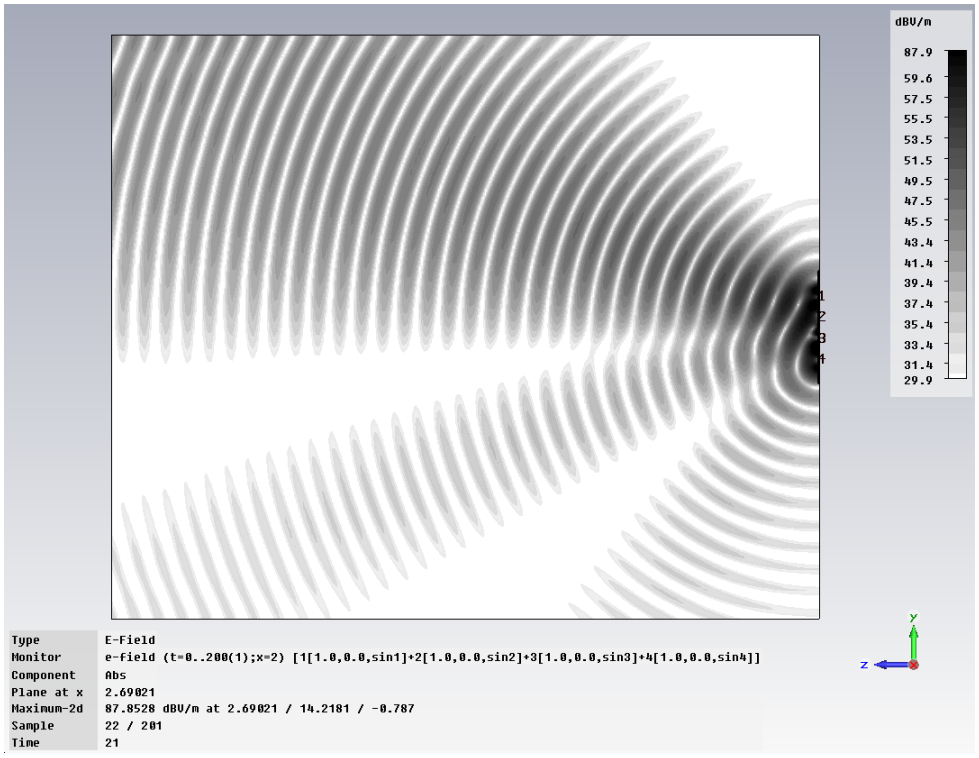

Figure 5.41: The transient E-field on plane x = 2 mm at 21 ns.

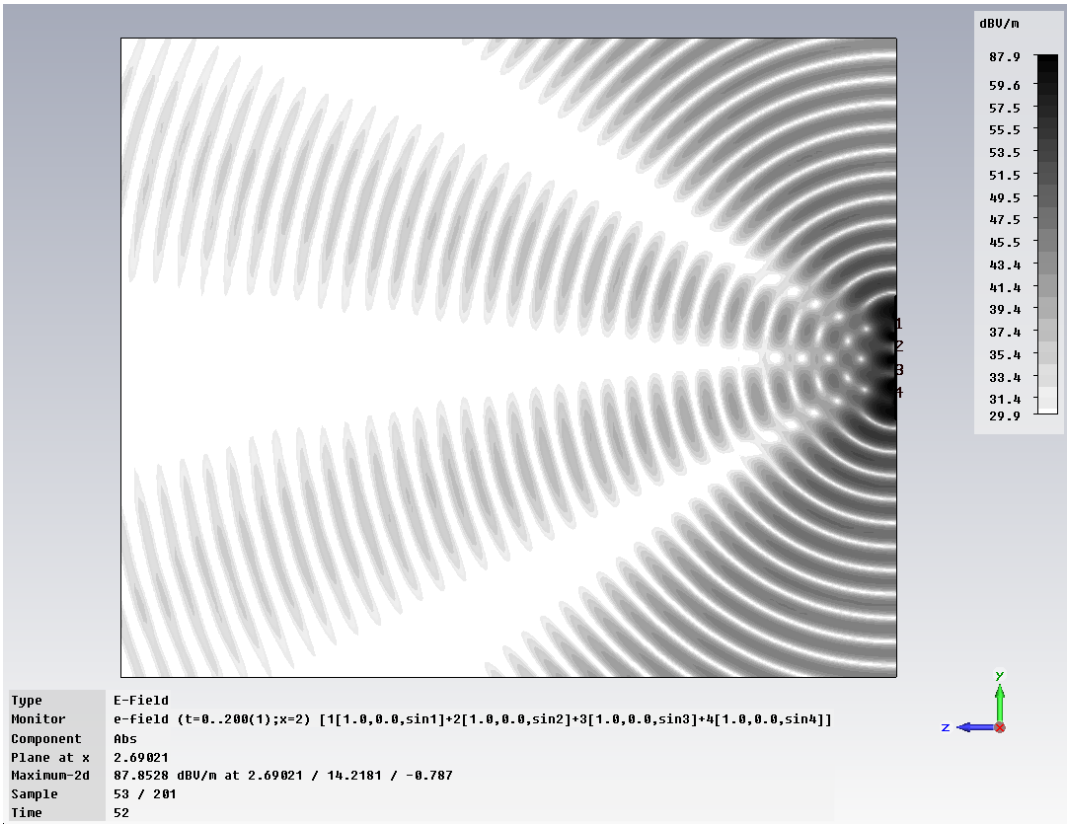

Figure 5.42: The transient E-field on plane x = 2 mm at 52 ns.

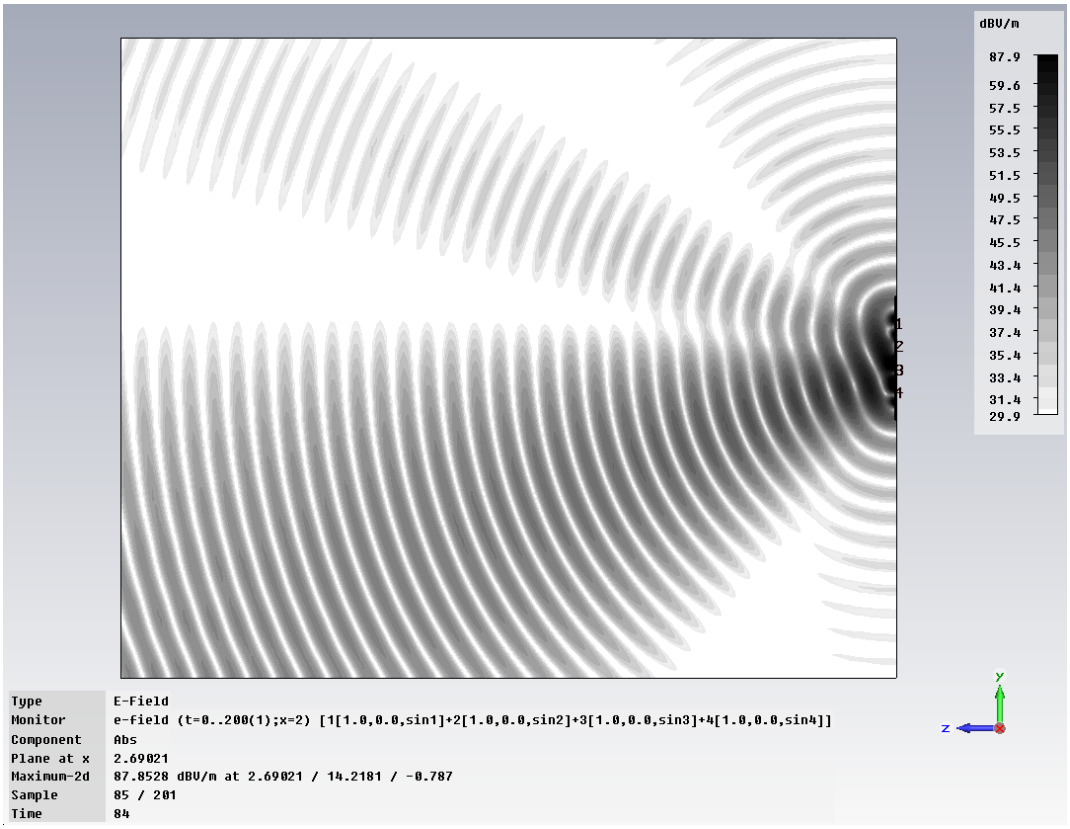

Figure 5.43: The transient E-field on plane x = 2 mm at 84 ns.

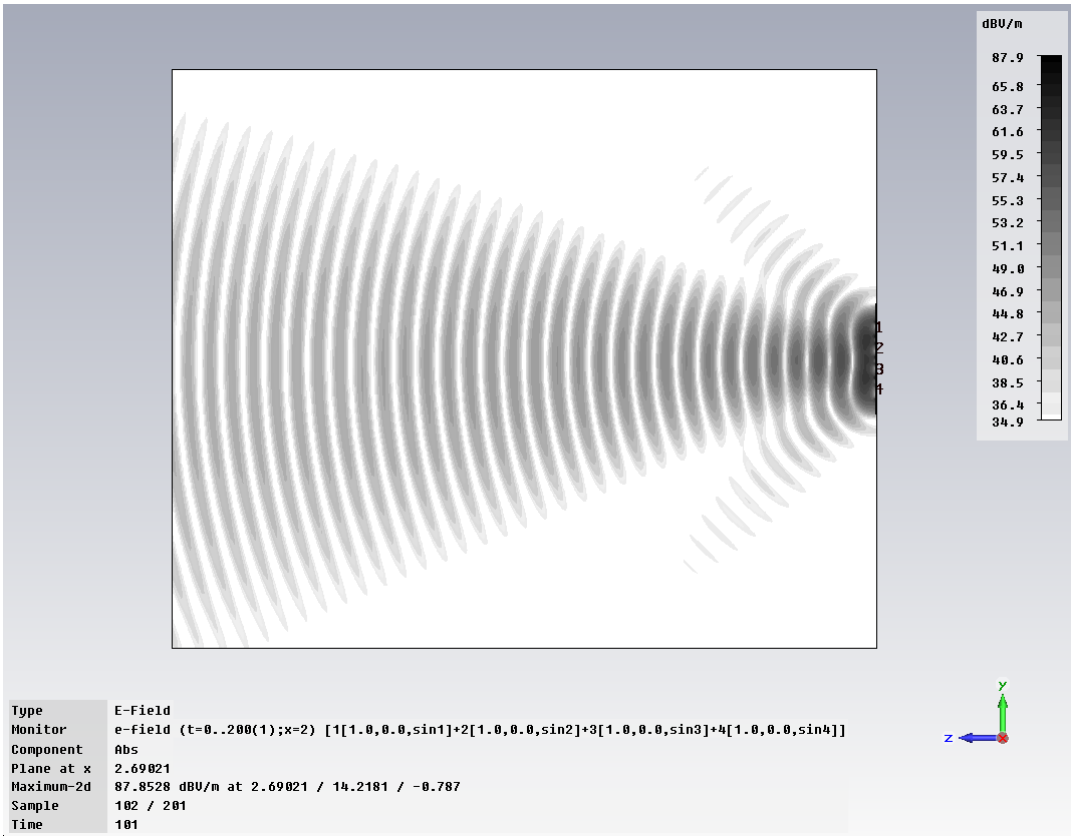

Figure 5.44: The transient E-field on plane x = 2 mm at 101 ns.

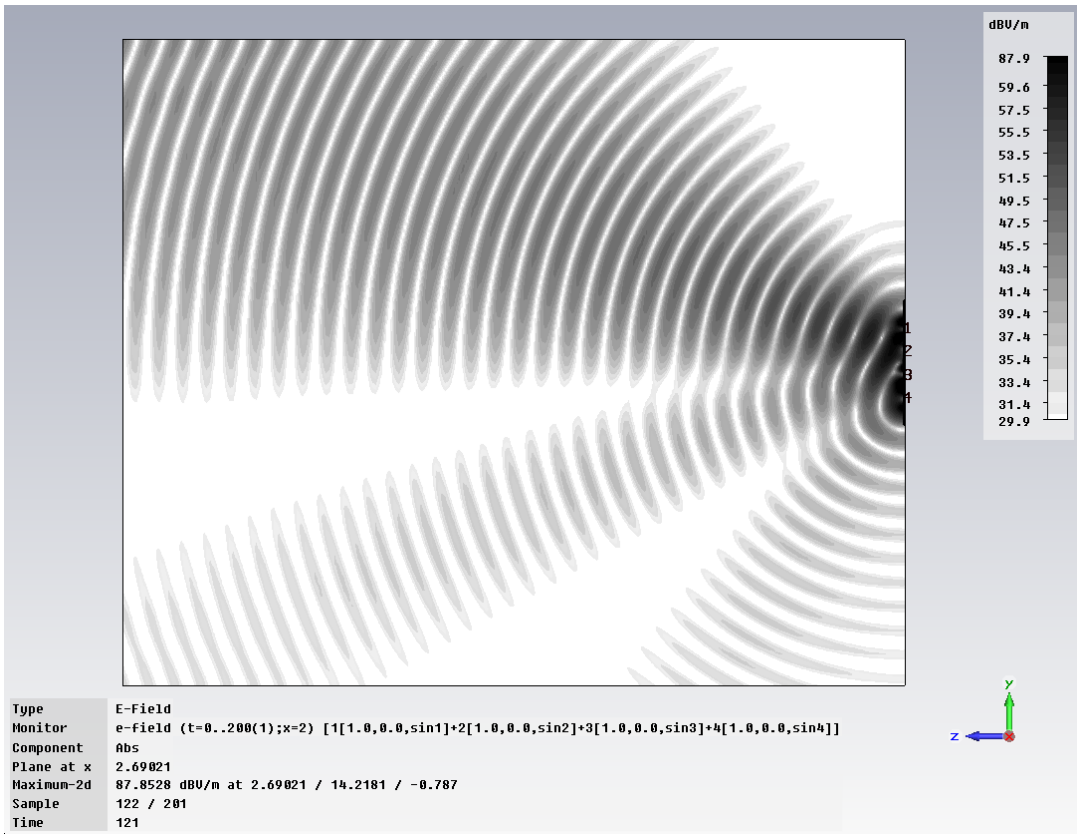

Figure 5.45: The transient E-field on plane x = 2 mm at 121 ns.

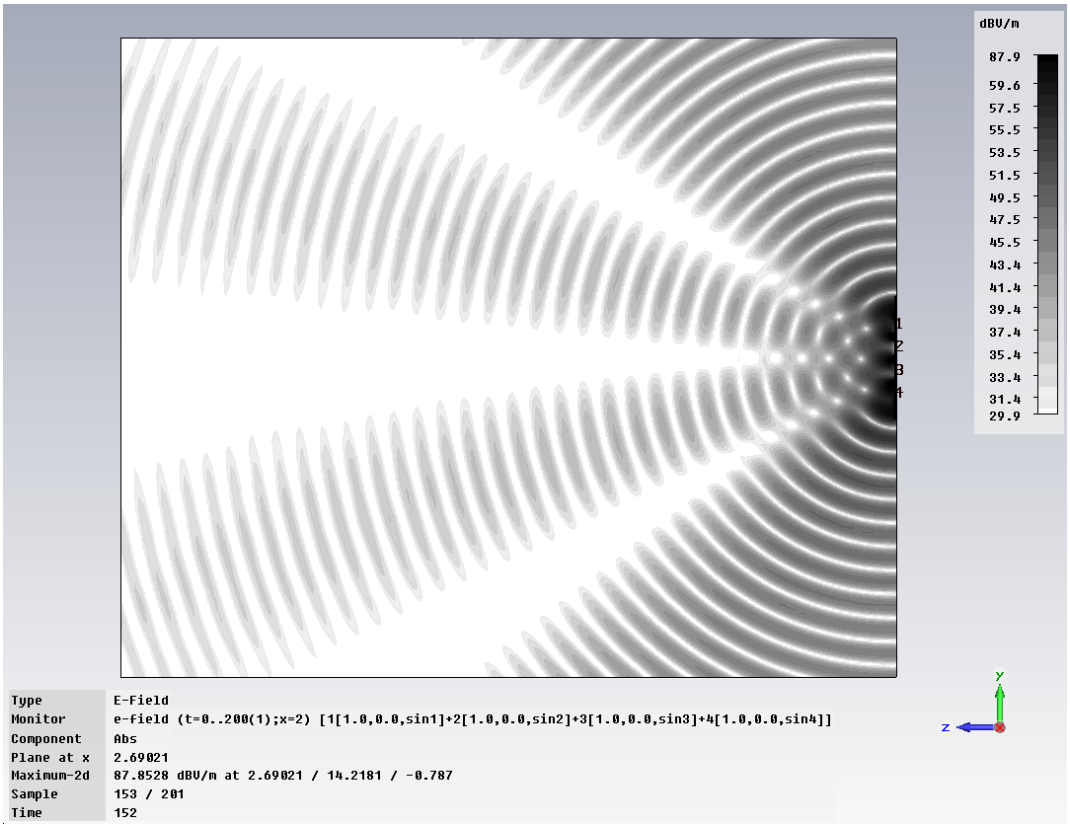

Figure 5.46: The transient E-field on plane x = 2 mm at 152 ns.

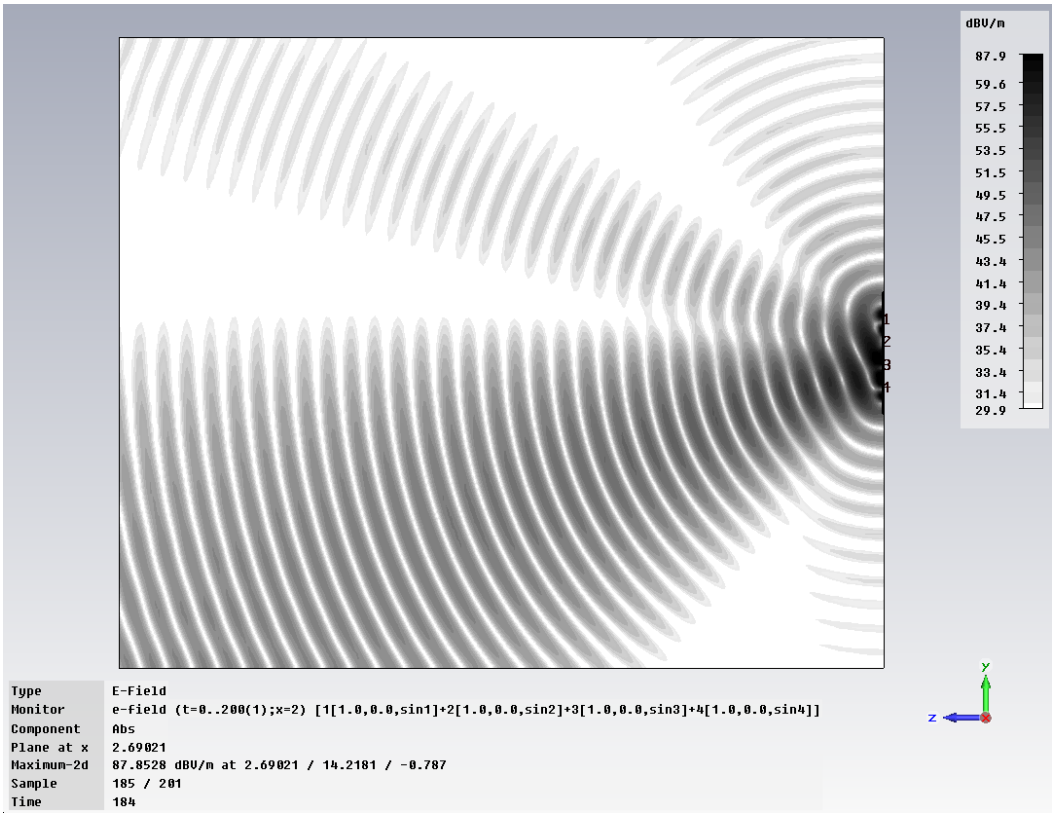

Figure 5.47: The transient E-field on plane x = 2 mm at 184 ns.

When $\Delta f = 0.01\,\text{GHz}$, the scanning period of is 100 ns (see Figures 5.40-5.46), which is again the inverse of frequency shift Δf. With the value of Δf being 0.025GHz, 0.02GHz and 0.01GHz, the scanning period of FDA shown by the electromagnetic simulation results is 40 ns, 50 ns and 100 ns respectively. Therefore the relationship between scanning period has been verified to be the inverse of Δf.

5.4. Summary

In this Chapter, the CW FDA is modeled and simulated in CST Microwave Studio where an 8-element linear microstrip patch antenna array is fed by sinuous signals whose frequencies are separated by $\Delta f = 0.025\,\text{GHz}$. With patch antenna element replacing isotropic point sources, periodically beam scanning phenomenon is still observed from electromagnetic simulation results. The scanning period is 40 *ns*, which is the inverse of Δf. Moreover, a 4-element FDA is simulated with 2 values of frequency shift. In both cases, the scanning period is the inverse of frequency shift. Thus, the relationship between scanning period and frequency shift Δf has been verified by electromagnetic simulation. The simulated S-parameters show that the mutual coupling between elements when the space is half wavelength is below -20dB, which means that mutual coupling causes very small deviation to single element's performance. The EM simulation results not only verify the theory of FDA in Chapter 4, but also provide proof for FDA's physical feasibility.

In Chapter 6, the discussions on FDA are broadened by changing CW signals to pulse signals. When a rectangular pulse is transmitted by an FDA given Δf and ρ,

the FDA's beam pattern during the pulse is examined. It is shown that when certain constraint is put on the pulse width, an FDA transmitting a pulse signal can be used to achieve beam forming. The transmitter employs an FDA so that a pulse signal can be transmitted to a desired direction; while at the receiver side a single carrier is required to demodulate the received signals.

Chapter 6

Beam Forming Using FDA

In Chapters 4 and 5, the discussion and analysis on the characteristics of FDA are made in the case of CW signals. In this Chapter, based on the results under CW condition, the mechanism of using FDA for beam forming purpose is explained.

6.1 Limitation of CW FDA

To better explain the limitation of CW FDA, we begin with conventional phased array. This can be done by assigning a zero value to the parameter Δf of an FDA $N = 8,\ \Delta f = 0$ kHz, $\rho = 0.45$. A zero value of Δf turns an FDA into a conventional single carrier array with zero phase shift, which results in a broadside radiation according to Section 3.1.4.

With $\Delta f = 0$, $AF(\theta, t)_{\Delta f, \rho} | r = r_0$ and $AF(\theta, r)_{\Delta f, \rho} | t = t_0$ are computed with $r_0 = 3 \times 10^5$ m , $t_0 = 3$ ms respectively. It is shown in Figure 6.1 and 6.2 that a conventional CW phased array has a time-range independent array factor. The angle position of maximum (broadside in Figure 6.3) stays unchanged at any time or distance.

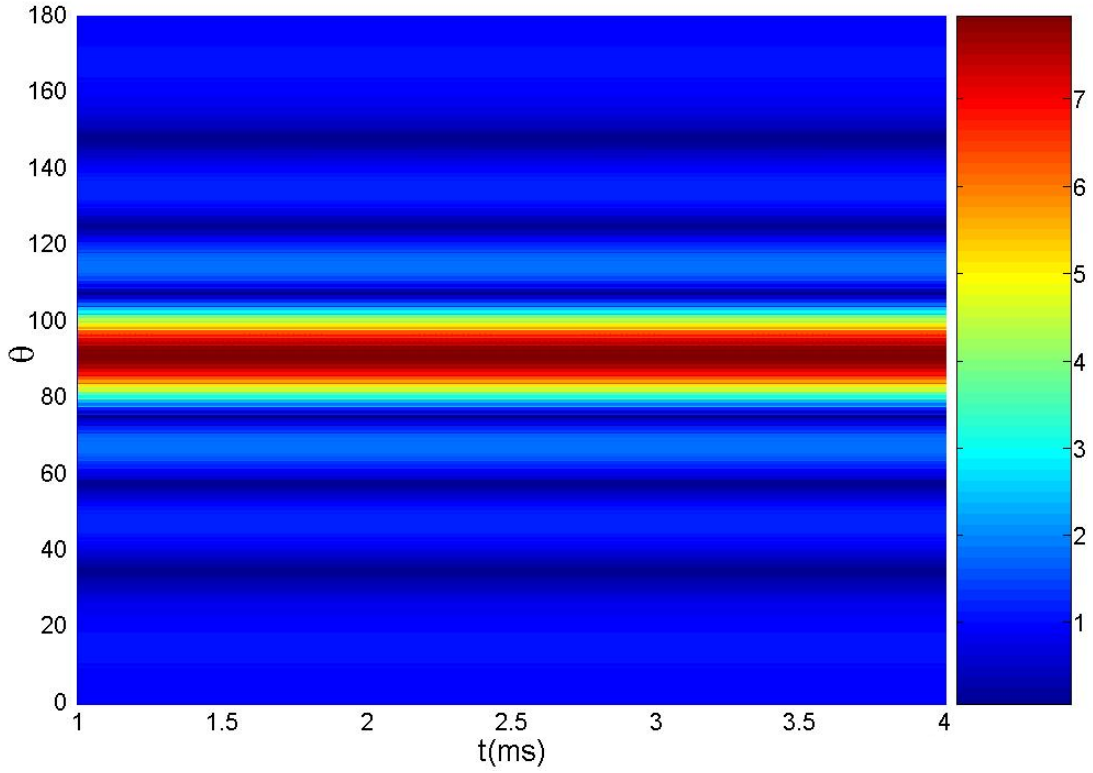

Figure 6.1: Array factor of a phased array at $r_0 = 3\times10^5\,\mathrm{m}$.

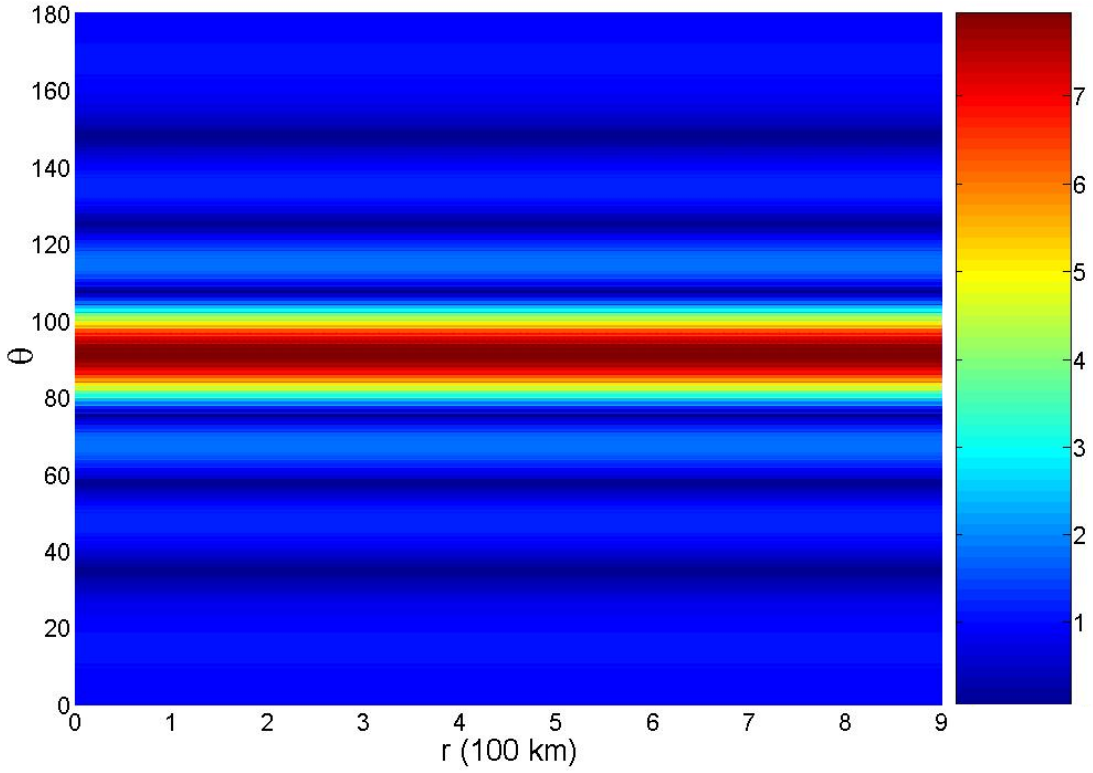

Figure 6.2: Array factor of a phased array at $t_0 = 3\ \mathrm{ms}$.

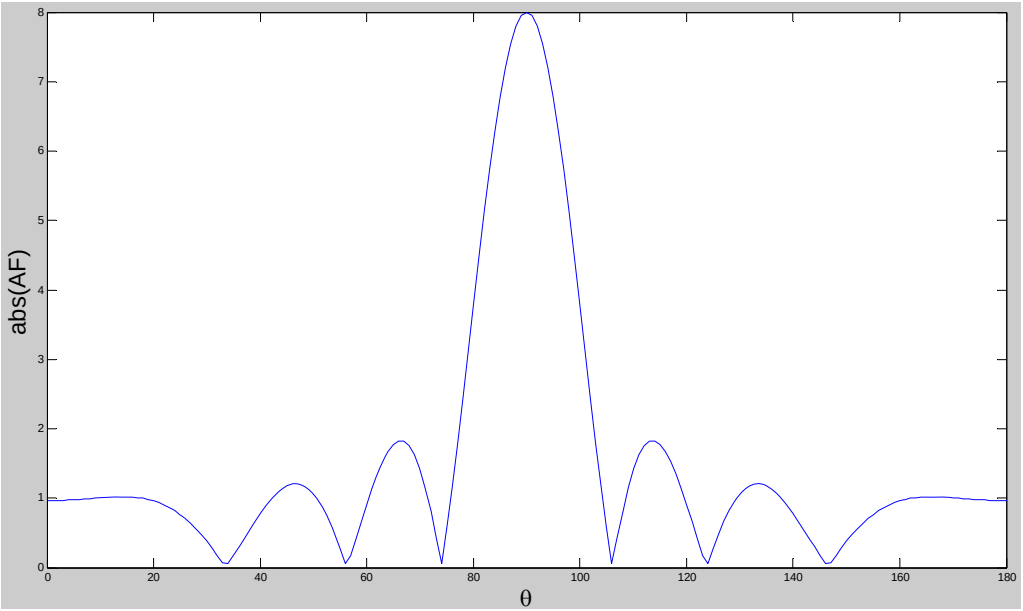

Figure 6.3: Main beam formed at broadside direction using a phased array.

Then the FDA ($N = 8,\ \Delta f = 1$ kHz, $\rho = 0.45$) is examined as comparison. The array factors at 2 different distances $r_0 = 3\times10^5 m$ and $r_1 = 4.5\times10^5 m$ are computed.

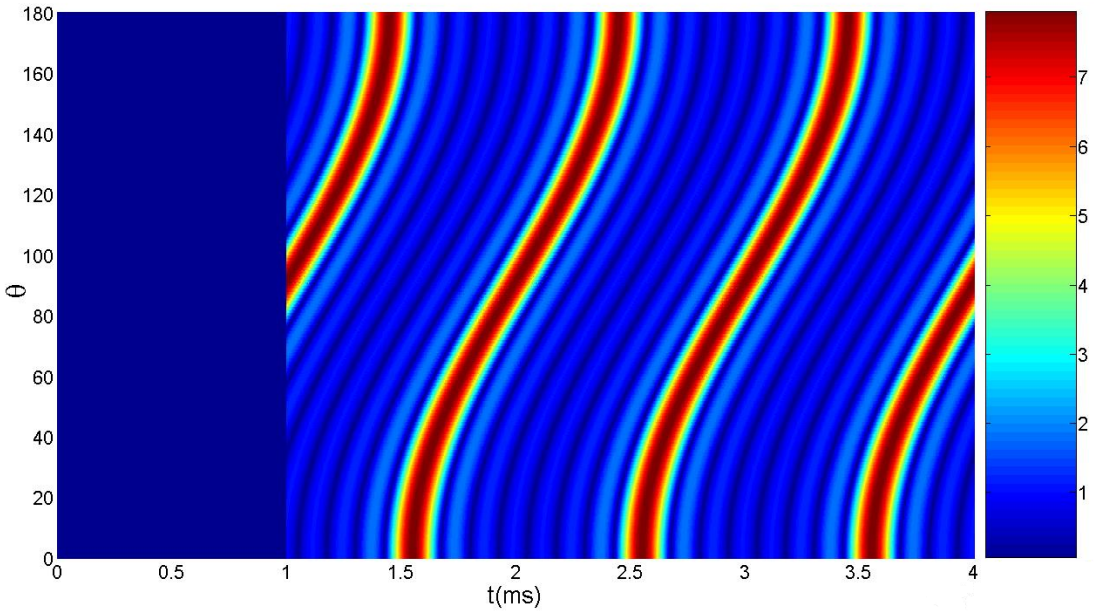

Figure 6.4: Array factor at $r_0 = 3\times10^5$ m .

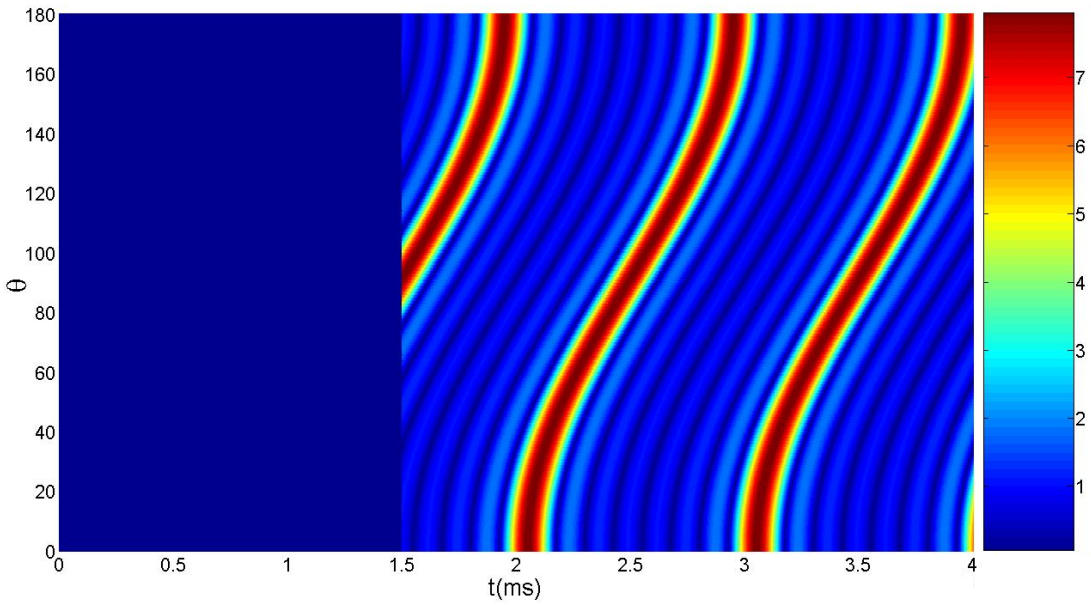

Figure 6.5: Array factor at $r_1 = 4.5\times10^5\,\mathrm{m}$.

From Figures 6.4 and 6.5, one can see that the only difference between $AF(\theta,t)_{\Delta f,\rho}\big|r=r_0$ *and* $AF(\theta,t)_{\Delta f,\rho}\big|r=r_1$ is the delay of starting time, which is caused by range difference. Although the CW FDA has a main beam all the time, due to periodicity in the long run the average energy received at all directions is same. In other words, the FDA only has a transient gain. This is the limitation of CW FDA. However, the periodicity and continuity of $AF(\theta,t,r)_{\Delta f,\rho}$ make it possible to use FDA for applications require beam forming . This will be discussed in next session.

6.2 Concept of an FDA Transmitting a Pulse

The concept of an FDA transmitting a pulse is explained in Figure 6.6 where time-limited ($t \in [t_s, t_e]$) diverse frequency signals are transmitted by an *N*-element FDA with specific parameters of Δf and ρ. This can be achieved by modulating the CW signal at each element with a rectangular pulse ($t \in [t_s, t_e]$). For CW signals, one can take t_s as 0 and t_e infinite.

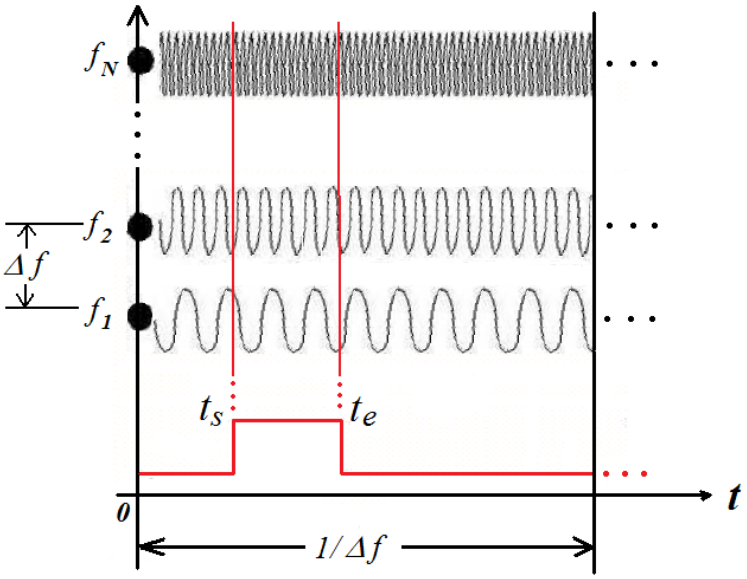

Figure 6.6: A pulse transmitted by an FDA.

Before we discuss the performance of an FDA transmitting a pulse signal, one assumption is made on the rectangular pulse. As it takes $1/\Delta f$ for the main beam of a CW FDA to complete one entire scan from 0° to 180°, the length of the rectangular pulse is limited to be less than $1/\Delta f$. Under this assumption, during the pulse signal, the main beam has an angle spread which is less than 180° during the pulse signal. That is,

$$0 \le t_s < t_e < t_s + 1/\Delta f \quad . \tag{6-1}$$

6.3 Array Factor of FDA Transmitting a Pulse Signal

Regarding time-limited ($0 \le t_s < t_e < t_s + 1/\Delta f$) frequency diverse signals, the array factor $AF(\theta,t,r)_{\Delta f,\rho}$ of FDA is re-visited to give insight to the mechanism of beam control.

A small modification to the CW array factor gives the pulsed array factor, marked as $AF(\theta,t,r)^{P}_{\Delta f,\rho}$.

$$AF(\theta,t,r)^{P}_{\Delta f,\rho} \triangleq \begin{cases} 0 & (0 \le t < r/c + t_s \ or \ t > r/c + t_e) \\ \sum_{n=1}^{N} e^{j(n-1)\psi} & \left(r/c + t_s \le t \le r/c + t_e\right) \end{cases} \tag{6-2}$$

where $\psi = 2\pi\cos\theta \times \rho + 2\pi \times \left(\frac{t}{1/\Delta f}\right) - 2\pi \times \left(\frac{r}{c/\Delta f}\right)$.

Accordingly,

$$AF(\theta,t)^{P}_{\Delta f,\rho}\,|r = r_0 \triangleq \begin{cases} 0 & (0 \le t < r_0/c + t_s \ or \ t > r_0/c + t_e) \\ \sum_{n=1}^{N} e^{j(n-1)\psi} & \left(r_0/c + t_s \le t \le r_0/c + t_e\right) \end{cases} \tag{6-3}$$

$$AF(\theta,r)^{P}_{\Delta f,\rho}\,|t = t_0 \triangleq \begin{cases} 0 & r > (t_0 - t_s)\times c \ \ or \ \ r < (t_0 - t_e)\times c \\ \sum_{n=1}^{N} e^{j(n-1)\psi} & (t_0 - t_e)\times c \le r \le (t_0 - t_s)\times c \end{cases} \quad (t_0 > t_e > t_s) \tag{6-4}$$

As an example, a rectangular pulse $\left[0.95\times 1/\Delta f\ ,1.05\times 1/\Delta f\right]$ is transmitted by an FDA ($N=8,\ \Delta f=1\,\text{kHz},\ \rho=0.45$) and $AF(\theta,t)^{P}_{\Delta f,\rho}\left|r=r_0\right.$ is computed with $r_0=3\times 10^5\,\text{m}$. It is shown in Figure 6.7(a)-(c) that a $\frac{1}{10}\times 1/\Delta f$ length pulse transmitted at 0.95 ms forms a scanning beam at the distance of $4.5\times 10^5\,\text{m}$ with 12° angle spread, from 84° at 1.95 ms to 96° at 2.05 ms.

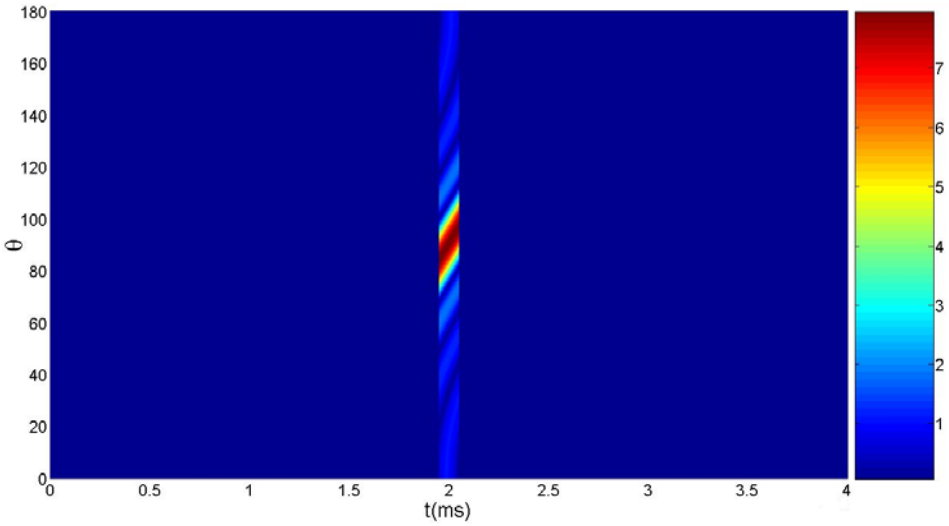

(a) Overview

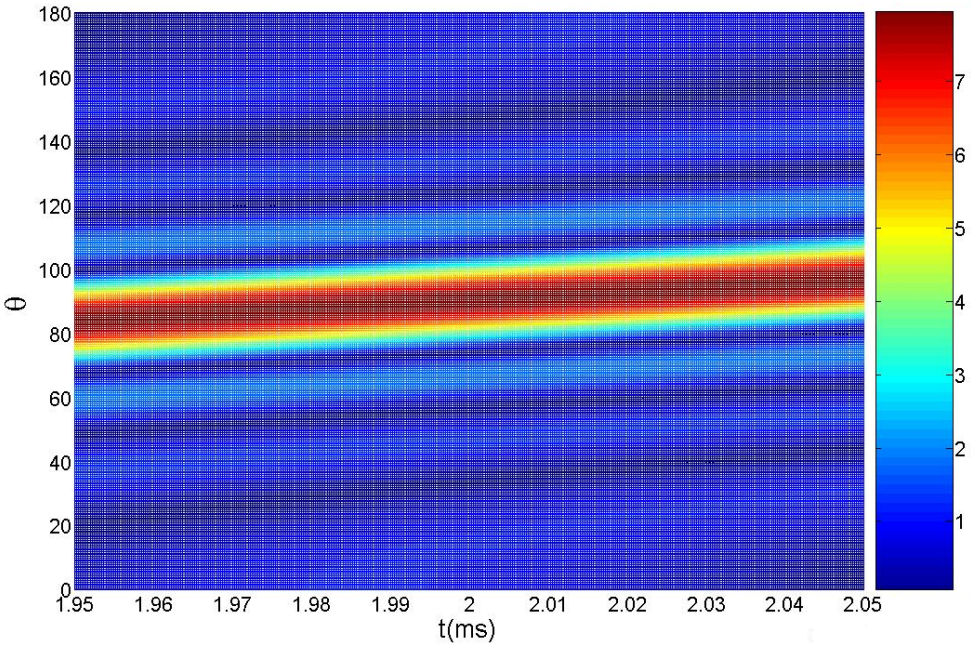

(b) From 1.95 ms to 2.05 ms

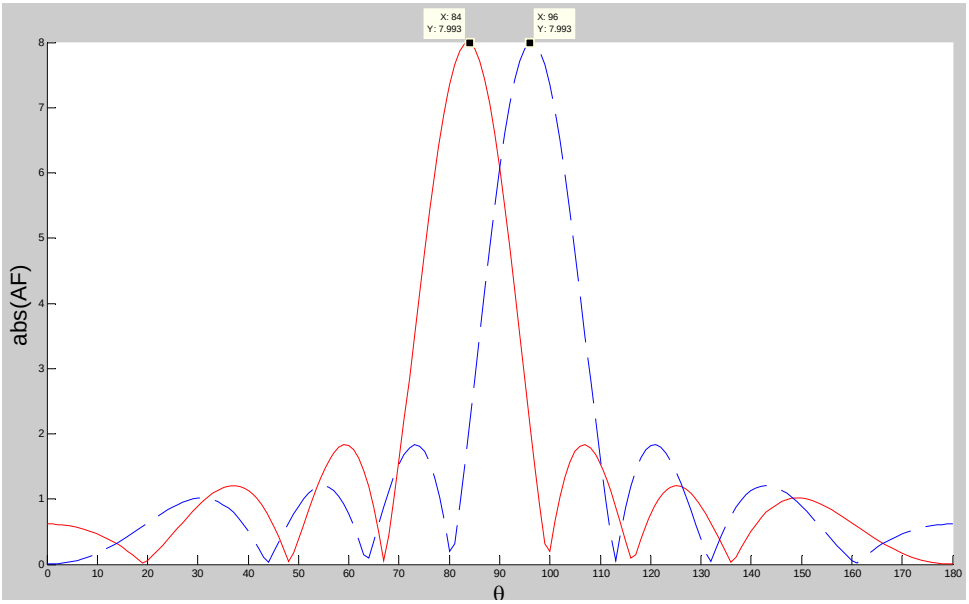

(c) 12° angle spread (solid line stands for 1.95 ms and dashed line for 2.05 ms)

Figure 6.7: Array factor at $r_0 = 3\times10^5\,\mathrm{m}$ of a $\left[0.95\times1/\Delta f\,,1.05\times1/\Delta f\right]$ pulse.

Actually, the same phenomenon is observed at different distances except that the starting time is delayed accordingly. For example, if observation point is moved to $r_0 = 4.5\times10^5\,\mathrm{m}$, the beam still scans from 84° to 96°, starting at 2.45 ms this time.

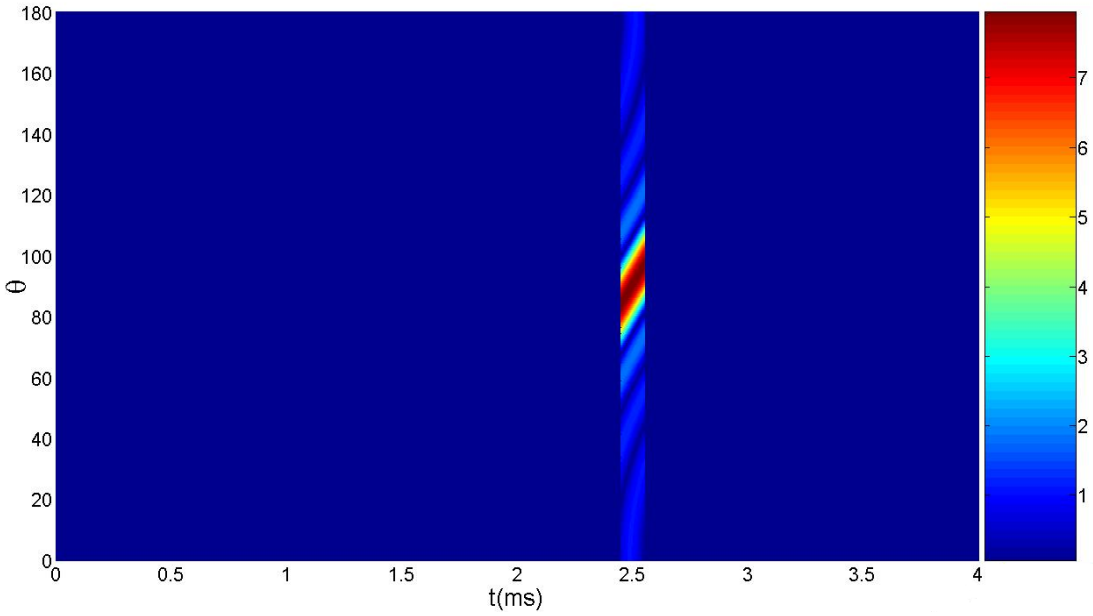

Figure 6.8: Array factor at $r_0 = 4.5\times10^5\,\mathrm{m}$ of a $\left[0.95\times1/\Delta f\,,1.05\times1/\Delta f\right]$ pulse.

To illustrate how the pulse $[0.95\times 1/\Delta f\ ,1.05\times 1/\Delta f\ ]$ propagates across space, $AF(\theta,r)^{P}_{\Delta f\ ,\rho}\left|t=t_0\right.$ is computed with $t_0=1.05$ ms, 2.5 ms and 4 ms respectively.

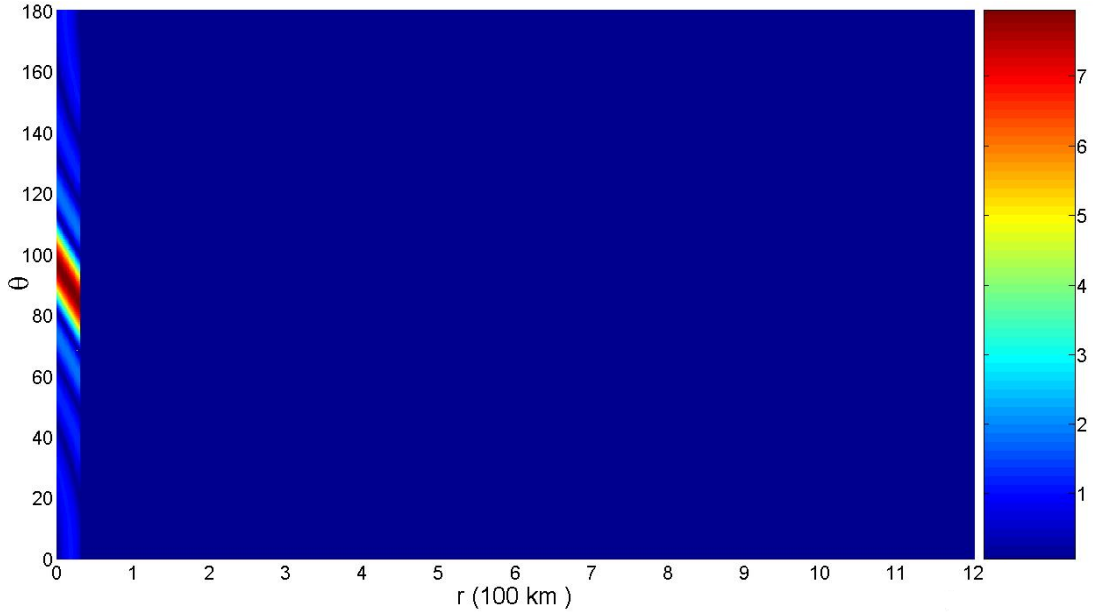

(a) Array factor at $t_0=1.05$ ms of $[0.95\text{ ms},1.05\text{ ms}]$ pulse

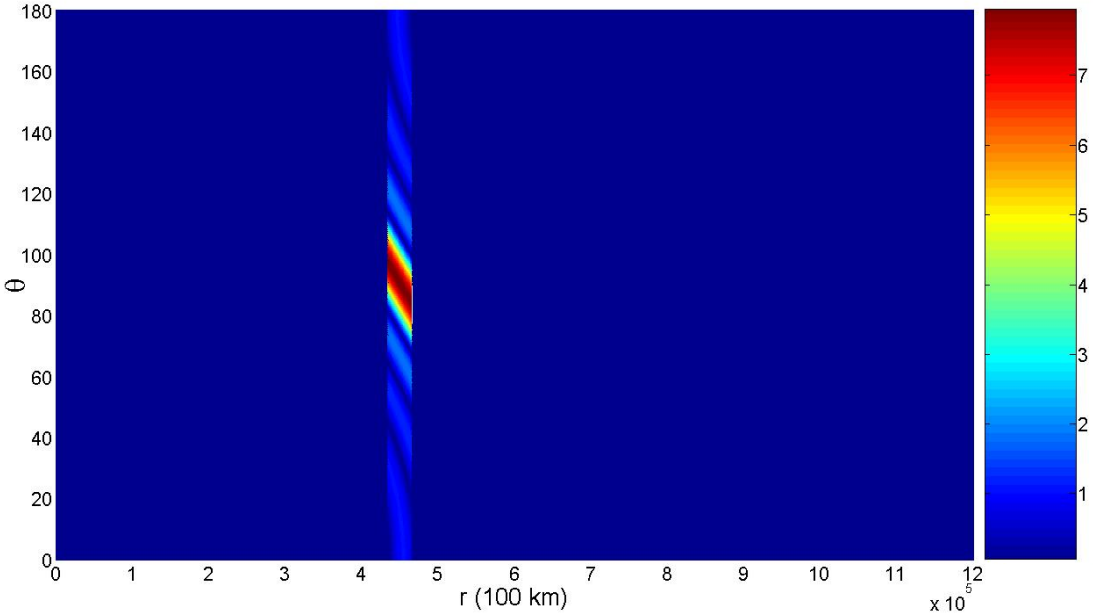

(b) Array factor at $t_0=2.5$ ms of $[0.95\text{ ms},1.05\text{ ms}]$ pulse

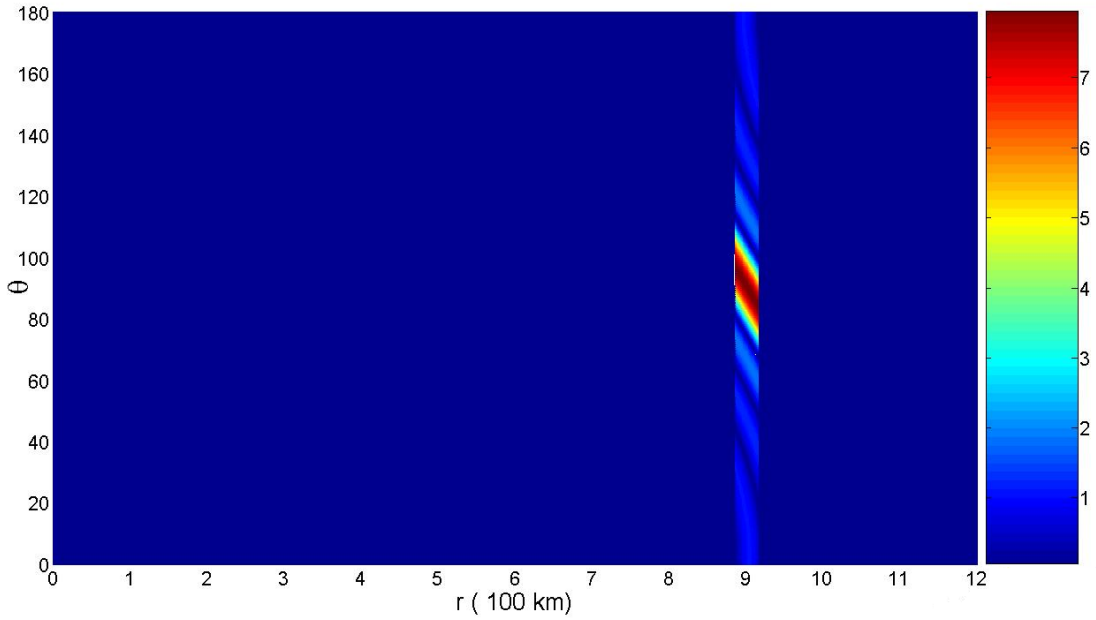

(c) Array factor at $t_0 = 4$ ms of $[0.95\text{ ms}, 1.05\text{ ms}]$ pulse

Figure 6.9: Propagation of beam pattern of a $[0.95\times 1/\Delta f\ , 1.05\times 1/\Delta f\ ]$ pulse.

It is shown in Figure 6.9 that at any time after the pulse $[0.95\times 1/\Delta f\ , 1.05\times 1/\Delta f\ ]$ is transmitted, a beam pattern with a $3\times 10^4 m$ spread in distance and 12° spread in angle propagates outwards from the origin.

6.4 Performance of pulse with $\frac{1}{100}\times 1/\Delta f$ length

In Chapter 6.3, the performance of a pulse with $\frac{1}{10}\times 1/\Delta f$ length is examined. A 12° spread in angle is obviously too big for beam forming purpose. In order to decrease the angle spread, the pulse length is shortened to $\frac{1}{100}\times 1/\Delta f$. The array factor of a $\frac{1}{100}\times 1/\Delta f$ pulse $[0.995\times 1/\Delta f\ , 1.005\times 1/\Delta f\ ]$ at $r_0 = 4.5\times 10^5$ m is computed again and depicted in Figure 6.10.

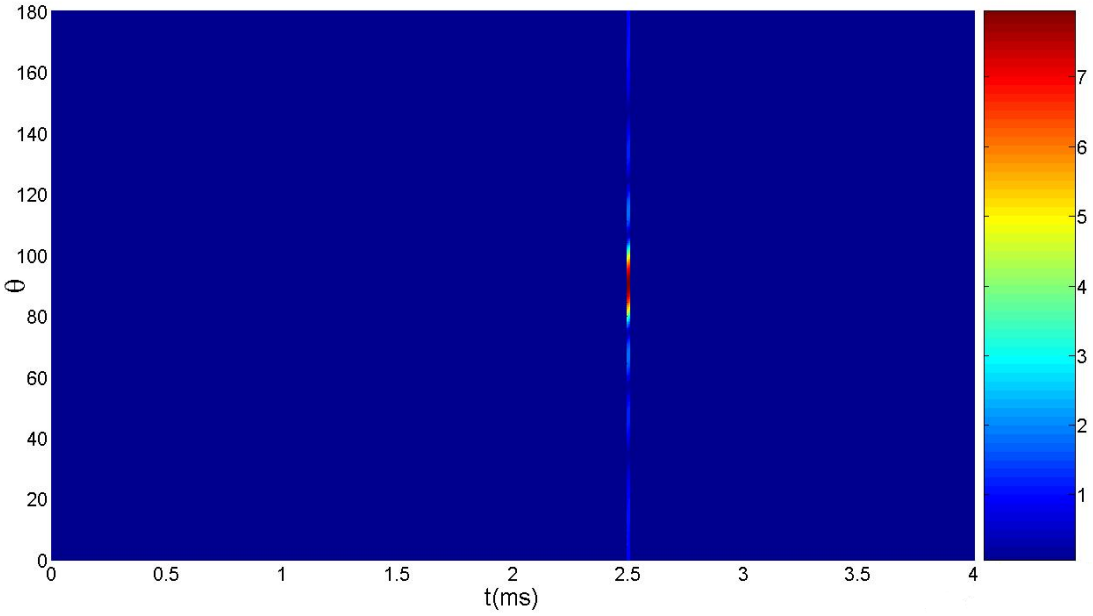

(a) Overview

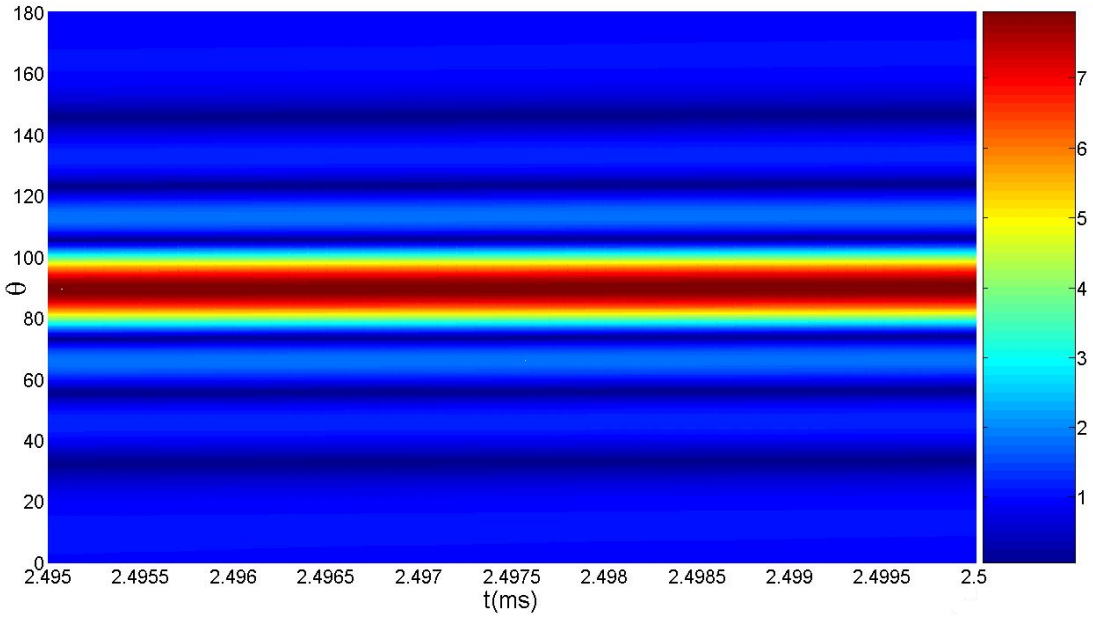

(b) From 2.495 ms to 2.505 ms

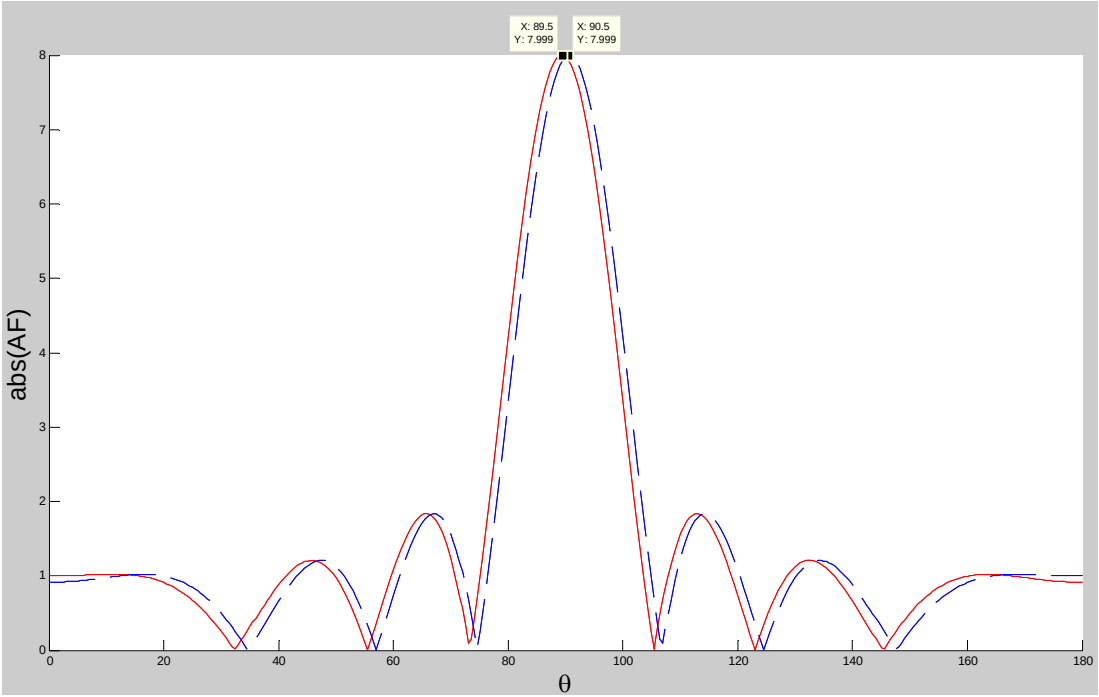

(c) 1° angle spread(solid line stands for 2.495 ms and dashed line for 2.505 ms)

Figure 6.10: Array factor at $r_0 = 4.5\times10^5$ m of a $\left[0.995\times1/\Delta f\ ,1.005\times1/\Delta f\right]$ pulse

It is shown in Figure 6.10 that the angle spread is just 1° for a pulse with a $\frac{1}{100}\times1/\Delta f$ length $\left(t\in\left[0.995\times1/\Delta f\ ,1.005\times1/\Delta f\right]\right)$ transmitted at 0.995 ms from the origin. This performance is very close to that of a conventional phased array. For even smaller angle spread, the pulse length should be even shorter. In following discussions, a $\frac{1}{100}\times1/\Delta f$ length pulse is used for beam steering while the pulse length can be adjusted to suit different circumstances.

6.5 Beam steering using $\frac{1}{100}\times 1/\Delta f$ length pulse

In previous Sections, the array factor of pulsed FDA is derived and analyzed. Given a pulse ($t \in [t_s, t_e], 0 \le t_s < t_e < t_s + 1/\Delta f$), its beam scanning performance can be evaluated through $AF(\theta,t)^P_{\Delta f,\rho}\,|r = r_0$ and $AF(\theta,r)^P_{\Delta f,\rho}\,|t = t_0$. It is shown that a $\frac{1}{100}\times 1/\Delta f$ length pulse has a beam forming effect which is very close to that of a conventional phased array. In this Section, we will discuss how to steer the beam of an FDA (e.g. $N = 8,\ \Delta f = 1$ kHz, $\rho = 0.45$) to a particular angle $\hat{\theta}$ with $\frac{1}{100}\times 1/\Delta f$ length pulse.

In Section 4.3.3.2 we have discussed the maximum of CW FDA's array factor. Similarly we can derive the maximum of pulsed FDA's array factor. Since a pulse has the same performance at any distance *r* except the starting time, we can choose a specific value of r_0 that is convenient for the computation of maximum of $AF(\theta,t)^P_{\Delta f,\rho}\,|r = r_0$.

When $r_0 = 0$ pulsed FDA's array factor (6-3) becomes

$$AF(\theta,t)^P_{\Delta f,\rho}\,|r = 0 \Box \begin{cases} 0 & (0 \le t < t_s \ or\ t > t_e) \\ \sum_{n=1}^{N} e^{j(n-1)\psi} & (t_s \le t \le t_e) \end{cases} \tag{6-5}$$

where $\psi = 2\pi\cos\theta\times\rho + 2\pi\times\left(\frac{t}{1/\Delta f}\right)$.

If a maximum occurs at $\hat{\theta}\ (\rho < 0.5)$, we have

$$t = \frac{m}{\Delta f} - \frac{\rho\cos\hat{\theta}}{\Delta f} \qquad (m = 0,1,2\ldots). \tag{6-6}$$

As one can always find multiple times for the array factor to achieve its maximum at $\hat{\theta}$. We assume that the array factor has a maximum at $\hat{\theta}_s$ at t_s and $\hat{\theta}_e$ at t_e respectively ($t \in [t_s, t_e], 0 \le t_s < t_e < t_s + 1/\Delta f$). That is,

$$t_s = \frac{m}{\Delta f} - \frac{\rho \cos \hat{\theta}_s}{\Delta f}, \tag{6-7}$$

$$t_e = \frac{m}{\Delta f} - \frac{\rho \times \cos \hat{\theta}_e}{\Delta f}. \tag{6-8}$$

Adding (6-7) to (6-8), we have

$$t_s + t_e = \frac{2m}{\Delta f} - \frac{\rho}{\Delta f} \times 2 \cos\left(\frac{\hat{\theta}_s + \hat{\theta}_e}{2}\right) \cos\left(\frac{\hat{\theta}_s - \hat{\theta}_e}{2}\right) \quad (m = 0,1,2...). \tag{6-9}$$

For a $\frac{1}{100} * 1/\Delta f$ length pulse we have $\hat{\theta}_s \approx \hat{\theta}_e$, $\cos\left(\frac{\hat{\theta}_s - \hat{\theta}_e}{2}\right) \approx 1$, (6-9) reduces to

$$2t_s + \frac{1}{100} \times \frac{1}{\Delta f} \approx \frac{2m}{\Delta f} - \frac{\rho}{\Delta f} \times 2 \cos \hat{\theta}. \tag{6-10}$$

Thus

$$t_s \approx \left(m - \rho \cos \hat{\theta} - \frac{1}{2} \times \frac{1}{100}\right) \times \frac{1}{\Delta f} \quad (m = 0,1,2...). \tag{6-11}$$

In Section 6.4, it is shown that a $\frac{1}{100} \times 1/\Delta f$ length transmitted at 0.995 ms from the origin forms a beam $\hat{\theta} = 90^\circ$ with an angle spread of 1°. If we let $\hat{\theta} = 90^\circ$ in (6-11),

we have $t_s \approx \left(m - \frac{1}{2} \times \frac{1}{100} \right) \times \frac{1}{\Delta f}$ $(m = 0,1,2...)$. When $m = 1$, $t_s \approx 0.995$ ms which agrees with previous result in Figure 6.10.

We give another example to illustrate the use of (6-11) in finding the proper time to transmit a $\frac{1}{100} \times 1/\Delta f$ pulse towards $\hat{\theta} = 60^\circ$. Let $\hat{\theta} = 60^\circ$ in (6-11), we have

$$t_s \approx \left(m - \frac{1}{2} \times \rho - \frac{1}{2} \times \frac{1}{100} \right) \times \frac{1}{\Delta f} \quad (m = 0,1,2...).$$

When $m = 1$, $t_s \approx 0.77$ms. And the array factor of an FDA $\left(N = 8,\ \Delta f = 1 \text{ kHz},\ \rho = 0.45\right)$ transmitting a $\frac{1}{100} \times 1/\Delta f$ length pulse ($t \in [0.77\text{ms}, 0.78\text{ms}]$) is computed and shown in Figure 6.8. One can see that a beam is formed at $\hat{\theta} = 60^\circ$ with an angle spread of 1°.

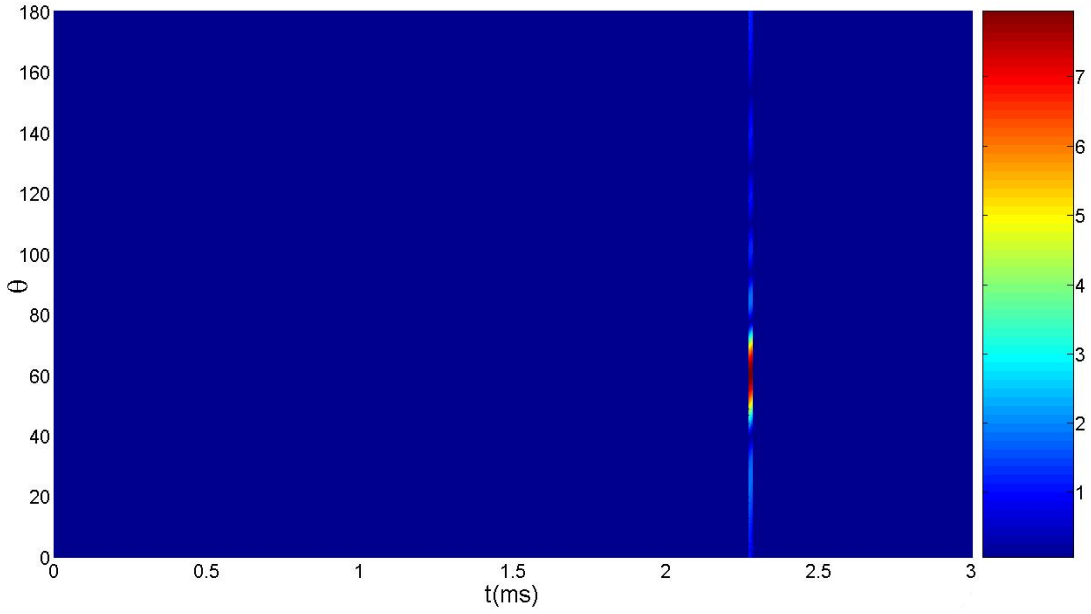

(a) Overview

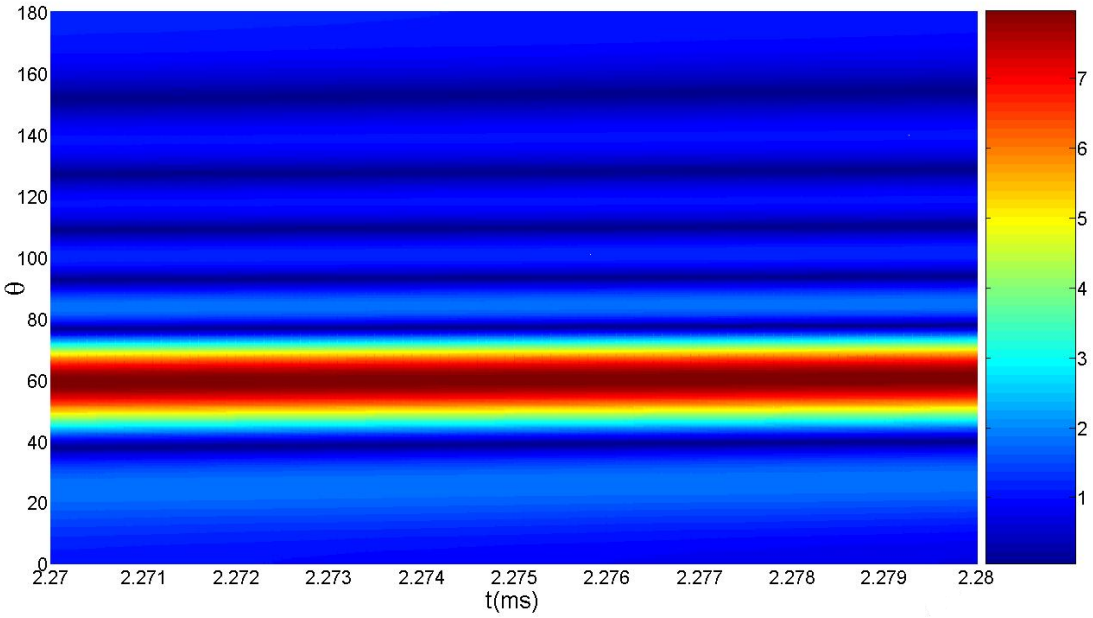

(b) From 2.27 ms to 2.28 ms

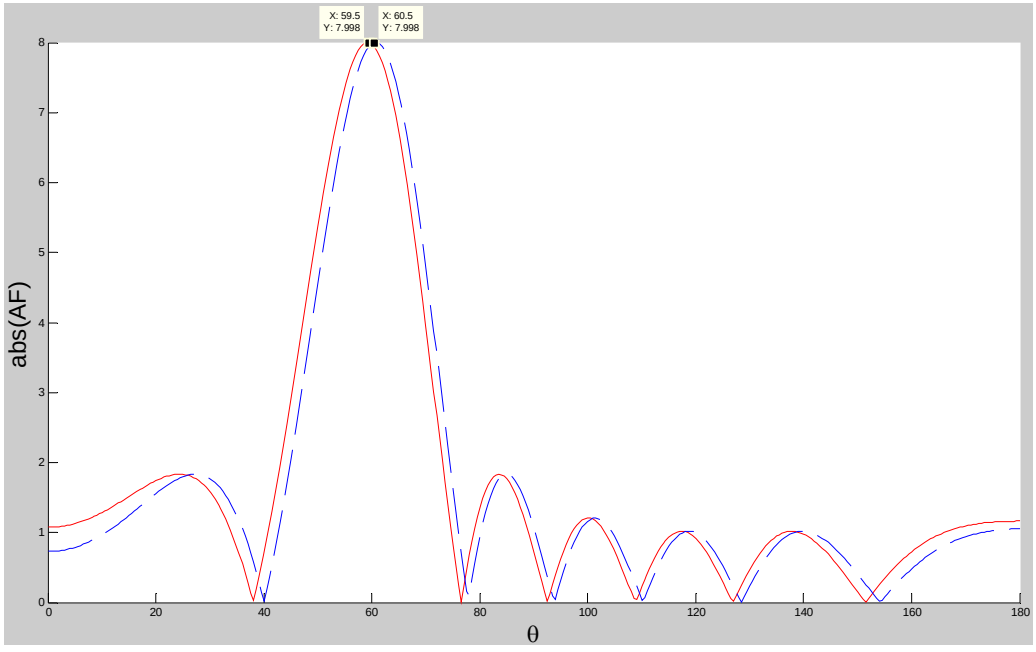

(c) 1° angle spread(solid line for 2.27 ms and dashed line for 2.28 ms).

Figure 6.11: Array factor at $r_0 = 4.5\times10^5\,\mathrm{m}$ of a $[0.77\ \mathrm{ms}, 0.78\ \mathrm{ms}]$ pulse

6.6 Signal Processing for an FDA Transmitting a Pulse Signal

In this Section, the signal processing technique in beam forming pulsed FDA will be discussed. Again we will a $\frac{1}{100}\times 1/\Delta f$ length pulse to illustrate the concept.

6.6.1 Basics of Radar Signal Processing

Let $s(t)$ be the baseband signal. After modulated by the carrier signal $f_0(t)$, the signal of $s(t)\,f_0(t)$ is transmitted by the antenna. Due to the time delay τ_0 and Doppler frequency shift ν_0, the received RF signal by the antenna will be $s(t-\tau_0)\,f_0(t-\tau_0)e^{j2\pi\nu_0 t}$.

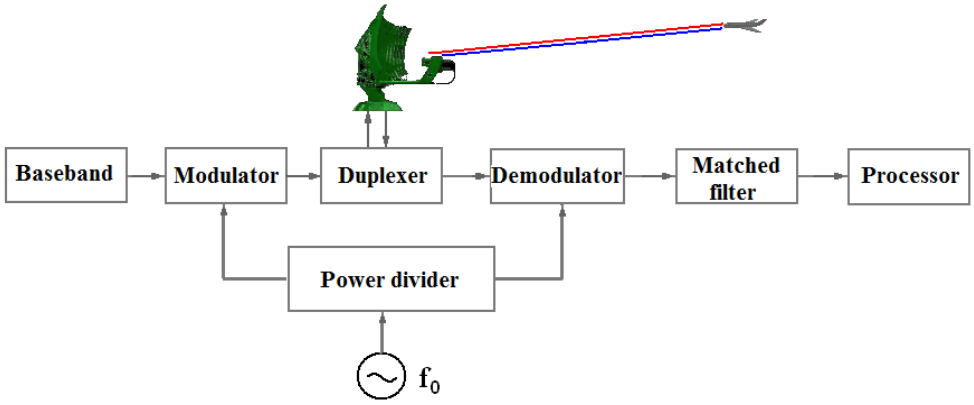

Figure 6.12: A typical pulsed radar system.

After being demodulated back to baseband, the received signal will be

$$r(t)=s(t-\tau_0)e^{j2\pi\nu_0 t}e^{j2\pi f_0\tau_0}. \tag{6-12}$$

This signal is processed by a matched filter

$$h_{\tau,\nu}(t)=s^*(T-t+\tau)e^{-j2\pi(T-t)}. \tag{6-13}$$

And the filter is matched to the signal

$$r(t) = s(t-\tau)e^{j2\pi\tau t}. \tag{6-13}$$

and designed to maximize the signal output at time *T*. The output of the matched filter at time *T* is given by [112]

$$o_T(\tau,\nu) = \int_{-\infty}^{+\infty} r(t)h_{\tau,\nu}(T-t)dt = e^{j2\pi f_0\tau_0}\chi_s(\tau-\tau_0,\nu-\nu_0), \tag{6-14}$$

which is referred to as the ambiguity function of baseband signal $s(t)$.

6.6.2 Time Domain Signal in the Main Beam Direction of a Pulsed FDA

In Chapter 4 where the array factor of FDA is derived, the total E-field radiated by *N* elements is given by

$$\overrightarrow{E_t} = \hat{a}_\theta e^{j(2\pi f_1 t - k_1 r_1)} j\eta \frac{kI_0 l}{4\pi r}\sin\theta \times \sum_{n=1}^{N} e^{j(n-1)\psi} \tag{6-15}$$

where

$$\begin{aligned}\psi &= 2\pi\cos\theta\times\rho + 2\pi\times\left(\frac{t}{1/\Delta f}\right) - 2\pi\times\left(\frac{r_1}{c/\Delta f}\right)\\ &= k_1 d\cos\theta + 2\pi t\times\Delta f - r_1\times\Delta k\end{aligned}.$$

(6-15) can be re-written as

$$\overrightarrow{E_t} = \hat{a}_\theta\ j\eta\frac{kI_0 l}{4\pi r}\sin\theta\times\frac{\sin\frac{N\psi}{2}}{\sin\frac{\psi}{2}}\times e^{j(2\pi f_1 t - k_1 r_1)}\times e^{j\frac{N-1}{2}\psi}. \tag{6-16}$$

Combining $e^{j\left(2\pi f_1 t - k_1 r_1\right)}$ and $e^{j\frac{N-1}{2}\psi}$ in (6-16), we have

$$\overrightarrow{E_t} = \hat{a}_\theta \; j\eta \frac{kI_0 l}{4\pi r}\sin\theta \times e^{-j\left(\frac{N-1}{2}\right)^2 \Delta k d\cos\theta} \times \frac{\sin\frac{N\psi}{2}}{\sin\frac{\psi}{2}} \times e^{j2\pi\left(f_1+\frac{N-1}{2}\Delta f\right)t - j\left(k_1+\frac{N-1}{2}\Delta k\right)\left(r_1-\frac{N-1}{2}d\cos\theta\right)}.$$

Referring to the geometry of the FDA in Figure 4.3, we have

$$f_1 + \frac{N-1}{2}\Delta f = \frac{f_1 + f_N}{2} \equiv f_c \tag{6-17}$$

$$k_1 + \frac{N-1}{2}\Delta k = \frac{k_1 + k_N}{2} \equiv k_c \tag{6-18}$$

$$r_1 - \frac{N-1}{2} d\cos\theta = \frac{r_1 + r_N}{2} \equiv r_c . \tag{6-19}$$

(5-16) can be reduced to

$$\overrightarrow{E_t} = \hat{a}_\theta \; j\eta \frac{kI_0 l}{4\pi r}\sin\theta \times \left(\frac{\sin\frac{N\psi}{2}}{\sin\frac{\psi}{2}}\right) \times \left(e^{-j\left(\frac{N-1}{2}\right)^2 \Delta k d\cos\theta} \times e^{j\left(2\pi f_c t - k_c r_c\right)}\right). \tag{6-20}$$

Now examine the time-domain signal received at $\hat{\theta}$ is examined using (6-20). When a beam is formed at angle $\hat{\theta}$ using a $\frac{1}{100}\times 1/\Delta f$ length pulse, from (6-20) we know that the value of $\left|\frac{\sin\frac{N\psi}{2}}{\sin\frac{\psi}{2}}\right|$ during the pulse is very close to its maximum N (starting from 7.999 to 8 then back to 7.999 as in Figure 5.8.c). Therefore when a $\frac{1}{100}\times 1/\Delta f$ length pulse is transmitted to form a beam at angle $\hat{\theta}$, the signal received at angle $\hat{\theta}$ is

$$\overrightarrow{E_t} \approx \hat{a}_\theta \; jN\eta \frac{kI_0 l}{4\pi r}\sin\theta \times e^{-j\left(\frac{N-1}{2}\right)^2 \Delta k d\cos\theta} \times e^{j\left(2\pi f_c t - k_c r_c\right)}. \tag{6-21}$$

From (6-21) we can see the received signal can be regarded as a pulse signal whose frequency is $f_c \approx \frac{f_1 + f_N}{2}$. This approximation makes it possible to use a single carrier f_c to retrieve the baseband signal from the received RF signal, as discussed in next session.

6.6.3 Signal Processing in a Pulsed Radar using FDA

Again let $s(t)$ be the baseband signal to be transmitted towards angle $\hat{\theta}$ by an FDA. In previous discussions, $s(t)$ is a rectangular pulse. $s(t)$ can also be other waveforms used in nowadays radar systems, such as chirp signals and phase modulated signals, We will not go further into the area of radar waveform design which is not in the scope of this thesis. Instead we will focus on how to demodulate the baseband signal in a pulsed radar using FDA.

From Section 6.6.2, it is proven that although modulated by *N* diverse frequency ($f_1 \approx f_N$) carriers, the signal received in the main beam direction can be regarded as a single frequency signal whose frequency is $f_c \approx \frac{f_1 + f_N}{2}$. If there is an object (τ_0, v_0) in the main beam direction of a pulsed frequency diverse array, the received RF signal will be $s(t-\tau_0) f_c(t-\tau_0) e^{j2\pi v_0 t}$, which can be demodulated by a synchronized carrier signal f_c. Based on above argument, an FDA pulsed radar is proposed. A synchronization module is required to adjust the relative time difference between the carrier signal and baseband signal, which determines the beam-forming angle of an FDA.

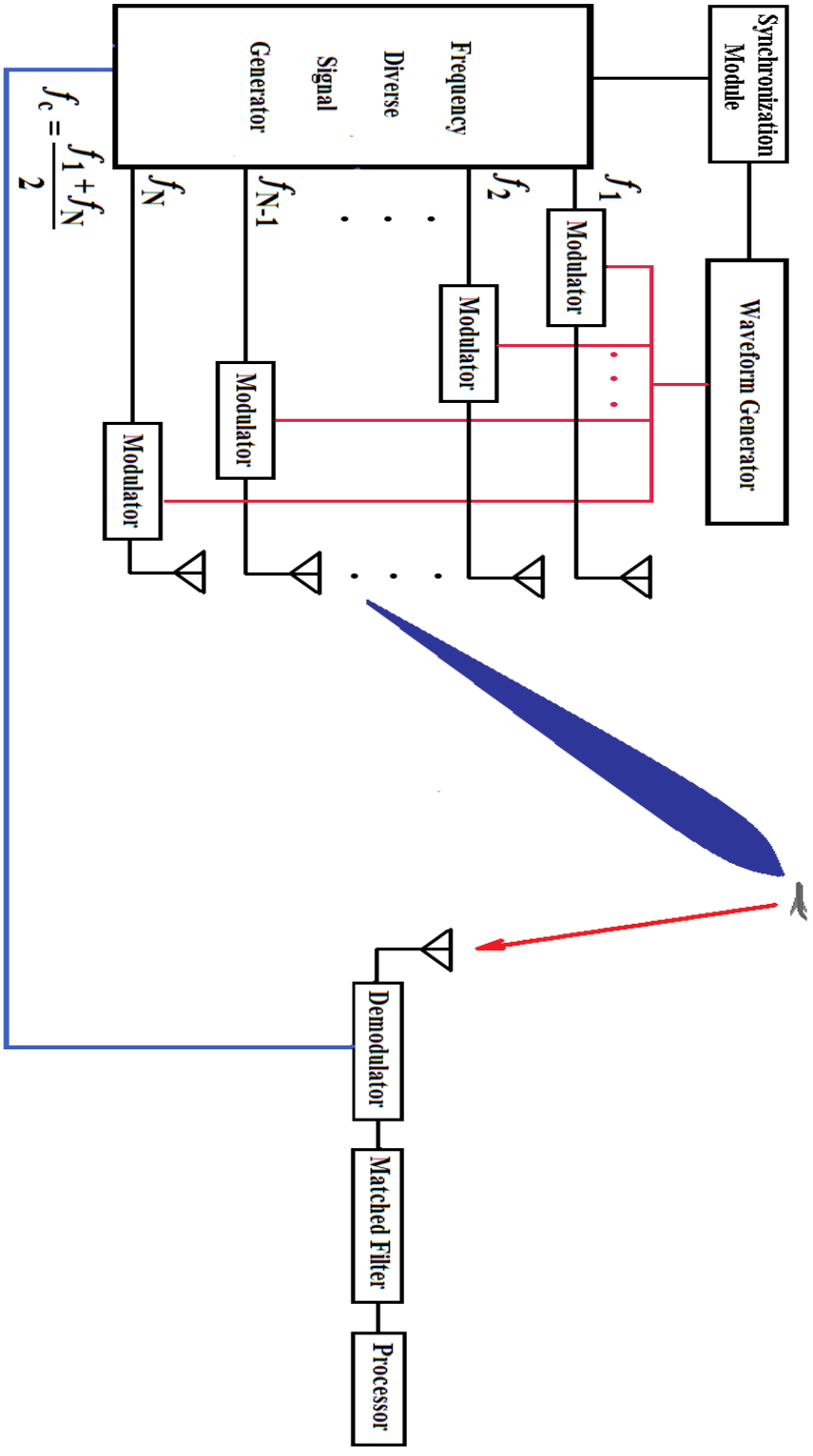

Figure 6.13: A pulsed radar using FDA

For an FDA pulsed radar with given Δf, the beam forming pulse width should be $\frac{1}{100}\times 1/\Delta f$ in order to have less than 1° angle spread (see Section 6.4). When a beam is desired to be formed towards $\hat{\theta}$, the transmitting time t_s can be chosen using (6-11). If the same pulse is transmitted again after $1/\Delta f$, the bean will still be formed towards $\hat{\theta}$ due to periodicity. In this way, the main beam is always formed towards $\hat{\theta}$ during every single pulse as shown in Figure 6.14.

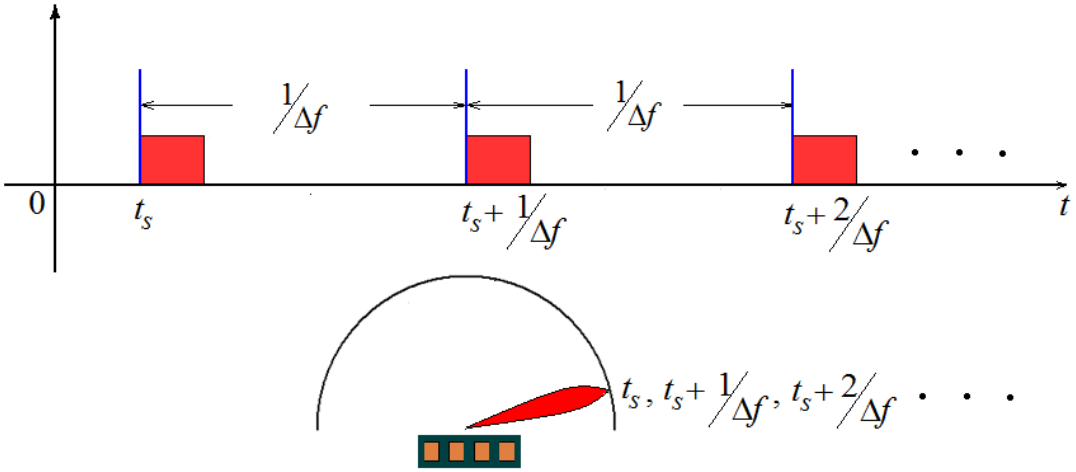

Figure 6.14: Beam Forming Using FDA Transmitting Pulses

6.7 Summary

In Chapter 5, our discussion is extended from CW FDA to pulsed FDA, since the CW FDA is not suitable for beam forming applications. The array factor of pulsed FDA $AF\left(\theta,t,r\right)_{\Delta f,\rho}^{P}$ is derived so that the beam pattern of an FDA transmitting a pulse signal can be analyzed. It is shown that a pulse length of $\frac{1}{100}\times 1/\Delta f$ can provide beam forming effect which is very close to that of a conventional phased array. Based on this result, the relationship between the beam steering angle $\hat{\theta}$ and the starting time t_s of a $\frac{1}{100}\times 1/\Delta f$ length pulse is given. More importantly, the signal processing technique in the pulsed FDA is developed on the analysis of time domain signal received in the main beam direction and the structure of a pulsed radar using FDA is described.

So far, the theory of FDA has been presented. Given an FDA with given ($N,\Delta f,\rho$), its radiation characteristics can be analyzed. Specific pulses can be designed for beam forming applications where the proposed signal processing technique can be utilized. One remaining question is how to physically implement an FDA. That is, how to choose the parameters of an FDA and further generate the required frequency diverse signals. This will be covered in Chapter 7.

Chapter 7

Physical Implementation of FDA

7.1 Background

When the physical implementation of FDA is concerned, our research leads to the PLL (phase locked loop) frequency synthesis techniques. As the focus of this thesis is a full investigation of FDA, the design of a novel frequency synthesizer with improved performance is not within the scope of this thesis. Therefore, only the basic mechanisms and key parameters of PLL are discussed, as they will determine the quality of the frequency diverse signals. PLL frequency synthesizer itself is not a new idea or design; but in this thesis it is first introduced to FDA as an effective hardware implementation approach.

Actually frequency synthesizers come in three varieties: Direct Analog Synthesizers, Direct Digital Synthesizers, and Indirect PLL Synthesizers. Because it is not convenient to achieve phase synchronization between multiple Direct Analog synthesizers, while the DDS is limited by the working frequency of digital circuitry and doesn't work at high frequency (above 1GHz), the indirect PLL frequency synthesizer becomes the best option.

7.2 Design of Frequency Diverse Signal Generator

In Chapter 4 when the concept of FDA is introduced and the array factor of FDA is derived, there are two assumptions which further discussions are based on. The first assumption is that the frequency increment Δf should be far less than the working frequency f ; while the second assumption is that all signals should have 0° phase at $t = 0$. Both assumptions are to be complied with when physically implementing the FDA.

When an FDA is designed for a specific application, f is usually fixed, such as 2.4 GHz for IEEE 802.11n, 5.8GHz for Broadband Wireless Access, etc. Assume a pulsed FDA for beam forming purpose operates at frequency f_p and transmits a pulse with length l_p. From Section 6.4 we know that the recommended pulse width l_p should be less than $\frac{1}{100} \times \frac{1}{\Delta f}$, that is

$$\Delta f \le \frac{1}{100} \times \frac{1}{l_p}. \tag{7-1}$$

Also the first assumption on frequency diversity in Chapter 4 gives

$$\Delta f \ll f_p. \tag{7-2}$$

Basically, the principle is to choose the largest Δf within the limits of (7-1) and (7-2), as too small Δf brings difficulties to hardware implementation and causes signal quality degration.

Usually the first constraint (7-1) is dominant especially when a long (several microseconds) pulse is transmitted. For example, Δf should be less than 1 Hz for 10ms pulse. For short pulses such as a 10ns pulse, Δf should be less than 1MHz according to (7-1). Since f_p is usually in the order of GHz, 1MHz is more than enough for (7-2). Therefore for pulse length longer than 10 ns, Δf can be derived using (7-1) so that

$$\Delta f = \begin{cases} \frac{1}{100} * \frac{1}{l_p} \text{ or smaller } \left(l_p \geq 10ns\right), \\ \frac{1}{1000} * f_p \text{ or smaller} \left(l_p < 10ns\right). \end{cases} \tag{7-3}$$

With Δf derived from f_p and l_p using (7-3), the left task is to obtain frequency diverse signals separated by Δf from each other, whose phases at $t = 0$ are all 0°. The solution to this problem is a frequency diverse signal generator composed of several synchronized PLL frequency synthesizers.

One may suggest the required diverse frequency signals can be generated by several synchronized signal generators, which are able to give tunable outputs with fine frequency steps. The problem is, even if one manages to perfectly synchronize several signal generators, the cost and volume of the system will be too big. Thus it becomes necessary to consider how to design a low cost and compact frequency diverse signal generator. In following Sections, the mechanism of PLL Frequency Synthesizer will be explained, including key parameters and basic design guidelines.

7.2.1 Mechanism of Phase/Frequency Lock

The block diagram of a basic PLL frequency synthesizer is shown in Figure 7.1. It comprises a phase frequency detector (PFD), voltage-controlled oscillator (VCO), frequency divider, and low pass filter (LPF) in a negative feedback arrangement such that the output frequency/phase (divided by N) is locked to the input frequency/phase. If the input frequency is obtained from a stable source, such as quartz crystal oscillator, then the output frequency may be stepped in integer multiples of this frequency and can therefore span many closely-spaced channels.

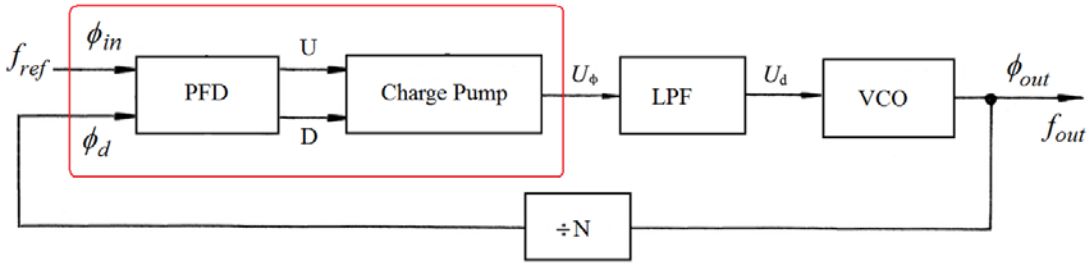

Figure 7.1: A block diagram of a PLL frequency synthesizer.

A VCO is designed to resonate at a frequency determined by a voltage input. A frequency divider is a circuit that takes an input signal of frequency f_{in}, and gives an output signal of frequency f_{out} ($f_{out} = \frac{f_{in}}{N}$, N is an integer). A PFD compares the phases of reference signal f_{ref} and divided VCO signal (f_{VCO}/N) and activates the charge pumps based on the phase difference between these two signals. Usually the charge pump and PFD (Figure 7.2) are integrated together [127], [128].

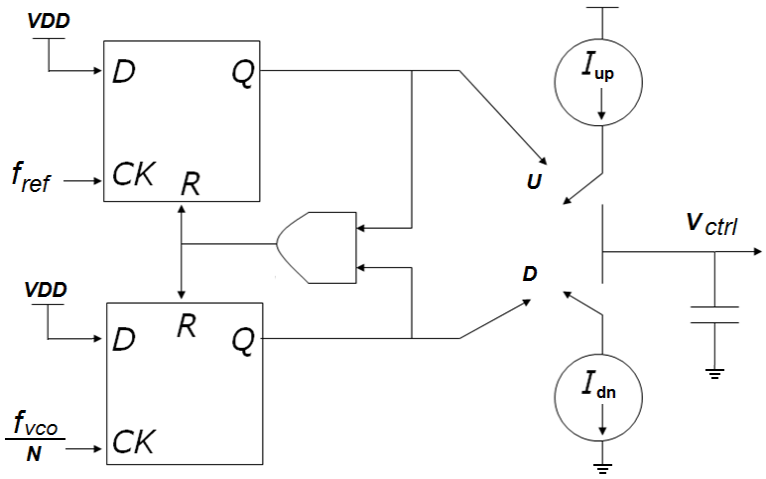

Figure 7.2: The PFD and charge pump.

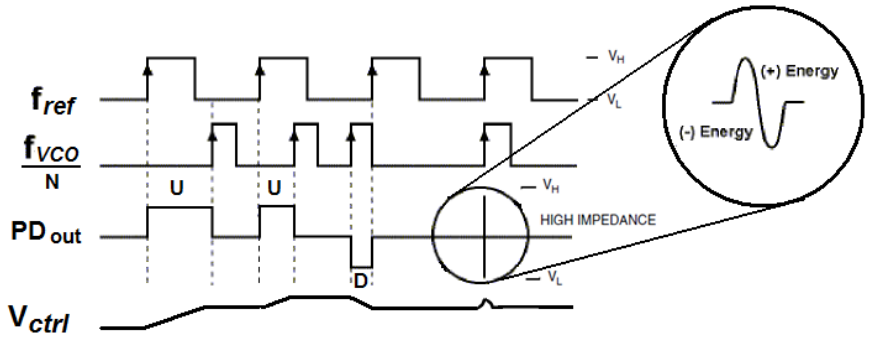

Figure 7.3: The output waveform of PFD and charge pump [129].

In a PLL the phase difference between the reference signal f_{ref} and the output signal f_{VCO}/N is translated into two signals - U and D, as in Figure 7.3. The two signals control switches to steer current into or out of a capacitor, causing the voltage across the capacitor V_{ctrl} to increase or decrease. In each cycle, the time during which the switch is turned on (length of U or D) is proportional to the phase difference; hence the charge delivered is dependent on the phase difference also. The voltage on the capacitor is used to tune a VCO, generating the desired output signal frequency.

When the phase difference is greater than $\pm 2\pi$, the output of the charge pump will be a constant current (e.g. the first pulse of PD_{out} in Figure 7.3), which results in a continuously changing control voltage applied to the VCO. The PFD will continue to operate like this until the phase error between the two input signals drops below 2π. Once the phase difference between the two signals is less than 2π, the charge pump is only active for a portion of each phase detector cycle (e.g. the second pulse of PD_{out} in Figure 7.3) that is proportional to the phase difference between the two signals. Once the phase difference between the two signals reaches zero, the device enters the phase locked state.

Further practical considerations include how much noise there is in the output. This is a function of the loop filter of the system, which is a low-pass filter placed between the output of the PFD and the input of the VCO. The role of the loop filter, which is a low-pass filter inserted between the PFD and the VCO, eliminates the high frequency component of the phase correction pulse generated by the phase comparator so that only the DC component is provided to the VCO. As a rule of thumb, the cut off frequency of the low-pass filter is chosen as equal or less than 1/10 of reference frequency f_{ref}. Heavy filtering will make the VCO slow to respond to changes, causing drift and slow response time, but light filtering will produce noise and other problems with harmonics. Thus the design of the filter is critical to the performance of the system and in fact the main area that a designer will concentrate on when building a synthesizer system.

When a PLL frequency synthesizer reaches the "phase locked state", theoretically the two signals of f_{vco}/N and f_{ref} shall have the same frequency and phase [127]-[129]. Therefore by aligning several PLL frequency synthesizers and applying a common reference signal, we will obtain the desired frequency diverse signals.

More specifically, the phases of all output signals should all be "0" when the phase of reference signal f_{ref} is "0". And the frequency increment Δf can be realized by assigning a linear increment to the divide ratio *N* across the synthesizers.

Since the desired frequency diverse signal generator is composed by several PLL frequency synthesizers sharing a common reference signal, it becomes necessary to find a suitable design for single PLL frequency synthesizer. We begin with the main parameters of a PLL synthesizer.

7.2.2 Main Parameters of a PLL Frequency Synthesizer

There are several important parameters of a PLL frequency synthesizer.

Frequency range - the output frequency band of a PLL frequency synthesizer, decided by VCO's tuning range.

Step size - the smallest frequency increment a PLL frequency synthesizer can produce

Phase noise - an indicator of the signal quality. An ideal signal's total energy is concentrated in a singular frequency. Real signals have a spectral distribution, and their energy is spread. For a carrier frequency at a given power level, the phase noise of a synthesizer is the ratio of the carrier power to the power in a 1Hz bandwidth at a defined frequency offset (usually 10 KHz), expressed in dBc/Hz.

Spurious signals - a measure of the discrete, deterministic "noise" in the signal spectrum. Spurs may come from a variety of sources, but one of the most common is PLL's reference signal, which is often referred to as reference spur, since many of

the PLL's components including the phase-frequency detector (PFD) and charge pump (CP) are clocked at the reference frequency. The spurs are caused by non-idealities of PLL's components such as charge pump leakage, inadequate decoupling of power supplies, mismatches in the up and down currents from the charge pump, etc.

Loop bandwidth - a measure of the dynamic speed of the feedback loop. Since the PLL acts as a narrow-band filter, this parameter indicates this filter's single sideband bandwidth. In general, the loop filter bandwidth should be 1/10 or less of the PFD frequency (channel spacing). Increasing the loop bandwidth will increase the switch speed, but the filter bandwidth should not be more than 1/5 of PFD, to avoid significantly increased risk of instability [127]-[129].

Switching speed - a measure of the time it takes the PLL circuit to re-tune the VCO from one frequency to another. This parameter usually depends on the size of the frequency step.

Other parameters deal with size, power, supply voltage, interface protocol, temperature range and reliability.

7.2.3 A Compact Design of Integer-N Frequency Synthesizer

In this section, a compact integer-N of PLL frequency synthesizer for FDA is presented. The design is based on the PLL IC MC145152, which when combined with an external LPF and VCO, can provide all the remaining functions for a PLL frequency synthesizer operating up to the device's frequency limit. For higher VCO frequency operation, a prescaler can be used between the VCO and the synthesizer IC when the desired output frequency is beyond the IC's frequency limit.

The block diagram is shown in Figure 7.4. The PLL IC MC145152 consists of a phase detector, 10-bit programmable "N" counter (N_0-N_9) and 6-bit programmable "A" counter (A_0-A_5) which require only a SPST switch to alter data to the zero state. Thus the output frequency is controlled only by 16-bit parallel programming without any other communication interfaces.

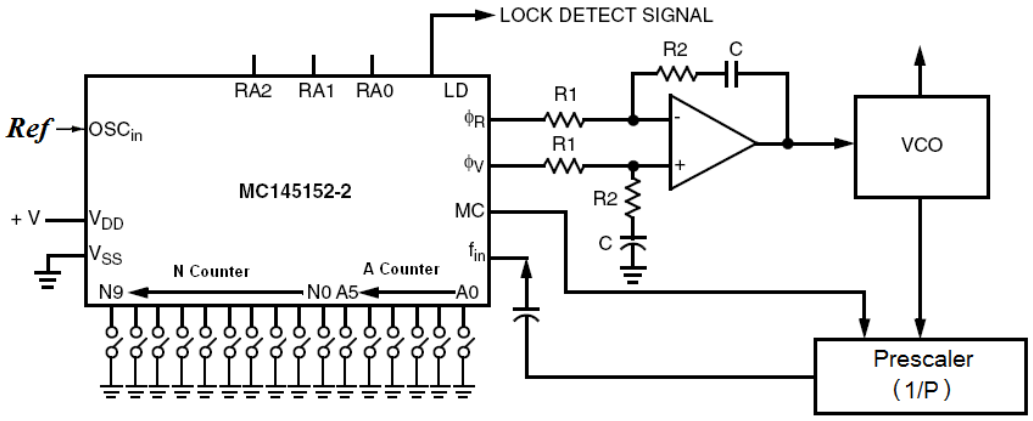

Figure 7.4: A typical application of MC145152 [130].

The system total divide value N_T will be:

$$N_T = \frac{\text{frequency into the prescaler}\left(f_{VCO}\right)}{\text{frequency into the PFD}\left(f_{REF}\right)} = N \times P + A. \qquad (7\text{-}4)$$

The 2-layer circuit in Figure 7.5 has a dimension of 8cm by 6cm.

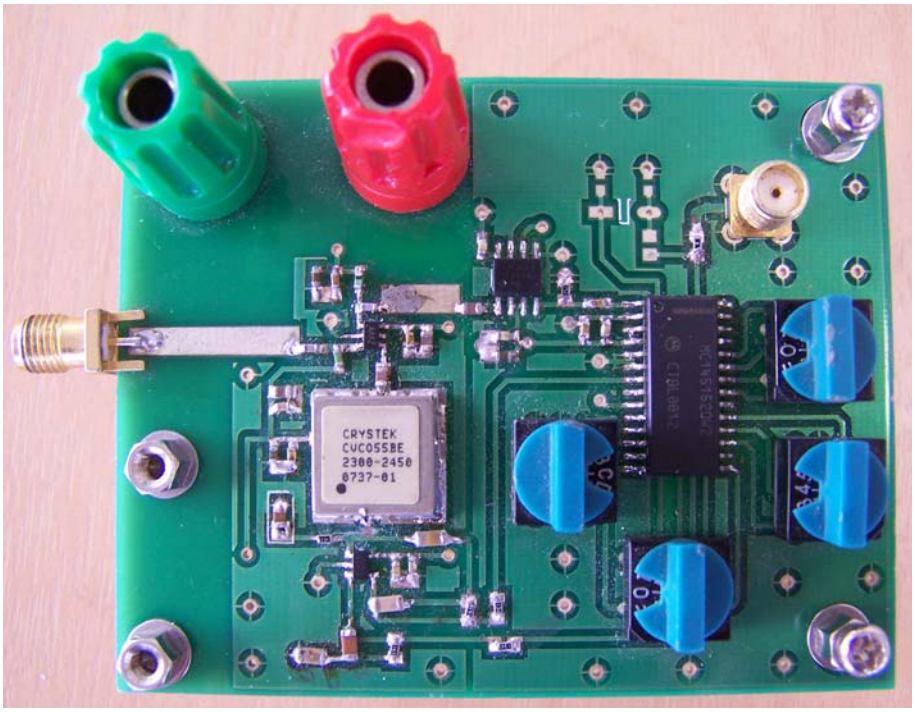

(a) Front

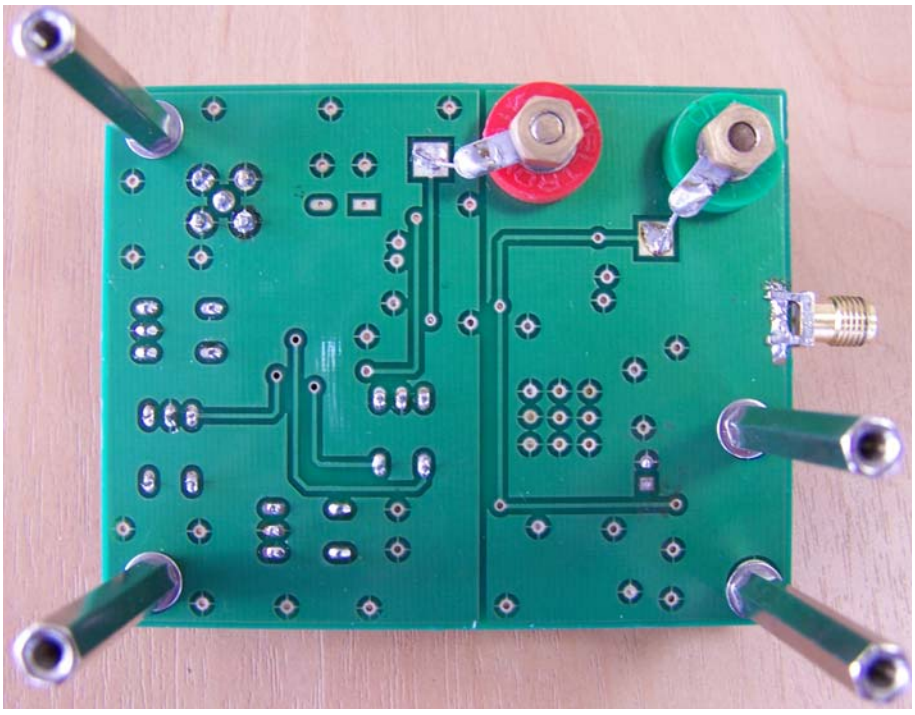

(b) Back

Figure 7.5: An integer-N frequency synthesizer for FDA.

In our design 4 hex rotary switches are employed to set the correct control bit (“0” or “1”) to “N” and “A” counter. A signal generator provides a flexible reference frequency which allows one to evaluate its affection on the quality of PLL output signal. The VCO output is fed to a spectrum analyzer.

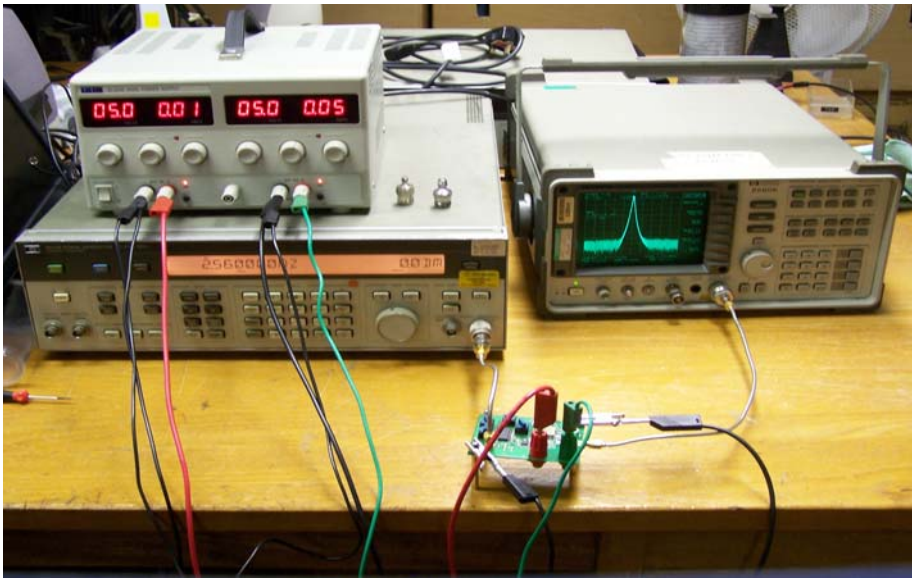

Figure 7.6: The measurement setup.

By changing the positions of 4 rotary switches, the frequency synthesizer gives outputs of different frequencies. For example, when the reference signal is 200 KHz, the frequency synthesizer can produce a step size of 200.3 KHz near 2.4 GHz as shown in Figure 7.7.

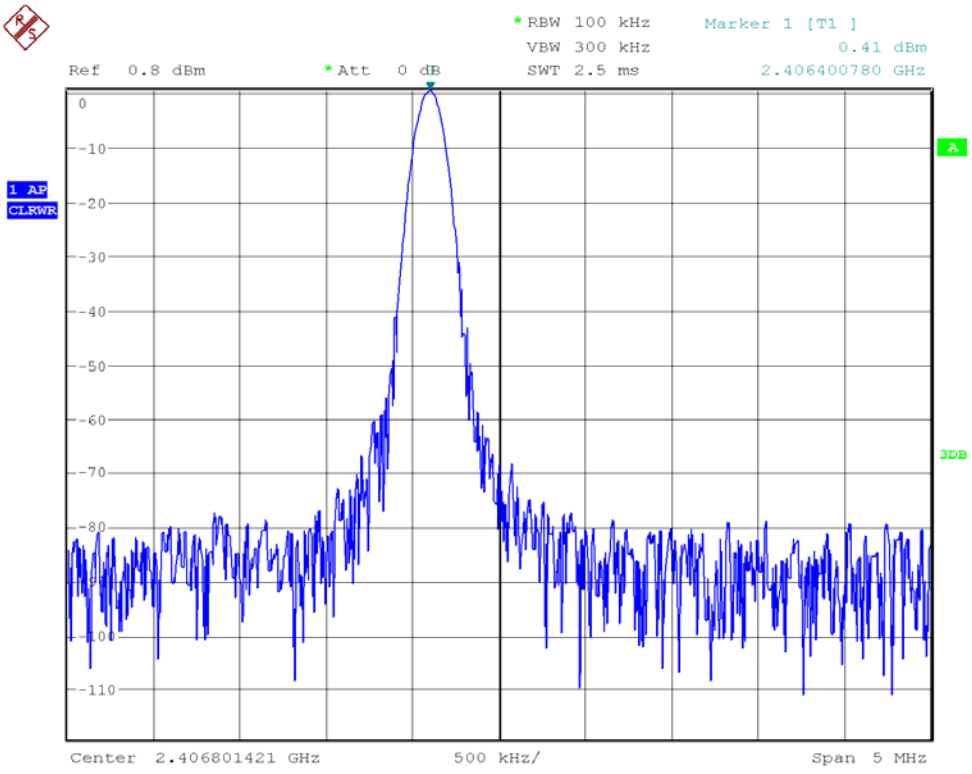

(a) 2406.4008MHz

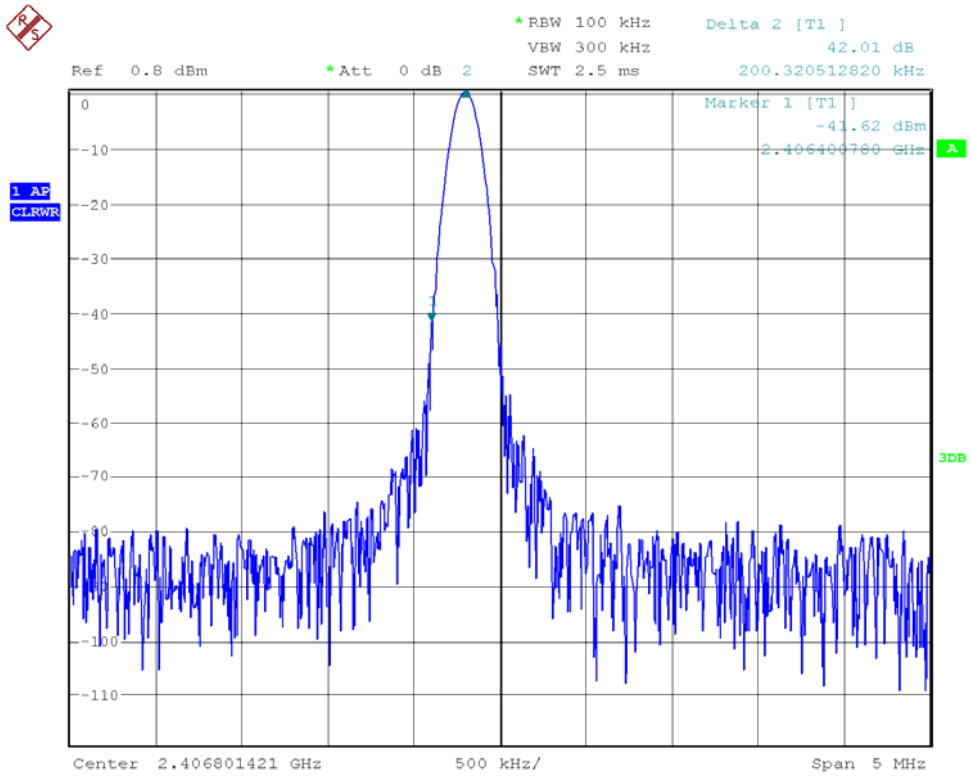

(b) 2406.6011MHz

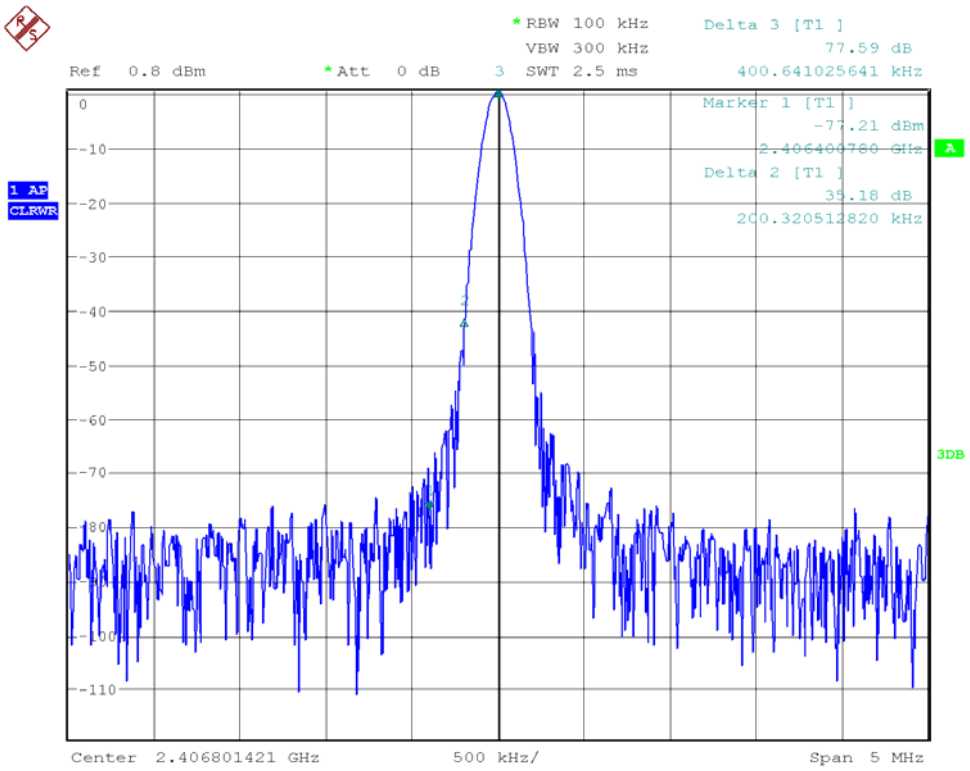

(c) 2406.8014GHz

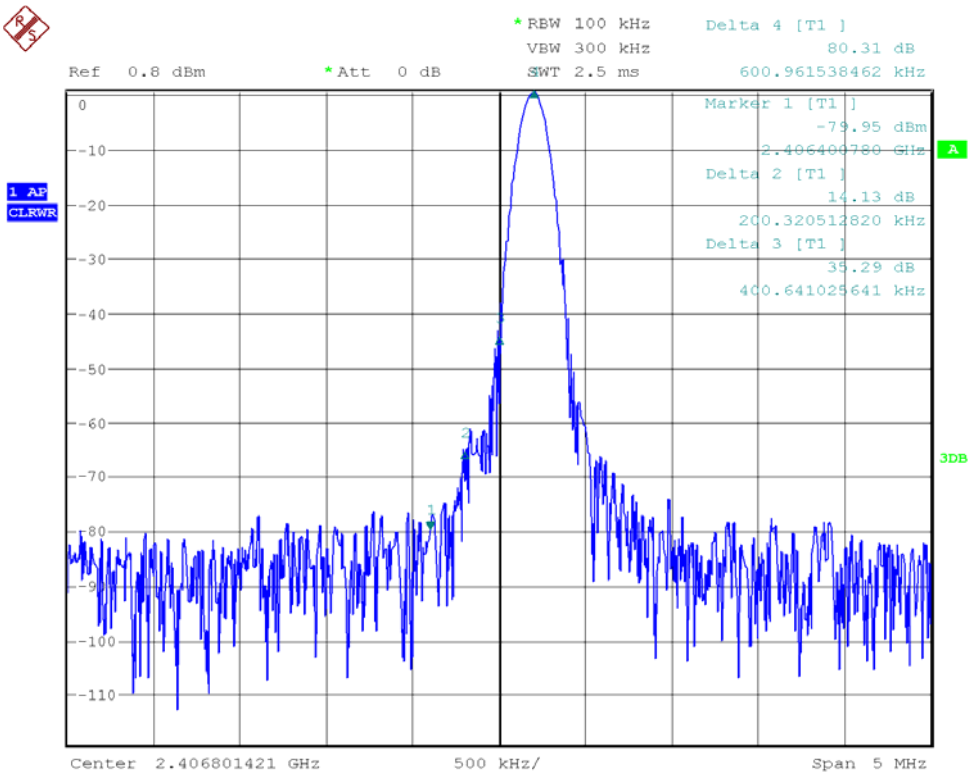

(d) 2407.0017MHz

Figure 7.7: The 200.3 KHz step size when $f_{ref} = 200KHz$.

When a PLL locks, the frequencies and phases of the two signals f_{ref} and f_{vco}/N become the same and the VCO frequency can be selected in steps of f_{ref}. In order to have a small step size, the reference frequency f_{ref} must be small and thus N shall be large. This requirement causes two problems. First, a large value of N results in an amplified phase-noise level at the VCO output. Second, the small reference frequency f_{ref} requires the low-pass filter to have a very small bandwidth to suppress harmonics and reference spurs.

7.2.4 Phase Noise of the Integer-N Frequency Diverse Signal Generator

Phase Noise is a method of describing the stability of a signal in frequency domain. As shown in Figure 7.8, for a central frequency at a certain power level, the phase noise of a synthesizer is the ratio of the central frequency power to the power in a 1Hz bandwidth at a defined frequency offset (usually 10 KHz), expressed in dBc/Hz.

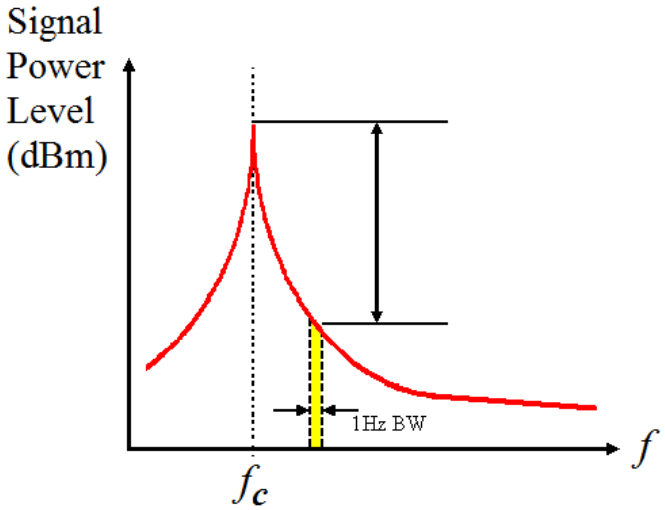

Figure 7.8: The phase noise in frequency domain.

If the output of a frequency synthesizer is examined in time domain with an

oscilloscope, some displacements of the up/down edge of the signal as shown in Figure 7.9, referred as jitter, can be observed. This is the influence of phase noise on signal in time domain. Since the FDA requires that all signals have 0° phase at one particular time, the phase noise shall be limited below certain level.

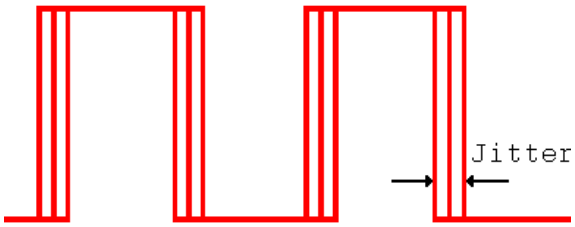

Figure 7.9: Jitter in the time domain.

The main internal sources of phase noise of a PLL frequency synthesizer are its components, including reference signal, VCO, PLL IC and loop filter. All these phase noises are very small and statistically independent thus can be analyzed separately and added together to the output of frequency synthesizer [127]-[129].

The phase noise of reference signal is amplified by 20log$N$ inside the loop filter's bandwidth while suppressed otherwise. Therefore, for a fixed output frequency, doubling the reference frequency provides 6dB improvement in output phase noise.

$$N_{ref}(f) = L_{ref}(f) + 20\log f_{out} - 20\log f_{ref} + 20\log\left|H(f)\right|. \tag{7-5}$$

The phase noise of VCO is different. It is suppressed inside the loop bandwidth, while suffers no attenuation outside of the loop bandwidth.

$$N_{VCO}(f) = L_{VCO}(f) + 20\log\left|1 - H(f)\right|. \tag{7-6}$$

The phase noise of PLL IC, similar to that of reference signal, is amplified by 10log$N$ inside the loop bandwidth.

$$N_{PLL-IC}(f) = PN_{1Hz} + 20\log f_{out} - 10\log f_{ref} + 20\log\left|H(f)\right|. \tag{7-7}$$

The phase noise of a loop filter comes from the thermal noise of resisters and active components such as operational amplifier in an active filter. There are other factors that may affect the phase noise of a PLL frequency synthesizer, like the decoupling of power supply, decoupling between RF ground and digital ground, shielding of loop filter and VCO, etc.

The measured phase noise of the proposed frequency diversity signal generator is shown in Figure 7.10. The output frequency f_{vco} is around 2.4GHz. The reference frequency f_{ref} has been set to be 400 KHz, 200 KHz, 100 KHz and 40 KHz, corresponding to a divide ratio N of 6000, 12000, 24000 and 60000 separately. As the designed bandwidth of loop filter is less than 10 KHz, the phase noise beyond 10 KHz is suppressed. One can see that the phase noise at 10 KHz offset is below -80dBc/Hz in 4 cases, while the phase noise at 1 KHz degrades with the increasing divide ratio N.

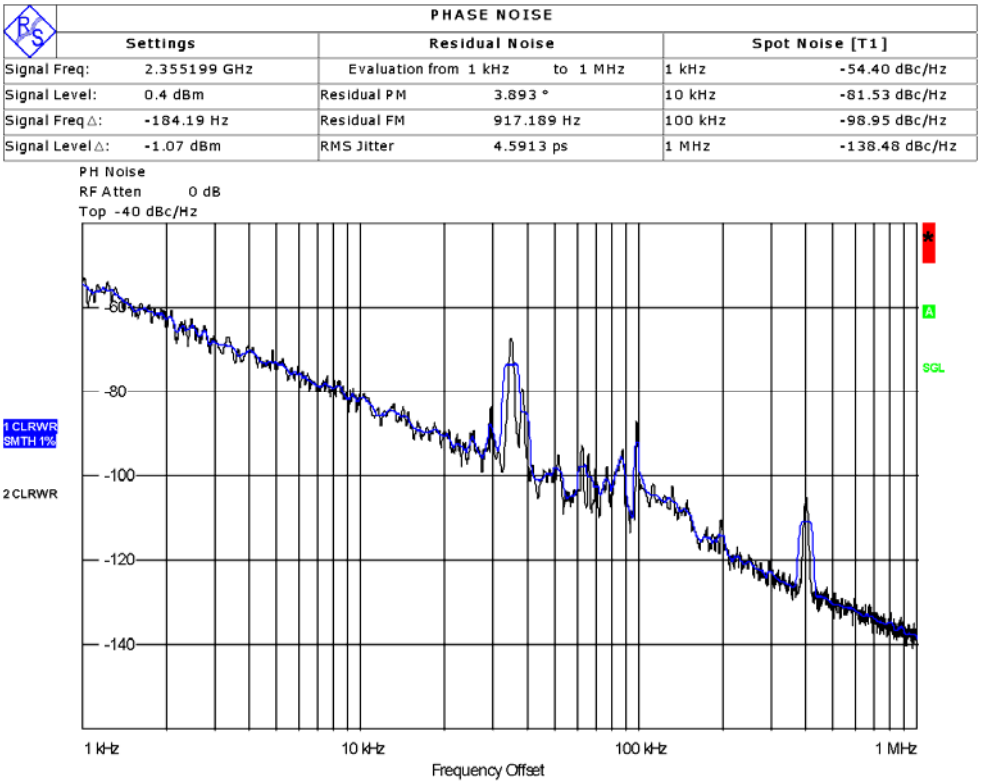

(a) $f_{ref} = 400KHz$, -54.40dBc/Hz at 1KHz offset

PHASE NOISE					
Settings		Residual Noise		Spot Noise [T1]	
Signal Freq:	2.406399 GHz	Evaluation from 1 kHz	to 1 MHz	1 kHz	-53.37 dBc/Hz
Signal Level:	0.4 dBm	Residual PM	3.976 °	10 kHz	-80.36 dBc/Hz
Signal Freq△:	-488.74 Hz	Residual FM	1.775 kHz	100 kHz	-95.46 dBc/Hz
Signal Level△:	-0.4 dBm	RMS Jitter	4.5899 ps	1 MHz	-138.93 dBc/Hz

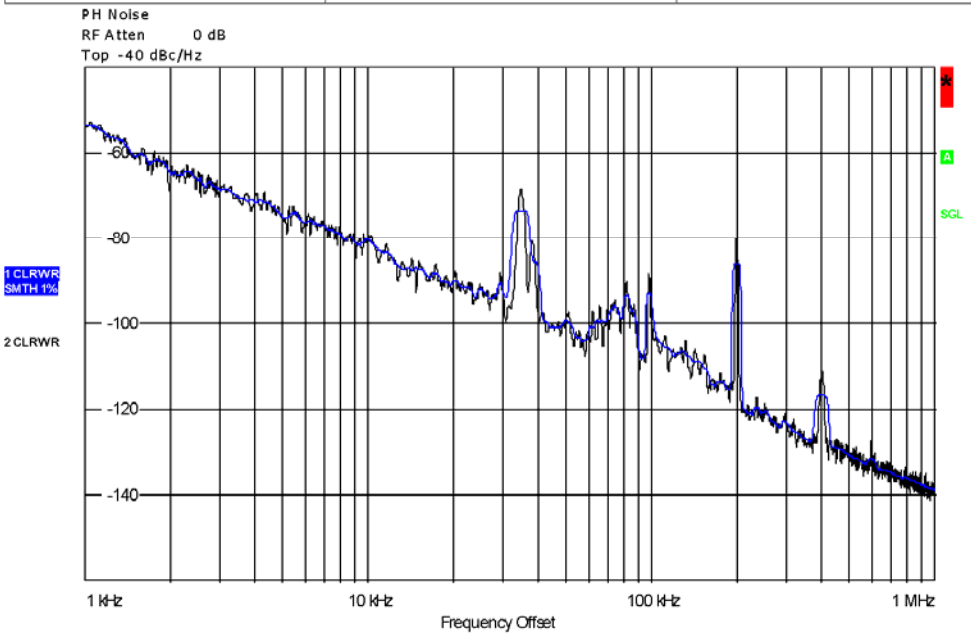

(b) $f_{ref} = 200KHz$, -53.37dBc/Hz at 1KHz offset

PHASE NOISE					
Settings		Residual Noise		Spot Noise [T1]	
Signal Freq:	2.406401 GHz	Evaluation from 1 kHz	to 1 MHz	1 kHz	-51.66 dBc/Hz
Signal Level:	0.8 dBm	Residual PM	4.618 °	10 kHz	-82.66 dBc/Hz
Signal Freq△:	-99.95 kHz	Residual FM	1.409 kHz	100 kHz	-84.85 dBc/Hz
Signal Level△:	-49.03 dBm	RMS Jitter	5.3312 ps	1 MHz	-139.29 dBc/Hz

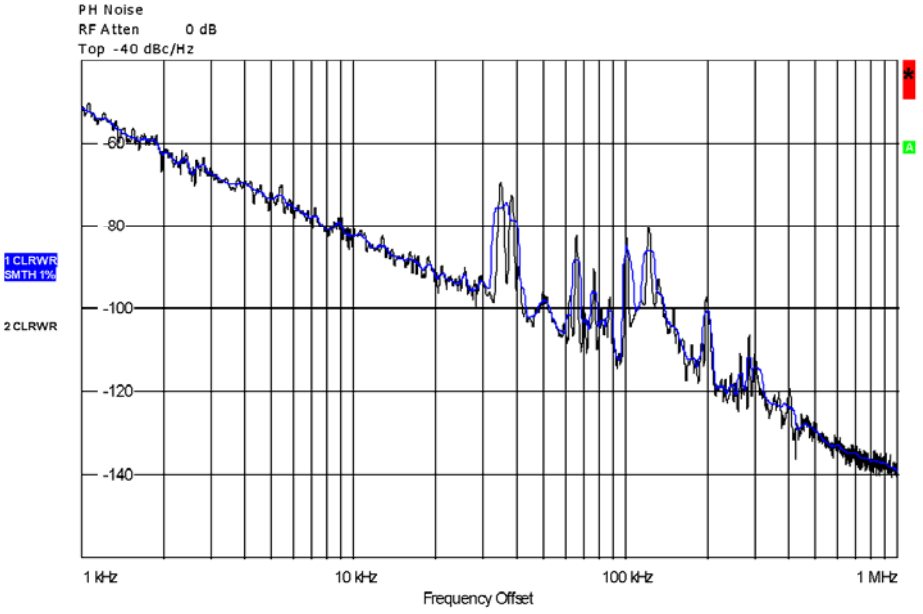

(c) $f_{ref} = 100KHz$, -51.66dBc/Hz at 1KHz offset

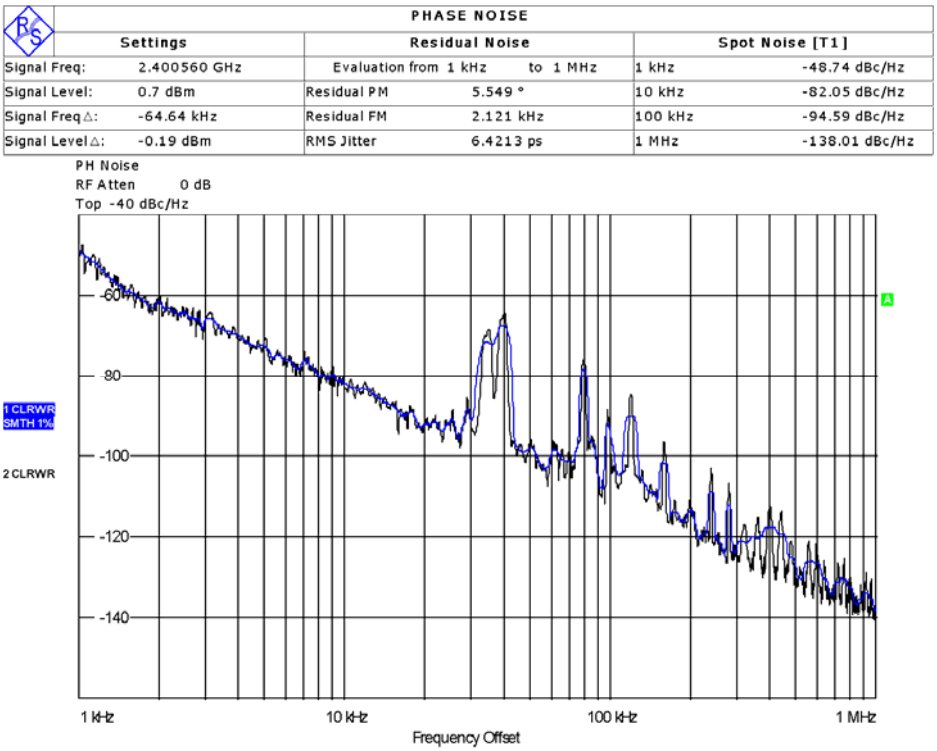

(d) $f_{ref} = 40KHz$, -48.74dBc/Hz at 1KHz offset

Figure 7.10: The measured phase noise of the frequency diversity signal generator.

The fabricated frequency synthesizer has a phase noise of -54.4dBc/Hz at 1KHz offset with a divide ratio of 6000, which raises the f_{ref} phase noise floor by 75dB. Figure 7.11 shows that the measured phase noise of f_{ref} is -126.32dBc/Hz at 1KHz offset, which is 72dB lower than -54.4dBc/Hz. This means that the fabricated integer-N synthesizer has a very good phase noise performance.

It will be shown in later Chapters that a commercial fractional-N frequency synthesizer produced by Analog Device has a phase noise of -88.11 dBc/Hz at 1KHz offset with a divide ratio of 580, which gives 20dB ($20\log\frac{6000}{580}$) improvement in phase noise. Considering a 10MHz TXCO (temperature compensated crystal oscillator) with phase noise of -140dBc/Hz at 1 KHz offset [129] is used to provide reference signal, which also gives 13dB (140 - 126.32) improvement, an estimated

value for the fabricated frequency synthesizer will be -55.11 dBc/Hz at 1 KHz offset. This again shows that the fabricated synthesizer has a very good performance of phase noise.

Although the proposed design has the advantages of compact size, low cost and simple parallel programming, it is not recommended that a divide ratio of over 6000 be used as it will significantly degrade the phase noise performance. A high value of divide ratio N not only degrades phase noise, but also increases the level of reference spurs, even if the loop filter suppresses reference spurs which are outside of its bandwidth.

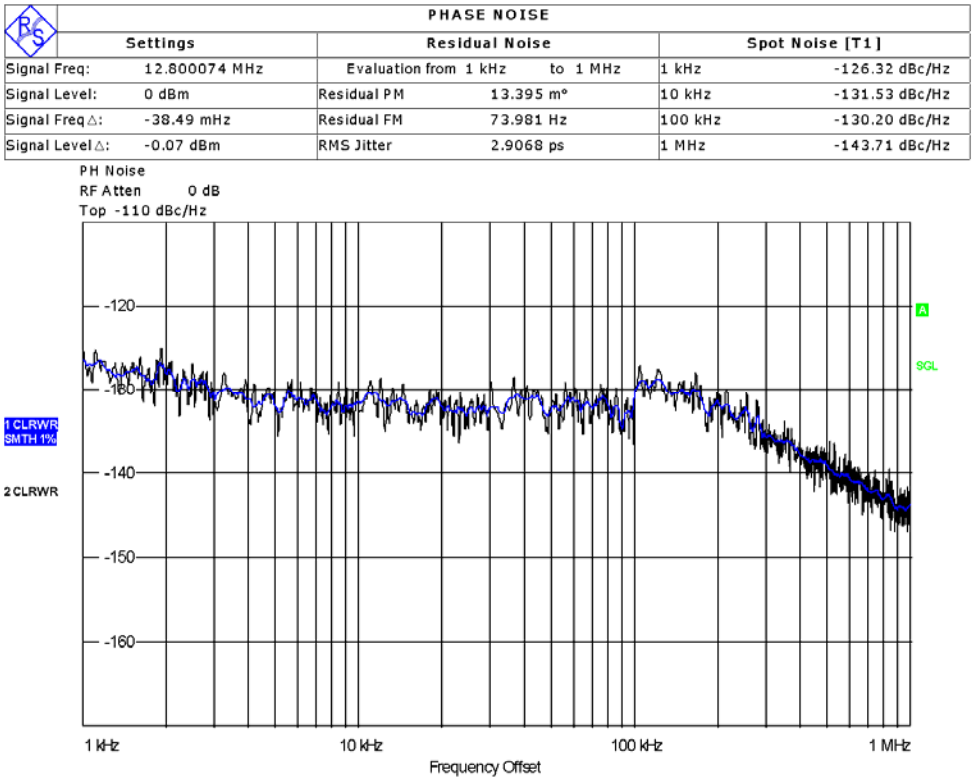

Figure 7.11: The measured phase noise of reference signal.

7.2.5 Reference Spurs of the Integer-N Frequency Diverse Signal Generator

In the phase locked state, the PFD output will be narrow "spikes" that occur at a frequency equal to f_{ref} as in Figure 7.12, but the input of the VCO should be a smooth noise-free DC voltage. Any noise on this signal naturally causes frequency modulation of the VCO. These "spikes" as shown in Figure 7.13 will cause spurs which can be seen in the PLL's output spectrum, offset from the PLL's output frequency (f_{out}) by $\pm f_{ref}$ [127],[128],[131] Reference spurs are mainly caused by source and sink current mismatches in the Charge Pump, leakage of reference signal and its harmonics. For integer-N frequency synthesizer, reference spurs not only increase phase noise level, but also cause interference to neighboring channel thus need to be filtered out. That is why the loop bandwidth is chosen as 1/10 of f_{ref} .

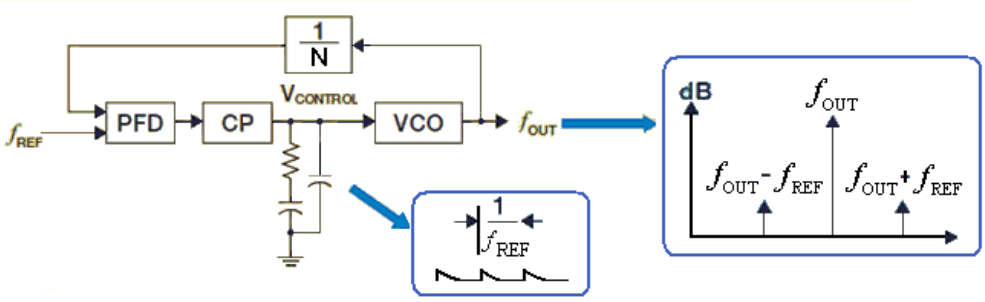

Figure 7.12: "Spikes" in PFD output and "spurs" in VCO output spectrum [132].

The measured reference spurs of the proposed frequency diversity signal generator is shown in Figure 7.13. The output frequency f_{vco} is around 2.4GHz. The reference frequency f_{ref} has been set to be 400 kHz, 200 kHz, 100 kHz and 40 kHz, corresponding to a divide ratio *N* of 6000, 12000, 24000 and 60000 separately. One can see that the reference spur level becomes higher with the increasing divide ratio.

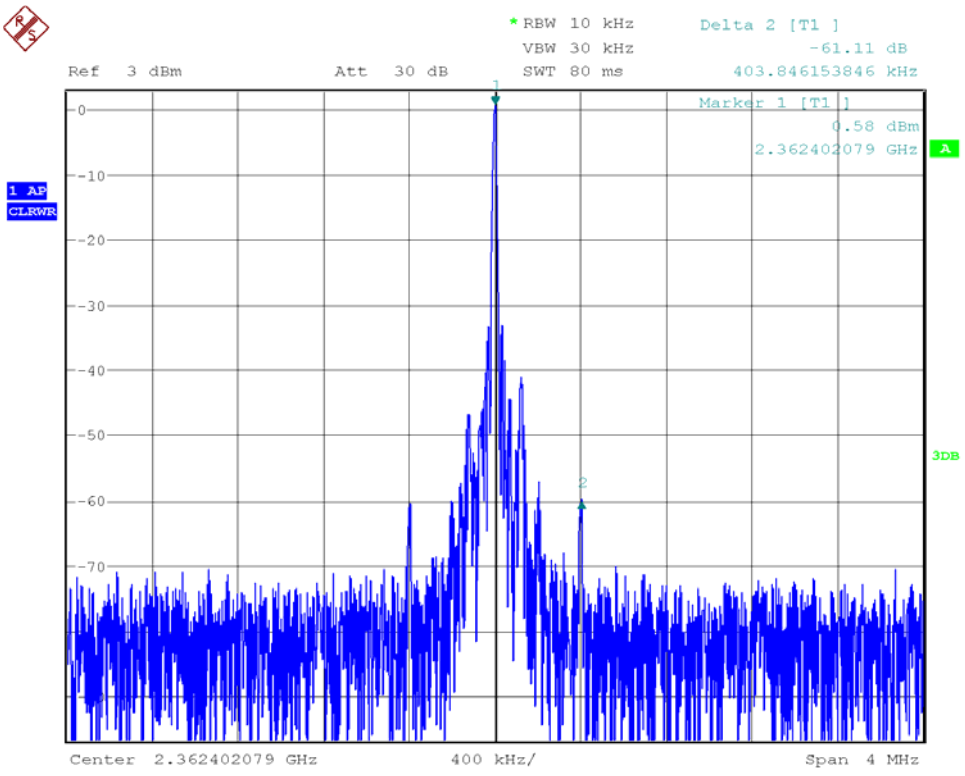

(a) Spur level = -61.11dB with $f_{ref} = 400KHz$

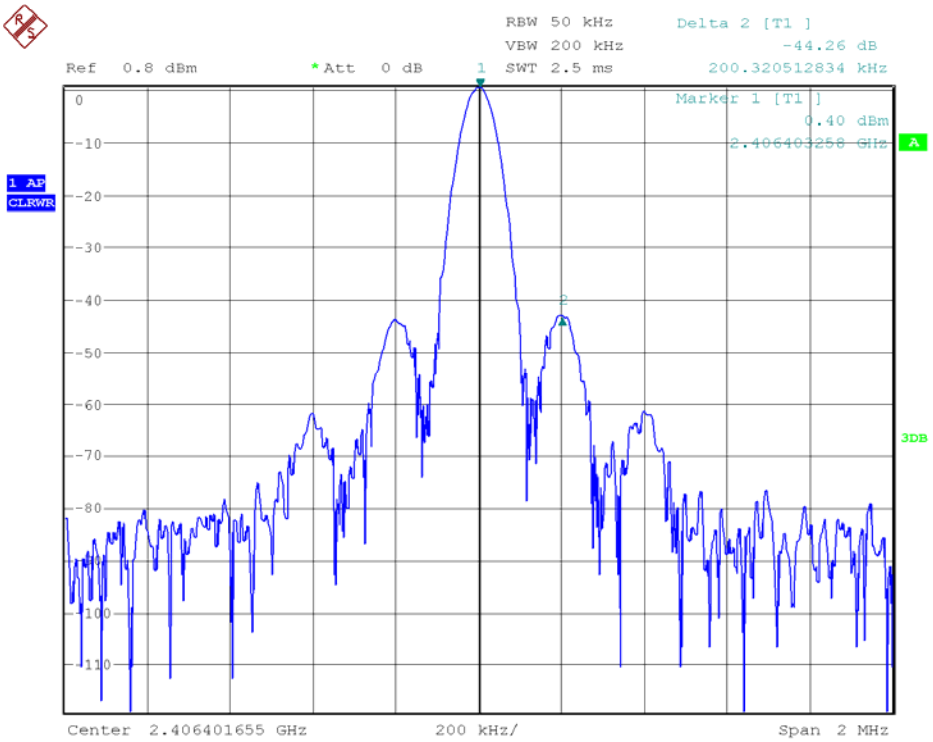

(b) Spur level = -44.26dB with $f_{ref} = 200KHz$

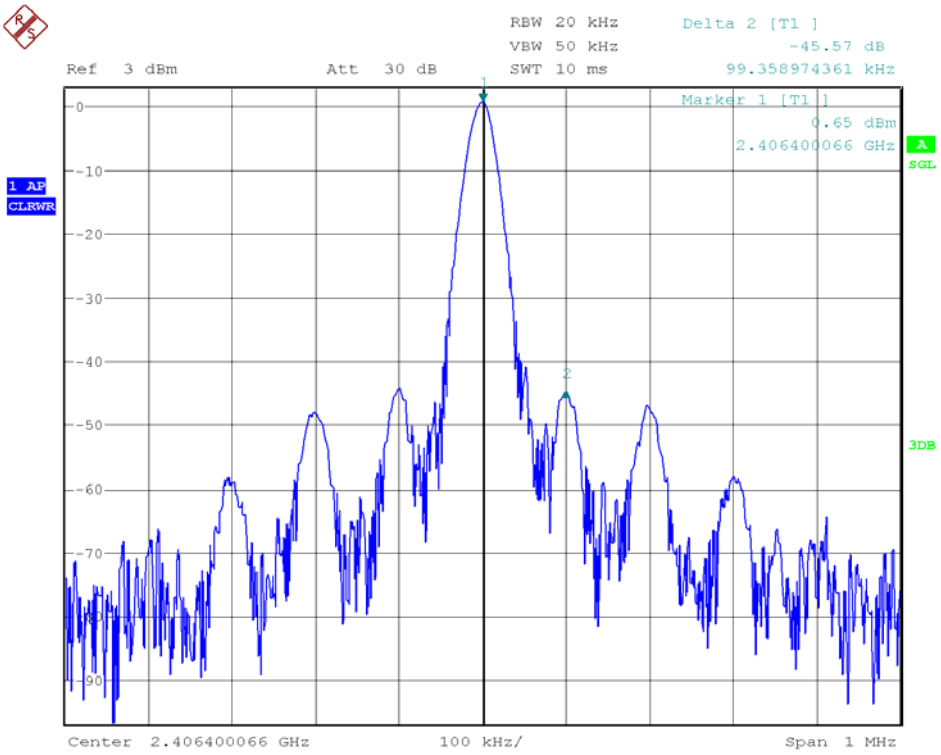

(c) Spur level = -45.57dB with $f_{ref} = 100KHz$

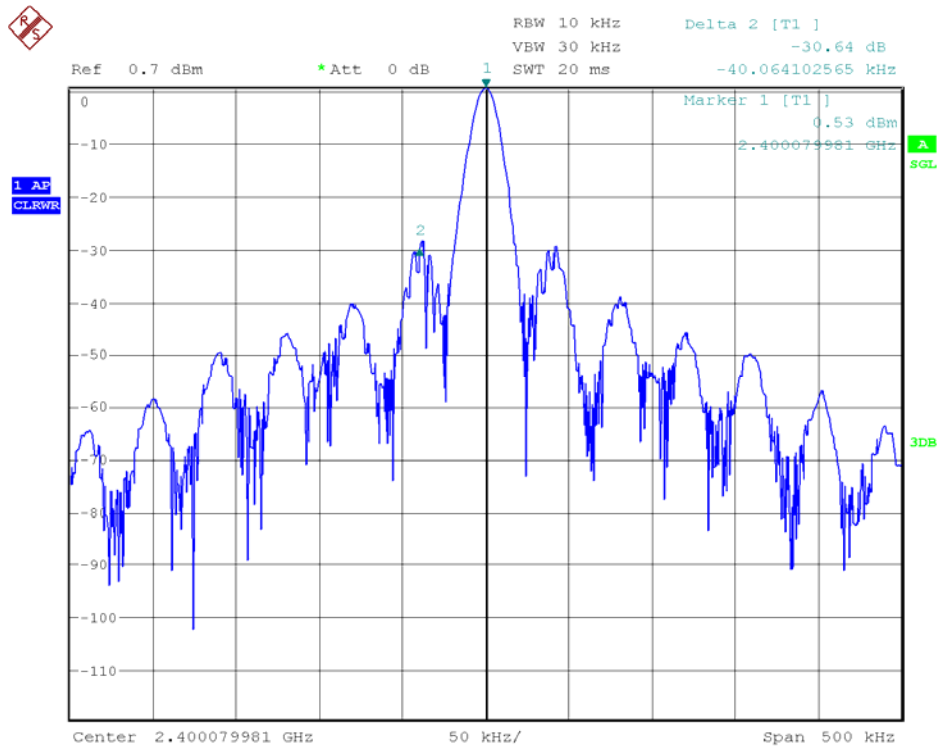

(d) Spur level = -30.64 dB with $f_{ref} = 40KHz$

Figure 7.13: The measured reference spur.

The spectrum of reference signal is shown in Figure 7.14. One can see that the reference signal is not clean because it contains 2nd and higher harmonics, which will cause raised level of reference spur in the output. In our design, the reference signal is provided by a signal generator which allows us to evaluate its influence on the phase noise and reference spurs of output signals. In practical designs, TXCO with better performance in phase noise and harmonics can be used.

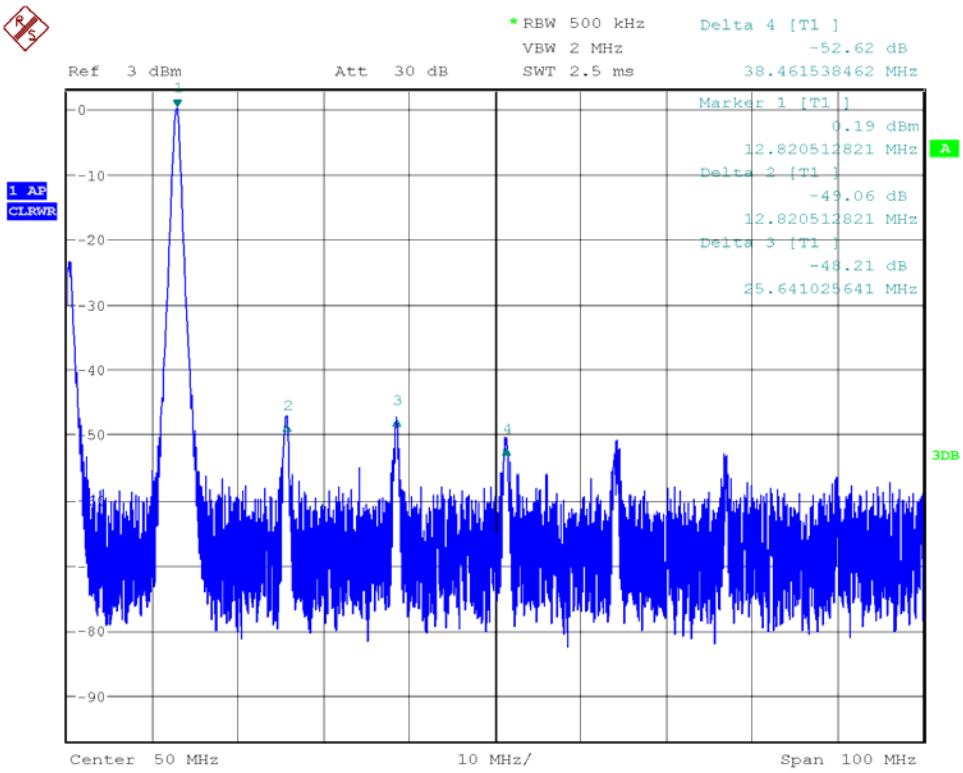

Figure 7.14: The measured spectrum of reference signal.

The inherit limitation of integer-N frequency synthesizer is that one cannot achieve fine frequency step and low phase noise/reference spur at the same time. A solution to this problem is the so called fractional-N frequency synthesizer, which can achieve fine frequency resolution with a higher f_{ref}. Higher reference frequency is also beneficial to the reduction of phase noise and reference. However, the improved performance has a cost of volume, price and complexity, which will be seen in next chapter.

7.3 $\Delta-\Sigma$ Fractional-N PLL Frequency Synthesizer

In integer-N PLL, the divide ratio *N* is fixed. Every reference cycle the VCO frequency is divided by *N*. In fractional-N, an average division of $\left(N+\frac{K}{F}\right)$ is achieved by periodically changing the divide ratio in such a way that in *F* reference cycles, *K* times the divide ratio is *N+1* and *F-K* times *N*. Thus, over *F* reference cycles, the total division is $N_T = K\left(N+1\right)+(F-K)N = FN+K$ and the average divide ratio is $\overline{N} = \frac{N_T}{F} = N+\frac{K}{F}$.

The output frequency in fractional-N designs is given by [127]

$$f_{VCO} = f_{ref}\left(N+\frac{K}{F}\right). \tag{7-8}$$

Fractional-N synthesizers provide an effective means of achieving fine frequency resolution ($\frac{f_{ref}}{F}$) with lower values of *N*, allowing less phase noise than integer-N frequency synthesizers with lower reference frequencies and higher *N* values. This reduction of *N* implies a theoretical reduction in phase noise.

Although a fractional-N synthesizer can achieve very fine granularity, if the sequence of divide by *N* and divide by *N+1* is periodic, spurious signals appear at the VCO output in addition to the desired frequency. This problem can be overcome by randomizing the selection of *N* and *N+1*. This class of fractional-n synthesizers is called $\Delta-\Sigma$ fractional-N synthesizers. The $\Delta-\Sigma$ fractional-N synthesizers can achieve a fine step size with a high reference frequency. The lowered *N* value not only provides low phase noise at the VCO output, it also allows the loop low-pass

filter to have a relatively wide bandwidth, without allowing high harmonic and spurious signals to reach the VCO-tuning port.

To give a comparison to the previous integer-N frequency synthesizer, an ADF4156 $\Delta-\Sigma$ fractional-N synthesizer produced by Analog Device is examined.

Figure 7.15: An ADF4156 $\Delta-\Sigma$ fractional-N synthesizer.

The ADF4146 $\Delta-\Sigma$ fractional-N synthesizer uses a 10MHz TXCO as reference signal and has a fractional index F of 50. Therefore the output frequency is $f_{VCO}=10MHz\times\left(N+\frac{K}{50}\right)$, which has a resolution of 200 KHz. The VCO on board resonates at around 5.8GHz, which gives an integer divide ratio of 580.

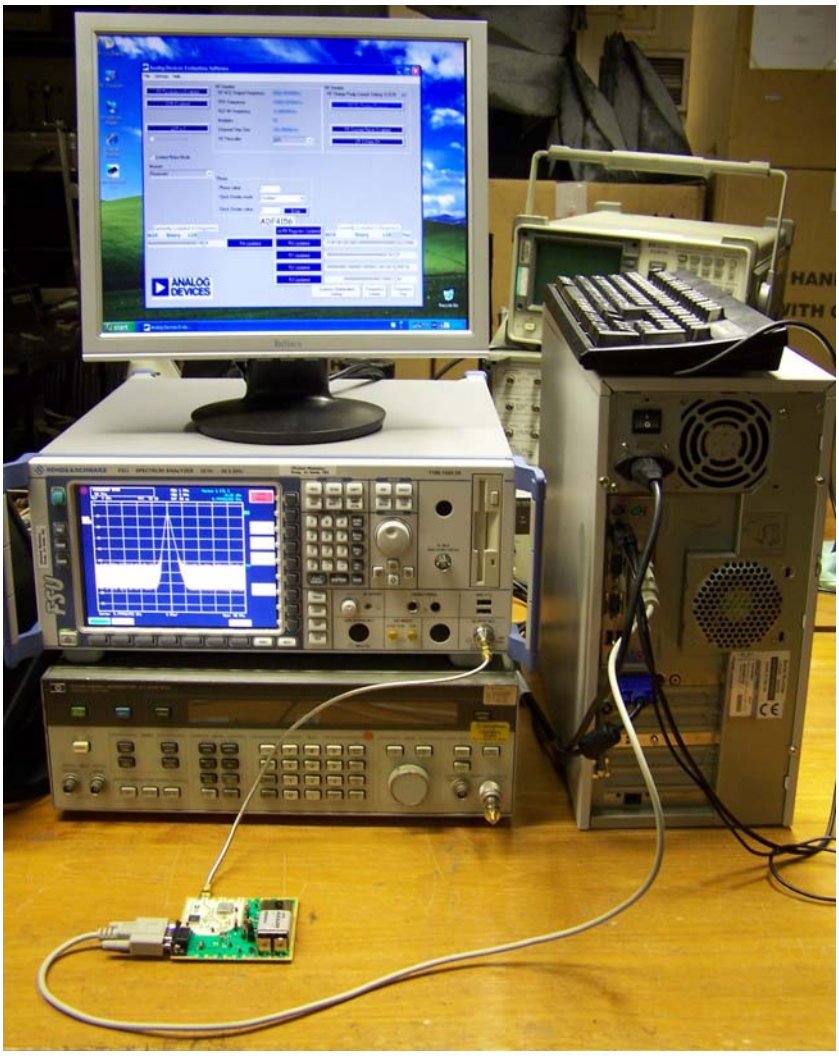

Figure 7.16: The measurement setup of AD4156 fractional frequency synthesizer.

The measurement is set up as in Figure 7.16. The synthesizer has a 9-pin port which is connected to a PC's 25-pin printer port. A software interface as in Figure 7.17 provided by Analog Device allows one to configure the output frequency.

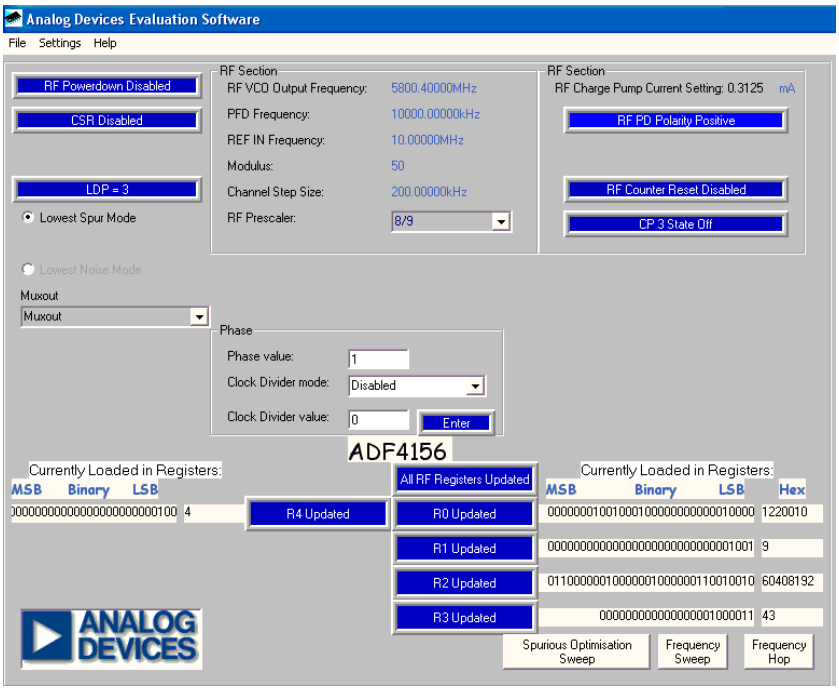

Figure 7.17: The software interface for configuring the output frequency of AD4156.

With a 10MHz reference and 50 fractional index, the output frequency can be tuned with a resolution of 200KHz. As shown in Figure 7.18, a fractional *N* of $580+\frac{2}{50}$ gives an output frequency of 5800.4MHz. 4 output frequencies separated by 200 KHz near 5.8GHz are shown in Figure 7.19.

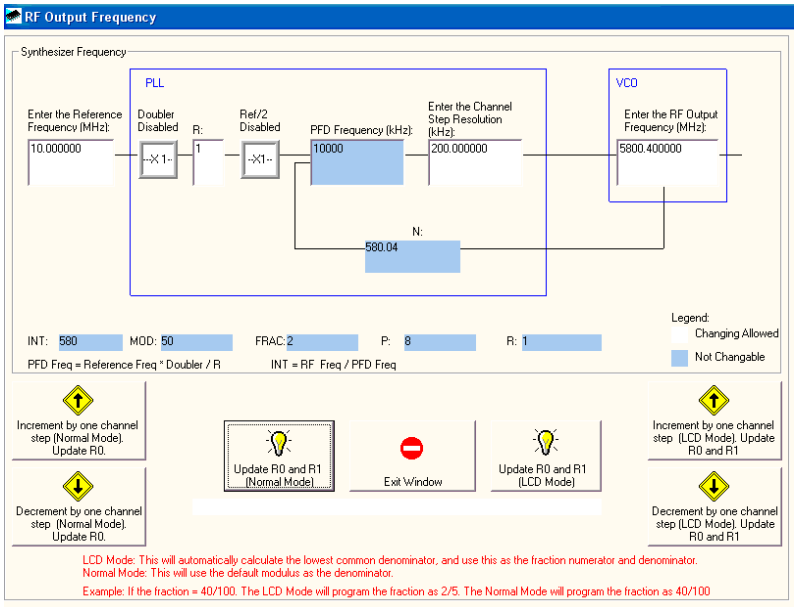

Figure 7.18: The output frequency set to be 5800.4MHz.

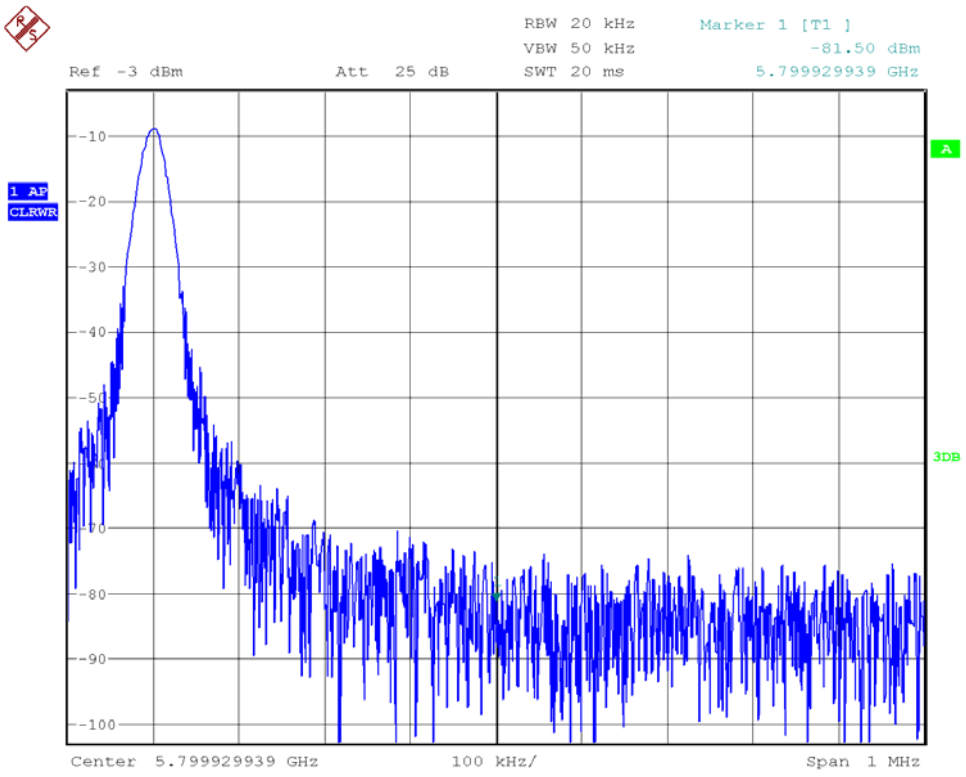

(a) 5800 MHz

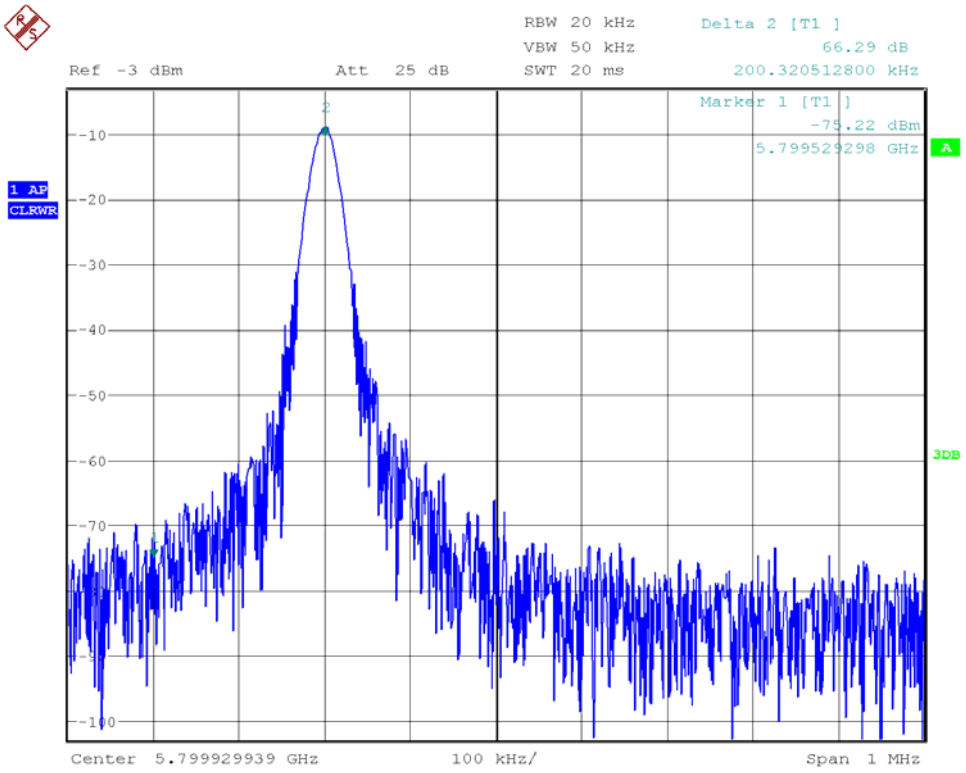

(b) 5800.2 MHz

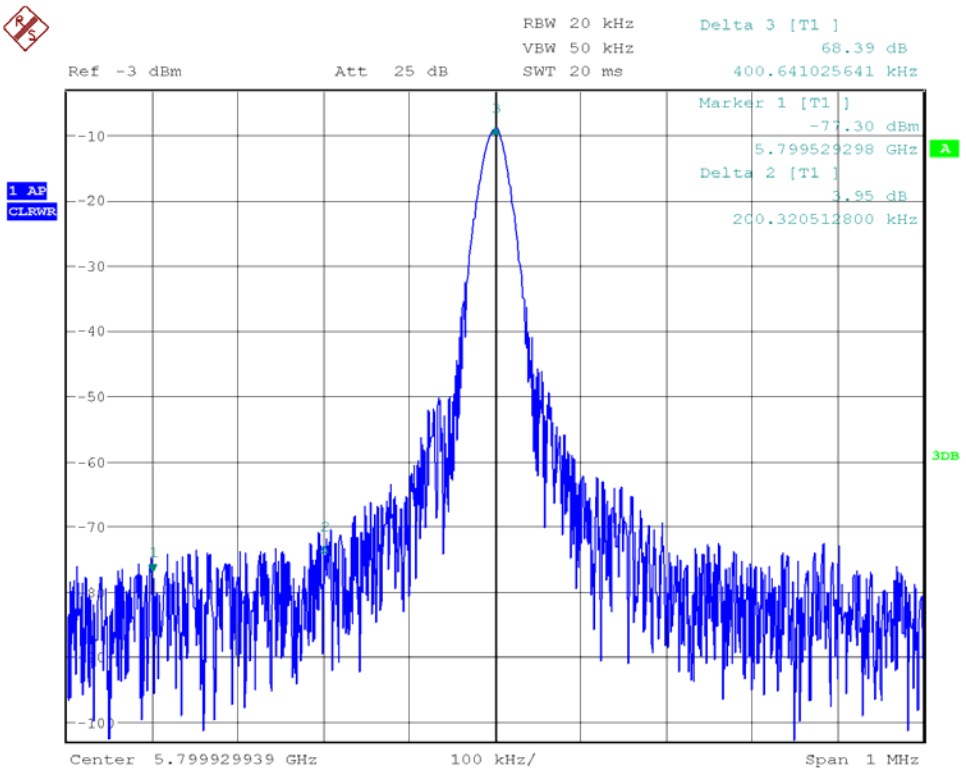

(c) 5800.4 MHz

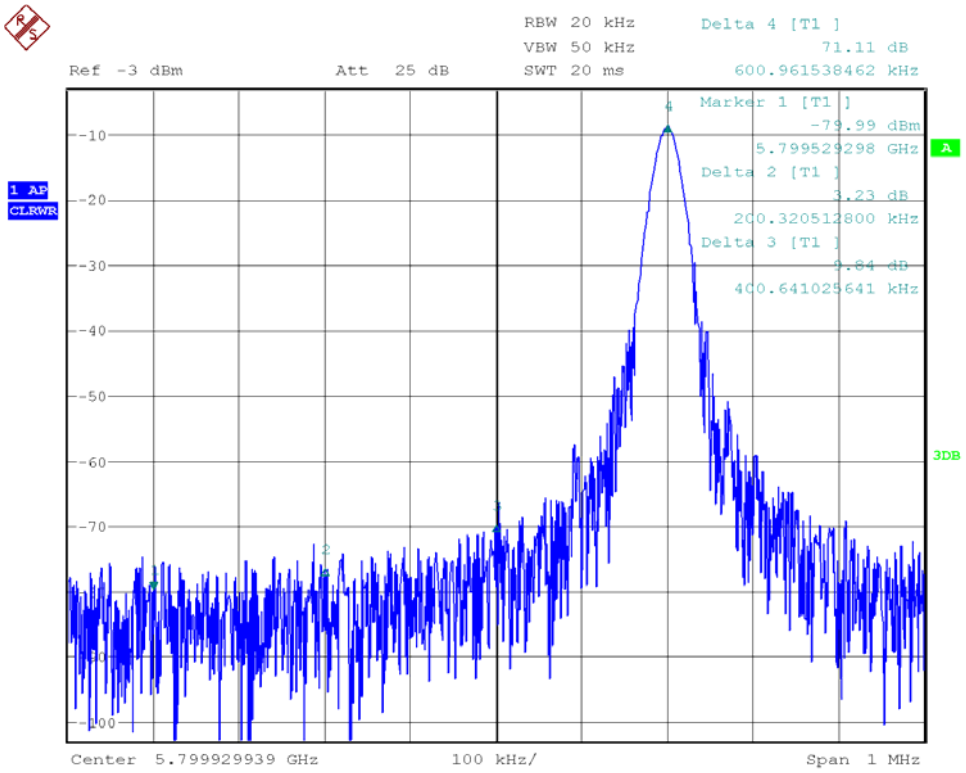

(d) 5800.6 MHz

Figure 7.19: Different output frequencies by ADF4156.

The measured phase noise of ADF4156 $\Delta-\Sigma$ fractional-N frequency synthesizer is -88.11dBc/Hz at 1KHz offset as shown in Figure 7.20. As analyzed in Chapter 7.2.4, the lowered divide ratio, as well as accurate TCXO, provides better phase noise performance.

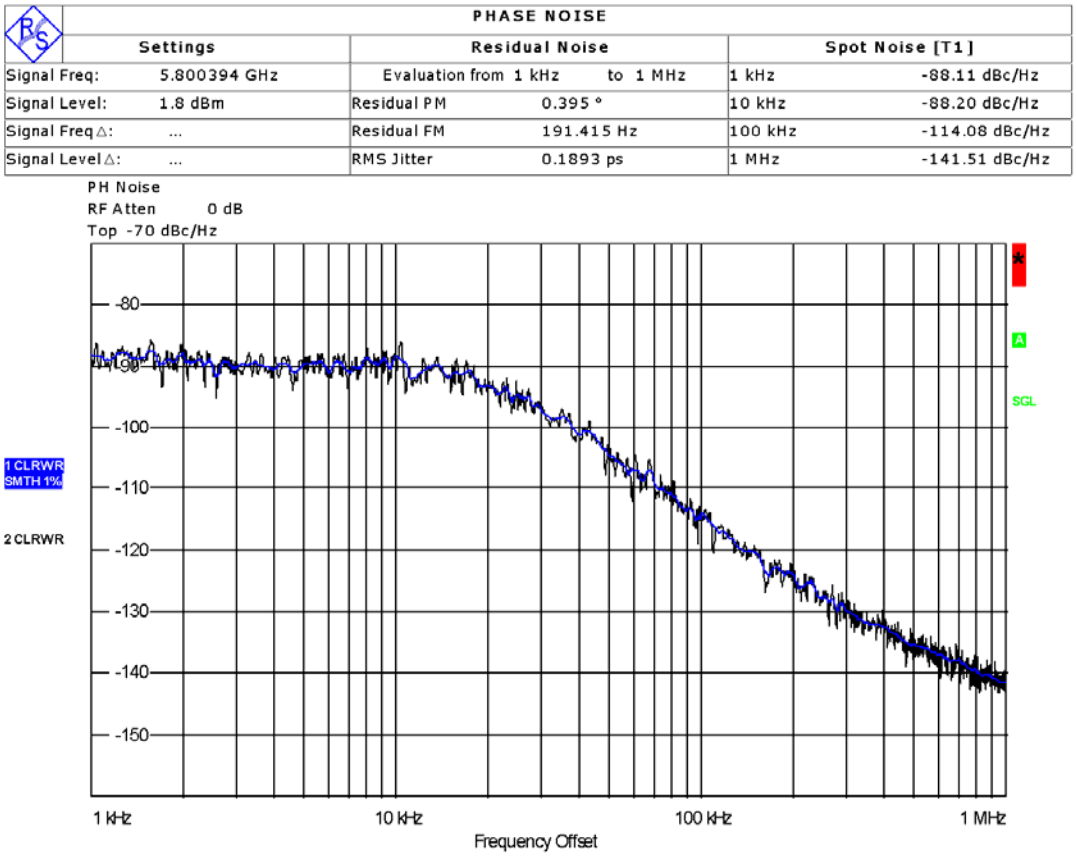

Figure 7.20: The measured phase noise of ADF4156.

The spectrum of the output frequency is shown in Figure 7.21 with a span of 100 MHz. Since the reference frequency is 10MHz, the reference spurs appearing at 10 MHz offset to the center frequency can be easily filtered by the loop filter, which has around 10KHz bandwidth seen from Figure 7.21. And the $\Delta-\Sigma$ technique eliminates the extra spurious signals caused by periodically changes between N and N+1. There are no obvious spurious signals seen in the spectrum.

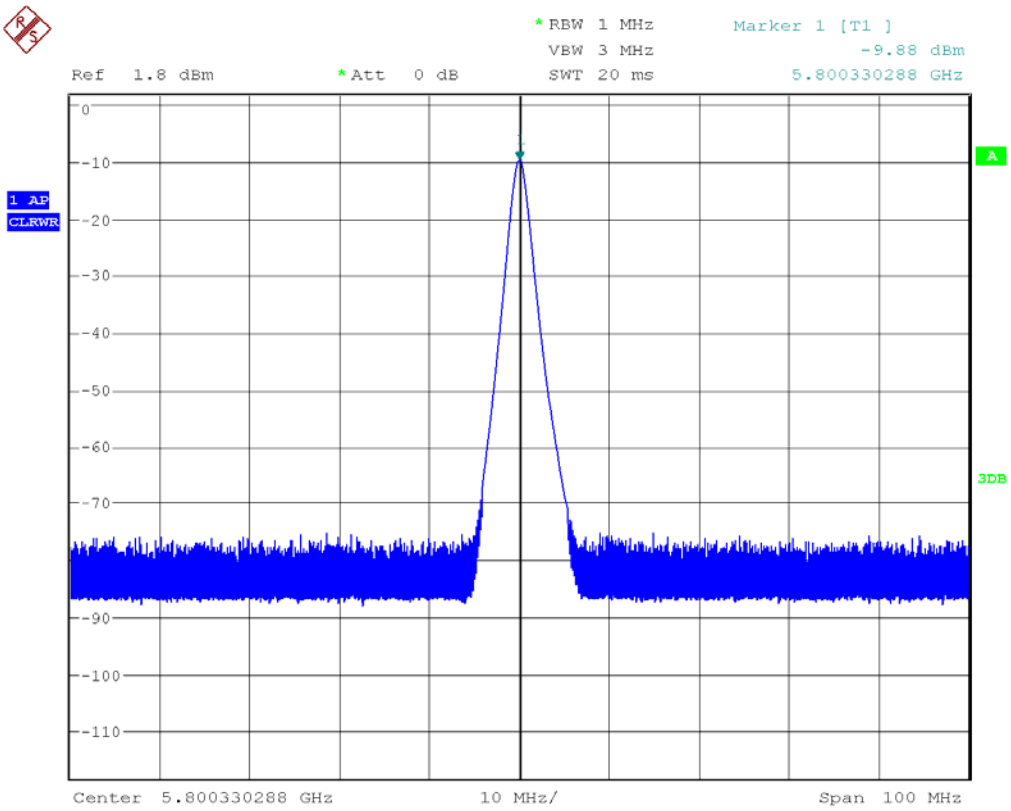

Figure 7.21: The measured spectrum of AD4156's output signal.

7.4 Summary

In this Chapter, the implementation of FDA is studied. To generate the required frequency diverse signals complying with the two assumptions in Chapter 4, the PLL frequency synthesis technique is introduced. Several PLL frequency synthesizers are employed to generate frequency diverse signals. To achieve phase synchronization among the frequency diverse signals, a common reference signal shall be shared by multiple synthesizers.

Then a compact design of integer-N frequency synthesizer is presented, which only requires parallel programming and thus no communicate interface to PC/FPGA is necessary. The influence of divide ratio *N* on the phase noise and reference spur is

evaluated through measurement. It is suggested that a less than 6000 divide ratio is suitable for integer-N frequency synthesizer which does not degrade the performance much. Due to the inherit limitation of integer-N frequency synthesizer, one cannot achieve fine frequency resolution and low phase noise at the same time. A solution to this problem is the $\Delta - \Sigma$ fractional-N frequency synthesizer, whose frequency resolution can be a fractional portion of the reference. The improved performance is obtained at the cost of increased cost and complexity. One can choose either integer-N or $\Delta - \Sigma$ fractional-N frequency synthesizer based on the budget and design requirements.

For the future work, a 4-element FDA using the compact design proposed in this thesis will be fabricated and its beam pattern will be measured, providing further support and proof for the theory on FDA described in this thesis.

Chapter 8

Conclusions and Future Work

8.1 Conclusions

This thesis presents a novel research on the theory and design of FDA for beam scanning and steering applications.

First the theory of the FDA is developed by deriving the array factor and analyzing its characteristics. The periodicity of FDA's array factor with respect to time and distance, together with the relationship between scanning period and frequency shift, is mathematically verified. Then the discussion is extended to pulsed case where the mechanism of beam steering using pulsed FDA is explained. Moreover, the signal processing technique for frequency diverse signals is also provided in this thesis, which makes the pulsed FDA suitable for pulsed radar applications.

Then the mathematical theory is verified by electromagnetic simulation, which considers the mutual coupling and element's radiation characteristics. The periodically beam scanning phenomenon is observed from the simulated results. And the relationship between scanning period and frequency shift is verified by 3 simulations where different frequency shift value is assigned.

The implementation of FDA is also considered. The basic two assumptions on FDA specify the requirements on the frequency diverse signals. In this thesis the PLL frequency synthesis technique is introduced as an effective approach of generating the desired frequency diverse signals. A compact design of integer-N frequency

synthesizer is presented with basic design considerations and guidelines. The $\Delta - \Sigma$ fractional-N frequency synthesizer with improved performance is also introduced.

The frequency diverse array concept provides new design freedom for beam forming and control. In the basic concept, a frequency shift is applied across the array elements. This results in a periodically scanning beam without mechanical rotation or electronic phase shifters. This feature of the FDA may result in an affordable beam scanning option. Actually the T/R (transmit/receive) module takes a significant part of the whole cost of a conventional phased array. Moreover, the FDA offers more flexible beam control with finer steering angle resolution, since the time to transmit the pulse can be chosen randomly and consecutively, while phase shifters can only provide limited phase resolution.

8.2 Future Work

Since the CW FDA has a periodically scanning beam and not suitable for beam steering applications, one remaining task is to measure the radiation pattern of pulsed FDA and verify the discussions in Chapter 5. Due to time and budget limitation, this has not been performed in this thesis. Thus, the future work is to fabricate a beam forming FDA and measure the radiation patterns of pulses transmitted at different time. The diagram of the whole system is shown in Figure 8.1.

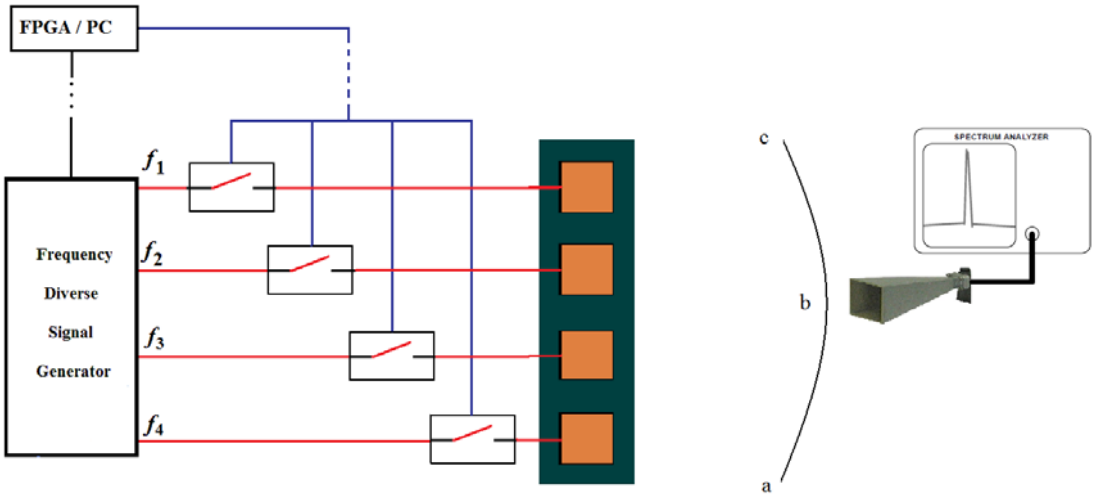

Figure 8.1: Measurement of radiation pattern of beam forming FDA

The frequency diverse signal generator discussed in Chapter 7 is employed to generate the required CW frequency diverse sinuous signals with frequency shift Δf . RF switches are inserted between the frequency diverse signal generator and antenna array. When a rectangular pulse with length of $\frac{1}{100}\times\frac{1}{\Delta f}$ is applied to turn on all the RF switches during the pulse, a fixed beam with 1° angle spread will be formed at certain angle. Moreover, if the rectangular pulse is repeated after multiples of scanning period ($n\times\frac{1}{\Delta f}$), the beam will be formed at the same angle due to periodicity. This makes it possible to obtain the radiation pattern by measuring the power level at different angles (from "a" to "c" in Figure 8.1) with a horn antenna connected to a spectrum analyzer.

If $\Delta-\Sigma$ fractional-N frequency synthesizer is used, an FPGA (or multiple PCs) is required to conFigure all the synthesizers because it is not convenient to connect each synthesizer to a separate PC. The whole volume and cost can be lower if the integer-N frequency synthesizer presented in Section 7.2 is used, since no FPGA or

PC is required. However, due to the limitation of integer-N frequency synthesizer, the frequency shift Δf cannot be too small in order to avoid a high value of divide ratio *N*. Therefore, the length of rectangular pulse $\frac{1}{100}\times\frac{1}{\Delta f}$ is very short. For example, when Δf is 400 kHz, the length of rectangular pulse will be 25 ns.

Another factor to be considered in both cases is the consistency of RF switches. The differences among the phase delay of RF switches may cause deviation to phase synchronization, which in turn changes the shape of radiation pattern.

8.3 Extension of the FDA Concept

In this thesis, the pulse transmitted by an FDA is a rectangular pulse with a width of $\frac{1}{100}\times\frac{1}{\Delta f}$. The type of pulse can be extended to linear frequency modulated (LFM or chirp) signal, which is widely used in radar systems. When a chirp signal is transmitted by an FDA, the relationship between the parameters of chirp signal and the radiation pattern of FDA can be explored. It is possible to use the FDA to transmit a chirp signal towards a desired direction at the transmitter end, while use a single carrier to demodulate the chirp signal at receiver end. This concept combines the flexible beam forming feature of FDA and improved target detection ability of chirp signals, at the same time eliminates the use of phase shifters.

References

[1] R. J. Mailloux, Phased Array Antenna Handbook. Norwood, MA:Artech House, 1994.

[2] D. Parker and D. C. Zimmermann, “Phased arrays—Part II: Implementations, applications, and future trends,” IEEE Trans. Microw. Theory Tech., vol. 50, no. 3, pp. 688–698, Mar. 2002.

[3] Rock, J.C.; Mullins, J.H.; Booth, J.P.; Hudson, T, “The Past, Present, and Future of Electronically-Steerable Phased Arrays in Defense Applications”, Aerospace Conference, 2008 IEEE, 2008 , Page(s): 1 - 7

[4] Naguib, A.F.; Arogyaswami Paulraj; Kailath, T., “Capcity improvement of base-station antenna arrays cellular CDMA”, Signals, Systems and Computers, 1993. 1993 Conference Record of The Twenty-Seventh Asilomar Conference on, vol.2, Page(s): 1437 - 1441

[5] Khalaj, B.H.; Paulraj, A.; Kailath, T., “Antenna arrays for CDMA systems with multipath”, Military Communications Conference, 1993. MILCOM '93. Conference record. 'Communications on the Move'., IEEE,Volume: 2, Page(s): 624 - 628

[6] E. Fishler, A. Haimovich, R. Blum, D. Chizhik, L. Cimini, and R. Valenzuela, “MIMO radar: an idea whose time has come,” Proceedings of the IEEE Radar Conference, pp. 71–78, April 2004.

[7] E. Fishler, A. Haimovich, R. Blum, L. Cimini, D. Chizhik, and R. Valenzuela, “Performance of MIMO radar systems: advantages of angular diversity,” 38th

Asilomar Conference on Signals, Systems and Computers, Pacific Grove, CA, vol. 1, pp. 305–309, Nov. 2004.

[8] F. Robey, S. Coutts, D. Weikle, J. McHarg, and K. Cuomo, "MIMO radar theory and experimental results," 38th Asilomar Conference on Signals, Systems and Computers, Pacific Grove, CA, vol. 1, pp. 300–304, Nov.2004.

[9] D. R. Fuhrmann and G. San Antonio, "Transmit beamforming for MIMO radar systems using partial signal correlation," 38th Asilomar Conference on Signals, Systems and Computers, Pacific Grove, CA, vol. 1, pp. 295– 299, Nov. 2004.

[10] A. Haimovich, R. Blum, and L. Cimini, "MIMO radar with widely separated antennas," IEEE Signal Processing Mag.,vol. 25, pp. 116–129, Jan. 2008.

[11] E. Fishler, A. Haimovich, R. Blum, L. Cimini, D. Chizhik, and R. Valenzuela, "Spatial diversity in radars—Models and detection performance," IEEE Trans. Signal Processing, vol. 54, pp. 823–838, Mar. 2006.

[12] N. Lehmann, E. Fishler, A. Haimovich, R. Blum, D. Chizhik, L. Cimini, and R. Valenzuela, "Evaluation of transmit diversity in MIMO-radar direction finding," IEEE Trans. Signal Processing, vol. 55, pp. 2215–2225, May 2007.

[13] J. Li, P. Stoica, and X. Zheng, "Signal synthesis and receiver design for MIMO radar imaging," IEEE Trans. Signal Processing, vol. 56, pp. 3959–3968, Aug. 2008.

[14] J. Li and P. Stoica, "MIMO radar with colocated antennas," IEEE Signal Processing Mag., vol. 24, pp. 106–114, Sept. 2007.

[15] C.-Y. Chen and P. Vaidyanathan, “MIMO radar space-time adaptive processing using prolate spheroidal wave functions,” IEEE Trans. Signal Processing, vol. 56, pp. 623–635, Feb. 2008.

[16] I. Bekkerman and J. Tabrikian, “Target detection and localization using MIMO radars and sonars,” IEEE Trans. Signal Processing, vol. 54, pp. 3873–3883, Oct. 2006.

[17] Y. Yang and R. Blum, “Minimax robust MIMO radar waveform design,” IEEE J. Select. Topics Signal Processing, vol. 1,pp. 147–155, Jun. 2007.

[18] A. Maio and M. Lops, “Design principles of MIMO radar detectors,” IEEE Trans. Aerosp. Electron. Syst., vol. 43, pp. 886–898, July 2007.

[19] D. Fuhrmann and G. Antonio, “Transmit beamforming for MIMO radar systems using signal cross-correlation,” IEEE Trans. Aerosp. Electron. Syst., vol. 44, pp. 171–186, Jan. 2008.

[20] P. Stoica, J. Li, and Y. Xie, “On probing signal design for MIMO radar,” IEEE Trans. Signal Processing, vol. 55, pp.4151–4161, Aug. 2007.

[21] J. Li, L. Xu, P. Stoica, K. Forsythe, and D. Bliss, “Range compression and waveform optimization for MIMO radar: A Cramer-Rao bound based study,” IEEE Trans. Signal Processing, vol. 56, pp. 218–232, Jan. 2008.

[22] A. Hassanien and S.A. Vorobyov, “Transmit/receive beamforming for MIMO radar with colocated antennas,” in Proc. IEEE Int. Conf. on Acoustic, Speech, Signal Processing (ICASSP’09), Taipei, Taiwan, Apr. 2009, pp. 2089–2092.

[23] J. P. Browning, D. R. Fuhrmann, and M. Rangaswamy, “A hybrid MIMO phased-array concept for arbitrary spatial beampattern synthesis,” in Proc. IEEE Digital Signal Processing and Signal Processing Education Workshop (DSP/SPE’09),Marco Island, FL, Jan. 2009, pp. 446–450.

[24] Y. Abramovich and G. Frazer, “Bounds on the volume and height distributions for the MIMO radar ambiguity function,”IEEE Signal Processing Lett., vol. 15, pp. 505–508, 2008.

[25] Andrea Goldsmith, Wireless communications, 2005

[26] D. W. Bliss and K. W. Forsythe, “Multiple-input multiple-output (MIMO) radar and imaging: degrees of freedom and resolution,” Proc. 37th IEEE Asilomar Conf. on Signals, Systems, and Computers, vol. 1, pp. 54–59, Nov. 2003.

[27] D. J. Rabideau and P. Parker, “Ubiquitous MIMO Multifunction Digital Array Radar,” Proc. 37th IEEE Asilomar Conf. on Signals, Systems, and Computers, vol. 1, pp. 1057–1064, Nov. 2003.

[28] V. F. Mecca, D. Ramakrishnan, and J. L. Krolik, “MIMO Radar Space-Time Adaptive Processing for Multipath Clutter Mitigation” IEEE Workshop on Sensor Array and Multichannel Signal Processing, pp. 249–253, July 2006.

[29] J. Li, P. Stoica, L. Xu, and W. Roberts, “On Parameter Identifiability of MIMO Radar,” IEEE Signal Processing Letters, Vol. 14, No. 12, pp. 968–971, Dec. 2007.

[30]Steinberg, B.; Yadin, E., “Effect of multipath and scattering on array gain of a large adaptive beam forming phased array”, Antennas and Propagation IEEE

Transactions on, Volume: 33 , Issue: 5, Year: 1985 , Page(s): 481 – 487

[31] Lee, J.-H.; Wu, J.-F.; “Adaptive beam forming without signal cancellation in the presence of coherent jammers”, Radar and Signal Processing, IEE Proceedings, Volume 136, Issue 4, Aug 1989 Page(s):169 – 173

[32] Chiba, I.; Takahashi, T.; Karasawa, Y.; “Transmitting null beam forming with beam space adaptive array antennas”, Vehicular Technology Conference, 1994 IEEE 44th, 8-10 June 1994 Page(s):1498 - 1502 vol.3

[33] Madan, B.; “A rapidly converging algorithm for adaptive beam forming”, Acoustics, Speech, and Signal Processing, IEEE International Conference on ICASSP '80. Volume 5, Apr 1980 Page(s):1052 – 1055

[34]Garcia-Ordonez, L.; Pages-Zamora, A.; Fonollosa, J.R.; “Diversity and multiplexing tradeoff of multiple beamforming in MIMO channels”, Information Theory, 2005. ISIT 2005. Proceedings. International Symposium on 4-9 Sept. 2005 Page(s):1808 – 1812

[35] Boche, H.; Jorswieck, E.; “Analysis of diversity and multiplexing tradeoff for multi-antenna systems with covariance feedback”, Vehicular Technology Conference, 2002. Proceedings. VTC 2002-Fall. 2002 IEEE 56th , Volume 2, 24-28 Sept. 2002 Page(s):864 - 868 vol.2

[36]Sarkar, T.K.; Adve, R.; Koh, J.; Park, S.; Salazar, M.; “Smart antennas and digital beam forming”, Antennas and Propagation Society International Symposium, 2000. IEEE Volume 3, 16-21 July 2000 Page(s):1245 vol.3

[37] R. C. Hansen, Ed., Microwave Scanning Antenna, Volume I Apertures. New York: Academic, 1964.

[38] Microwave Scanning Antenna, Volume II Array Theory and Practice. New York: Academic, 1966.

[39] R. C. Hansen, Ed., Microwave Scanning Antenna, Volume III Array Systems New York: Academic, 1966.

[40] J. L. Allen, "The theory of array antennas," MIT Lincoln Lab., Lexington, MA, Tech. Rep. 323, 1963.

[41] R. S. Elliott, "Beamwidth and directivity of large scanning arrays," Microwave J., pt. 1, vol. 6, pp. 53–60, Dec. 1963.

[42] A. A. Oliner and G. H. Knittel, Phased-Array Antennas. Norwood, MA: Artech House, 1972.

[43] R. C. Hansen, Significant Phased Array Papers. Norwood, MA: Artech House, 1973.

[44] E. Brookner, Practical Phased-Array Antenna Systems. Norwood, MA: Artech House, 1991.

[45] http://www.radartutorial.eu/19.kartei/karte423.en.html

[46] http://en.wikipedia.org/wiki/Radar

[47] http://www.es.northropgrumman.com/ASD/combat/APG-77.html

[48] Cohen, E. D., "Trends in the Development of MMICs and Packages for Active Electronically Scanned Arrays (AESAs)," 1996 IEEE International Symposium on Phased Arrays Systems and Technology, October 15-18, 1996, pp. 1-4, Boston, MA.

[49] B. Kopp, "X-band T/R module overview," in IEEE MTT-S Int. Microwave Symp. Dig., 2000, pp. 705–708

[50] F.E. van Vliet, M. van Wanum, A.W. Roodnat, M.Alfredson, "Fully-integrated wideband TTD core chip with serial control",Conf. Proc. GaAs2003, Munich, Germany, 2003

[51] K. Van Caekenberghe, T. Vaha-Heikkila, G. Rebeiz, and K. Sarabandi, "Ka-band MEMS TTD passive electronically scanned array (ESA)," in IEEE Antennas Propag. Symp. Dig., Jul. 2006, pp. 513–516.

[52] K. Topalli, M. Unlu, O. A. Civi, S. Demir, S. Koc, and T. Akin, "A monolithic phased array using 3-bit DMTL RF MEMS phase shifters,"in IEEE Antennas Propag. Symp. Dig., Jul. 2006, pp. 517–520.

[53] M. Kim, J. B. Hacker, R. E. Mihailovich, and J. F. DeNatale, "A DC-to-40 GHz four-bit RF MEMS true-time delay network," IEEE Microw. Wireless Compon. Lett., vol. 11, no. 2, pp. 56–58, Feb. 2001.

[54] B. Pillans, S. Eshelman, A. Malczewski, J. Ehmke, and C. Goldsmith, "Ka-band RF MEMS phase shifters," IEEE Microw. Guided Wave Lett., vol. 9, no. 12, pp. 520–522, Dec. 1999.

[55] Smith, J. K., F. W. Hopwood and K. A. Leahy, "MEM Switch Technology in Radar," IEEE 2000 lnteinational Radar Conference, pp. 193.198.

[56]. J. Frank, “Bandwidth criteria for phased array antennas”, in Phased Array Antennas, A.A. Oliner & G.H. Knittel, Artech House, pp. 243-253, 1972.

[57] J.S. Ajoika & J.L. McFarland, “Beam Forming Feeds”, Chap. 19 of Antenna Handbook: Theory, Applications, and Design, Y.T. Lo and S.W. Lee (eds.), Van Nostrand, pp. 19-7 – 19-8, 1988.

[58] R. Tang, “Survey of Time Delay Beam Steering Techniques”, in Phased Array Antennas, A.A. Oliner & G.H. Knittel, Artech House, pp. 254-260, 1972.

[59] W.B. Adams, “The broad-band signal response of a phase-steered linear receiving array”, Proc. IEEE, vol. 52, issue 1, p. 106, Jan 1964

[60] Lu Jiaguo; Wu Manqin; Jin Xueming; Fang Zhengxing; “Active phased array antenna based on DDS”,Phased Array Systems and Technology, 2003. IEEE International Symposium on, 2003 , Page(s): 511 – 516

[61] Nishio, T.; Hsiao-Ping Tsai; Yuanxun Wang; Itoh, T.; “A high-speed adaptive antenna array with simultaneous multibeam-forming capability”,Microwave Theory and Techniques, IEEE Transactions on,Volume: 51 , Issue: 12, 2003 , Page(s): 2483 – 2494

[62] van Dijk, R.; van der Houwen, E.H.; Maas, A.P.M.; “Multi-mode FMCW radar array with independent digital beam steering for transmit and receive”,Radar Conference, 2008. EuRAD 2008. European, 2008 , Page(s): 412 – 415

[63] 1. R. Klauder, A. C. Price, S. Darlington, and W. 1.Albersheim, "The theory and design of chirp radars," Bell Syst. Tech. vol. XXXIX, no. 4, p. 745-808, July 1960.

[64] R. Manasse, "The use of pulse coding to discriminate against clutter," M.1.T. Lincoln Lab., Lexington, MA, Group Rept. 312-12, June 1961.

[65] S. Sussman, "Least-square synthesis of radar ambiguity functions, " IEEE Trans.Information Theory vol. 8, issue 3, pp. 246-254, Apr. 1962.

[66] L. J. Spafford, "Optimum radar receive waveforms in the presence of clutter," General Electric, Syracuse, NY, Technical Information Series Report R65EMHI4, June 1965.

[67] H. L. VanTrees, "Optimum signal design and processing for reverberation-limited environments, " IEEE Trans. Military Electronics, vol. MIL-9, issues 3-4, pp. 212-229, Jul.-Oct. 1965.

[68] M. Ares, "Optimum burst waveforms for detection of targets in uniform range-extended clutter,"GeElectric,Syracuse, NY, Technical Information Series Report R66EMH16 Rept., Mar. 1966.

[69] W. D. Rummier, "Clutter suppression by complex weighting of coherent pulse trains," IEEE Trans. Aerospace and Electronics Systems, vol. AES-2, pp. 689699, Nov. 1966.

[70] D. DeLong and E. Hofstetter, "On the design of optimum radar waveforms for clutter rejection," IEEE Trans.Information Theory, vol. 13, issue 3, pp. 454 463, Jul. 1967.

[71] C. A. Stutt and L. 1. Spafford , "A 'best' mismatched filter response for radar clutter discrimination," IEEE Trans.Information Theory, vol. IT-14, no. 2, pp. 280287, Mar. 1968.

[72] A. Farina, “Waveform diversity: Past, present, and future,” in Proc. 3rd Int. Waveform Diversity Des. Conf., Plenary Talk, Pisa, Italy, Jun.2007

[73] A. Nehorai, F. Gini, M. S. Greco, A. Papandreou-Suppappola, and M.Rangaswamy, Eds., “Adaptive waveform design for agile sensing and communications,” IEEE J. Sel. Topics Signal Process., vol. 1, no. 1, pp.2–213.

[74] J. W. Garnham, J. R. Roman, and P. Antonik, “Application of waveform diversity to improve SMTI system performance,” Fourth Tri-Service Waveform Diversity Workshop, Naval Research Lab,Wash. DC, USA, 14-15 Nov. 2006.

[75] S. Sira, A. Papandreou-Suppappola, and D. Morrell, “Time-varying waveform selection and configuration for agile sensors in tracking applications,” in Proc. of the 2005 Int. Conf. on Acoustics, Speech and Signal Processing, Mar. 2005.

[76] J. S. Bergin, P. M. Techau, J. E. Don Carlos, and J. R. Guerci, “Radar waveform optimization for colored noise mitigation,” in Proc.2005 IEEE Int. Radar Conf., Alexandria, VA, May 9–12, 2005, pp.149–154.

[77] B. Friedlander, “A subspace framework for adaptive radar waveform design,” in Conf. Rec. 39th Asilomar Conf. Signals, Syst. Comput. 2005, Pacific Grove, CA, Oct. 28–Nov. 1 2005, pp. 1135–1139.

[78] M. Bell, J. G. Webster, Ed., “Information Theory of Radar and Sonar

Waveforms," in Wiley Encyclopedia of Electrical and Electronic Engineering. New York: Wiley-Intersci., 1999, vol. 10, pp. 180–190.

[79] S.U. Pillai, H. S. Oh, D. C. Youla, and J. Guerci , "Optimum transmit-receiver design in the presence of signal-dependent interference and channel noise," IEEE Trans. Information Theory, vol. 46, no. 2, pp. 577–584, Mar. 2000.

[80] D. A. Garren, M. K. Osborn, A. C. Odom, J. S. Goldstein, S. U. Pillai, and J. Guerci, "Enhanced target detection and identification via optimized radar transmission pulse shape", Proc. Inst. Elect. Eng., Radar, Sonar, Navigation, vol. 148, no. 3, pp. 130-138, Jun. 2001.

[81] R. S. Adve, R. A. Schneible, G. Genello, P. Antonik, "Waveform-space-time adaptive processing for distributed aperture radars", Proc.2005 IEEE Intl. Radar Conference, pp. 93-97, 2005.

[82] Lin, J.; Chiu, M.; Lee, R.; "Spreadspectrum Communications", Communications Engineering:E ssentials for Computer Scientists and Electrical Engineers ch7, 2007 , Page(s): 209 – 230

[83] Jung, P.; Baier, P.W.; Steil, A.; "Advantages of CDMA and spread spectrum techniques over FDMA and TDMA in cellular mobile radio applications", Vehicular Technology, IEEE Transactions on Volume: 42 , Issue: 3,1993 , Page(s): 357 - 364

[84] Gaston, D.; "Applications of spread spectrum radio technology for the security market", Security Technology, 1994. Proceedings. Institute of Electrical and Electronics Engineers 28th Annual 1994 International Carnahan Conference on, 1994 , Page(s): 86 - 91

[85] Mingqi Li; Qicong Peng; Yulin Liu; “Performance analysis of a two dimensional spread spectrum multicarrier system in Rayleigh fading channel”, Communication Technology Proceedings, 2003. ICCT 2003. International Conference on Volume: 2 ,2003 , Page(s): 1911 - 1914

[86] Choi, J.D.; Stark, W.E.; “Performance analysis of ultra-wideband spread-spectrum communications in narrowband interference”, MILCOM 2002. Proceedings, Volume: 2, 2002, Page(s): 1075 - 1080

[87] Sturman, T.A.; Guidi, A.M.; Dingley, P.; Bowyer, M.D.J.; Petfield, N.R.; Moseley, M.; “Waveform diversity and design: Part II - Issues for waveforms and applications”, 2008 IET Waveform Diversity & Digital Radar Conference,1 – 13, 2008

[88] Ilteris Demirkiran, Donald D. Weiner, Pramod K. Varshney, “ A General Approach for Performance Evaluation of Multi-user Direct-Sequence Spread Spectrum (DSSS) Systems.” The 2004 Conference on Information Sciences and Systems (CISS), Princeton, NJ, March 2004. EMC

[89] S. B. Weinstein and P. M. Ebert, “Data Transmission by Frequency-Division Multiplexing using the Discrete Fourier Transform,” IEEE Trans. on Communications, vol. 19, no. 5, pp. 628–634, Oct. 1971.

[90] R. van Nee and R. Prasad, OFDM for Wireless Multilmedia Communications, Artech House Publishers, Boston, USA, 2000.

[91] L. Brennan and I. Reed, “Theory of adaptive radar,” IEEE Transactions on Aerospace and Electronic Systems, vol. 9, pp. 237–252, March 1973.

[92] I. S. Reed, J. Mallett, and L. Brennan, “Rapid convergence rate in adaptive arrays,” IEEE Transactions on Aerospace and Electronic Systems, vol. 10, No. 6, pp. 853–863, Nov. 1974.

[93] B. Friedlander, “A Subspace Method for Space Time Adaptive Processing,” IEEE Trans. On Signal Processing, vol. 53, Issue 1, pp. 74–82, Jan. 2005.

[94] J. S. Goldstein, I. Si. Reed, and L. L. Scharf, “A Multistage Representation of the Wiener Filter Based on Orthogonal Projections,” IEEE Trans. on Information Theory, vol. 44, Issue 7, pp. 2943–2959, Nov. 1998.

[95] J. R. Guerci, J. S. Goldstein, and I. S. Reed, “Optimal and Adaptive Reduced-Rank STAP,” Special Section on Space-Time Adaptive Processing, IEEE Trans. on Aerospace and Electronic Systems, vol. 36, Issue 2, pp. 647–663, April 2000.

[96] J. R. Guerci, Space-time adaptive processing, Artech House, 2003.

[97] A. M. Haimovich and M. Berin, “Eigenanalysis-based space-time adaptive radar: performance analysis,” IEEE Trans. on Aerospace and Electronic Systems, vol. 33, Issue 4, pp. 1170–1179, Oct. 1997.

[98] R. Klemm, Principles of Space-Time Adaptive Processing, IEE, 2002.

[99] W. L. Melvin, G. A. Showman, and J. R. Guerci, “A knowledge-aided GMTI detection architecture,” in Proc. of 2004 IEEE Radar Conference, Apr. 2004. Philadelphia.

[100] J. S. Bergin, C. M. Teixeira, P. M. Techau, and J. R. Guerci, “STAP with knowledge-aided data pre-whitening,” in Proc. of 2004 IEEE Radar Conference, Apr. 2004. Philadelphia.

[101] M. Rangaswamy, F. C. Lin, and K. R. Gerlach, “Robust adaptive signal processing methods for heterogeneous radar clutter scenarios,” Signal Proc., vol. 84, pp. 1653–1665, Sept. 2004.

[102] S. Blunt, K. R. Gerlach, and M. Rangaswamy, “The enhanced FRACTA algorithm with knowledge aided covariance estimation,” in Proc. of 2004 Sensor Array and Multichannel Sig. Proc. Workshop, July 2004.

[103] W. Baldygo, M. Wicks, R. Brown, P. Antonik, G. Capraro, and L. Hennington, "Artificial Intelligence Applications to Constant False Alarm Rate (CFAR) Processing," in Proc. 1993 National Radar Conference, Boston, 1993.

[104] C. Morgan and L. Moyer, "Knowledge Base Applications to Adaptive Space-Time Processing, Vol. IV: Knowledge-Based Tracking," USAF Res. Lab., Rome, NY Rep. AFRL-SN-RS-TR-2001-146 (IV), 2001,vol. IV.

[105] McLaughlin, D.J.; Allan, N.; Twarog, E.M.; Trizna, D.B.; “High resolution polarimetric radar scattering measurements of low grazing angle sea clutter”, Oceanic Engineering, IEEE Journal of Volume: 20 , Issue: 3, 1995 , Page(s): 166 – 178

[106]D. A. Garren, et al, "Full-polarization marched-illumination for target detection and identification," IEEE Transactions on Aerospace and Electronic System. vol. 38. no. 3. pp. 824-837. 2002.

[107] Cloude, S.R.; Papathanassiou, K.P.; “Polarimetric SAR interferometry”, Geoscience and Remote Sensing, IEEE Transactions on, Volume: 36 , Issue: 5 , Part: 1, 1998 , Page(s): 1551 - 1565

[108] J. P. Costas, “A Study of a Class of Detection Waveforms Having Nearly Ideal Range-Doppler Ambiguity Properties,” Proc. IEEE, Vol. 72, pp. 996–1009, Aug. 1984.

[109] S. W. Golomb and H. Taylor, “Construction and Properties of Costas Arrays,” Proc. IEEE, Vol. 72, pp. 1143–1163, Sept. 1984.

[110] N. Levanon and E. Mozeson, Radar Signals,Wiley-IEEE Press, 2004.

[111] Jiann-Ching Guey; Bell, M.R.; “Diversity waveform sets for delay-Doppler imaging”,Information Theory, IEEE Transactions on Volume 44, Issue 4, July 1998 Page(s):1504 – 1522

[112] Shu-Ming Tseng; Der-Feng Tseng; Guan-Fu Huang; Yuan Ching Tzeng; Wen-Chi Tseng; “A realization of diversity waveform sets for delay-Doppler imaging”,Circuits and Systems, 2004. Proceedings. The 2004 IEEE Asia-Pacific Conference on,Volume 1, 6-9 Dec. 2004, Page(s):237 – 240, vol.1

[113] Wing-Kit Chung; Kainam Thomas Wong; “Pulse-diverse radar waveform design for accurate joint estimation of time delay and Doppler shift”, Acoustics, Speech, and Signal Processing, 2000. ICASSP’00 Proceedings of 2000 IEEE International Conference on, Volume 5, 5-9 June 2000 Page(s):3037 - 3040 vol.5

[114] Chieh-Fu Chang; Bell, M.R.; “Frequency-coded waveforms for enhanced

delay-Doppler resolution", Information Theory, IEEE Transactions on, Volume: 49 , Issue: 11, 2003 , Page(s): 2960 – 2971

[115] S. U. Pillai, H. S. Oh, D. C. Youla, and 1. Guerci, "Optimum transmit-receiver design in the presence of signal-dependent interference and channel noise," IEEE Trans.Information Theory, vol. 46, no. 2, pp. 577-584, Mar. 2000.

[116] D. A. Garren, M. K. Osborn, A. C. Odom, 1. S. Goldstein, S. U. Pillai, and 1. Guerci, "Enhanced target detection and identification via optimized radar transmission pulse shape," Proc. Inst. Elect. Eng., Radar, Sonar, Navigation, vol. 148, no. 3, pp. 130-138, Jun.2001.

[117] A. R. Kaye and D. A. George, "Transmission of multiplexed PAM signals over multiple channel and diversity systems," IEEE Trans.Commun. Technol., vol. COMM-18, pp. 520–526, Oct. 1970.

[118] P. Antonik, M. C. Wicks, H. D. Griffiths, C. J. Baker, "Frequency diverse array radars", Proc. 2006 IEEE Radar Conf., Verona, NY, pp. 215-217, 24-27 April 2006.

[119]Jingjing Huang, Kin-Fai Tong, Chris Baker, "Frequency Diverse Array with Beam Scanning Feature", The 2008 IEEE International Symposium on Antennas and Propagation, San Diego, USA, July 2008,Page(s):1-4

[120] Jingjing Huang, Kin-Fai Tong, Karl Woodbridge, Chris Baker, "Frequency Diverse Array: Simulation and Design", 2009 IEEE Radar Conference, Pasadena, USA, May 2009, Page(s): 1-4

[121]Jingjing Huang, Kin-Fai Tong, Chris Baker, “Frequency Diverse Array: Simulation and Design”, Antennas & Propagation Conference, 2009. LAPC 2009. Loughborough, UK, Nov 2009, Page(s): 253-256

[122] http://eprints.ucl.ac.uk/18746/1/18746.pdf

[123] W. L. Stutzman, G. A. Thiele: Antenna Theory and Design, Wiley, Second Edition, New York, 1998.

[124] Jiann-Ching Guey; Bell, M.R.; “Diversity waveform sets for delay-Doppler imaging”,Information Theory, IEEE Transactions on Volume 44, Issue 4, July 1998, Page(s):1504 – 1522

[125] Constantine A. Balanis, “Antenna Theory: Analysis and Design”, 3rd Edition, , 2005

[126] Visser, Hubregt J., “Array and Phased Array Antenna Basics”, 2005 John Wiley & Sons

[127]Rolland E. Best, “Phase Locked Loops: Theory, Design, and Applications”, 2007 Mcgraw-Hill

[128]Venceslav F. Kroupa, “Phase Lock Loops and Frequency Synthesis”,April 2003

[129] Curtis Barrett, “Fractional/Integer-N PLL Basics”, Technical Brief SWRA029, http://focus.ti.com.cn/cn/lit/an/swra029/swra029.pdf

[130] http://www.freescale.com/files/rf_if/doc/data_sheet/MC145151-2.pdf

[131] Steve Williams and Tony Caviglia, "Simulating PLL reference spurs", http://rfdesign.com/mag/605RFD33.pdf

[132] http://datasheets.maxim-ic.com/en/ds/DS4026.pdf